UNIVERSIDAD DE MURCIA

ESCUELA INTERNACIONAL DE DOCTORADO

Molecular mechanism of cap-independent translation of MNSV. Structural and functional analysis of the viral and host factors involved

Mecanismos moleculares de la traducción cap-independiente de MNSV. Análisis estructural y funcional de los factores virales y del huésped

D. MANUEL MIRAS MARÍN

2016

Molecular mechanism of cap-independent translation of MNSV. Structural and functional analysis of the viral and host factors involved

Mecanismos moleculares de la traducción cap-independiente de MNSV. Análisis estructural y funcional de los factores virales y del huésped

D. MANUEL MIRAS MARÍN

Directores: Dra. Verónica Truniger

Dr. Miguel Ángel Aranda

TABLE OF CONTENTS

List of Figures

List of Tables

List of Supplementary Tables

SUMMARY

Cap-independent translation is frequent for viral RNAs, which are often devoid of 5'-cap structure or/and 3'-poly(A) tail typical of eukaryotic mRNAs. Instead, many plant RNA viruses contain in their 3´-UTRs RNA elements able to enhance their cap-independent translation (3´-CITEs). It has been reported that 3´-CITEs directly bind and require eukaryotic translation initiation factors (eIF) for their function. We have shown that cap-independent translation of *Melon necrotic spot virus* (MNSV, family *Tombusviridae*) RNAs is controlled by a 3´-CITE *in cis.* Genetic evidence indicates that the eIF4E subunit of melon eIF4F is necessary for cap-independent translation of avirulent MNSV RNAs. However, the interaction between 3'-CITE and eIF4E remains uncharacterized. The study of this interaction may be used in antiviral strategies. Importantly, MNSV resistance was showed to be eIF4E-mediated and recently, a new resistance-breaking MNSV isolate was identified. Thus, the aims of this thesis is focused on elucidating the mechanisms of cap-independent translation of MNSV RNAs and characterize this new resistance- breaking isolate

In the first chapter, we characterized the newly resistance-breaking MNSV isolate, MNSV-N. It was found a 55 nucleotide insertion in its 3'-UTR which was acquired by interfamilial recombination with the 3'-UTR of an Asiatic *Cucurbit aphid-borne yellows virus* (CABYV, family *Luteoviridae*) isolate. By constructing chimeric viruses and assaying their properties, we showed that the recombined sequence is responsible for the MNSV-N ability to break down the eIF4E-mediated resistance. Analysis of the translation effiency showed that the insertion funcstions as a 3'-CITE. The structural and functional characterization of this 3'-CITE showed that it belongs to a new structural class that we called CXTE (CABYV *Xinjiang*-like translation element) and functions in absence of eIF4E.

In the second chapter, to understand the cap-independent translation of MNSV RNAs, we performed a structural and functional analysis of the 3'-CITE of avirulent MNSV isolates and its partner eIF4F. Thus, we defined the minimal size of the 3´-CITE

in "*in vivo*" translation assays to a sequence of 45 nucleotides. Hereafter, we studied its secondary structure and its ability to bind eIF4F. *In vitro* binding assays revealed eIF4F-binding sites on a bulge of 3'-CITE. Mutational analyses in eIF4E revealed amino acids involved in cap-independent translation and suggested that the eIF4F complex is necessary for an efficient translation because the disruption of the complex is associated with a loss in translation activity.

Finally, in the third chapter we studied the binding mode of the eIF4E:eIF4G interaction. We previously showed that this binding is required for MNSV RNAs efficiently translate. Thus, subunit eIF4E free and in complex with a truncated $eIF4G_{1003-1092}$ were crystallized. X-ray data revealed a second eIF4E-binding domain in eIF4G. This second binding domain, or non-canonical binding motif, contacts with the lateral surface of eIF4E which it is shared with other eIF4E-binding proteins (4E-BPs). This data suggests a bipartite eIF4E:eIF4G binding mode that competes with 4E-BPs in translation regulation.

List of viruses

- AMV: *Alfalfa mosaic virus*
- BMV: *Brome mosaic virus*
- BRV: *Blackcurrant reversion virus*
- BYDV: *Barley yellow dwarf virus*
- CABYV: *Cucurbit aphid-borne yellows virus*
- CarMV: *Carnation mottle virus*
- CbMV: *Calibrachoa mottle virus*
- CBV: *Cucumber Bulgarian virus*
- CIRV: *Carnation Italian ringspot virus*
- CLSV: *Cucumber leaf spot virus*
- CMV: *Cucumber mosaic virus*
- CrPV: *Cricket paralysis virus*
- CrTMV: *Crucifer-infecting tobamovirus*
- CYVV: *Clover yellow vein virus*
- FDMV: *Foot and mouth disease virus*
- FMDV: *Foot-mouth disease virus*
- HCV: *Hepatitis C virus*
- HIV-1: *Human immunodeficiency virus type 1*
- JCSMV: *Johnsongrass chlorotic stripe mosaic virus*
- LMV: *Lettuce mosaic virus*
- MNeSV: *Maize necrotic spot virus*
- MNSV: *Melon necrotic spot virus*
- MWLMV: *Maize white line mosaic virus*
- PEMV2: *Pea enation mosaic virus RNA 2*
- PLPV: *Pelargonium line pattern virus*
- PMV: *Panicum mosaic virus*
- PnLV: *Poinsettia latent virus*
- PSNV: *Pea stem necrosis virus*
- PV: *Poliovirus*
- PVA: *Potato virus A*
- PVY: *Potato virus Y*
- RCNMV: *Red clover necrotic mosaic virus*
- STNV *Satellite tobacco necrosis virus*
- TBSV: *Tomato bushy stunt virus*
- TCV: *Turnip crinkle virus*
- TEV: *Tobacco etch virus*
- TMV: *Tobacco mosaic virus*
- TriMV: *Triticum mosaic virus*
- TSWV: *Tomato spotted wilt virus in pepper*
- TuMV: *Turnip mosaic virus*

List of acronyms

- +ssRNA: Positive single-stranded RNA
- -ssRNA: Negative single-stranded RNA
- 3'-CITE: Cap-independent translation element
- 4E-BM: Canonical eIF4E-binding motif
- 4E-BPs: eIF4E-binding proteins
- 4E-T: eIF4E transporter
- aa-tRNA: amino acyl-tRNAs
- AtLOX2: Arabidopsis thaliana lipoxygenase 2
- BTE: *Barley yellow dwarf virus*-like translational element
- BzCN: Benzoyl cynide
- *Cm*eIF4E: *Cucumis melo* eIF4E
- CP: Coat protein
- CXTE: CABYV-Xinjiang-like translation element
- DMSO: Dimethyl sulfoxide
- dNTP: Deoxynucleotide tripphospahte
- dpi: Days post inoculation
- ds: Double stranded
- DTT: Dithiothreitol
- EDTA: Ethylenediaminetetraacetic acid
- eIF2: Eukaryotic initiation factor 2
- eIF4A: Eukaryotic initiation factor 4A
- eIF4B: Eukaryotic initiation factor 4B
- eIF4E: Eukaryotic initiation factor 4E
- eIF4G: Eukaryotic initiation factor 4G
- eIF5: Eukaryotic initiation factor 5
- ESTs: Expressed sequence tag
- F-Luc: Firefly luciferase
- GDP: Guanosine-5´-diphosphate
- gRNA: Genomic RNA
- GTP: Guanosine triphosphate
- ICTV: International Committee on Taxonomy of Virus
- IRES: Internal ribosome entry site
- ISS: I-shaped structure
- m7G: 7-methyl-gunosine
- Ma5TE: MNSValpha5-like translation element
- MBP: Maltose binding protein
- Met-tRNA: Methionine initiator transfer RNA
- mg: Milligram
- ml: Milliliter
- MNK1-2: Mitogen-activated protein kinase-interacting kinases 1 and 2
- mRNA: Messenger RNA
- mTOR: Mammalian target of rapamycin

- NAC: Nascent polypeptide-associate complex
- NC 4E-BM: Non-canonical binding motif
- nt: Nucleotide
- ORF: Open reading frame
- PAPB: Poly-A binding protein
- PIC: Preinitiation complex
- Pmol: Picomole
- PNK: Polynucleotide Kinase
- PTE: *Panicum mosaic virus*-like translation element
- R-Luc: Renilla luciferase
- RB: Resistance breaking
- RdRp: RNA dependent RNA polymerase
- RNA: Ribonucleic acid
- RT: Reverse transcriptase
- SDS-PAGE: Sodium dodecyl sulfate polyacrylamide gel eletrophoresis
- SDS: Sodium dodecyl sulfate
- sgRNA: Subgenomic
- sgRNA: Subgenomic RNA
- SHAPE: Selective 2'-hydroxyl acylation analyzed by primer extensión
- SL: Stem-loop structure
- TED: Translation enhancer domain
- TILLING: Targeting induced local lesions in genomes
- TSS: tRNA-shaped structure
- UTR: Untranslated region
- UV: Ultraviolet
- VPg: Viral protein genome-linked
- VRC: Viral replication complex
- wt: Wild type
- YSS: Y-shaped structure

INTRODUCTION

Introduction

Plant virology is primarily concerned with the diseases that viruses may cause and their control. Along the years, plant virology has also used viruses as very efficient tools to dissect fundamental processes in the biology of the plants and, more generally, of eukaryotic organisms. Examples include the very same discovery of the existence of viruses (reviewed in (Zaitlin 1998; Scholthof 2004) and the contribution to the discovery of the RNA silencing phenomenon and its mechanisms (Hamilton & Baulcombe 1999). Plant viruses are obligate parasites which posses very small genomes. They are strictly dependent on their hosts metabolic machineries for energy generation and proteins synthesis. This has two main consequences to which this Thesis makes reference to: (i) Viral genomes consist of a compact mosaic of functional modules with many times overlapping functions, and (ii) Viruses are strictly dependent on hosts factors with which viral factors need to interact to complete viruses infectious cycles. In the following sections I will briefly review the viral cycle of the most abundant class of plant viruses, with special emphasis on the step leading to the translation of viral mRNAs into proteins. I will also comment on an important evolutionary mechanism that may lead to the sudden acquisition of a functional competence by viral genomes. As the reader will see, these two aspects are central to the fundamental findings of this Thesis. Finally, I will review the most important aspects of the experimental system that I have used and end up identifying the major goals of this Thesis.

1. Viral cycle

Positive sensed single-stranded RNA (+ssRNA) viruses constitute the largest group of RNA viruses with more than 30 families. Main steps in the +ssRNA plant virus cycles include entry in the cell, uncoating, translation, replication, assembly and shedding. Plant viruses enter cells of initially infected plants following transmission by insect vectors or after mechanical injury. No cell surface receptors have been identified for plant virus entry. Uncoating of the viral RNA is poorly understood for most plant

viruses. First evidence of this process was shown for *Tobacco mosaic virus* (TMV) (Shaw *et al.* 1986). TMV viral RNA is initially uncoated in the 5'-to-3' direction and the process is completed by the removal of coat protein molecules (subunits) in the 3'-to-5' direction. *In vivo* uncoating begins by a cotranslational disassembly mechanism in which the removal of subunits in the 5'-to-3' direction is coincident with ribosome translocation during translation of the first ORF of the viral RNA ((Michael & Wilson 1984). Subsequent studies with *Cowpea chlorotic mottle virus* (CCMV) and *Flock house virus* (FHV) suggested that this process might be a general mechanism of viral particles disassembly (Roenhorst *et al.* 1989; Hiscox & Ball 1997). Viral replication is a multi-step process that requires the viral encoded RNA dependent RNA polymerase (RdRp), other viral proteins, numerous host proteins and the host endomembrane system (Ahlquist *et al.* 2003; Nagy & Pogany 2008; Nagy *et al.* 2012; Nagy & Pogany 2012) (Figure 2). Binding of viral-encoded proteins selectively to the viral RNA is proposed to switch the conformation of the viral RNA from a translationally to a replication competent template (Gamarnik et al., 1998). Replication takes place in a viral-induced, membrane-bound, multi-protein complex known as the viral replication complex (VRC). The viral replication complexes utilize different subcellular membranes as "platforms" for replication, including endoplasmic reticulum, mitochondria, vacuoles, Golgi, chloroplasts, and peroxisomal membranes (Salonen *et al.* 2004). For example, *Melon necrotic spot virus* (MNSV) (genus *Carmovirus*, family *Tombusviridae*) alters host mitochondria to transform them into viral factories (Gomez-Aix et al., 2015). RdRp and auxiliary replication proteins are involved in the following processes: 1) to detect the +ssRNA template, 2) to move factors involved to the replication sites, 3) to assemble viral replication complexes and finally, 4) to transcribe the viral RNA into a negative ssRNA, which is subsequently used as a template for the synthesis of the +ssRNA progeny (Nagy & Pogany 2006). In addition to viral proteins, host factors have crucial roles in all steps of (+)RNA virus replication. Genome-wide approaches have emerged as a powerful tool to identify these host factors. For example, genome-wide screenings of *Saccharomyces cerevisiae* led to the identification of host genes that affect *Brome mosaic virus* (BMV) and *Tomato bushy stunt virus* (TBSV) replication (Panavas *et al.* 2005; Cheng *et al.* 2006; Jiang *et al.* 2006).

To express the 3’ proximal ORFs, many +ssRNA viruses generate subgenomic RNAs (sgRNAs) during the late stages of infection, either via premature termination of transcription by the RdRp during (-)-strand RNA synthesis or internal initiation on the (-)-strand during (+)-strand RNA synthesis. These ORFs usually encode structural and movement proteins. The newly synthesized genomic RNAs are used either for a new round of translation and production of more replicase and structural proteins, or are encapsidated to produce viral particles. For example, in *Pepino mosaic virus* (PepMV) each virus particle contains a single molecule of RNA, which is protected by hundreds of copies of a coat protein (Agirrezabala *et al.* 2015). Encapsidation signals for many RNA viruses are *cis*-acting RNA sequences that are located either in the 5’ or the 3’ end of the viral RNA (Sasaki & Taniguchi 2003). Plant viral progeny moves from cell to cell *via* plasmodesmata as a nucleoprotein complex, though viral particles have been observed in plasmodesmata in a number of cases.

Thus, an initial and fundamental step is the translation of the gRNA to produce the viral proteins required for the early steps of the viral cycle. A significant proportion of +ssRNA viruses utilize non-canonical mechanisms of translation that allow them to compete with cellular mRNAs for the translational machinery (Simon & Miller 2013). Canonical and non-canonical translation mechanisms will be reviewed in the following sections.

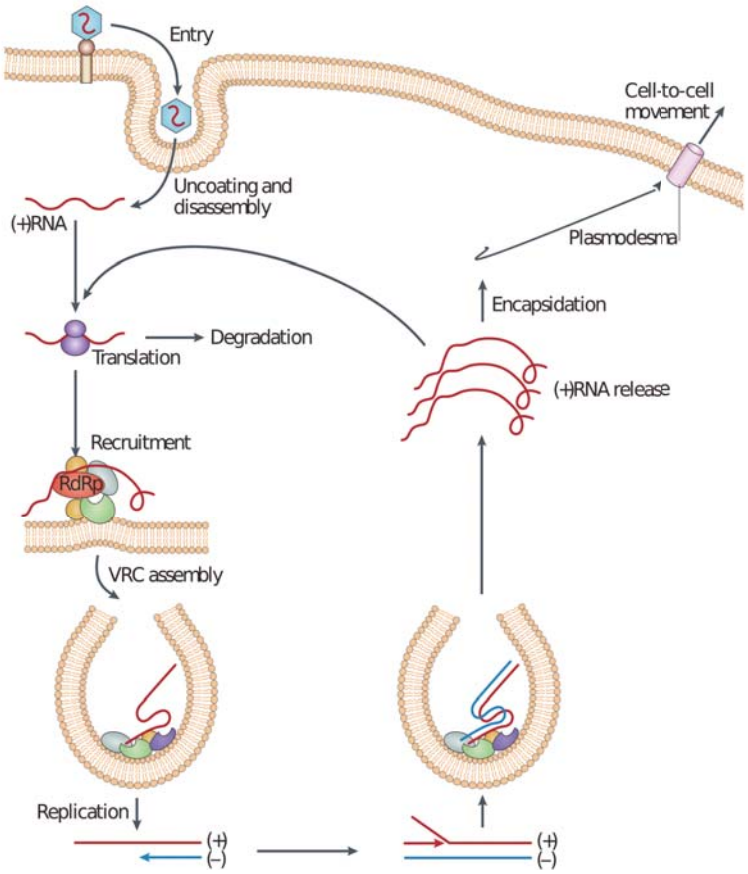

Figure 1. Schematic infection cycle of positive-sense RNA viruses. (+)RNA viruses enter plant cells through wounds or vectors. When the virus is inside the cell, the (+)RNA genome is released into the cytosol, where it is translated by the host ribosomes. The resulting viral replication proteins then recruit the (+)RNA to subcellular membrane compartments, where functional viral replication complexes (VRCs) are assembled. A small amount of negative-sense RNA ((−)RNA) is synthesized and serves as a template for the synthesis of a large number of (+)RNA progeny. The new (+)RNAs are released from the VRCs, whereas the (−)RNA is retained. The released (+)RNAs start a new cycle of translation and replication, become encapsidated, and move to neighboring cells through plasmodesmata (adapted from Nagy and Pogany, 2012).

2. Translation of mRNAs

Translation consists of the processes needed for converting genetic information from messenger RNAs into proteins. For cellular mRNAs, after their synthesis in the nucleus (transcription) and export to the cytosol through specialized channels, mRNAs serve as templates for protein synthesis, which is carried out by the cellular machines called ribosomes (Lackner & Bähler 2008). Ribosomes, which are large complexes, are composed of proteins and non-coding RNAs and catalyze eukaryotic protein synthesis from mRNA templates (Varani 1997). Translation is functionally divided into three

distinct steps: initiation, elongation and termination (Fig. 2) (Merrick 1992). Initiation consists of the recruitment of ribosomal subunits to the mRNA. This is followed by elongation, during which amino acids are added to the nascent peptide. Next, in the termination step, the ribosomal subunits dissociate and protein and mRNA are released. Finally, a last step of recycling takes place (Dever & Green 2012).

1.1. Canonical translation initiation

Translation initiation is the rate limiting (Gallie 2002; Pestova *et al.* 2007) and most highly regulated step (Aitken & Lorsch 2012) in translation. In higher eukaryotes, the structure of the mRNA plays an important role in translation initiation and regulation (Gallie & Browning 2001; Pestova & Kolupaeva 2002). Most eukaryotic mRNAs are appended at their 5'-end with a 7-methyl-guanosine (m7G)-pppN structure, where N is any nucleotide (Perry *et al.* 1975), which is called cap. The cap has been shown to significantly enhance translation of reporter constructs *in vitro* and is thus considered a pivotal *cis*-acting element for the translatability of the majority of eukaryotic mRNAs (Both *et al.* 1975). Apart from being crucial for translation initiation, the 5´cap also facilitates nuclear export and protects from cytosolic degradation pathways (Varani 1997). In addition to the 5' cap, all eukaryotic mRNAs, except histone mRNAs (Adesnik *et al.* 1972), carry a polyadenosine (poly(A)) tail at their 3´-end, which is co-transcriptionally added to the nascent mRNA. The poly(A) tail is a key determinant of transcript stability and enhances translation of mRNAs, being recognized and bound by the poly(A) binding-protein (PABP) (Sachs 1990; Kahvejian *et al.* 2005). These structural features are required for recruitment of the protein synthesis machinery during translation initiation via the cap-dependent pathway. This pathway involves numerous initiation factors (eIFs) (Gallie 2002) and the interplay of a succession of protein-protein and RNA-protein interactions (Hershey & Merrick 2000). This process has been divided in five steps (Fig. 3):

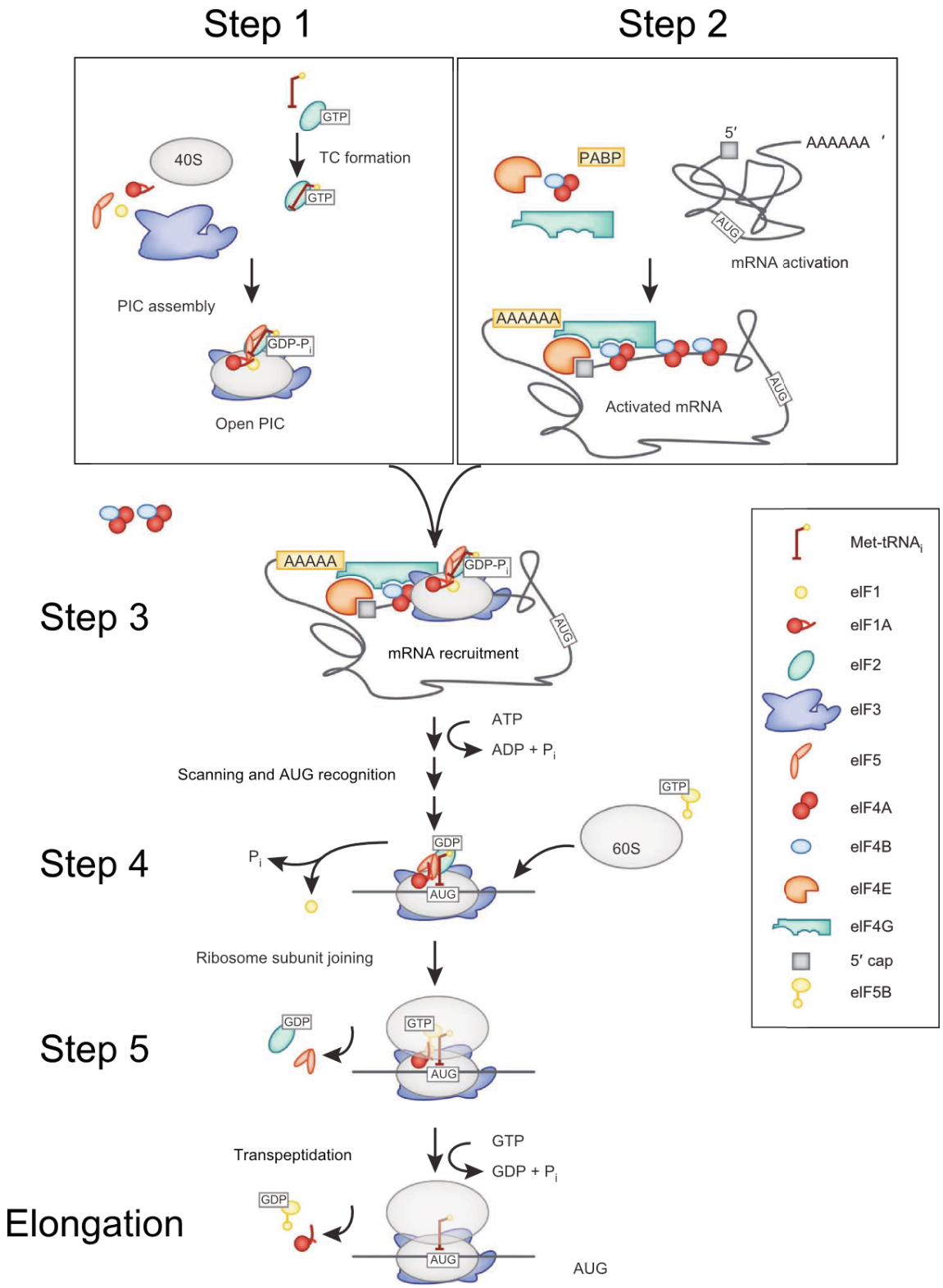

Figure 2. Cap-dependent translation. Cap-dependent translation begins with the formation of the ternary complex, the activated mRNA, and the pre-initiation complex (PIC). After the mRNA is recruited to the pre-initiation complex and the ribosome is properly assembled, translation may occur (adapted from Aitken, 2012).

Step 1. Formation of 43S preinitiation complex

Some eIFs bind to the 5'-end of the transcript while others bind first to the small subunit of the ribosome (40S), which contains three tRNA binding sites: A, P, and E sites (Rodnina & Wintermeyer 2009). The ternary complex (TC) composed of eIF2 bound to GTP and the initiator methionine bound tRNA (Met-tRNA^{Met}) interacts with the 40S ribosome through the P-site bound to initiation factors eIF3, eIF1A, and eIF1 to form the 43S preinitiation complex (PIC) (Sonenberg & Hinnebusch 2009). EIF2 interacts with eIF3 directly via the eIF3a subunit and indirectly via eIF5 bridging the two factors. EIF3, which is a huge multicomponent complex (Sun *et al.* 2011; Smith *et al.* 2016), can support dissociation of 80S in the presence of the mRNA or the TC and eIF1A (Unbehaun *et al.* 2004; Kolupaeva *et al.* 2005). EIF3 binds mostly on the solvent-accessible side of the 40S ribosome (Srivastava *et al.* 1992), but one of its domains wraps around to block part of the binding site of the 60S ribosome (Siridechadilok *et al.* 2005). EIF1A blocks the A-site to prevent premature entry of tRNAs, and eIF1 binds near to the P-site (Carter *et al.* 2001; Lomakin *et al.* 2003; Yu *et al.* 2009). These factors are important in PIC formation and selection of the start codon (Pestova *et al.* 1998; Battiste *et al.* 2000; Martin-Marcos *et al.* 2011).

Step 2. Priming of the mRNA 5´-cap structure by eIF4F, eIF4A and eIF4B

The mRNA is recognized and bound by eIF4F, which in mammals is a heterotrimer composed of the cap-binding factor eIF4E, the ATP-dependent RNA helicase eIF4A and the scaffolding protein eIF4G, which contains binding domains for eIF4E, eIF4A and PABP (Grifo *et al.* 1983; Jaramillo *et al.* 1990; Pestova *et al.* 2001). In plants, eIF4F is a heterodimer composed of eIF4E and eIF4G. The isoforms eIFiso4E and eIFiso4G are found only in plants and show preference for initiation at unstructured non-coding regions (Gallie & Browning 2001). EIF4B, which assists in the eIF4A helicase function, binds to the complex eIF4F (Grifo *et al.* 1982; Grifo *et al.* 1984). Recognition of mRNA by eIF4F in both plants and mammals is facilitated through binding of the eIF4E subunit to the 5'-cap (Sonenberg *et al.* 1980; Pestova *et al.* 2001). EIF4G can recruit other factors, including eIF3 and the PABPs through direct protein-protein interactions. It is thought that this last interaction promotes the circularization of the

message enhancing translation efficiency (Sachs & Davis 1989; Tarun *et al.* 1997; Wells *et al.* 1998; Paek *et al.* 2015). The formation of this closed-loop may also allow coupling of translation termination and recycling events with subsequent rounds of initiation on the same mRNA (Uchida *et al.* 2002).

Step 3. Binding of mRNA to the 43S complex

The ternary complex, 40S ribosome and initiation factors are known as the 43S ribosomal PIC (Pestova *et al.* 2007; Rodnina & Wintermeyer 2009). The 43S PIC interacts with the activated mRNA. Multiple factors (eIF4A, eIF4B, and possibly PABP) work to unwind the secondary structure naturally present in most 5'-untranslated regions (UTRs) of mRNAs (Hinnebusch 2011). EIF4G serves as organizing center for loading of the 43S PIC to the 5´-end of the mRNA, mainly via interactions between PABP, eIF4G, eIF4B, eIF3, eIF2 and mRNA (Sachs & Varani 2000; Jivotovskaya *et al.* 2006).

Step 4. Scanning of the mRNA leader and start codon recognition

The 43S PIC loaded at the capped 5´-end of the mRNA scans the downstream leader sequence until it finds the first start codon in an optimal initiation context, known as the Kozak sequence: GCC(**A**/**G**)CCAUG**G** (with most important bases in bold; (Kozak 1984; Kozak 1986)). The scanning process of the 43S PIC requires ATP hydrolysis and is dependent of eIF1 and eIF1A, which are required for selection of the correct codon by discriminating incorrect codon-anticodon interactions between the message and the initiator Met-tRNA^{Met} (Pestova & Kolupaeva 2002). Start site selection requires cooperation between the scanning ribosome and eIF1, eIF2 and eIF5, which form the 48S preinitiation complex (Pestova & Kolupaeva 2002). As a result, the anticodon of the initiator tRNA interacts with the AUG codon (Pestova *et al.* 2007).

Step 5. 60S subunit joining

After the start codon is selected, eIF5 stimulates the hydrolysis of the GTP associated with eIF2, and eIF2-bound GDP is released from 48S preinitiation complex (Merrick 1992). Joining of the 60S subunit requires an additional factor, eIF5B, which bound to GTP joins the free A-site, preventing tRNAs from enter to it before the 60S

ribosome joins (Pestova *et al.* 2001). This leads to a conformational change that allows the initiation factors to leave, including eIF3 (Aitken & Lorsch 2012). The 60S ribosome joins the 40S ribosome, hydrolyzing the GTP molecule associated with eIF5B and releasing eIF5B (Pestova *et al.* 2001). The resulting 80S complex is ready to enter the elongation phase of translation.

2.1. Translation elongation and termination

In the elongation phase, entering amino acyl-tRNAs (aa-tRNA) bind the mRNA through an anti-codon-codon interaction at the A-site (Lewin *et al.* 2008). This binding is accompanied by the hydrolysis of GTP and the release of the eIF1/GDP complex (Rodnina & Wintermeyer 2009). Transpeptidation is catalyzed by the ribosome itself and occurs between aa-tRNA at the A-site and the peptidyl-tRNA at the P-site. As a result, the peptidyl-tRNA occupies the A-site while the deacylated-tRNA formed is relocated at the P-site. After formation of the peptide bond, the translocation step occurs in which the ribosome ratchets in the 3' direction along the transcript, the new peptidyl-tRNA is moved to the P-site to make room for the incoming aa-tRNA and the deacylated tRNA in the P-site is shuttled to the exit (E)-site (Julián *et al.* 2008) and from there exits the ribosome (Rodnina & Wintermeyer 2009).

2.2. Ribosomal recyling

Ribosome recycling occurs after the nascent polypeptide has been released during the termination step. Despite the release of the polypeptide, ribosomes remain bound to the mRNA and tRNA. It is only during the fourth step of translation that ribosomes are ultimately released from the mRNA, split into subunits, and are free to bind new mRNA (Pisarev *et al.* 2011; Dever & Green 2012).

3. Non-canonical translation initiation mediated by viral RNA structures

As obligate parasites viruses, rely on their hosts translational machinery for translating viral proteins. However, many plant and animal viral mRNAs lack a functional 5' cap and /or a poly(A) tail. In fact, about 80 % of the plant viruses have mRNAs that lack either the 5´cap and/or the poly(A) tail. In the absence of these elements, viruses have evolved alternative elements to efficiently translate their viral RNAs, including internal ribosome entry sites (IRESes) and cap-independent translation enhancers (CITEs).

3.1. IRESes

IRESes are mainly harbored in the 5´-UTRs of predominantly animal viruses as alternative structures to the cap (Hellen & Sarnow 2001; Tuplin 2015). The first IRES to be characterized was in the 5´-UTR of *Poliovirus* (PV, family *Picornaviridae*) (Pelletier & Sonenberg 1988). IRESes are highly structured *cis*-acting RNA elements which recruit ribosomes or ribosomal subunits to the vicinity of the initiation codon in the presence or absence of translational initiation factors (Hertz & Thompson 2011). There is little similarity in sequence, structure and translation factor requirements among different classes of IRESes. For example, IRESes of *Foot-mouth disease virus*, *Poliovirus* and *Hepatitis C virus* (FMDV, PV and HCV, family *Picornaviridae* and *Flaviviridae*, respectively) require different combinations of translational initiation factors to recruit the 43S preinitiation complex, while the *Cricket paralysis virus* (CrPV, family *Dicistroviridae*) IRES recruits the 43S complex independently of any initiation factor (Tuplin 2015).

Some plant viruses which RNAs lack 5´-cap contain IRESes, as for example *Tobacco etch virus* (TEV, family *Potyviridae*). The TEV 5´-leader sequence contains two IRESes that were named cap-independent regulatory elements (CIREs), both needed for an efficient translation initiation (Niepel & Gallie 1999). Other examples of plant IRESes include the 5´-leader sequence of genomic RNAs of *Blackcurrant reversion virus* (BRV, family *Comoviridae*) and that of *Crucifer-infecting tobamovirus* (CrTMV, family *Virgaviridae*) which harbor two IRESes, one upstream of the coat protein ORF and the second upstream of movement protein gene. Interestingly, this last IRES promotes

highly efficient translation of a mRNA reporter construct not only in plant but also in animal cells (Dorokhov *et al.* 2002). Recently, a novel translation enhancer in the 5´-UTR of *Triticum mosaic virus* (TriMV, family *Potyviridae*) has been described. The 5´-UTR of TriMV is capable of driving cap-independent translation iniation in an eIF4E-independent manner (Roberts *et al.* 2015).

3.2. CITEs

Members of the *Tombusviridae* and *Luteoviridae* plant virus families lack both 5´cap and 3´poly(A) elements but contain in their 3' ends RNA elements capable of enhancing translation in the absence of cap (cap-independent translation elements, CITEs). In contrast to IRESes, 3'-CITEs do not allow internal ribosome entry. It has been shown for some 3´-CITEs that they can functionally substitute the 5´cap with high efficiency, recruiting translation initiation factors, leading to ribosome entry at or near the 5´terminus followed by ribosome scanning to the initiation codon (Fabian & White 2004; Rakotondrafara & Miller 2008; Nicholson & White 2011). Location of the 3´-CITE in the 3´-end may provide three advantages: a) preventing the translation initiation of truncated or degraded RNAs; b) allowing to share the same RNA element for genomic RNA and subgenomic RNAs; c) allowing to regulate the switch between translation and replication (Barry & Miller 2002; Miller & White 2006). Thus far, six different classes of 3´-CITEs have been characterized (Simon & Miller 2013); they share little secondary structure similarity (Figure 4), as described next.

Translation Enhancer Domain

The first 3´-CITE was discovered in *Satellite tobacco necrosis virus* (STNV) and termed translation enhancer domain (TED) (Meulewaeter *et al.* 1998). The TED is predicted to form a long stem loop with several internal bulges (Van Lipzig *et al.* 2002). This element was shown to be functional *in vitro* (wheat germ extracts) and *in vivo* (Danthinne *et al.* 1993; Timmer *et al.* 1993). The proposed mechanism of translation mediated by TED involves binding of eIF4F or eIFiso4F followed by a predicted RNA:RNA long-distance interaction with the apical loop of the 5´-end (Gazo *et al.*

2004). The STNV 3´-CITE confers cap-independent translation *in vitro* when it is moved to the 5´-UTR of an uncapped reporter (Meulewaeter *et al.* 1998). Another member of the *Tombusviridae* family, *Pelargonium line pattern virus* (PLPV) was recently shown to harbor a TED 3'-CITE (Blanco-Pérez *et al.* 2016). These authors showed that the PLPV TED required a long-range RNA:RNA interaction with a hairpin in the coding sequence of p27 for efficient translation activity (Blanco-Pérez *et al.* 2016).

Y-Shaped Structure

3´-CITEs with Y-shaped structure (YSS) were identified in several genomes of viruses belonging to the Tombusvirus genus. YSS are formed by three helical regions. The efficiency of translation controlled by the YSS of *Tomato bushy stunt virus* (TBSV) was shown to depend on a long-distance interaction with the 5´-UTR of the genome. Mutational analysis of TBSV YSS showed that alterations in junction residues between helices and in a large asymmetric bulge in the major supporting stem disrupted translation (Fabian & White 2006)(Fabian and White, 2006). Moreover, the YSS of *Carnation Italian ringspot virus* (CIRV) requires the addition of the eIF4F or eIFiso4F complex to a factor-depleted wheat germ extract to promote efficient translation (Nicholson *et al.* 2013). Translation assays showed the ability of the CIRV YSS to function efficiently in *in vitro* and *in vivo*, whereas TBSV YSS was only shown to be functional in *in vivo*.

Barley yellow dwarf virus-Like Translation Element

The Barley yellow dwarf virus-like translation element (BTE) is one of the best characterized 3´-CITEs and it can be found in the luteovirus, dianthovirus, necrovirus and umbravirus genera (Wang *et al.* 2010; Simon & Miller 2013a). All BTEs share a long basal helix from which three to six helices radiate, containing a highly conserved sequence of 17 nucleotides localized in SL-I. The BTE binds preferentially to the eIF4G subunit of the eIF4F complex and requires long-distance basepairing with a stem-loop in the 5´-UTR for promoting efficient translation (Treder *et al.* 2007; Rakotondrafara &

Miller 2008). Footprinting experiments revealed that eIF4G protects SL-I as well as additional bases around the hub (Kraft *et al.* 2013a). Addition of eIF4E enhanced the level of protection. The interaction based on sequence complementarity occurs between a stable hairpin outside of the 17-nucleotide conserved sequence and the 5´-UTR (Wang *et al.* 2010). This long-distance RNA:RNA interaction is required for efficient translation by the BTE but can be replaced by complementary nonviral sequences outside the BTE (Rakotondrafara & Miller 2008). This interaction is conserved among all BTEs except the BTE of *Red clover necrotic mosaic virus* (RCNMV), in which mutations in the complementary loop had no effect on translation (Sarawaneeyaruk *et al.* 2009). Recently, it was shown that the 40S ribosomal subunit binds to the BTE and that this interaction is more efficient in the presence of the complex eIF4F, ATP and the helicase factors eIF4A and eIF4B (Sharma *et al.* 2015).

***Panicum mosaic virus*-like Translation Element**

The *Panicum mosaic virus*-like Translation Element (PTE) was first identified in *Panicum mosaic virus* (PMV, panicovirus, family *Tombusviridae*) and later in *Pea enation mosaic virus RNA 2* (PEMV2, umbravirus)(Batten *et al.* 2006). The PEMV PTE consists of a three-way branched helix with a large G-rich bulge in the main stem (Wang *et al.* 2009). The formation of a pseudoknot between the G-rich bulge and C-rich sequence at the three-helix junction of the PTE has been proposed which is critical for eIF4E recruitment by the PTE (Wang *et al.* 2011). Unlike most other CITEs, the PEMV PTE does not participate in a long-distance RNA:RNA interaction with the 5´-UTR. Instead, upstream the PTE, there is an element, the kl-TSS, that contribute in a long range RNA:RNA interaction with a 5´proximal hairpin located in the p33 ORF (Gao *et al.* 2012a). Interestingly, kl-TSS can also bind the 60S ribosomal subunit (Gao *et al.* 2013).

Another member of the *Tombusviridae*, *Saguaro cactus virus* (SCV) harbor a PTE conferring cap-independent translation and participate in a long-distance RNA:RNA interaction with hairpin located in the p26 ORF (Chattopadhyay *et al.* 2011).

Interestingly, the sequence involved in the interaction has the same conserved motif found in carmovirus TED-like elements and I-shaped structures (Simon & Miller 2013a).

T-Shaped Structure

The 3´-UTR of another member of *Tombusviridae*, *Turnip crinkle virus* (TCV), contains an internal T-shaped structure (TSS) and consists in three hairpins, two pseudoknots and multiple unpaired single stranded linker regions (Zuo *et al.* 2010). Interestingly, the TSS resembles a three-dimensional tRNA-like structure (Zuo *et al.* 2010). The TCV TSS recruits and binds the 60S subunit of the 80S ribosome (Stupina *et al.* 2008b). For this element, no base pairing between 3'-CITE and 5´-UTR has been identified. It is proposed that both ribosomal subunits form a protein bridge with the UTRs, where the 40S subunit binds the 5´-UTR and the 60S subunit binds the TSS (Stupina *et al.* 2008b). An additional TSS was found in PEMV RNA-2 upstream of the PTE (Gao *et al.* 2012a).

I-Shaped Structure

The smallest CITEs of all, the I-shaped structure (ISS) of *Maize necrotic spot virus* (MNeSV) and MNSV (tombusvirus and carmovirus, respectively) have been shown to preferentially interact with the eIF4E subunit of eIF4F. A model has been proposed suggesting that interaction between the 3' CITE and the 5'UTR modulates the delivery of the 3' bound initiation factors to the 5' end of the genome, subsequently facilitating recruitment of the 43S preinitiation complex (Nicholson *et al.* 2010). In support of this model, it has been shown that the interacting 5'UTR:I-shaped 3'CITE of MNeSV together with eIF4F form a complex *in vitro*. In addition, ribosome toe printing has demonstrated that while bound to eIF4F, the I-shaped CITE can simultaneously base pair with the 5' UTR and recruit ribosomes to the 5' end of the viral fragment (Nicholson *et al.* 2010). Direct genetic evidence for the interaction between the MNSV ISS and eIF4E has been shown in melon. A single amino acid change in eIF4E renders

the I-shaped CITE less effective as a translational enhancer and makes melon resistant to MNSV infection. Interestingly, this resistance is overcome by mutations in the MNSV I-shaped CITE that correspondingly restore the translation enhancing activity of the element (Nieto *et al.* 2006b; Truniger *et al.* 2008c).

Shape of RNA 2ª structure	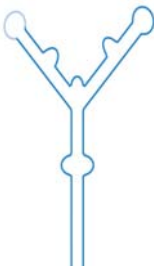 Y-shaped	 BTE	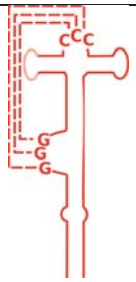 PTE	 TED	 T-shaped	 I-shaped
Translation initiation factor	eIF4F or eIFisoF	eIF4G	eIF4E	eIF4F	60S ribosome	eIF4F
Tombusviridae						
Tombusvirus	+			+		+
Necrovirus		+				
Carmovirus			+	+	+	+
Dianthovirus		+				
Aureusvirus			+	+		+
Panicovirus			+			
Luteoviridae						
Luteovirus		+				
Umbravirus		+		+	+	

Figure 3. Summary of the RNA secondary structures, ligands and phylogenetic distribution of 3'-CITEs. Basic RNA secondary structure cartoon are shown with consensus sequence. All 3'-CITEs with a RNA long-distance interaction described was shown in secondary structure with a shift in loop colored. Initiation factors known to bind are shown (adapted from Nicholson and White, 2011 and Simon and Miller, 2013).

4. The cap-binding protein eIF4E

EiF4E was identified as the component of the cap-binding protein complex, that crosslinks specifically with the m^7G cap structure (Sonenberg *et al.* 1979). Since then,

isoforms and homologues of eIF4E have been identified in a broad range of organisms including mammals, plants, nematodes, flies and yeast (Allen *et al.* 1992; Gingras *et al.* 1999; Browning 2004; Hernández *et al.* 2005; Joshi *et al.* 2005). EIF4E forms the eIF4F complex by binding to the scaffold protein eIF4G. Biochemical evidence supporting direct binding of eIF4E to the m^7G cap comes from functional studies, finding that depletion of eIF4E from cellular extracts dramatically reduces cap-dependent translation (Sonenberg *et al.* 1979). Crystal structures from mammalian, yeast, wheat and pea eIF4E have been already solved (Marcotrigiano *et al.* 1997; Niedzwiecka *et al.* 2002a; Brown *et al.* 2007; Monzingo *et al.* 2007; Ashby *et al.* 2011) (Fig. 4). Interestingly, they show a strong conservation across eukaryotic kingdoms (Tomoo *et al.* 2003; Monzingo *et al.* 2007). The structure of eIF4E resembles that of a cupped hand, like a baseball catcher glove, pinching the cap between finger and thumb, consisting of eight anti-parallel b-sheets and a dorsal side composed of three a-helices (Marcotrigiano *et al.* 1997; Matsuo *et al.* 1997; Tomoo *et al.* 2005). The cap structure is recognized and sandwiched between two parallel tryptophan residues in this formed cap-binding pocket. The most important interaction is the stacking of a guanine, which is strengthened by the delocalized positive charges arising from the methyl group of the cap structure (Marcotrigiano *et al.* 1997). The eIF4G-binding site is localized in the dorsal surface (Gingras *et al.* 1999).

The role of eIF4E in translation has been intensely studied, in particular in mammalian and yeast. In mammals, eIF4E regulation is carried out by direct phosphorylation of Serine 209 by kinases MNK1 and MNK2 (Waskiewicz *et al.* 1997; Raught & Gingras 2007). Studies have reported contrary results on the impact of eIF4E phosphorylation on cap-binding, suggesting that it increases or decreases its affinity for the cap structure (Shibata *et al.* 1998; Zuberek *et al.* 2003). The potential mechanisms derived from phosphorylation include: alteration of the affinity for 5´cap, the stability of the eIF4F complex and modulation of the rate of eIF4F formation (Morley *et al.* 1993)

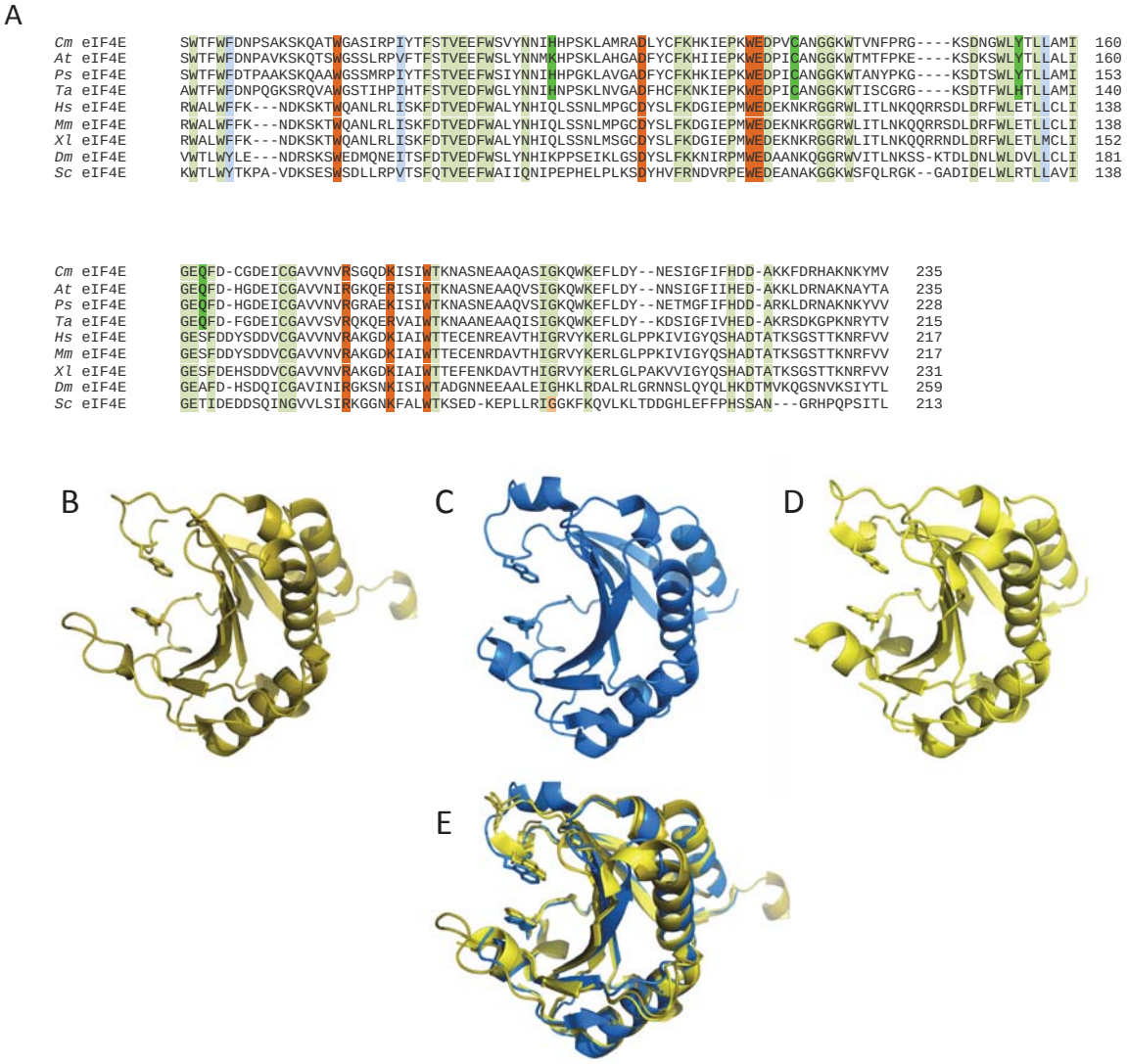

Figure 4. eIF4E alignment and crystal structures. A) Multiple alignment of eIF4E sequences from *Cucumis melo* (Cm), *Arabidopsis thaliana* (At), *Pisum sativum* (Ps), *Triticum aestivum* (Ta), *Homo sapiens* (Hs), *Mus musculus* (Mm), Xenopus, laevis (Xl), Drosophila melanogaster (Dm) and *Saccharomyces cerevisiae* (Sc). Residues that are most directly involved in binding m7GTP are marked in red. Amino acids marked in green and blue are highly conserved (in >95% and >85% of sequences, respectively) across all eukaryota. Plant-specific amino acids are boxed in bright green. Consensus secondary structures are represented above the alignment. B), C) and D) Crystal structures from *H. sapiens, P. sativum* and *M. musculus*, respectively. Cap-binding tryptophans are shows as sticks. E) 3-D alignment of previous crystal structures.

In plants, an additional form of eIF4F has been identified, absent in animals: the isoform of eIF4F (eIFiso4F) formed by the subunits eIFiso4E and eIFiso4G (Browning 2004). EIF4E and eIFiso4E differ slightly in molecular weight and show ~50% amino acid homology (Browning 2004; Monzingo *et al.* 2007; Mayberry *et al.* 2011). On the other hand, eIFiso4G is about half size of eIF4G (Browning 2004; Mayberry *et al.* 2011). In

addition, it has been reported that binding affinities between eIF4E:eIF4G and eIFiso4E:eIFiso4G are similar (0.18 nM and 0.08 nM K_D, respectively). The different isoforms have different expression patterns during plant development in *Arabidopsis thaliana*, with eIF4E being expressed in all tissues except certain root cells, while eIFiso4E is particularly abundant in floral organ cells and young developing tissues (Rodriguez *et al.* 1998). Both forms seem to be required for plant growth regulation and polyribosome formation, since simultaneous downregulation of eIF4E and eIFiso4E has been shown to affect plant development (Combe *et al.* 2005). Although eIFiso4E forms its own translational complexes, it is believed that eIFiso4E displays similar activities as eIF4E in translation initiation(Browning 2004). Knocked-down eIF4E or eIFiso4E tobacco plants showed normal development and fertility (Combe *et al.* 2005), suggesting that one is able to assume the functions of the other one. On the other hand, some evidences exist that support a functional specialization between both isoforms. For example, translation of uncapped mRNAs and highly structured 5´-UTR mRNAs have been shown to be promoted to a greater extend by eIF4F than by eIFiso4F (Gallie & Browning 2001).

The *eIF4E* and *eIFiso4E* genes have been shown to provide resistance to members of the family *Potyviridae* disrupting its interaction with VPg of *Turnip mosaic virus* (TuMV), *Tobacco etch virus* (TEV) or *Pea seed-borne mosaiv virus* (PSbMV) (Wittmann *et al.* 1997; Kang *et al.* 2005; Ashby *et al.* 2011) or P1 of *Clover yellow vein virus* (ClYVV) (Nakahara *et al.* 2010), HC-Pro of *Potato virus A* (PVA), *Potato virus Y* (PVY) and TEV (Ala-Poikela *et al.* 2011) and CI of *Lettuce mosaic virus* (Abdul-Razzak *et al.* 2009). Adaptation of viruses to eIF4E-mediated resistances (leading to resistance breakdown) is common and results usually from amino acid substitutions in the VPg (Keller *et al.* 1998; KüHne *et al.* 2003; Ayme *et al.* 2006), although other viral proteins have also been involved, like the CI (Abdul-Razzak *et al.* 2009) and P1 (Nakahara *et al.* 2010).

Moreover, eIF4E has been shown to be involved in recessive resistance to the non-potyvirus MNSV (Diaz-Pendon *et al.* 2004; Nieto *et al.* 2006b).

5. eIF4E-binding proteins

The inhibition of cap-dependent translation initiation is a widespread and reversible mechanism for regulating gene expression in eukaryotes (Kong & Lasko 2012). In animal and yeast cells, this type of regulation is mediated by a family of eIF4E-binding proteins (4E-BPs), which play essential roles in diverse biological processes, including cell proliferation and development (Banko *et al.* 2005; Kong & Lasko 2012) (Dowling *et al.* 2010; Gkogkas *et al.* 2013) (Tabla 1). The 4E-BPs are proteins of variable molecular weight (~15-120kDa) able to interact with eIF4E (Pause *et al.* 1994). These translation regulators share the canonical eIF4E-binding motif (4E-BM, YXXXXLϕ) with eIF4G and possess similar affinities for eIF4E (Fletcher & Wagner 1998; Marcotrigiano *et al.* 1999; Gosselin *et al.* 2011). The canonical binding motifs found in eIF4G and 4E-BPs adopt similar α-helical conformations and compete for binding to a conserved patch of hydrophobic residues on the dorsal surface of eIF4E that is opposite to the cap-binding pocket (Mader *et al.* 1995; Matsuo *et al.* 1997; Gross *et al.* 2003). Some 4E-BPs have been described to contain a second binding domain, the non-canonical binding motif (NC 4E-BM), suggesting a bipartite binding mode to form eIF4E complexes (Mizuno *et al.* 2008; Kinkelin *et al.* 2012; Igreja *et al.* 2014; Peter *et al.* 2015a; Peter *et al.* 2015b). Although non-canonical motifs are not conserved among different 4E-BPs, they contain common features: 1) they are located ~15-30 residues downstream from canonical motifs, 2) they contain hydrophobic residues, and 3) in the case of Cup (which is involved in embryogenesis repression), they exhibit helical propensity. The 4E-BPs exert their inhibitory effect on protein synthesis by interfering with the formation of the eIF4F complex, through their competition with eIF4G. Binding of eIF4E to either the 4E-BPs or eIF4G is mutually exclusive (Gingras *et al.* 1999). Furthermore, phosphorylation of residues in 4E-BPs *via* the mTOR pathway prevents its binding to eIF4E, allowing eIF4G to do it (Peter *et al.* 2015a).

No homolog to the 4E-BPs has been found in plants to date. Two proteins, the beta subunit of nascent polypeptide-associate complex (NAC) and the plant lipoxygenase 2 (AtLOX2), have been shown to interact with AteIF4E and AteIFiso4E

(Freire *et al.* 2000; Freire 2005), but no evidence for their role in translation was found. Nevertheless, the presence of other plant 4E-BP analogs cannot be dismissed.

Table 1. eIF4E-binding partners (adapted from Rhoads et al., 2009).

Organism	Protein	Consequences of binding	Canonical binding sequence
Homo sapiens	4E-BP1	Repression of cap-dependent mRNA translation	RIIYDRKFLMECR
	4E-BP2		RIIYDRKFLMDRR
	4E-BP3		RIIYDRKFLMECK
	4E-T	Transport of eIF4E into the nucleus	PHRYTKEELLDIK
	Angel1	Repression of translation of specific mRNAs in the ER membrane	RRKYGRDFLLRFR
Drosophila melanogaster	Thor/4E-BP	Repression of cap-dependent mRNA translation	KLIYERAFMKNLR
	Cup	Repression of translation of *nano* and *oskar* mRNAs	VKSYTRSRLMDIR
	4E-T	Transport of eIF4E into the nucleus	SARYSKVDLLALR
	Mextli	Role in germline stem cell maintenance and early embryogenesis	RVSYDIEHLLYYS
Saccharomyces cerevisiae	CAF20/4E-BP	Repression of cap-dependent mRNA translation	MIKYTIDELFQLK
	EAP1		TYAYSMNELYHLK
Arabidopsis thaliana	AtLOX2	Competition with eIF4G for binding to eIF4E	LKKYRKEELE
	NAC		RLQSTLKRIG

6. RNA recombination as an evolutionary mechanism for the acquisition of functional modules

The ability of viruses to change underlies many disease management concerns. Excepting migration from distant locations, variability in plant pathogen populations is the necessary initial step in adaptation to new plants (host shifting), resistance breaking (RB), and changes in symptoms and virulence. RNA viruses have a large

potential of variability in their genetic information, due to either mutations, RNA recombination or reassortment.

6.1. Mutations

Mutation is the initial source of variation in populations. RNA viruses show rates of mutation and substitution that are orders of magnitude higher than those of their DNA-based hosts and in the range of 0.03–2 per genome and replication round (Sanjuan *et al.* 2010; Lauring *et al.* 2013; Acevedo *et al.* 2014; Duchêne *et al.* 2014). This difference results from the lack of proofreading activity of the virus-encoded RNA-dependent RNA polymerases together with the viruses large population numbers (Steinhauer *et al.* 1992). It is commonly accepted that high mutation rates may be beneficial as a mechanism to escape from the strong selective pressures imposed by the host's defense mechanisms. However, high mutation rates have not necessarily evolved in response to natural selection (Elena & Sanjuán 2005; Clune *et al.* 2008), as a too high mutation rate may have pernicious effects on viral fitness since most of the mutations are deleterious (Bonhoeffer *et al.* 2004; Sanjuán *et al.* 2004).

6.2. Recombination

Similar to genetic recombination in DNA-based organisms, viral RNA recombination is defined as the process of swapping RNA fragments among RNA molecules. If crossovers occur amongst the same RNA templates in a homologous fashion, the exchanges are functionally equivalent to DNA meiotic crossing-over. In some viruses, the frequency of homologous crossing-over is very high and practically every replicated viral RNA molecule can be considered as chimeric in nature, as it has been demonstrated for *Brome mosaic virus* (BMV, family *Bromoviridae*) RNAs (Urbanowicz *et al.* 2005). The generally accepted mechanism of RNA recombination is currently explained by a copy-choice model where the viral RNA polymerase (RdRp) complex in RNA viruses [reverse transcriptase (RT) in retroviruses] changes templates during synthesis while remaining bound to the nascent strand, thereby generating an RNA molecule with mixed ancestry (Galetto *et al.* 2006) (Fig. 5). Template switching is

thought to be guided by the sequence similarity between the nascent and the acceptor nucleic acid molecules (Zhang & Temin 1994). Accordingly, RNA recombination is usually 'homologous', as it occurs most often between regions of high sequence similarity. Interestingly, the critical sequence similarity between the two parental sequences may be present close to, although not necessarily at, the crossover site. However, exchange between different, and hence genetically dissimilar, genomic regions or between non-related RNA molecules, leading to 'non-homologous' recombination, can also occur (Nagy *et al.* 1997). As non-homologous RNA recombination involves regions with little sequence similarity, it will often produce deleterious genotypes. This is probably the reason for its less frequent observation in comparison to homologous recombination (Voigt *et al.* 2002; Drummond *et al.* 2005; Simon-Loriere *et al.* 2009).

Most RNA recombination events have been identified between viral genomes of the same species (Moury *et al.* 2006a; Pagán & Holmes 2010). Phylogenetic analyses of *Luteoviridae* family viral genome sequences suggest that viral speciation events tended to occur within the same plant host species and country of origin Pagán, 2010 #1079}. Moreover, RNA recombination between viral and cellular RNAs have been observed for both plant and animal RNA viruses. One example is RNA recombination between *Human immunodeficiency virus* type 1 (HIV-1, family retroviridae) and host RNAs. HIV-1 is known to recombine effectively with host tRNAs after introducing its strong secondary structure elements into the HIV RNA (Konstantinova *et al.* 2007). HIV-1 is capable of acquiring new genetic material, especially to the RT-encoding ORF (van der Hoek *et al.* 2005; Berkhout 2011). The reverse scenario was also observed in nonretroviral RNA sequences of Bornaviruses and other (−) strand RNA viruses that were integrated into the host genome, including the human genome (Belyi *et al.* 2010; Horie *et al.* 2010). Also, mRNA viruses were described to leave their sequences in the cellular DNA of infected hosts (Crochu *et al.* 2004; Tanne & Sela 2005; Maori *et al.* 2007; Zemer *et al.* 2008; Geuking *et al.* 2009). These results demonstrate that RNA viruses can serve as a source of genetic innovation for their hosts.

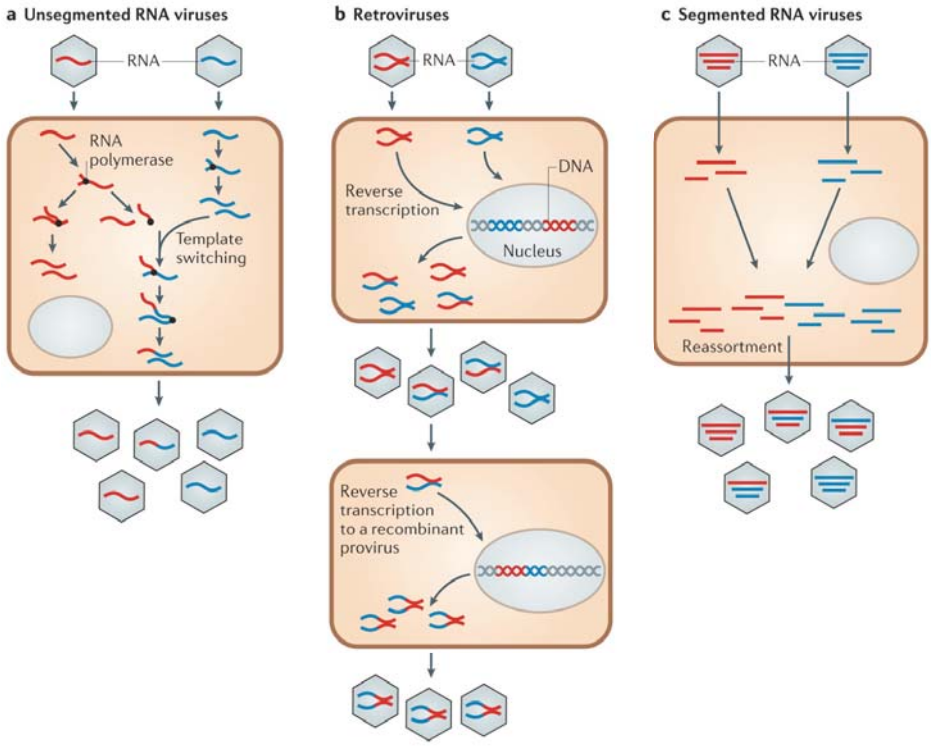

Figure 5. Generation of recombinant and reassortant RNA viruses. A) Co-infection of a cell by genetically distinct viral strains can lead to the generation of recombinant viruses. B) Co-infection of a cell by genetically distinct strains of a retrovirus can lead to the generation of 'heterozygous' virus particles, after which a template-switching event can lead to a recombinant provirus. C) Co-infection of a cell by genetically distinct strains of a segmented virus can generate different combinations of reassortant progeny.

RNA recombination occurs at highly variable frequencies in RNA viruses, although there are few instances in which precise rates of recombination per nucleotide or genome have been determined. For example, recombination appears to occur frequently in some retroviruses (Mansky & Wisniewski 1998)— most notably HIV, which has an estimated recombination rate of between 1.38×10^{-4} and 1.4×10^{-5} per site per generation (Shriner *et al.* 2004; Neher & Leitner 2010) — and in some (+)ssRNA viruses, such as enteroviruses (of the family *Picornaviridae*) and viruses of the families *Coronaviridae, Bromoviridae* and *Potyviridae* (Tomimura *et al.* 2004; Urbanowicz *et al.* 2005; Gibbs & Ohshima 2010; Savolainen-Kopra & Blomqvist 2010). Importantly, these differences in recombination frequency correspond to some major

biological differences between these viral groups, indicating that major aspects of genome architecture at least partially determine recombination rate.

6.3. Reassortment

Reassortment is restricted to viruses that possess segmented genomes and involves packaging of segments with different ancestry into a single virion (Fig. 5). As with RNA recombination, reassortment requires that a cell be infected with more than one virus. Although reassortment does not require the physical proximity of parental genomes during replication, the packaging process that results in reassortant viruses may not be entirely random (McDonald & Patton 2011).

7. Evolutionary role of RNA recombination

From the evolutionary standpoint, RNA recombination may have played a key role during virus speciation and emergence. Comparative analyses of sequences of plant virus species allow the development of evolutionary models to associate adaptive phenotypic changes with evolving sites within viral genomes (Pond *et al.* 2012)). Thus, wide imprints of RNA recombination were found within plant viruses. RNA recombination seems to be particularly frequent among members of the family *Potyviridae*, the largest family of plant RNA viruses. Frequent recombinational footprints were detected within the ORFs of both structural and nonstructural proteins (Bousalem *et al.* 2000; Visser & Bellstedt 2009; Yamasaki *et al.* 2010). Phylogenetic surveys indicate not only intraspecies and intragenus, but also intergenus recombination crossover's footprints among potyviruses (Valli *et al.* 2007; Desbiez *et al.* 2011), supporting their apparent modular evolution. Recombination with host RNAs was also detected, likely via retrotransposable elements (Tanne & Sela 2005) demonstrating that, like animal viruses, plant viruses can expand their coding capacity via recombination with the host's messenger RNA pool (Chare & Holmes 2006).

For most RNA viruses, cross-species transmission is the most common way for a virus to enter a new host. Recombination could assist in this process because it enables

viruses to explore a greater proportion of the sequence space than is accessible by mutation at any time, thereby increasing the likelihood of finding a genetic configuration that facilitates host adaptation (Lindstrom *et al.* 2004). Changes in ecological conditions brings together the reservoir viruses and their crop hosts, often as a result of interplay among the environment, genetic plasticity, and the required host factors (Elena *et al.* 2011).

8. The experimental system MNSV/melon

8.1. Melon necrotic spot virus

Melon necrotic spot virus (MNSV) is a *Carmovirus* within the family *Tombusviridae* (Hibi & Furuki 1985), which is present in cucurbit crops worldwide. MNSV can be transmitted mechanically, by the zoospores of the fungus *Olpidium bornovanus* and through the seed (Lange & Insunza 1977; Campbell & Sim 1994). Characteristic symptoms of diseased plants include local necrotic spots or large necrotic lesions on leaves, and necrosis on stems and petioles (Fig. 6) (Matsuo *et al.* 1991). The MNSV host range is restricted to members of the *Cucurbitaceae* family. In inoculated melon cotyledons, necrotic spots of approximately 2 mm in diameter appear at about 3 days post-inoculation (p.i.). These lesions grow to reach approximately 5 mm at 7 d p.i; eventually, lesions coalesce resulting in the complete necrosis of the cotyledon at 15 to 20 d p.i. Variations in the lesion's size, shape and speed of size increase depend on the MNSV strain. The ability of MNSV to systemically infect melon plants also depends on the melon genotype, the virus strain and the environmental conditions, but very often occurs in just a small percentage of the inoculated plants. In systemically infected melon plants, necrotic spots start to appear in the upper non-inoculated leaves at about 7 to 10 d p.i. The MNSV genome is a single-stranded (+)-sense RNA molecule of 4.3 kb with at least five open reading frames (ORF) (Fig. 6). (Riviere & Rochon 1990; Díaz *et al.* 2004). This RNA, as well as the subgenomic RNAs derived from it, is uncapped and lacks a poly(A) tail at its 5'- and 3'-ends, respectively (Riviere & Rochon 1990; Díaz *et al.* 2004). Instead, it posses nucleotide sequences at the 3'-UTR of the MNSV RNAs that function as cap-

independent translation enhancers (3'-CITE)(Truniger *et al.* 2008c). MNSV has been included in *Carmovirus* genera on the basis of its genomic distribution and replication strategy.

The 5'-proximal ORF encodes a protein of 29 kDa (p29) terminating with an amber codon, its read-through results in a larger gene product of 89 kDa (p89). Two small, centrally located ORFs encode two consecutive proteins of 7 kDa (p7A and p7B), separated by an amber codon located at the end of p7A. Finally, the 3'-proximal ORF encodes a coat protein of 42 kDa (p42), which is related to those of the genus Tombusvirus (Riviere *et al.* 1989; Riviere & Rochon 1990; Canizares *et al.* 2001). p29 and its read-through protein p89 are expressed from the genomic-length RNA (gRNA), whereas the small p7A and p7B proteins and the coat protein are translated from two 1.9 and 1.6 kb subgenomic RNAs (sgRNAs), respectively (Riviere & Rochon 1990).

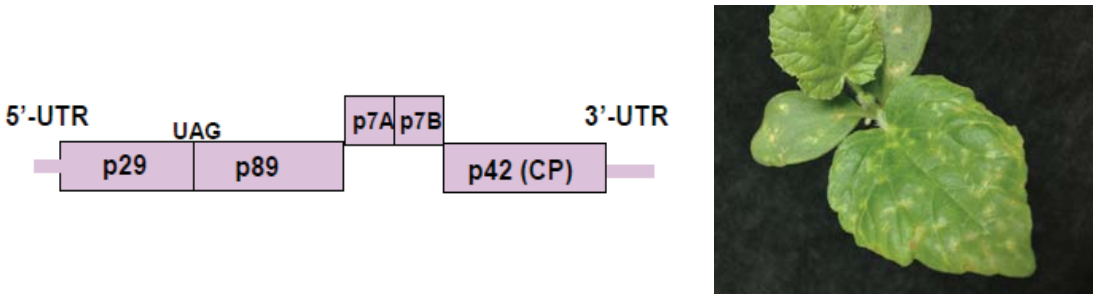

Figure 6. MNSV genome and symptoms in melon plant.

P29 and p89 are essential for MNSV replication and probably components of the replication complex (Riviere & Rochon 1990; Genoves *et al.* 2006; Gomez-Aix *et al.* 2015). The MNSV p29 contains three transmembrane domains, two of them shared with p89, and it was identified as being responsible for the induction of necrosis in *N. benthamiana* (Mochizuki *et al.* 2008). Importantly, the transient expression of p29 revealed that was able to specifically target mitochondria, where it could induce its reorganization and the formation of membranous structures where the viral RNA replication could take place (Gomez-Aix *et al.* 2015). The two central ORFs, p7A and p7B, are involved in cell-to-cell movement (Genoves *et al.* 2006; Navarro *et al.* 2006;

Martínez-Gil *et al.* 2007; Genovés *et al.* 2010; Genovés *et al.* 2011). P7A binds RNA and localizes to the cell periphery in structures that probably correspond to plasmodesmata (Genovés *et al.* 2006; Navarro *et al.* 2006). MNSV p7B protein inserts into membranes of the endoplasmic reticulum in a cotranslational process and moves to Golgi and plasmodesmata, forming part of the early secretory pathway (Martínez-Gil *et al.* 2007; Genovés *et al.* 2010; Genovés *et al.* 2011; Serra-Soriano *et al.* 2015). The protein p42 is the capsid protein (CP), which in addition to its structural role, is implicated in systemic movement, plays a role as a weak silencing suppressor and is involved in virus transmission (Genovés *et al.* 2006; Ohki *et al.* 2010).

8.2. The melon/MNSV model

Melon (*Cucumis melo* L.) is a eudicot diploid plant species (2n = 2x = 24) of interest because of its specific biological properties and its economic importance. Melon, with 29 million tons of melons produced worldwide in 2013 (http://faostat.fao.org) is an important fruit crop. It is particularly important in Mediterranean and East Asian countries, where hybrid varieties have a significant and growing economic value. It belongs to the *Cucurbitaceae* family, which also includes cucumber (*Cucumis sativus* L.), watermelon (*Citrullus lanatus* (Thunb.) Matsum. & Nakai), and squash (*Cucurbita* spp.). Melon is an attractive model for studying valuable biological characters, such as fruit ripening (Nuñez-Palenius *et al.* 2008), sex determination (Martin *et al.* 2009; Foucart *et al.* 2011), and phloem physiology (Zhang *et al.* 2006).

In line with the scientific and economic interest of this species, a number of genetic and molecular tools have been developed over the last years, including genetic maps (Diaz *et al.* 2011), sequencing of ESTs collections (Gonzalez-Ibeas *et al.* 2007; Clepet *et al.* 2011), microarrays (Mascarell-Creus *et al.* 2009), a physical map (González *et al.* 2010), BAC sequences (González *et al.* 2010), generation of a TILLING platform (Dahmani-Mardas *et al.* 2010), mitochondrial and chloroplast genome sequence (Rodríguez-Moreno *et al.* 2011) and, to complete the repertoire of genomic tools, de novo sequencing of the melon genome (Garcia-Mas *et al.* 2012).

Viral infections are a serious threat for melon commercial quality and production. Especially, there are numerous RNA viruses affecting cucurbit crops, including MNSV (Kassem *et al.* 2007b).

This research group has studied extensively aspects related to MNSV genome translation and eIF4E-mediated resistance mechanisms. In melon, *nsv*-mediated natural recessive resistance is effective against all MNSV isolates except for the resistance-breaking isolate MNSV-264 (Díaz *et al.* 2004). The *nsv* gene was shown to correspond to a melon eIF4E allele containing a single nucleotide change, with respect to the susceptible eIF4E allele, resulting in one amino acid substitution at 228 position (Histidine228Leucine) leading to resistance to MNSV (Nieto *et al.* 2006b). To map the virulence determinant, the sequence required for resistance breaking, quimeric mutants between avirulent and virulent MNSVs (the former not able to infect resistant melon) were constructed and analyzed for their multiplication capacity in protoplasts from susceptible and resistant melon. Results showed that the virulence determinant resides in the 3'-UTR and that *nsv*-mediated resistance acts at the single-cell level (Díaz *et al.* 2004). Interestingly, the MNSV-264 3'-UTR has <50% nucleotide sequence identity compared with that of avirulent MSNV isolates and was proposed to have a recombinant, non-MNSV, origin (Nieto *et al.* 2011a). Specifically, the critical region for overcoming the resistance has been mapped to a 67 nucleotide sequence of the 3'-UTR that acts as a cap-independent translation enhancer (3'-CITE) (Truniger *et al.* 2008c). This 3'-CITE was shown to be control MNSV RNA translation in both susceptible and resistant melon (Díaz *et al.* 2004; Truniger *et al.* 2008c). On the other hand, the 3'-CITE of avirulent MNSV can only mediate MNSV RNA translation in susceptible melon. Therefore, transgenic melon lines knocked-down for eIF4E were resistant to all MNSV strains except MNSV-264 (Rodríguez-Hernández *et al.* 2012). These results suggest an interaction with melon eIF4E. Moreover, the presence of the 5'-UTR *in cis* is required for efficient translation being involved in a long-distance RNA:RNA interaction based on sequence complementarity with the 3'-CITE (Truniger *et al.* 2008c); Truniger, unpublished). Recently, a new resistance-breaking isolate, MNSV-N, has been identified in the field that may be a threat.

9. REFERENCES

Abdul-Razzak A., Guiraud T., Peypelut M., Walter J., Houvenaghel M.C., Candresse T., Le Gall O. and German-Retana S. 2009. Involvement of the cylindrical inclusion (CI) protein in the overcoming of an eIF4E-mediated resistance against Lettuce mosaic potyvirus. *Molecular plant pathology* **10**: 109-113.

Acevedo A., Brodsky L. and Andino R. 2014. Mutational and fitness landscapes of an RNA virus revealed through population sequencing. *Nature* **505**: 686-690.

Adesnik M., Salditt M., Thomas W.t. and Darnell J.E. 1972. Evidence that all messenger RNA molecules (except histone messenger RNA) contain poly (A) sequences and that the poly (A) has a nuclear function. *J Mol Biol* **71**: 21-30.

Agirrezabala X., Méndez-López E., Lasso G., Sánchez-Pina M.A., Aranda M. and Valle M. 2015. The near-atomic cryoEM structure of a flexible filamentous plant virus shows homology of its coat protein with nucleoproteins of animal viruses. *eLife* **4**: e11795.

Ahlquist P., Noueiry A.O., Lee W.-M., Kushner D.B. and Dye B.T. 2003. Host factors in positive-strand RNA virus genome replication. *Journal of virology* **77**: 8181-8186.

Aitken C.E. and Lorsch J.R. 2012. A mechanistic overview of translation initiation in eukaryotes. *Nature Structural and Molecular Biology* **19**: 568-576.

Ala-Poikela M., Goytia E., Haikonen T., Rajamäki M.-L. and Valkonen J.P.T. 2011. Helper component proteinase of the genus Potyvirus is an interaction partner of translation initiation factors eIF (iso) 4E and eIF4E and contains a 4E binding motif. *Journal of virology* **85**: 6784-6794.

Allen M.L., Metz A.M., Timmer R.T., Rhoads R.E. and Browning K.S. 1992. Isolation and sequence of the cDNAs encoding the subunits of the isozyme form of wheat protein synthesis initiation factor 4F. *Journal of Biological Chemistry* **267**: 23232-23236.

Ashby J.A., Stevenson C.E.M., Jarvis G.E., Lawson D.M. and Maule A.J. 2011. Structure-based mutational analysis of eIF4E in relation to sbm1 resistance to Pea seed-borne mosaic virus in Pea. *PloS one* **6**.

Ayme V., Souche S., Caranta C., Jacquemond M., Chadœuf J., Palloix A. and Moury B. 2006. Different mutations in the genome-linked protein VPg of Potato virus Y confer virulence on the pvr23 resistance in pepper. *Molecular plant-microbe interactions* **19**: 557-563.

Banko J.L., Poulin F., Hou L., DeMaria C.T., Sonenberg N. and Klann E. 2005. The translation repressor 4E-BP2 is critical for eIF4F complex formation, synaptic plasticity, and memory in the hippocampus. *The Journal of neuroscience* **25**: 9581-9590.

Barry J.K. and Miller W.A. 2002. A– 1 ribosomal frameshift element that requires base pairing across four kilobases suggests a mechanism of regulating ribosome and replicase traffic on a viral RNA. *Proceedings of the National Academy of Sciences* **99**: 11133-11138.

Batten J.S., Desvoyes B., Yamamura Y. and Scholthof K.-B.G. 2006. A translational enhancer element on the 3'-proximal end of the Panicum mosaic virus genome. *FEBS letters* **580**: 2591-2597.

Battiste J.L., Pestova T.V., Hellen C.U.T. and Wagner G. 2000. The eIF1A solution structure reveals a large RNA-binding surface important for scanning function. *Molecular cell* **5**: 109-119.

Belyi V.A., Levine A.J. and Skalka A.M. 2010. Unexpected inheritance: multiple integrations of ancient bornavirus and ebolavirus/marburgvirus sequences in vertebrate genomes. *PLoS Pathog* **6**: e1001030.

Berkhout B. 2011. HIV-1 as RNA evolution machine. *RNA biology* **8**: 225-229.

Blanco-Pérez M., Pérez-Cañamás M., Ruiz L. and Hernández C. 2016. Efficient Translation of Pelargonium line pattern virus RNAs Relies on a TED-Like 3´-Translational Enhancer that Communicates with the Corresponding 5´-Region through a Long-Distance RNA-RNA Interaction. *PloS one* **11**: e0152593.

Bonhoeffer S., Chappey C., Parkin N.T., Whitcomb J.M. and Petropoulos C.J. 2004. Evidence for positive epistasis in HIV-1. *Science* **306**: 1547-1550.

Both G.W., Banerjee A.K. and Shatkin A.J. 1975. Methylation-dependent translation of viral messenger RNAs in vitro. *Proceedings of the National Academy of Sciences* **72**: 1189-1193.

Bousalem M., Douzery E.J.P. and Fargette D. 2000. High genetic diversity, distant phylogenetic relationships and intraspecies recombination events among natural populations of Yam mosaic virus: a contribution to understanding potyvirus evolution. *Journal of General Virology* **81**: 243-255.

Brown C.J., McNae I., Fischer P.M. and Walkinshaw M.D. 2007. Crystallographic and mass spectrometric characterisation of eIF4E with N 7-alkylated cap derivatives. *J Mol Biol* **372**: 7-15.

Browning K.S. 2004. Plant translation initiation factors: it is not easy to be green. *Biochemical Society Transactions* **32**: 589-591.

Campbell R.N. and Sim S.T. 1994. Host specificity and nomenclature of Olpidium bornovanus (= Olpidium radicale) and comparisons to Olpidium brassicae. *Canadian Journal of Botany* **72**: 1136-1143.

Canizares M.C., Marcos J.F. and Pallas V. 2001. Molecular variability of twenty-one geographically distinct isolates of Carnation mottle virus (CarMV) and phylogenetic relationships within the Tombusviridae family. *Arch Virol* **146**: 2039-2051.

Carter A.P., Clemons W.M., Brodersen D.E., Morgan-Warren R.J., Hartsch T., Wimberly B.T. and Ramakrishnan V. 2001. Crystal structure of an initiation factor bound to the 30S ribosomal subunit. *Science* **291**: 498-501.

Chare E.R. and Holmes E.C. 2006. A phylogenetic survey of recombination frequency in plant RNA viruses. *Arch Virol* **151**: 933-946.

Chattopadhyay M., Shi K., Yuan X. and Simon A.E. 2011. Long-distance kissing loop interactions between a 3' proximal Y-shaped structure and apical loops of 5' hairpins enhance translation of Saguaro cactus virus. *Virology* **417**: 113-125.

Cheng C.P., Serviene E. and Nagy P.D. 2006. Suppression of viral RNA recombination by a host exoribonuclease. *Journal of Virology* **80**: 2631-2640.

Clepet C., Joobeur T., Zheng Y., Jublot D., Huang M., Truniger V., Boualem A., Hernandez-Gonzalez M.E., Dolcet-Sanjuan R., Portnoy V. et al. 2011. Analysis of expressed sequence tags generated from full-length enriched cDNA libraries of melon. *BMC Genomics* **12**.

Clune J., Misevic D., Ofria C., Lenski R.E., Elena S.F. and Sanjuán R. 2008. Natural selection fails to optimize mutation rates for long-term adaptation on rugged fitness landscapes. *PLoS Comput Biol* **4**: e1000187.

Combe J.P., Petracek M.E., van Eldik G., Meulewaeter F. and Twell D. 2005. Translation initiation factors eIF4E and eIFiso4E are required for polysome formation and regulate plant growth in tobacco. *Plant molecular biology* **57**: 749-760.

Crochu S., Cook S., Attoui H., Charrel R.N., De Chesse R., Belhouchet M., Lemasson J.-J., de Micco P. and de Lamballerie X. 2004. Sequences of flavivirus-related RNA viruses persist in DNA form integrated in the genome of Aedes spp. mosquitoes. *Journal of General Virology* **85**: 1971-1980.

Dahmani-Mardas F., Troadec C., Boualem A., Leveˆque S., Alsadon A.A., Aldoss A.A., Dogimont C. and Bendahmane A. 2010. Engineering melon plants with improved fruit shelf life using the TILLING approach. *PloS one* **5**: e15776.

Danthinne X., Seurinck J., Meulewaeter F., Van Montagu M. and Cornelissen M. 1993. The 3′ untranslated region of satellite tobacco necrosis virus RNA stimulates translation in vitro. *Molecular and Cellular Biology* **13**: 3340-3349.

Desbiez C., Moury B. and Lecoq H. 2011. The hallmarks of "green" viruses: Do plant viruses evolve differently from the others? *Infection, Genetics and Evolution* **11**: 812-824.

Dever T.E. and Green R. 2012. The elongation, termination, and recycling phases of translation in eukaryotes. *Cold Spring Harbor perspectives in biology* **4**: a013706.

Diaz A., Fergany M., Formisano G., Ziarsolo P., Blanca J., Fei Z., Staub J.E., Zalapa J.E., Cuevas H.E. and Dace G. 2011. A consensus linkage map for molecular markers and quantitative trait loci associated with economically important traits in melon (Cucumis melo L.). *BMC plant biology* **11**: 1.

Díaz J.A., Nieto C., Moriones E., Truniger V. and Aranda M.A. 2004. Molecular characterization of a Melon necrotic spot virus strain that overcomes the resistance in melon and nonhost plants. *Molecular Plant-Microbe Interactions* **17**: 668-675.

Diaz-Pendon J.A., Truniger V., Nieto C., Garcia-Mas J., Bendahmane A. and Aranda M.A. 2004. Advances in understanding recessive resistance to plant viruses. *Molecular Plant Pathology* **5**: 223-333.

Dorokhov Y.L., Skulachev M.V., Ivanov P.A., Zvereva S.D., Tjulkina L.G., Merits A., Gleba Y.Y., Hohn T. and Atabekov J.G. 2002. Polypurine (A)-rich sequences promote cross-kingdom conservation of internal ribosome entry. *Proceedings of the National Academy of Sciences of the United States of America* **99**: 5301-5306.

Drummond D.A., Silberg J.J., Meyer M.M., Wilke C.O. and Arnold F.H. 2005. On the conservative nature of intragenic recombination. *Proceedings of the National Academy of Sciences of the United States of America* **102**: 5380-5385.

Duchêne S., Holmes E.C. and Ho S.Y.W. 2014. Analyses of evolutionary dynamics in viruses are hindered by a time-dependent bias in rate estimates. *Proceedings of the Royal Society of London B: Biological Sciences* **281**: 20140732.

Echevarría-Zomeño S., Yángüez E., Fernández-Bautista N., Castro-Sanz A.B., Ferrando A. and Castellano M. 2013. Regulation of translation initiation under biotic and abiotic stresses. *International journal of molecular sciences* **14**: 4670-4683.

Elena S.F., Bedhomme S., Carrasco P., Cuevas J.M., De la Iglesia F., Lafforgue G., Lalic J., Pròsper À., Tromas N. and Zwart M.P. 2011. The evolutionary genetics of emerging plant RNA viruses. *Molecular Plant-Microbe Interactions* **24**: 287-293.

Elena S.F. and Sanjuán R. 2005. Adaptive value of high mutation rates of RNA viruses: separating causes from consequences. *Journal of virology* **79**: 11555-11558.

Fabian M.R. and White K.A. 2004. 5′-3′ RNA-RNA interaction facilitates Cap- and poly(A) tail-independent translation of tomato bushy stunt virus mRNA: A potential common mechanism for tombusviridae. *Journal of Biological Chemistry* **279**: 28862-28872.

-. 2006. Analysis of a 3′-translation enhancer in a tombusvirus: A dynamic model for RNA-RNA interactions of mRNA termini. *RNA* **12**: 1304-1314.

Fletcher C.M. and Wagner G. 1998. The interaction of eIF4E with 4E-BP1 is an induced fit to a completely disordered protein. *PROTEIN SCI* **7**: 1639-1642.

Foucart C., Boualem A., Lasseur B., Eleblu J., Fahraj I. and Bendahmane A. 2011. [Sex determination in cucurbits]. *Biologie aujourd'hui* **206**: 57-62.

Freire M.A. 2005. Translation initiation factor (iso) 4E interacts with BTF3, the β subunit of the nascent polypeptide-associated complex. *Gene* **345**: 271-277.

Freire M.A., Tourneur C., Granier F., Camonis J., El Amrani A., Browning K.S. and Robaglia C. 2000. Plant lipoxygenase 2 is a translation initiation factor-4E-binding protein. *Plant molecular biology* **44**: 129-140.

Galetto R., Giacomoni V., Véron M. and Negroni M. 2006. Dissection of a circumscribed recombination hot spot in HIV-1 after a single infectious cycle. *Journal of Biological Chemistry* **281**: 2711-2720.

Gallie D.R. 2002. Protein-protein interactions required during translation. *Plant molecular biology* **50**: 949-970.

Gallie D.R. and Browning K.S. 2001. eIF4G functionally differs from eIFiso4G in promoting internal initiation, cap-independent translation, and translation of structured mRNAs. *Journal of Biological Chemistry* **276**: 36951-36960.

Gao F., Gulay S.P., Kasprzak W., Dinman J.D., Shapiro B.A. and Simon A.E. 2013. The kissing-loop T-shaped structure translational enhancer of Pea enation mosaic virus can bind simultaneously to ribosomes and a 5′ proximal hairpin. *Journal of virology* **87**: 11987-12002.

Gao F., Kasprzak W., Stupina V.A., Shapiro B.A. and Simon A.E. 2012. A ribosome-binding, 3' translational enhancer has a T-shaped structure and engages in a long-distance RNA-RNA interaction. *Journal of Virology* **86**: 9828-9842.

Garcia-Mas J., Benjak A., Sanseverino W., Bourgeois M., Mir G., González V.M., Hénaff E., Câmara F., Cozzuto L. and Lowy E. 2012. The genome of melon (Cucumis melo L.). *Proceedings of the National Academy of Sciences* **109**: 11872-11877.

Gazo B.M., Murphy P., Gatchel J.R. and Browning K.S. 2004. A Novel Interaction of Cap-binding Protein Complexes Eukaryotic Initiation Factor (eIF) 4F and eIF(iso)4F with A Region in the 3′-Untranslated Region of Satellite Tobacco Necrosis Virus. *Journal of Biological Chemistry* **279**: 13584-13592.

Genoves A., Navarro J.A. and Pallas V. 2006. Functional analysis of the five melon necrotic spot virus genome-encoded proteins. *Journal of general virology* **87**: 2371-2380.

Genovés A., Navarro J.A. and Pallás V. 2006. Functional analysis of the five melon necrotic spot virus genome-encoded proteins. *Journal of General Virology* **87**: 2371-2380.

Genovés A., Navarro J.A. and Pallás V. 2010. The intra-and intercellular movement of Melon necrotic spot virus (MNSV) depends on an active secretory pathway. *Molecular plant-microbe interactions* **23**: 263-272.

Genovés A., Pallás V. and Navarro J.A. 2011. Contribution of topology determinants of a viral movement protein to its membrane association, intracellular traffic, and viral cell-to-cell movement. *Journal of Virology* **85**: 7797-7809.

Geuking M.B., Weber J., Dewannieux M., Gorelik E., Heidmann T., Hengartner H., Zinkernagel R.M. and Hangartner L. 2009. Recombination of retrotransposon and exogenous RNA virus results in nonretroviral cDNA integration. *Science* **323**: 393-396.

Gibbs A. and Ohshima K. 2010. Potyviruses and the digital revolution. *Annual review of phytopathology* **48**: 205-223.

Gingras A.-C., Raught B. and Sonenberg N. 1999. eIF4 initiation factors: effectors of mRNA recruitment to ribosomes and regulators of translation. *Annual review of biochemistry* **68**: 913-963.

Gomez-Aix C., García-García M., Aranda M.A. and Sanchez-Pina M.A. 2015. Melon necrotic spot virus replication occurs in association with altered mitochondria. *Molecular Plant-Microbe Interactions* **28**: 387-397.

González V.M., Garcia-Mas J., Arús P. and Puigdomènech P. 2010. Generation of a BAC-based physical map of the melon genome. *BMC genomics* **11**: 1.

Gonzalez-Ibeas D., Blanca J., Roig C., González-To M., Picó B., Truniger V., Gómez P., Deleu W., Caño-Delgado A., Arús P. et al. 2007. MELOGEN: An EST database for melon functional genomics. *BMC Genomics* **8**.

Gosselin P., Oulhen N., Jam M., Ronzca J., Cormier P., Czjzek M. and Cosson B. 2011. The translational repressor 4E-BP called to order by eIF4E: new structural insights by SAXS. *Nucleic acids research* **39**: 3496-3503.

Grifo J.A., Abramson R.D., Satler C.A. and Merrick W.C. 1984. RNA-stimulated ATPase activity of eukaryotic initiation factors. *Journal of Biological Chemistry* **259**: 8648-8654.

Grifo J.A., Tahara S.M., Leis J.P., Morgan M.A., Shatkin A.J. and Merrick W.C. 1982. Characterization of eukaryotic initiation factor 4A, a protein involved in ATP-dependent binding of globin mRNA. *Journal of Biological Chemistry* **257**: 5246-5252.

Grifo J.A., Tahara S.M., Morgan M.A., Shatkin A.J. and Merrick W.C. 1983. New initiation factor activity required for globin mRNA translation. *Journal of Biological Chemistry* **258**: 5804-5810.

Gross J.D., Moerke N.J., Von Der Haar T., Lugovskoy A.A., Sachs A.B., McCarthy J.E.G. and Wagner G. 2003. Ribosome loading onto the mRNA cap is driven by conformational coupling between eIF4G and eIF4E. *Cell* **115**: 739-750.

Hamilton A.J. and Baulcombe D.C. 1999. A species of small antisense RNA in posttranscriptional gene silencing in plants. *Science* **286**: 950-952.

Hellen C.U.T. and Sarnow P. 2001. Internal ribosome entry sites in eukaryotic mRNA molecules. *Genes & development* **15**: 1593-1612.

Hernández G., Altmann M., Sierra J.M., Urlaub H., del Corral R.D., Schwartz P. and Rivera-Pomar R. 2005. Functional analysis of seven genes encoding eight translation initiation factor 4E (eIF4E) isoforms in Drosophila. *Mechanisms of development* **122**: 529-543.

Hershey J.W.B. and Merrick W.C. 2000. 2 The Pathway and Mechanism of Initiation of Protein Synthesis. *Cold Spring Harbor Monograph Archive* **39**: 33-88.

Hertz M.I. and Thompson S.R. 2011. Mechanism of translation initiation by Dicistroviridae IGR IRESs. *Virology* **411**: 355-361.

Hibi T. and Furuki I. 1985. Melon necrotic spot virus. *CMI/AAB descriptions of plant viruses* **302**.

Hinnebusch A.G. 2011. Molecular mechanism of scanning and start codon selection in eukaryotes. *Microbiology and Molecular Biology Reviews* **75**: 434-467.

Hiscox J.A. and Ball L.A. 1997. Cotranslational disassembly of flock house virus in a cell-free system. *Journal of virology* **71**: 7974-7977.

Horie M., Honda T., Suzuki Y., Kobayashi Y., Daito T., Oshida T., Ikuta K., Jern P., Gojobori T. and Coffin J.M. 2010. Endogenous non-retroviral RNA virus elements in mammalian genomes. *Nature* **463**: 84-87.

Igreja C., Peter D., Weiler C. and Izaurralde E. 2014. 4E-BPs require non-canonical 4E-binding motifs and a lateral surface of eIF4E to repress translation. *Nature Communications* **5**.

Jaramillo M., Browning K., Dever T.E., Blum S., Trachsel H., Merrick W.C., Ravel J.M. and Sonenberg N. 1990. Translation initiation factors that function as RNA helicases from mammals, plants and yeast. *Biochimica et Biophysica Acta (BBA)-Gene Structure and Expression* **1050**: 134-139.

Jiang Y., Serviene E., Gal J., Panavas T. and Nagy P.D. 2006. Identification of essential host factors affecting tombusvirus RNA replication based on the yeast Tet promoters hughes collection. *Journal of Virology* **80**: 7394-7404.

Jivotovskaya A.V., Valášek L., Hinnebusch A.G. and Nielsen K.H. 2006. Eukaryotic translation initiation factor 3 (eIF3) and eIF2 can promote mRNA binding to 40S subunits independently of eIF4G in yeast. *Molecular and Cellular Biology* **26**: 1355-1372.

Joshi B., Lee K., Maeder D.L. and Jagus R. 2005. Phylogenetic analysis of eIF4E-family members. *BMC Evol Biol* **5**.

Julián P., Konevega A.L., Scheres S.H.W., Lázaro M., Gil D., Wintermeyer W., Rodnina M.V. and Valle M. 2008. Structure of ratcheted ribosomes with tRNAs in hybrid states. *Proceedings of the National Academy of Sciences* **105**: 16924-16927.

Kahvejian A., Svitkin Y.V., Sukarieh R., M'Boutchou M.-N. and Sonenberg N. 2005. Mammalian poly (A)-binding protein is a eukaryotic translation initiation factor, which acts via multiple mechanisms. *Genes & development* **19**: 104-113.

Kang B.C., Yeam I., Frantz J.D., Murphy J.F. and Jahn M.M. 2005. The pvr1 locus in Capsicum encodes a translation initiation factor eIF4E that interacts with Tobacco etch virus VPg. *The Plant Journal* **42**: 392-405.

Kassem M.A., Sempere R.N., Juárez M., Aranda M.A. and Truniger V. 2007. Cucurbit aphid-borne yellows virus is prevalent in field-grown cucurbit crops of southeastern Spain. *Plant Disease* **91**: 232-238.

Keller K.E., Johansen E., Martin R.R. and Hampton R.O. 1998. Potyvirus genome-linked protein (VPg) determines pea seed-borne mosaic virus pathotype-specific virulence in Pisum sativum. *Molecular plant-microbe interactions* **11**: 124-130.

Kinkelin K., Veith K., Grünwald M. and Bono F. 2012. Crystal structure of a minimal eIF4E–Cup complex reveals a general mechanism of eIF4E regulation in translational repression. *Rna* **18**: 1624-1634.

Kolupaeva V.G., Unbehaun A., Lomakin I.B., Hellen C.U. and Pestova T.V. 2005. Binding of eukaryotic initiation factor 3 to ribosomal 40S subunits and its role in ribosomal dissociation and anti-association. *Rna* **11**: 470-486.

Kong J. and Lasko P. 2012. Translational control in cellular and developmental processes. *Nat Rev Gen* **13**: 383-394.

Konstantinova P., Ter Brake O., Haasnoot J., De Haan P. and Berkhout B. 2007. Trans-inhibition of HIV-1 by a long hairpin RNA expressed within the viral genome. *Retrovirology* **4**: 15.

Kozak M. 1984. Compilation and analysis of sequences upstream from the translational start site in eukaryotic mRNAs. *Nucleic acids research* **12**: 857-872.

-. **1986**. Point mutations define a sequence flanking the AUG initiator codon that modulates translation by eukaryotic ribosomes. *Cell* **44**: 283-292.

Kraft J.J., Treder K., Peterson M.S. and Miller W.A. 2013. Cation-dependent folding of 3' cap-independent translation elements facilitates interaction of a 17-nucleotide conserved sequence with eIF4G. *Nucleic Acids Research* **41**: 3398-3413.

KüHne T., Shi N., Proeseler G., Adams M.J. and Kanyuka K. 2003. The ability of a bymovirus to overcome the rym4-mediated resistance in barley correlates with a codon change in the VPg coding region on RNA1. *Journal of general virology* **84**: 2853-2859.

Lackner D.H. and Bähler J. 2008. Translational Control of Gene Expression: From Transcripts to Transcriptomes. *International review of cell and molecular biology* **271**: 199-251.

Lange L. and Insunza V. 1977. Root-inhabiting Olpidium species: the O. radicale complex. *Transactions of the British Mycological Society* **69**: 377-384.

Lauring A.S., Frydman J. and Andino R. 2013. The role of mutational robustness in RNA virus evolution. *Nature reviews Microbiology* **11**: 327-336.

Lewin A., Crow A., Hodson C.T.C., Hederstedt L. and Le Brun N.E. 2008. Effects of substitutions in the CXXC active-site motif of the extracytoplasmic thioredoxin ResA. *Biochemical Journal* **414**: 81-91.

Lindstrom S.E., Cox N.J. and Klimov A. 2004. Genetic analysis of human H2N2 and early H3N2 influenza viruses, 1957–1972: evidence for genetic divergence and multiple reassortment events. *Virology* **328**: 101-119.

Lomakin I.B., Kolupaeva V.G., Marintchev A., Wagner G. and Pestova T.V. 2003. Position of eukaryotic initiation factor eIF1 on the 40S ribosomal subunit determined by directed hydroxyl radical probing. *Genes & development* **17**: 2786-2797.

Mader S., Lee H., Pause A. and Sonenberg N. 1995. The translation initiation factor eIF-4E binds to a common motif shared by the translation factor eIF-4 gamma

and the translational repressors 4E-binding proteins. *Molecular and cellular biology* **15**: 4990-4997.

Mansky L.M. and Wisniewski R.M. 1998. The bovine leukemia virus encapsidation signal is composed of RNA secondary structures. *Journal of virology* **72**: 3196-3204.

Maori E., Lavi S., Mozes-Koch R., Gantman Y., Peretz Y., Edelbaum O., Tanne E. and Sela I. 2007. Isolation and characterization of Israeli acute paralysis virus, a dicistrovirus affecting honeybees in Israel: evidence for diversity due to intra- and inter-species recombination. *Journal of General Virology* **88**: 3428-3438.

Marcotrigiano J., Gingras A.C., Sonenberg N. and Burley S.K. 1997. Cocrystal structure of the messenger RNA 5' cap-binding protein (eIF4E) bound to 7-methyl-GDP. *Cell* **89**: 951-961.

-. 1999. Cap-dependent translation initiation in eukaryotes is regulated by a molecular mimic of eIF4G. *Molecular Cell* **3**: 707-716.

Martin A., Troadec C., Boualem A., Rajab M., Fernandez R., Morin H., Pitrat M., Dogimont C. and Bendahmane A. 2009. A transposon-induced epigenetic change leads to sex determination in melon. *Nature* **461**: 1135-1138.

Martin-Marcos P., Cheung Y.-N. and Hinnebusch A.G. 2011. Functional elements in initiation factors 1, 1A and 2β discriminate against poor AUG context and non-AUG start codons. *Molecular and cellular biology*: MCB. 05819-05811.

Martínez-Gil L., Saurí A., Vilar M., Pallás V. and Mingarro I. 2007. Membrane insertion and topology of the p7B movement protein of Melon Necrotic Spot Virus (MNSV). *Virology* **367**: 348-357.

Mascarell-Creus A., Cañizares J., Vilarrasa-Blasi J., Mora-García S., Blanca J., Gonzalez-Ibeas D., Saladié M., Roig C., Deleu W. and Picó-Silvent B. 2009. An oligo-based microarray offers novel transcriptomic approaches for the analysis of pathogen resistance and fruit quality traits in melon (Cucumis melo L.). *BMC genomics* **10**: 467.

Matsuo H., Li H., McGuire A.M., Fletcher C.M., Gingras A.-C., Sonenberg N. and Wagner G. 1997. Structure of translation factor eIF4E bound to m7GDP and interaction with 4E-binding protein. *Nature Structural & Molecular Biology* **4**: 717-724.

Matsuo K., Soda E., Baba S. and Ota T. 1991. Occurrence of mosaic disease of melon caused by the lagenaria strain of cucumber mosaic virus in Nagasaki prefecture [Japan]. *Proceedings of the Association for Plant Protection of Kyushu (Japan)*.

Mayberry L.K., Allen M.L., Nitka K.R., Campbell L., Murphy P.A. and Browning K.S. 2011. Plant cap-binding complexes eukaryotic initiation factors eIF4F and eIFISO4F: Molecular specificity of subunit binding. *Journal of Biological Chemistry* **286**: 42566-42574.

McDonald S.M. and Patton J.T. 2011. Assortment and packaging of the segmented rotavirus genome. *Trends Microbiol* **19**: 136-144.

Merrick W.C. 1992. Mechanism and regulation of eukaryotic protein synthesis. *Microbiological reviews* **56**: 291-315.

Meulewaeter F., Danthinne X., Va M. and Cornelissen M. 1998. 5′-and 3′-sequences of satellite tobacco necrosis virus RNA promoting translation in tobacco. *The Plant Journal* **14**: 169-176.

Michael T. and Wilson A. 1984. Cotranslational disassembly increases the efficiency of expression of TMV RNA in wheat germ cell-free extracts. *Virology* **138**: 353-356.

Miller W.A. and White K.A. 2006. Long-distance RNA-RNA interactions in plant virus gene expression and replication. (ed. DB Alfen), pp. 447-467.

Mizuno A., In Y., Fujita Y., Abiko F., Miyagawa H., Kitamura K., Tomoo K. and Ishida T. 2008. Importance of C-terminal flexible region of 4E-binding protein in binding with eukaryotic initiation factor 4E. *FEBS letters* **582**: 3439-3444.

Mochizuki T., Ohnishi J., Ohki T., Kanda A. and Tsuda S. 2008. Amino acid substitution in the coat protein of Melon necrotic spot virus causes loss of binding to the surface of Olpidium bornovanus zoospores. *Journal of General Plant Pathology* **74**: 176-181.

Monzingo A.F., Dhaliwal S., Dutt-Chaudhuri A., Lyon A., Sadow J.H., Hoffman D.W., Robertas J.D. and Browning K.S. 2007. The structure of eukaryotic translation initiation factor-4E from wheat reveals a novel disulfide bond. *Plant Physiology* **143**: 1504-1518.

Morley S.J., Rau M., Kay J.E. and Pain V.M. 1993. Increased phosphorylation of eukaryotic initiation factor 4α during early activation of T lymphocytes correlates with increased initiation factor 4F complex formation. *EUR J BIOCHEM* **218**: 39-48.

Moury B., Desbiez C., Jacquemond M. and Lecoq H. 2006. Genetic diversity of plant virus populations: towards hypothesis testing in molecular epidemiology. *Adv Virus Res* **67**: 49-87.

Muñoz A. and Castellano M. 2012. Regulation of translation initiation under abiotic stress conditions in plants: is it a conserved or not so conserved process among eukaryotes? *Comparative and functional genomics* **2012**.

Nagy P.D., Barajas D. and Pogany J. 2012. Host factors with regulatory roles in tombusvirus replication. *Current Opinion in Virology* **2**: 691-698.

Nagy P.D., Carpenter C.D. and Simon A.E. 1997. A novel 3'-end repair mechanism in an RNA virus. *Proceedings of the National Academy of Sciences of the United States of America* **94**: 1113-1118.

Nagy P.D. and Pogany J. 2006. Yeast as a model host to dissect functions of viral and host factors in tombusvirus replication. *Virology* **344**: 211-220.

-. 2008. Multiple roles of viral replication proteins in plant RNA virus replication. *Plant Virology Protocols: From Viral Sequence to Protein Function*: 55-68.

-. 2012. The dependence of viral RNA replication on co-opted host factors. *Nature Reviews Microbiology* **10**: 137-149.

Nakahara K.S., Shimada R., Choi S.-H., Yamamoto H., Shao J. and Uyeda I. 2010. Involvement of the P1 cistron in overcoming eIF4E-mediated recessive resistance against Clover yellow vein virus in pea. *Molecular plant-microbe interactions* **23**: 1460-1469.

Navarro J.A., Genoves A., Climent J., Sauri A., Martinez-Gil L., Mingarro I. and Pallas V. 2006. RNA-binding properties and membrane insertion of Melon necrotic spot virus (MNSV) double gene block movement proteins. *Virology* **356**: 57-67.

Neher R.A. and Leitner T. 2010. Recombination rate and selection strength in HIV intra-patient evolution. *PLoS Comput Biol* **6**: e1000660.

Nicholson B.L. and White K.A. 2011. 3′ Cap-independent translation enhancers of positive-strand RNA plant viruses. *Current Opinion in Virology* **1**: 373-380.

Nicholson B.L., Wu B., Chevtchenko I. and White K.A. 2010. Tombusvirus recruitment of host translational machinery via the 3' UTR. *RNA* **16**: 1402-1419.

Nicholson B.L., Zaslaver O., Mayberry L.K., Browning K.S. and White K.A. 2013. Tombusvirus Y-shaped translational enhancer forms a complex with eIF4F and can be functionally replaced by heterologous translational enhancers. *Journal of Virology* **87**: 1872-1883.

Niedzwiecka A., Marcotrigiano J., Stepinski J., Jankowska-Anyszka M., Wyslouch-Cieszynska A., Dadlez M., Gingras A.-C., Mak P., Darzynkiewicz E. and Sonenberg N. 2002. Biophysical studies of eIF4E cap-binding protein: recognition of mRNA 5' cap structure and synthetic fragments of eIF4G and 4E-BP1 proteins. *J Mol Biol* **319**: 615-635.

Niepel M. and Gallie D.R. 1999. Identification and characterization of the functional elements within the tobacco etch virus 5' leader required for cap-independent translation. *Journal of virology* **73**: 9080-9088.

Nieto C., Morales M., Orjeda G., Clepet C., Monfort A., Sturbois B., Puigdomènech P., Pitrat M., Caboche M., Dogimont C. et al. 2006. An eIF4E allele confers resistance to an uncapped and non-polyadenylated RNA virus in melon. *Plant Journal* **48**: 452-462.

Nieto C., Rodríguez-Moreno L., Rodríguez-Hernández A.M., Aranda M.A. and Truniger V. 2011. Nicotiana benthamiana resistance to non-adapted Melon necrotic spot virus results from an incompatible interaction between virus RNA and translation initiation factor 4E. *Plant Journal* **66**: 492-501.

Nuñez-Palenius H.G., Gomez-Lim M., Ochoa-Alejo N., Grumet R., Lester G. and Cantliffe D.J. 2008. Melon fruits: genetic diversity, physiology, and biotechnology features. *Critical reviews in biotechnology* **28**: 13-55.

Ohki T., Akita F., Mochizuki T., Kanda A., Sasaya T. and Tsuda S. 2010. The protruding domain of the coat protein of Melon necrotic spot virus is involved in compatibility with and transmission by the fungal vector Olpidium bornovanus. *Virology* **402**: 129-134.

Paek K.Y., Hong K.Y., Ryu I., Park S.M., Keum S.J., Kwon O.S. and Jang S.K. 2015. Translation initiation mediated by RNA looping. *Proceedings of the National Academy of Sciences of the United States of America* **112**: 1041-1046.

Pagán I. and Holmes E.C. 2010. Long-term evolution of the Luteoviridae: time scale and mode of virus speciation. *Journal of Virology* **84**: 6177-6187.

Panavas T., Serviene E., Brasher J. and Nagy P.D. 2005. Yeast genome-wide screen reveals dissimilar sets of host genes affecting replication of RNA viruses. *Proceedings of the National Academy of Sciences of the United States of America* **102**: 7326-7331.

Pause A., Belsham G.J., Gingras A.-C., Donze O., Lin T.-A., Lawrence J.C. and Sonenberg N. 1994. Insulin-dependent stimulation of protein synthesis by phosphorylation of a regulator of 5'-cap function. *Nature* **371**: 762-767.

Pelletier J. and Sonenberg N. 1988. Internal initiation of translation of eukaryotic mRNA directed by a sequence derived from poliovirus RNA. *Nature* **334**: 320-325.

Perry R.P., Kelley D.E., Friderici K.H. and Rottman F.M. 1975. Methylated constituents of heterogeneous nuclear RNA: presence in blocked 5′ terminal structures. *Cell* **6**: 13-19.

Pestova T.V., Borukhov S.I. and Hellen C.U.T. 1998. Eukaryotic ribosomes require initiation factors 1 and 1A to locate initiation codons. *Nature* **394**: 854-859.

Pestova T.V. and Kolupaeva V.G. 2002. The roles of individual eukaryotic translation initiation factors in ribosomal scanning and initiation codon selection. *Genes & development* **16**: 2906-2922.

Pestova T.V., Kolupaeva V.G., Lomakin I.B., Pilipenko E.V., Shatsky I.N., Agol V.I. and Hellen C.U.T. 2001. Molecular mechanisms of translation initiation in eukaryotes. *Proceedings of the National Academy of Sciences* **98**: 7029-7036.

Pestova T.V., Lorsch J.R. and Hellen C.U.T. 2007. 4 The Mechanism of Translation Initiation in Eukaryotes. *Cold Spring Harbor Monograph Archive* **48**: 87-128.

Peter D., Igreja C., Weber R., Wohlbold L., Weiler C., Ebertsch L., Weichenrieder O. and Izaurralde E. 2015a. Molecular architecture of 4E-BP translational inhibitors bound to eIF4E. *Molecular cell* **57**: 1074-1087.

Peter D., Weber R., Köne C., Chung M.-Y., Ebertsch L., Truffault V., Weichenrieder O., Igreja C. and Izaurralde E. 2015b. Mextli proteins use both canonical bipartite and novel tripartite binding modes to form eIF4E complexes that display differential sensitivity to 4E-BP regulation. *Genes & development* **29**: 1835-1849.

Pisarev A.V., Skabkin M.A., Pisareva V.P., Skabkina O.V., Hellen C.U.T. and Pestova T.V. 2011. *The mechanism of ribosome recycling in eukaryotes*. Springer.

Pond S.L.K., Murrell B. and Poon A.F.Y. 2012. Evolution of viral genomes: interplay between selection, recombination, and other forces. *Evolutionary Genomics: Statistical and Computational Methods, Volume 2*: 239-272.

Rakotondrafara A.M. and Miller W.A. 2008. In vitro analysis of translation enhancers. (eds. GD Foster, E Johansen, Y Hong, PD Nagy), pp. 113-124.

Raught B. and Gingras A.-C. 2007. 14 Signaling to Translation Initiation. *Cold Spring Harbor Monograph Archive* **48**: 369-400.

Riviere C.J., Pot J., Tremaine J.H. and Rochon D.M. 1989. Coat protein of melon necrotic spot carmovirus is more similar to those of tombusviruses than those of carmoviruses. *Journal of general virology* **70**: 3033-3042.

Riviere C.J. and Rochon D.M. 1990. Nucleotide sequence and genomic organization of melon necrotic spot virus. *Journal of General Virology* **71**: 1887-1896.

Roberts R., Zhang J., Mayberry L.K., Tatineni S., Browning K.S. and Rakotondrafara A.M. 2015. A Unique 5′ Translation Element Discovered in Triticum Mosaic Virus. *Journal of virology* **89**: 12427-12440.

Rodnina M.V. and Wintermeyer W. 2009. Recent mechanistic insights into eukaryotic ribosomes. *Current opinion in cell biology* **21**: 435-443.

Rodriguez C.M., Freire M.A., Camilleri C. and Robaglia C. 1998. The Arabidopsis thaliana cDNAs coding for eIF4E and eIF (iso) 4E are not functionally equivalent for yeast complementation and are differentially expressed during plant development. *The Plant Journal* **13**: 465-473.

Rodríguez-Hernández A.M., Gosalvez B., Sempere R.N., Burgos L., Aranda M.A. and Truniger V. 2012. Melon RNA interference (RNAi) lines silenced for Cm-eIF4E show broad virus resistance. *Molecular Plant Pathology* **13**: 755-763.

Rodríguez-Moreno L., González V.M., Benjak A., Martí M.C., Puigdomènech P., Aranda M.A. and Garcia-Mas J. 2011. Determination of the melon chloroplast and mitochondrial genome sequences reveals that the largest reported mitochondrial genome in plants contains a significant amount of DNA having a nuclear origin. *BMC genomics* **12**: 424.

Roenhorst J.W., Verduin B.J.M. and Goldbach R.W. 1989. Virus-ribosome complexes from cell-free translation systems supplemented with cowpea chlorotic mottle virus particles. *Virology* **168**: 138-146.

Sachs A. 1990. The role of poly (A) in the translation and stability of mRNA. *Current opinion in cell biology* **2**: 1092-1098.

Sachs A.B. and Davis R.W. 1989. The poly (A) binding protein is required for poly (A) shortening and 60S ribosomal subunit-dependent translation initiation. *Cell* **58**: 857-867.

Sachs A.B. and Varani G. 2000. Eukaryotic translation initiation: there are (at least) two sides to every story. *Nature Structural & Molecular Biology* **7**: 356-361.

Salonen A., Ahola T. and Kääriäinen L. 2004. Viral RNA replication in association with cellular membranes. in *Membrane trafficking in viral replication*, pp. 139-173. Springer.

Sanjuán R., Moya A. and Elena S.F. 2004. The distribution of fitness effects caused by single-nucleotide substitutions in an RNA virus. *Proceedings of the National Academy of Sciences of the United States of America* **101**: 8396-8401.

Sanjuan R., Nebot M.R., Chirico N., Mansky L.M. and Belshaw R. 2010. Viral mutation rates. *Journal of virology* **84**: 9733-9748.

Sarawaneeyaruk S., Iwakawa H.-o., Mizumoto H., Murakami H., Kaido M., Mise K. and Okuno T. 2009. Host-dependent roles of the viral 5′ untranslated region (UTR) in RNA stabilization and cap-independent translational enhancement mediated by the 3′ UTR of Red clover necrotic mosaic virus RNA1. *Virology* **391**: 107-118.

Sasaki J. and Taniguchi K. 2003. The 5′-end sequence of the genome of Aichi virus, a picornavirus, contains an element critical for viral RNA encapsidation. *Journal of virology* **77**: 3542-3548.

Savolainen-Kopra C. and Blomqvist S. 2010. Mechanisms of genetic variation in polioviruses. *Reviews in medical virology* **20**: 358-371.

Scholthof K.-B.G. 2004. Tobacco mosaic virus: a model system for plant biology. *Annu Rev Phytopathol* **42**: 13-34.

Serra-Soriano M., Navarro J.A., Genoves A. and Pallás V. 2015. Comparative proteomic analysis of melon phloem exudates in response to viral infection. *J Proteomics* **124**: 11-24.

Sharma S.D., Kraft J.J., Miller W.A. and Goss D.J. 2015. Recruitment of the 40S ribosomal subunit to the 3'-untranslated region (UTR) of a viral mRNA, via the eIF4 complex, facilitates cap-independent translation. *Journal of Biological Chemistry* **290**: 11268-11281.

Shaw J.G., Plaskitt K.A. and Wilson T.M.A. 1986. Evidence that tobacco mosaic virus particles disassemble contranslationally in vivo. *Virology* **148**: 326-336.

Shibata S., Morino S., Tomoo K., In Y. and Ishida T. 1998. Effect of mRNA cap structure on eIF-4E phosphorylation and cap binding analyses using Ser209-mutated eIF-4Es. *Biochemical and Biophysical Research Communications* **247**: 213-216.

Shriner D., Rodrigo A.G., Nickle D.C. and Mullins J.I. 2004. Pervasive genomic recombination of HIV-1 in vivo. *Genetics* **167**: 1573-1583.

Simon A.E. and Miller W.A. 2013. 3’ cap-independent translation enhancers of plant viruses. in *Annual Review of Microbiology*, pp. 21-42.

Simon-Loriere E., Galetto R., Hamoudi M., Archer J., Lefeuvre P., Martin D.P., Robertson D.L. and Negroni M. 2009. Molecular mechanisms of recombination restriction in the envelope gene of the human immunodeficiency virus. *PLoS Pathog* **5**: e1000418.

Siridechadilok B., Fraser C.S., Hall R.J., Doudna J.A. and Nogales E. 2005. Structural roles for human translation factor eIF3 in initiation of protein synthesis. *Science* **310**: 1513-1515.

Smith M.D., Arake-Tacca L., Nitido A., Montabana E., Park A. and Cate J.H. 2016. Assembly of eIF3 Mediated by Mutually Dependent Subunit Insertion. *Structure*.

Sonenberg N. and Hinnebusch A.G. 2009. Regulation of translation initiation in eukaryotes: mechanisms and biological targets. *Cell* **136**: 731-745.

Sonenberg N., Morgan M.A., Merrick W.C. and Shatkin A.J. 1978. A polypeptide in eukaryotic initiation factors that crosslinks specifically to the 5'-terminal cap in mRNA. *Proceedings of the National Academy of Sciences* **75**: 4843-4847.

Sonenberg N., Rupprecht K.M., Hecht S.M. and Shatkin A.J. 1979. Eukaryotic mRNA cap binding protein: purification by affinity chromatography on sepharose-coupled m7GDP. *Proceedings of the National Academy of Sciences* **76**: 4345-4349.

Sonenberg N., Trachsel H., Hecht S. and Shatkin A.J. 1980. Differential stimulation of capped mRNA translation in vitro by cap binding protein.

Srivastava S., Verschoor A. and Frank J. 1992. Eukaryotic initiation factor 3 does not prevent association through physical blockage of the ribosomal subunit-subunit interface. *J Mol Biol* **226**: 301-304.

Steinhauer D.A., Domingo E. and Holland J.J. 1992. Lack of evidence for proofreading mechanisms associated with an RNA virus polymerase. *Gene* **122**: 281-288.

Stupina V.A., Meskauskas A., McCormack J.C., Yingling Y.G., Shapiro B.A., Dinman J.D. and Simon A.E. 2008. The 3’ proximal translational enhancer of Turnip crinkle virus binds to 60S ribosomal subunits. *Rna* **14**: 2379-2393.

Sun C., Todorovic A., Querol-Audí J., Bai Y., Villa N., Snyder M., Ashchyan J., Lewis C.S., Hartland A. and Gradia S. 2011. Functional reconstitution of human eukaryotic translation initiation factor 3 (eIF3). *Proceedings of the National Academy of Sciences* **108**: 20473-20478.

Tanne E. and Sela I. 2005. Occurrence of a DNA sequence of a non-retro RNA virus in a host plant genome and its expression: evidence for recombination between viral and host RNAs. *Virology* **332**: 614-622.

Tarun S.Z., Wells S.E., Deardorff J.A. and Sachs A.B. 1997. Translation initiation factor eIF4G mediates in vitro poly (A) tail-dependent translation. *Proceedings of the National Academy of Sciences* **94**: 9046-9051.

Timmer R.T., Benkowski L.A., Schodin D., Lax S.R., Metz A.M., Ravel J.M. and Browning K.S. 1993. The 5'and 3'untranslated regions of satellite tobacco necrosis virus RNA affect translational efficiency and dependence on a 5'cap structure. *Journal of Biological Chemistry* **268**: 9504-9510.

Tomimura K., Špak J., Katis N., Jenner C.E., Walsh J.A., Gibbs A.J. and Ohshima K. 2004. Comparisons of the genetic structure of populations of Turnip mosaic virus in West and East Eurasia. *Virology* **330**: 408-423.

Tomoo K., Matsushita Y., Fujisaki H., Abiko F., Shen X., Taniguchi T., Miyagawa H., Kitamura K., Miura K.-i. and Ishida T. 2005. Structural basis for mRNA Cap-Binding regulation of eukaryotic initiation factor 4E by 4E-binding protein, studied by spectroscopic, X-ray crystal structural, and molecular dynamics simulation methods. *Biochimica et Biophysica Acta (BBA)-Proteins and Proteomics* **1753**: 191-208.

Tomoo K., Shen X., Okabe K., Nozoe Y., Fukuhara S., Morino S., Sasaki M., Taniguchi T., Miyagawa H. and Kitamura K. 2003. Structural features of human initiation factor 4E, studied by X-ray crystal analyses and molecular dynamics simulations. *J Mol Biol* **328**: 365-383.

Treder K., Kneller E.L., Allen E.M., Wang Z., Browning K.S. and Miller W.A. 2007. The 3' cap-independent translation element of Barley yellow dwarf virus binds eIF4F via the eIF4G subunit to initiate translation. *RNA (New York, NY)* **14**: 134-147.

Truniger V., Nieto C., González-Ibeas D. and Aranda M. 2008. Mechanism of plant eIF4E-mediated resistance against a Carmovirus (Tombusviridae): cap-independent translation of a viral RNA controlled in cis by an (a) virulence determinant. *The Plant Journal* **56**: 716-727.

Tuplin A. 2015. Diverse roles and interactions of RNA structures during the replication of positive-stranded RNA viruses of humans and animals. *Journal of General Virology* **96**: 1497-1503.

Uchida N., Hoshino S.-i., Imataka H., Sonenberg N. and Katada T. 2002. A novel role of the mammalian GSPT/eRF3 associating with poly (A)-binding protein in Cap/Poly (A)-dependent translation. *Journal of Biological Chemistry* **277**: 50286-50292.

Unbehaun A., Borukhov S.I., Hellen C.U.T. and Pestova T.V. 2004. Release of initiation factors from 48S complexes during ribosomal subunit joining and the link between establishment of codon-anticodon base-pairing and hydrolysis of eIF2-bound GTP. *Genes & development* **18**: 3078-3093.

Urbanowicz A., Alejska M., Formanowicz P., Błażewicz J., Figlerowicz M. and Bujarski J.J. 2005. Homologous crossovers among molecules of brome mosaic bromovirus RNA1 or RNA2 segments in vivo. *Journal of virology* **79**: 5732-5742.

Valli A., Lopez-Moya J.J. and Garcia J.A. 2007. Recombination and gene duplication in the evolutionary diversification of P1 proteins in the family Potyviridae. *Journal of General Virology* **88**: 1016-1028.

van der Hoek L., Back N., Jebbink M.F., de Ronde A., Bakker M., Jurriaans S., Reiss P., Parkin N. and Berkhout B. 2005. Increased multinucleoside drug resistance and decreased replicative capacity of a human immunodeficiency virus type 1 variant with an 8-amino-acid insert in the reverse transcriptase. *Journal of virology* **79**: 3536-3543.

Van Lipzig R., Gultyaev A.P., Pleij C.W.A., Van Montagu M., Cornelissen M. and Meulewaeter F. 2002. The 5′ and 3′ extremities of the satellite tobacco necrosis virus translational enhancer domain contribute differentially to stimulation of translation. *Rna* **8**: 229-236.

Varani G. 1997. RNA-protein intermolecular recognition. *Accounts of chemical research* **30**: 189-195.

Visser J.C. and Bellstedt D.U. 2009. An assessment of molecular variability and recombination patterns in South African isolates of Potato virus Y. *Arch Virol* **154**: 1891-1900.

Voigt C.A., Martinez C., Wang Z.-G., Mayo S.L. and Arnold F.H. 2002. Protein building blocks preserved by recombination. *Nature Structural & Molecular Biology* **9**: 553-558.

Wang Z., Kraft J.J., Hui A.Y. and Miller W.A. 2010. Structural plasticity of Barley yellow dwarf virus-like cap-independent translation elements in four genera of plant viral RNAs. *Virology* **402**: 177-186.

Wang Z., Parisien M., Scheets K. and Miller W.A. 2011. The cap-binding translation initiation factor, eIF4E, binds a pseudoknot in a viral cap-independent translation element. *Structure* **19**: 868-880.

Wang Z., Treder K. and Miller W.A. 2009. Structure of a viral cap-independent translation element that functions via high affinity binding to the eIF4E subunit of eIF4F. *Journal of Biological Chemistry* **284**: 14189-14202.

Waskiewicz A.J., Flynn A., Proud C.G. and Cooper J.A. 1997. Mitogen-activated protein kinases activate the serine/threonine kinases Mnk1 and Mnk2. *The EMBO journal* **16**: 1909-1920.

Wells S.E., Hillner P.E., Vale R.D. and Sachs A.B. 1998. Circularization of mRNA by eukaryotic translation initiation factors. *Molecular cell* **2**: 135-140.

Wittmann S., Chatel H., Fortin M.G. and Laliberté J.-F. 1997. Interaction of the Viral Protein Genome Linked of Turnip Mosaic Potyvirus with the Translational Eukaryotic Initiation Factor (iso) 4E ofArabidopsis thalianaUsing the Yeast Two-Hybrid System. *Virology* **234**: 84-92.

Yamasaki S., Sakai J., Fuji S., Kamisoyama S., Emoto K., Ohshima K. and Hanada K. 2010. Comparisons among isolates of Sweet potato feathery mottle virus using complete genomic RNA sequences. *Arch Virol* **155**: 795-800.

Yu Y., Marintchev A., Kolupaeva V.G., Unbehaun A., Veryasova T., Lai S.-C., Hong P., Wagner G., Hellen C.U.T. and Pestova T.V. 2009. Position of eukaryotic translation initiation factor eIF1A on the 40S ribosomal subunit mapped by directed hydroxyl radical probing. *Nucleic acids research*: gkp519.

Zaitlin M. 1998. The discovery of the causal agent of the tobacco mosaic disease. *Discoveries in plant biology* **1**: 105-110.

Zemer R., Cohen Y.K., Naftaly T. and Klein A. 2008. Presence of hepatitis C virus DNA sequences in the DNA of infected patients. *European journal of clinical investigation* **38**: 845-848.

Zhang J. and Temin H.M. 1994. Retrovirus recombination depends on the length of sequence identity and is not error prone. *Journal of virology* **68**: 2409-2414.

Zhang X.-Y., Wang X.-L., Wang X.-F., Xia G.-H., Pan Q.-H., Fan R.-C., Wu F.-Q., Yu X.-C. and Zhang D.-P. 2006. A shift of phloem unloading from symplasmic to apoplasmic pathway is involved in developmental onset of ripening in grape berry. *Plant Physiology* **142**: 220-232.

Zuberek J., Wyslouch-Cieszynska A., Niedzwiecka A., Dadlez M., Stepinski J., Augustyniak W., Gingras A.-C., Zhang Z., Burley S.K. and Sonenberg N. 2003. Phosphorylation of eIF4E attenuates its interaction with mRNA 5′ cap analogs

by electrostatic repulsion: Intein-mediated protein ligation strategy to obtain phosphorylated protein. *Rna* **9**: 52-61.

Zuo X., Wang J., Yu P., Eyler D., Xu H., Starich M.R., Tiede D.M., Simon A.E., Kasprzak W., Schwieters C.D. et al. 2010. Solution structure of the cap-independent translational enhancer and ribosome-binding element in the 3' UTR of turnip crinkle virus. *Proceedings of the National Academy of Sciences of the United States of America* **107**: 1385-1390.

Aims of the study

This work is focused on elucidating the molecular mechanism of cap-independent translation of MNSV RNAs and an structural and functional analysis of the viral and host factors involved. In particular, a more detailed understanding of the role and function of avirulent 3'-CITE, which may have a critical contribution in translation initiation and overcome resistance, and how this element interacts with host factors.

Specific aims of the study:

1. Characterization of the new resistance-breaking isolate.
2. Study the interaction between 3'-CITE and eukaryotic initiation translation factors and how this binding affects cap-independent translation.
3. Crystalize *Cm*eIF4E alone and in complex with a eIF4G peptide and study the high resolution structures obtained for new binding motifs.

Chapter 1

Interfamilial recombination between viruses led to acquisition of a novel translation enhancing RNA element that allows resistance breaking

1. INTRODUCTION

Mutation, recombination and reassortment and combinations of these molecular events can produce new viral forms, a minority of which might become competent enough for replication in a new environment (see, for instance (Escriu *et al.* 2007)). While mutation is a universal and important mechanism of genetic variation that affects all viruses, the occurrence of recombination appears to vary greatly among different viruses, and can be also dependent on the host and the environment (Jaag & Nagy 2010). For plant RNA viruses, recombination seems to be one of the strongest forces shaping their genomes, and the end results are detectable in phylogenetic analysis. It is likely that plant RNA viruses appear to have tested recombination with all types of genetic material, because indications of recombination have been identified between closely related, but also distantly related, virus genomes and even with host genes. While intraspecific recombination was detected in many RNA viruses (Moury *et al.* 2006b; Ohshima *et al.* 2007; Pagán & Holmes 2010), intergeneric recombinants are rare (aus dem Siepen *et al.* 2005). Moreover, some plant viruses seem to have acquired host genes through recombination (Dolja *et al.* 2006).

The evolutionary effect of recombination has been the subject of a wealth of theoretical papers. On the one hand, recombination may play a fundamental role in compensating deleterious mutations caused by low fidelity polymerases (Chao & Matthews 1992; Chao & Trang 1997). On the other, recombination may lead to the acquisition of nonself sequences. Thus, recombination may result in dramatic changes in the biological properties of the virus, potentially playing a role in the emergence of new viral pathogens (Fernández-Cuartero *et al.* 1994; Domingo 2010), including resistance-breaking and host-switching strains (García-Arenal & McDonald 2003; Jegouic *et al.* 2009; Sztuba-Solińska *et al.* 2011; Bujarski 2013). The acquisition of the host-switching ability may force a reduction in the virus' fitness in the original host, because the new host may impose different selective requirements (Elena *et al.* 2011). While some studies indicate that recombination may assist host switch (Chare & Holmes 2006; Codoñer & Elena 2008; Sztuba-Solińska *et al.* 2011), others do not support an association between recombination and emergence, suggesting instead

that it is circumstantial (Holmes 2008; Holmes 2009). The results presented here support the first statement.

In principle, recombination may affect any function in the viral cycle, including translation of viral RNAs. Viral mRNAs have evolved numerous mechanisms to recruit the translational machinery of the host, allowing them to compete with host mRNAs and avoid defense mechanisms that act at the translation level. Only *c.* 20% of known positive-strand RNA viruses have genomic and subgenomic RNAs with the 5′-cap structure and 3′-poly(A) tail typical of eukaryotic mRNAs (van Regenmortel *et al.* 2000). Thus, most lack one or both of these features, and often use their 5′- and/or 3′-termini in alternative gene expression strategies (Dreher & Miller 2006; Kneller *et al.* 2006). Plant viruses of the families *Tombusviridae* and *Luteoviridae* lack both the cap and poly(A) tail. Several of the species from these two families have been shown to control their cap-independent translation with a cap-independent translational enhancer element residing within or near their 3′-UTR (3′-CITE) (Miller & White 2006b). Different 3′-CITEs with distinct properties have been described, but all have in common the general mechanistic steps involving recruitment of the translation initiation factors at the 3′-CITE and delivery of these near the translation start site through communication with the 5′-UTR (Simon & Miller 2013b). All members of the genus *Luteovirus* (family *Luteoviridae*), and all members of the *Necrovirus* and *Dianthovirus* genera (family *Tombusviridae*) carry 3′-CITEs similar to that of *Barley yellow dwarf virus* (BYDV Translational Enhancer, BTE) (Shen & Miller 2004; Kneller *et al.* 2006). Other structurally unrelated 3′-CITEs are found within the 3′-UTRs of the members of the *Tombusviridae* family, such as I-shaped, Y-shaped and 3′-CITEs similar to the one of *Panicum mosaic virus* (PMV Translational Enhancer, PTE) (Miller *et al.* 2007; Simon & Miller 2013b). BTE- and PTE-like 3′-CITEs have been also identified in umbraviruses (Wang *et al.* 2010). Several 3′-CITEs have been shown to bind the eukaryotic translation initiation factor (eIF) 4F, but with variations in the directly bound subunits, either eIF4E or eIF4G: for the BTE 3′-CITE of BYDV (genus *Luteovirus*) it was shown to be eIF4G (Treder *et al.* 2008), while for the PTE-like 3′-CITE of PMV (genus *Panicovirus*) (Wang *et al.* 2011), for the Y-shaped 3′-CITE of *Carnation italian ringspot virus* (CIRV, genus *Tombusvirus*) (Nicholson *et al.* 2013) and for the I-shaped 3′-CITE of *Maize*

necrotic streak virus (MNeSV, genus *Tombusvirus*) it was shown to be eIF4E (Nicholson *et al.* 2010).

In the case of the I-shaped 3´-CITE of *Melon necrotic spot virus* (MNSV, family *Tombusviridae*, genus *Carmovirus*) genetic evidence for an interaction with melon eIF4E exists: melon resistance against MNSV was shown to act at the level of translation, being mediated by eIF4E (Nieto *et al.* 2006a; Truniger *et al.* 2008b). The *eIF4E* allele from resistant melon varieties differs from the susceptibility allele in a single amino acid residue (Nieto *et al.* 2006a). A resistance breaking isolate, MNSV-264, was described (Diaz *et al.* 2002) , but this isolate did not prevail under field conditions (M.A. Aranda, unpublished results). The critical region in this isolate for overcoming the resistance was resolved to a 3'-CITE element. This 3´-CITE was active not only in susceptible melon, as the corresponding 3´-CITEs of avirulent strains, but also in resistant melon (Diaz *et al.* 2004; Truniger *et al.* 2008b). Thus, it was proposed that an inefficient interaction between the host-specific 3´-CITE of avirulent isolates and eIF4E of resistant melon impedes the correct formation of the translation initiation complex at the viral RNA ends and thereby leads to resistance (Truniger *et al.* 2008b).

In 2011 a new virulent MNSV isolate, that we named MNSV-N, was identified on MNSV-resistant melon plants in southeastern Spain. We set out to determine the resistance-breaking mechanism of MNSV-N. We found that MNSV-N contains a 55 nucleotide (nt) insertion in its 3´-UTR that functions as a virulence determinant. This inserted sequence has the capacity to act as a 3´-CITE in resistant and susceptible melon. Even though, the I-shaped 3´-CITE described for avirulent MNSV isolates, only functional in susceptible melon, is also present in this isolate. Both 3´-CITEs required the presence of the 5´-UTR of MNSV *in cis* for efficient translation to occur. Results show strong evidence that this 55 nt insertion has been acquired by interfamilial recombination with the 3´-UTR of an Asiatic *Cucurbit aphid-borne yellows virus* (CABYV) isolate. Thus, the sequence acquired by MNSV by recombination is a functional element able to control cap-independent translation of MNSV-N in the otherwise resistant host. To our knowledge this is the first direct proof for the previously proposed modularity and transferability in nature of 3´-CITEs. Additionally, it is one of the first rare recombination events in a plant RNA virus that has been

proven to result in resistance breaking. Thus, our results support the hypothesis that recombination in positive sense RNA viruses can widen host range, giving rise to new emergent strains.

2. EXPERIMENTAL PROCEDURES

2.1. Plants, viruses and virus inoculations

The susceptible (*Nsv/-*) *Cucumis melo* L. cultivars used were the cantaloupe-type accession C-35 ("La Mayora" germplasm collection, Málaga, Spain). The resistant *C. melo* cultivar (*nsv/nsv*) is the cantaloupe-type accession C-46 ("La Mayora" collection).

We used MNSV resistance-breaking isolates MNSV-N and MNSV-264 (Diaz *et al.* 2002) and nonresistance-breaking isolates MNSV-Al (Dutch-type) (Genoves *et al.* 2006) and MNSV-Mα5 (Díaz *et al.* 2003). MNSV-N came to our hands through our diagnosis service during the spring of 2011. MNSV-N was biologically cloned by four serial single necrotic lesion passages onto healthy resistant melon C-46 (*nsv/nsv*), as described in (Diaz *et al.* 2004). MNSV was inoculated mechanically on expanded melon cotyledons as described before (Díaz *et al.* 2003; Diaz *et al.* 2004). Plants were grown and maintained after inoculation in a glasshouse with a 16-h photoperiod, day/night temperature of 25/18^{o}C, and day/night relative humidity of 70/60%.

For the host range study (Table 2) 10 plants from different species from the families *Cucurbitaceae* (*Cucumis melo* (C35, C46; "La Mayora" collection)*, Citrullus lanatus* (cv. Sugar Baby; Semillas Battle)*, Cucurbita pepo* (cv. Pastelera; Semillas Battle) and *Cucumis sativus* (cv. Marketmore; Semillas Arnedo)), *Chenopodiaceae* (*Chenopodium amaranticolor* and *Chenopodium quinoa* ("La Mayora" collection)), *Amaranthaceae* (*Gomphrena globosa* ("La Mayora" collection)) and *Solanaceae* (*Nicotiana benthamiana* ("La Mayora" collection)) were mechanically inoculated on expanded cotyledons for the cucurbit species, and on young but fully expanded leaves of seedlings for the other species (20 cucurbits for inoculations with MNSV-264, because of very low systemic infection frequency). Infection was visually evaluated by

the appearance of necrotic lesions and by dot-blot hybridization using a MNSV-specific probe at 7 dpi (inoculated leaves) and 14 dpi (evaluation of systemic infection).

2.2. Analysis of viral virulence

For this experiment cotyledons of resistant melons were mechanically rub-inoculated with purified virions (Díez *et al.* 1998) of MNSV-264 or MNSV-N, while cotyledons of susceptible melon were additionally inoculated with MNSV-Al, at a concentration of 1 mg/ml in 10 mM potassium phosphate buffer. The diameters (mm) of the single necrotic lesions induced by each isolate in at least 10 plants were measured at 3, 5 and 7 dpi. Viral RNA accumulation at 7 dpi was determined by RT-qPCR, as previously described (Gómez *et al.* 2009). Briefly, total RNA extractions of three biological replicates from a mix of three lesions (6 mm diameter discs) were performed using Tri-Reagent (Sigma-Aldrich, St. Louis, MO, USA). RT-qPCR was performed using the Power SYBR® Green RNA-to-CT™ 1-Step Kit (Life Technologies) with 100 ng of total RNA following the manufacturer's protocol. *In vitro* transcripts were used in serial dilutions to generate standard curves. Primers for qPCR were designed by using Primer Express software (Applied Biosystems International, Foster City, CA, USA) targeting the 3´-UTR region. Primers for MNSV-Al were 5´-ATTTGGTCTCCCATATTCCTAC-3´ (CE-1291) and 5´-ATACGCCGTTACGGTTAGCCAG-3´ (CE-1292), for MNSV-264 were 5´-GACGAGGTCCAGCCAATCAA-3´(CE-1289) and 5´-GGCTCCGATAGAACCCCTCA-3´(CE-1290), and for MNSV-N were 5´-TTGTGGAGATGAGCGTGACT-3´ (CE-1293) and 5´-GAGACCGGGGTTGGAGTACA-3´(CE-1294). Virus concentration in each sample (ng of viral RNA per 100 ng of total RNA) was estimated by interpolating the threshold cycle (Ct) in standard curves. Slope values for each standard curve were as following: MNSV-Al -3.47 and R^2= 0.998; MNSV-N -3.60 and R^2= 0.997; and MNSV-264 -3.48 and R^2= 0.997. Reaction efficiency was above 90% in all cases.

2.3. cDNA synthesis and sequencing

RNA from MNSV-N infected cotyledons (5 dpi) was extracted using TRI reagent (Sigma-Aldrich). cDNA was obtained with Expand Reverse Transcriptase (Roche) using two different reverse primers: primer A contains the 3'-terminal 10 last nucleotides in the genome that are conserved in all MNSV isolates except MNSV-264 (Fig. 9b)(Truniger *et al.*, 2008), and primer B contains the sequence complementary to the 10 nucleotides at the 3' end of the MNSV-264 genome. PCR reactions for amplification of the 3´-end were performed with the Prime Star HS DNA polymerase (high fidelity) (Takara) using either of these two primers together with primer MA245, that lies in a conserved region of the CP-gene. Amplification was only obtained with primer A. This can be explained by the in average higher nucleotide similarity found between the 3´-UTR of MNSV-N with that of avirulent isolates than with that of MNSV-264. This PCR fragment was sequenced. The complete MNSV-N sequence was obtained by sequencing in both directions overlapping PCR fragments obtained with primers designed in conserved regions: CE-830: 5´-CAGCACAATTGTCTTCCACATC-3´; CE-831: 5´-TTCTATACTGGCAGGAGGCG -3´; CE-832: 5´-CATGGTAAGGCACTGGAGAC -3´; CE-833: 5´-TCAATGGGGCGAAAGATAGCC -3´; CE-834: 5´-ACATGGCTTCAGGGACAAGC-3´; CE-835: 5´- CCCGGGACTTATCTCGTCAC-3´. The whole MNSV genome sequence showed high similarity to the Dutch-type subgroup of MNSV (95 %).

2.4. Construction and analysis of chimeric viruses

The amplified 3´end of MNSV-N was cloned directionally into *Hpa*I/*Pst*I sites of the chimeric clone pBSK+-264/3´-Mα5 (Truniger *et al.* 2008b), resulting in the exchange of its 3´-UTR of MNSV-Mα5 with that of MNSV-N, resulting in pBSK+-264/3´-N (264/3´-N). Deletion of the 55 nt insertion (see alignment in Fig. 9) in the 3´-UTR of MNSV-N in pBSK+-264/3´-N was obtained by amplification of the whole plasmid with primers lacking this insertion. Subsequently, *Dpn*I digestion was used to select for the mutant plasmids (*in vitro* mutagenesis (Sambrook & Russell 2001)). *In vitro* transcribed RNA (RiboMAX Large Scale RNA production, Promega) from the above constructs, linearized with *Pst*I, was inoculated mechanically onto cotyledons (Diaz *et al.* 2004) or electroporated into protoplasts from resistant and susceptible melon plants (Truniger

et al. 2008b). The appearance of necrotic lesions was recorded after visual inspection. The ability of mutants to multiply in melon protoplasts was studied by dot-blot or Northern blot using a cRNA probe complementary to the 3´-UTR of MNSV-Mα5 (Diaz *et al.* 2004). Each experiment was carried out at least three times. The last 600 nt from the 3´-end of progeny virus genomes was amplified by RT-PCR and sequenced.

2.5. Luc-constructs

The MNSV-N 5´-UTR was amplified from cDNA (see above) by PCR using a primer that contained restriction sites and the T7 promoter sequence directly in front of the first 10 nt of the 5´-UTR sequence which is highly conserved in all MNSV isolates. The fragment was directionally cloned into the *Kpn*I/*Nco*I sites of the T7-luc plasmid (modified pGL3, resulting in 5´-N-luc) (Truniger *et al.* 2008b). The 3´-UTRs were directionally cloned after PCR amplification with primers containing restriction sites into the *Xba*I/*Hpa*I sites of the T7-luc or 5´-N-luc plasmid (resulting in 3´-N-luc or 5´-N-luc-3´-N, respectively). Deletion of the 55 nt insertion was achieved by *in vitro* mutagenesis (see above). The constructs (5´-end-luc-3´-end) were amplified by PCR with the high fidelity Prime Star HS DNA polymerase and transcribed *in vitro* (RiboMAX). Constructs containing only the first 81, 65 and 37 nucleotides of the 3´-UTR of MNSV-N were obtained by PCR amplification of plasmid 5´-N-luc-3´-N with reverse primers ending at the corresponding position (N81-5´-CCGGGGTTGGAGTACAAGACC; N65-5´-AGACCAGTGATTTGGACAGGC; N37-5´-ATGCCGGGTGGAGTCACGCTC; underlined in. 3b), *Dpn*I digestion of the input plasmid, followed by *in vitro* transcription (RiboMAX Large Scale RNA production, Promega).

2.6. *In vivo* translation in melon protoplasts

In vivo translation in melon protoplasts (susceptible or resistant) was performed as described in (Truniger *et al.* 2008b). Briefly, 10 μg of *in vitro* transcribed RNA was electroporated into 1x 10^6 protoplasts (Diaz *et al.* 2004). To minimize variations between samples, 2 μg of capped *Renilla* luciferase reporter RNA (pRL-null vector (Promega)) were introduced along with the virus RNA. After 5-6 h incubation in

the dark at 25°C, protoplasts was lysed in 1xPLB (Promega). *Firefly* and *Renilla* luciferase activities were measured with the Dual-Glo™ Luciferase assay system (Promega). These experiments were carried out at least five times for each construct.

2.7. Analysis of RNA structure

The 65 nt of the new 3´-CITE were inserted into the previously described SHAPE cassette (Wang *et al.* 2010). This plasmid was linearized with *Sma* I and transcribed using MEGAshortscript™ Kit (Ambion). SHAPE experiments were performed essentially as previously reported (Kraft *et al.* 2013b). Briefly, 500 ng of RNA refolded in SHAPE buffer were treated with 60mM of benzoyl cyanide (BzCN; Sigma–Aldrich) and reverse transcribed by primer extension of a radiolabeled primer. Products were resolved on an 8% denaturing polyacrylamide gel after primer extension. Normalized BzCN reactivity values for each nucleotide position were calculated by SAFA Footprinting Software (Das *et al.* 2005). RNA secondary structure was determined by using the MC-Fold computer program (Parisien & Major 2008b), using SHAPE reactivity data. *Trans*-inhibition assays of *in vitro* translation with wheat germ extract (Promega) were performed as described (Kraft *et al.* 2013b).

2.8. Nucleotide sequence accession numbers

The sequence of the genomic RNA of MNSV-N obtained here has been made available in GenBank (accession number KF060715).

3. RESULTS

3.1. MNSV-N breaks down the melon *nsv* resistance and is more virulent than MNSV-264

After its biological cloning, the host range and multiplication efficiency of MNSV-N were studied and compared to those of MNSV-Al (Genoves *et al.*, 2006) and the previously described resistance-breaking MNSV-264 (Diaz *et al.*, 2004). The result

of the host range study presented in Table 1 showed that MNSV-N infected the same hosts as MNSV-Al, but additionally, like MNSV-264, it also infected plants of the resistant melon cultivar (*nsv/nsv* genotype). On directly inoculated leaves or cotyledons virus multiplication was evaluated by the appearance of necrotic lesions and dot-blot analysis and occurred (NL/+) or not (-), always in 100 % of the plants tested (Table 2). The number of systemically infected plants was detected by appearance of necrotic lesions on upper non-inoculated leaves and confirmed by dot-blot (Table 2). The ability of MNSV to systemically infect melon plants depends on the plant genotype, the virus isolate and the environmental conditions. Very often systemic infection occurs in < 10 % of the inoculated plants (Mallor *et al.*, 2006; Gosalvez-Bernal *et al.*, 2008). Under our conditions, systemic infection of the resistant melons (C46) was never observed with MNSV-264 (Table 2). However, 30 % of the resistant melons (C46) singly inoculated with MNSV-N showed systemic infection. These results substantiated previous observations under field and laboratory conditions, suggesting that this new isolate was more virulent than MNSV-264.

Table 2. Host range study of MNSV isolates, including the new isolate MNSV-N

		MNSV-N (RB)		MNSV-Al (NRB)		MNSV-264 (NRB)	
Family	Species	IC/L	NIL	IC/L	NIL	IC/L	NIL
Cucurbitaceae	*C. melo cv.* C35 *(Nsv/-)*	NL/+(10/10)	SN/+(1/10)	NL/+(10/10)	SN/+(1/10)	NL/+(20/20)	SN/+(1/20)
	C. melo cv. C46 *(nsv/nsv)*	NL/+	SN/+(3/10)	- (0/10)	- (0/10)	NL/+(20/20)	- (0/20)
	C. lanatus cv. Sugar Baby	NL/+(10/10)	SN/+(3/10)	NL/+(10/10)	SN/+(3/10)	NL/+(20/20)	SN/+(1/20)
	C. pepo cv. pastelera	NL/+(10/10)	SN/+(8/10)	NL/+(10/10)	SN/+(8/10)	NL/+(20/20)	SN/+(1/20)
	C. sativus cv. Marketmore	NL/+(10/10)	SN/+(4/10)	NL/+(10/10)	SN/+(3/10)	NL/+(20/20)	SN/+(1/20)
Chenopodiaceae	*C. amaranticolor*	- (0/10)	- (0/10)	- (0/10)	- (0/10)	- (0/10)	- (0/10)
	C. quinoa	- (0/10)	- (0/10)	- (0/10)	- (0/10)	- (0/10)	- (0/10)
Amaranthaceae	*G. globosa*	- (0/10)	- (0/10)	- (0/10)	- (0/10)	NL/+(10/10)	- (0/10)
Solanaceae	*N. benthamiana*	- (0/10)	- (0/10)	- (0/10)	- (0/10)	NL/+(10/10)	SN/+(10/10)

IC/L: inoculated cotyledons/leaves; NIL: upper non-inoculated leaves; NL/+: necrotic lesions and dot blot positive; SN/+: systemic necrotic symptoms and dot blot positive; -: no symptoms and dot blot negative; RB: resistance-breaking; NRB: non resistance-breaking isolates; MNSV: Melon necrotic spot virus; nsv/nsv: genotype of resistance to MNSV; Nsv/-: genotype of susceptibility to MNSV.

Thus, the multiplication efficiency of MNSV-N was estimated in susceptible and resistant melons and compared to those of MNSV-264 and MNSV-Al. Measuring lesion

diameter in a time course experiment showed that MNSV-264 lesions did not increase much with time in either melon genotype. However, the diameter of lesions induced by the other two isolates increased significantly with time, resulting in 3-4 fold bigger lesions (Fig. 7a).

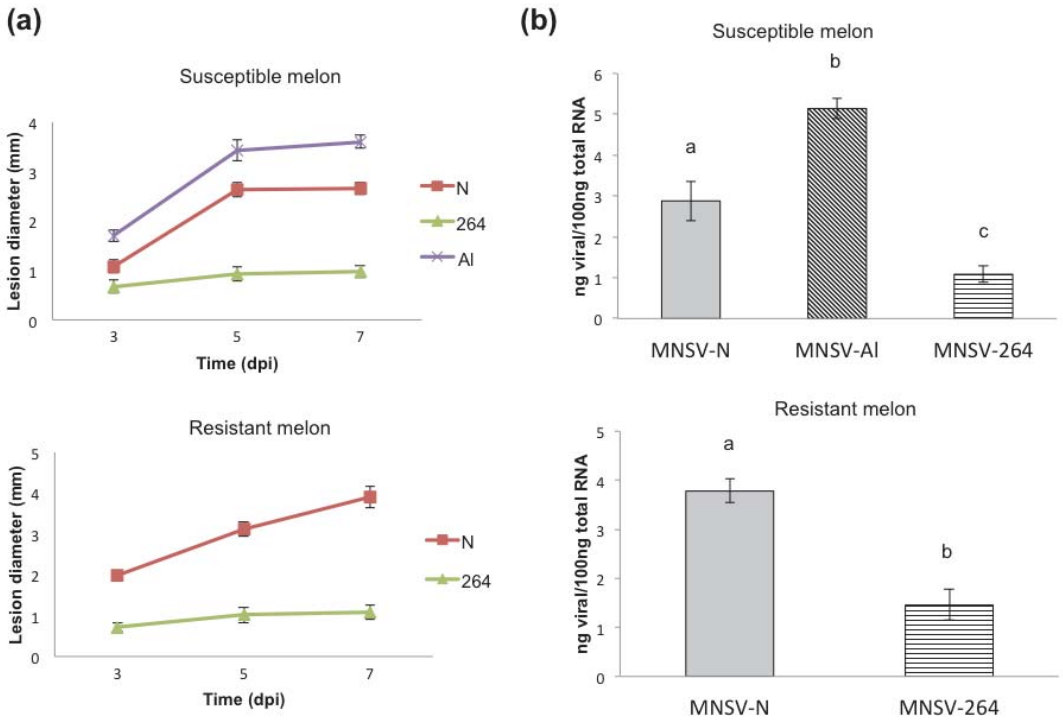

Figure 7. MNSV-N is more virulent than MNSV-264. (**a**) Evaluation of *Melon necrotic spot virus* (MNSV) infections in melon of susceptible (*Nsv/-*) and resistant (*nsv*/*nsv*) genotypes (C-35 and C46, respectively). Isolates MNSV-N and MNSV-264 were mechanically inoculated onto resistant melon cotyledons, while in susceptible melon MNSV-Al was also studied. (**a**) Infection was followed by measuring the diameters (mm) of single local lesions at 3, 5 and 7 days post inoculation (dpi). The significance was analyzed by the ANOVA test, with Bonferroni multiple comparison test P=0.0001 (susceptible) and P=0.0001 (resistant) for data obtained at 7 dpi, concluding that differences between MNSV-N, -264 and -Al were significant. (**b**) Virus accumulation in single lesions (ng of viral RNA/100 ng of total RNA) at 7 dpi, determined by RT-qPCR. For this assay three total RNA extractions from a mix of three lesions were performed per virus isolate and melon genotype. The significance of data was analyzed by the ANOVA test with Bonferroni multiple comparison test P=0.0021 (susceptible) and P=0.0005 (resistant). Error bars are +/-.

Virus RNA accumulation in single lesions was measured by RT-qPCR at 7 dpi, showing significant variations depending on the melon genotype and isolate inoculated: In susceptible melon, MNSV-Al RNA accumulated to higher levels than MNSV-N RNA which, in turn, accumulated more than MNSV-264 RNA. In resistant melon, MNSV-N RNA concentration was again nearly three-fold higher than that of

MNSV-264 (Fig. 7b). Additionally, as mentioned above, MNSV-N was the only isolate able to systemically infect resistant melon plants. Therefore, while MNSV-N is not more virulent than MNSV-Al in susceptible melons, its virulence is higher than that of MNSV-264 in resistant melons.

3.2. MNSV-N is a natural recombinant between MNSV and CABYV

The nucleotide sequence from the complete genome of MNSV-N was determined and compared with known MNSV sequences. In general terms, MNSV-N complete genome sequence showed high similarity to the ones of avirulent MNSV isolates (>92 %). A sharp decrease in similarity was detected in a small region of the 5´end of its 3´-UTR (Fig. 9). However, a general decrease in sequence similarity in the 3´-UTR was found between the genome sequences of MNSV-N and MNSV-264 (Fig. 9a), the region where the virulence determinant of MNSV-264 had been localized before (Diaz-Pendon *et al.*, 2005; Truniger *et al.*, 2008). Conversely, the 3´-UTR of MNSV-N had, on average, a much higher similarity to the 3´-UTRs of avirulent isolates (>76 %) than to that of MNSV-264 (<50 %).

Alignment of the 3´-UTR sequences of MNSV-N and avirulent MNSV isolates clearly showed that a fragment size of 55 nt had been inserted at its 5´-end, after the tenth nucleotide of its 3´-UTR (Fig. 9). Thus, if this insertion was excluded, the sequence similarity of the 3´-UTR of MNSV-N with the ones of avirulent isolates increased to 95 %. A BLAST search with the first 65 nt of the 3´-UTR of MNSV-N, including the 55-nt sequence insertion, identified a highly similar sequence in the 3´-UTR of an Asiatic isolate of the polerovirus *Cucurbit aphid-borne yellows virus* (CABYV) (family *Luteoviridae*). As can be observed in Fig. 9 (c), 49 nt of the 55-nt insertion were identical to the 5´-end of the 3´-UTR of the isolate CABYV-Xinjiang. Similarly, high conservation was observed with the 3´-UTRs of all other Asiatic CABYV isolates (Fig. 8).

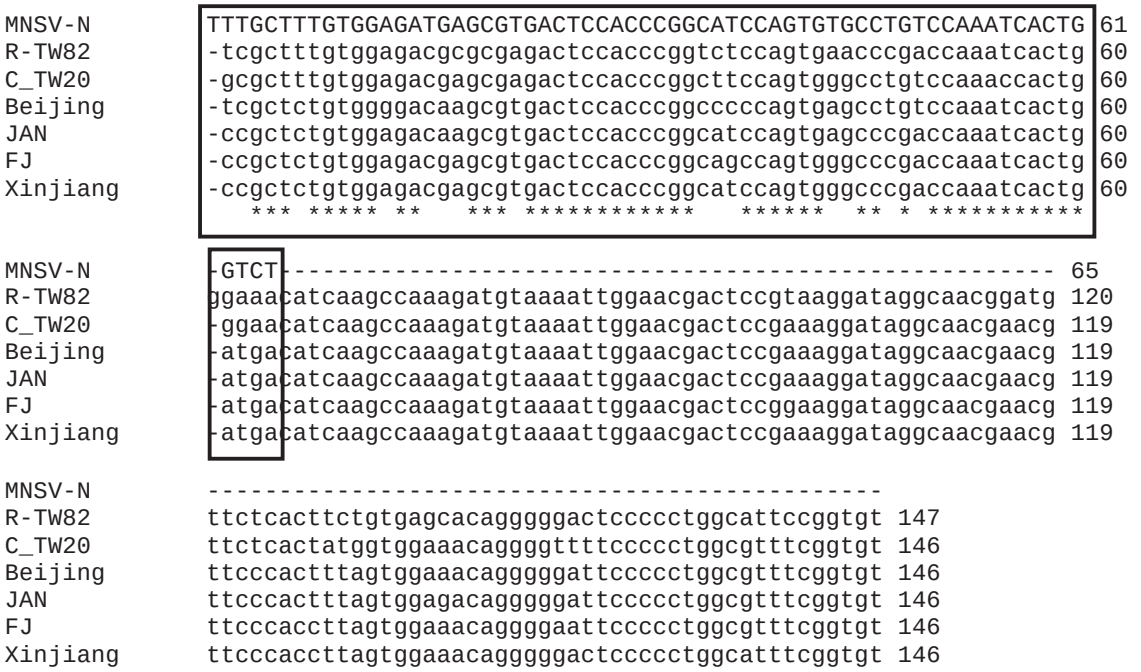

Figure 8. Sequence alignment of the 3´-UTR of Asiatic CABYV isolates with the recombined sequence of MNSV-N. Alignment performed with ClustalX with the 3´-UTR sequences of asiatic *Cucurbit aphid-borne yellows virus* (CABYV) isolates and the first 65 nt of the 3´-UTR of *Melon necrotic spot virus* (MNSV) isolate MNSN-N.

Interestingly, CABYV has a worldwide distribution in cucurbits, including melon, and co-infection with MNSV has been reported (Kassem *et al.* 2007a; Juarez *et al.* 2013). This high sequence identity suggested the occurrence of an recombination event. Thus, we carried out a recombination occurrence analysis using the RDP3 software, which implements several recombination-detecting algorithms (Martin *et al.* 2010) (Fig. 9d). As hypothesized, a recombination event with very high statistical significance (*P*-value <0.01) was detected by all methods implemented in RDP3, strongly suggesting that the 55-nt insertion in MNSV-N was acquired through recombination between MNSV and CABYV, both belonging to different virus families.

(a)

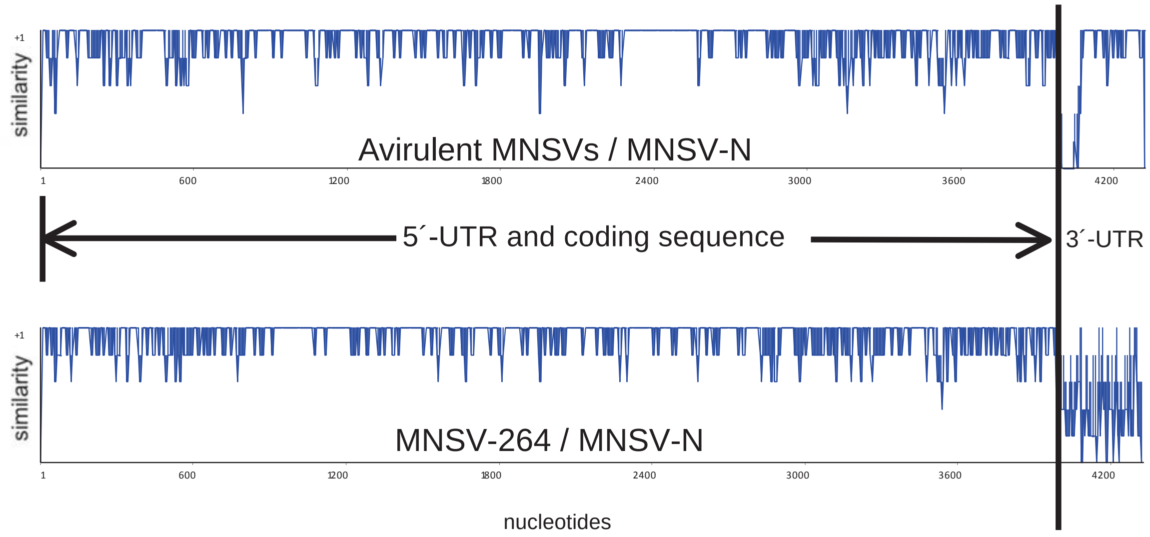

(b)

```
                                                                            N37                         N65
Dutch       ---TTTGATTTAC-------------------------------------------------------TGCA 14
MNSV-N      ---TTTGCTTTGTGGAGATGAGCGTGACTCCACCCGGCATCCAGTGTGCCTGTCCAAATCACTGGTCTTGTA 69
AI          ---TTTGATTTAT-------------------------------------------------------TGTA 14
Ma71        ---TTTGATTTAC-------------------------------------------------------TGTA 14
Ma24        ---TTTGATTTAC-------------------------------------------------------TGTA 14
Ma3         ---TTTGATTTAC-------------------------------------------------------TGTA 14
ISR         ---TTCGATT-AA-------------------------------------------------------TGTA 13
Pa58        ---TTTGACTTAC-------------------------------------------------------TGTA 14
Ma68        ---CTTGATTTAC-------------------------------------------------------TACA 14
Chiba       -AATTTAATTTAC-------------------------------------------------------TATA 16
Yamaguchi   --ATTTAATTTAC-------------------------------------------------------TATA 15
YS          --ATTAAATTTAC-------------------------------------------------------TATA 15
1Kochi      -AATTACATTTAC-------------------------------------------------------TATA 16
Nagasaki    GAATTA-ATTTAC-------------------------------------------------------TATA 16
KS          -TATGAAATA-AC-------------------------------------------------------TACA 15
Kouchi      -TATGAAATA-AC-------------------------------------------------------TACA 15
HM          ---TTTAATTTAC-------------------------------------------------------TGCA 16
                                                                                *  *

                       N81
Dutch       CTCCAAAT-CCGGTCTCCCTTGTTCCTACCTGTTCTCAGCCTGATATCTGTTCTGGTGTCCTATAGGCGTCC 85
MNSV-N      CTCCAACC-CCGGTCTCCCTTGTTCCTACCTGTTCTCAGCCAGATCTCTGTTCTGGTGTCCTATAGGCGTCC 140
AI          CTCCAAAT-TTGGTCTCCCATATTCCTACCTGTTCTCAGCCAGATCTCTGTTCTGGTGTCCTATAGGCATCC 85
Ma71        CTCCAAAT-TTGGTCTCCCATATTCCCACCTGTTCTCAGCCAGATATCTGTTCTGGTGTCCTATAGGCGTCC 85
Ma24        CTCCAAAT-TTGGTCTCCCATATTCCTACCTGTTCTCTGCCAGATCTCTGTTCTGGTGTCCTATAGGCGTCC 85
Ma3         CTCCAAAT-TTGGTCTCCCATATTCCTACATGTTCTCAGCCAGATCTCTGTTCTGGTGTCCTATAGGCGTCC 85
ISR         CTCCAAAAATTGGCCTCCCTTATTCCTACCCGTTCTCAGCCAGATCTCTGTTCTGGTGTCCTACAGGCGTTC 85
Pa58        CTCCAAAT-TTGGTCTCCCATATTCCTACCTGCTCTCAGCCAGATCTCTGTTCTGGTGTCCTATAGGCGTCC 85
Ma68        CTCCAAAT-TTTGTCTCCCATATTCCTACCTGTTCTCAGCCAGATCTCTGTTCTGGTGTCCTATAGGTGTCC 85
Chiba       CTCC-AAATCTGGTCTCTCTCATACCTTCCTGTTCTCAGCCAGATCTCTGTTCTGGTGTCCTATAGGTGTCC 87
Yamaguchi   CTCC-AAATCTGGTCTCTCTTATACCTACCTGTTCTCAGCCAGATCTCTGTTCTGGTGTCCTATAGGTGTCC 86
YS          CTCC-AAATCTGGTCTCTCTTATACCTACCTGTTCTCAGCCAGATCTCTGTTCTGGTGTCCTATAGGTGTCC 86
1Kochi      CTCCGAAATCTGGTCTCCCTTATACCTACCTGTTCTCAGCCAGATCTCTGTTCTGGTGTCCTATAGGTGTCC 88
Nagasaki    CTCCAAAATCTGGTCTCCCCTATACCTACCTGTTCTCAGCCAGATCTCTGTTCTGGTGTCCTATAGGTGTCC 88
KS          CTCCAAAATCTGGTCTCCCTTATTCCTACCTGTTCTCAGCCAGATCTCTGTTCTGGTGTCCTATAGGTGTCC 87
Kouchi      CTCCAAAATCTGGTCTCCCTTATTCCTACCTGTTCTCAGCCAGATCTCTGTTCTGGTGTCCTATAGGTGTCC 87
HM          CTCC-AAATCTGGTCTC-CTTATTCCTACCTGTTCTCAGCCAGATCTCTGTTCTGGTGTCCTATAGACGTCC 84
            **** *       * *** *    * **   *  * **** *** *** ***************** **    * *
```

```
Dutch       TTGTCGTGTGTAGTGCGGTCTGGCTAACCGTAATGGCGTATCGGCTTGG-ATTTCCGATGATTTGGCTCCGG 156
MNSV-N      TTGTCGTGTGTAGTGCGGTCTGGCTAACCGTAACAGCGTATCGGCTCGG-ATCTCCGATGATTAGGCTCCAG 211
AI          TTGTCGTGTGTAGTGCGGTCTGGCTAACCGTAACGGCGTATCGGCTTGG-CTTTCCAATGATTAGGCTCCGG 156
Ma71        TTGTCGTGTGTAGTGCGGCCTGGCTAACCGTAACGGCGTATCGGCTTGG-TTTTCCAATGATTAGGCTCCGG 156
Ma24        TTGTCGTGTGTAGTGCGGTCTGGCTAACCGTAACGGCGTATCGGCTTGG-GTTTCCAATGATTAGGCTCCCG 156
Ma3         TTGTCGTGTGTAGTGCGGTCTGGCTAACCGTAACGGCGTATCGGCTTGGGTTTTCCAATGATTAGGCTCCGG 157
ISR         ATGTCGTGTGTAGTGCGGTCTGGCTAACCGTAACGGCGTATCGGCTTGG-ATTTCCAATGATTAGGCTCCAG 156
Pa58        TTGTCGTGTGTAGTGCGGTCTGGCTAACCGTAACGGCGTATCGGCTTGG-TTTTCCGATGATTAGGCTCCGG 156
Ma68        TTGTCGTGTGTAGTGCGGTCTGGCTAACCGTAACGGCGTATCGGCTTGA-ACTTCCAATGATTAGGCTCCGG 156
Chiba       TTGTCGTGTGTAGTGCGGTCTGGCTAACCGTAACGGCGTATCGGCTTGG-TTCTCCGACGATTAGGCTCCGG 158
Yamaguchi   TTGTCGTGTGTAGTGCGGTCTGGCTAACCGTAACGGCGTATCGGCTTGG-TTCTCCGATGATTAGGCTCCGG 157
YS          TTGTCGTGTGTAGTGCGGTCTGGCTAACCGTAACGGCGTATCGGCTTGG-TTCTCCGACGATTAGGCTCCGG 157
1Kochi      TTGTCGTGTGTAGTGCGGTCTGGCTAACCGTAACGGCGTATCGGCTCGG-TTCTCCGACGATTAGGCTCTGG 159
Nagasaki    TTGTCGTGTGTAGTGCGGTCTGGCTAACCGTAACGGCGTATCGGCTCGG-TTCTCCGATGATTAGGCTCCGG 159
KS          TTGTCGTGTGTAGTGCGGTCTGGCTAACCGTAACGGCGTATCGGCTCGG-TTCTTCGATGATTAGGCTCCGG 158
Kouchi      TTGTCGTGTGTAGTGCGGTCTGGCTAACCGTAACGGCGTATCGGCTCGG-TTCTTCGATGATTAGGCTCCGG 158
HM          TTGTCGTGTGTAGTGCGGTCTGGCTACCCGTAACGGCGTATCGGCTTGG-GTCTTCGATGATTAGGCTCCGG 155
             ***************** ******* ******  *********** *     * * * **** *****  *

Dutch       GATGTACGACATAGCTGAAGATGGTTGGAGTTTGGTGGACCACCGCTAGCAAAATACACTCTGTGTGGGGCG 228
MNSV-N      GATGTACGACATAGCCGAAGATGGATGGAGCTTGGTAGACCACCGCTAGCAAAATACACTCTGTGTGGGGCG 283
AI          GATGTACGACATAGCTGAAGATGGATGGAGTTCGGTAGACCACCGCTAGCAAAATACACTCTGTGTGGGGCG 228
Ma71        GATGTACGACATAGCTGAAGATGGATGGAGTTCGGTAGACCACCGCTAGCAAAATACACTCTGTGTGGGGCG 228
Ma24        GATGTACGACATAGCTGAAGATGGATGGAGTTCGGTAGACCACCGCTAGCAAAATACACTCTGTGTGGGGCG 229
Ma3         GATGTACGACATAGCTGAAGATTGATGGAGTTTGGTAGACCACCGCTAGCAAAATACACTCTGTGTGGGGCG 228
ISR         GATGTACGACATAGTTGAAGATGGATGGAGTTTGGTAGACCACCGCTAGCAAAATACACTCTGTGTGGGGCG 228
Pa58        GATGTACGACATAGCTGAAGATGGATGGCGTTCGGTAGGCCACCGCTAGCAAAATACACTCTGTGTGGGGCG 228
Ma68        GATGTACGACATAGCTGAAGATGGATGGCGTTTGGTAGACCACCGCTAGCAAAATACACTCTGTGTGGGGCG 228
Chiba       GATGTACGACATAGTTGAAGATGGATGGTGTTTGGTAGATCACCGCTAGCAAAATACACTCTGTGTGGGGCG 230
Yamaguchi   GATGTACGACATAGTTGAAGATGGATGGTGTTTGGTAGATCACCGCTAGCAAAATACACTCTGTGTGGGGCG 229
YS          GATGTACGACATAGTTGAAGATGGATGGTGTTTGGTAGATCACCGCTAGCAAAATACACTCTGTGTGGGGCG 229
1Kochi      GATGTACGACATAGCTGAAGATGGATGGTGTTCGGTAGATCACCGCTAGCAAAATACACTCTGTGTGGGGCG 231
Nagasaki    GATGCACGACATAGCTGAAGATGGATGGTGTTCGGTAGATCACCGCTAGCAAAATACACTCTGTGTGGGGCG 231
KS          GATGTACGACATAGCTGAAGATGGATGGCGTTCGGTGGATCACCGCTAGCAAAATACACTCTGTGTGGGGCG 230
Kouchi      GATGTACGACATAGCTGAAGATGGATGGCGTTCGGTGGATCACCGCTAGCAAAATACACTCTGTGTGGGGCG 230
HM          AATGTACGACATAGCTGAAGATGGATGGAGTTTGGTAGATCACCGCTAGCAAAATACACTCTGTGTGGGGCG 227
             *** *********  ****** * *** * * *** *  ********************************

Dutch       TGCTAGTGGATAGTCATGTATGTTTGAGATGGGTTATAGGCCCATCCCGCCC 280
MNSV-N      TGCTAGTGGATAGTCATGTATGTTTGAGATGGGTTTTAGGCCCATCCCGCCC 335
AI          TGCTAGTGGATAGTCATGTATGTTTGAGATGGGTTATAGGCCCATCCCGCCC 280
Ma71        TGCTAGTGGATAGTCATGTATGTTTGAGATGGGTTATAGGCCCATCCCGCCC 280
Ma24        TGCTAGTGGATAGTCATGTATGTTTGAGATGGGTTATAGGCCCATCCCGCCC 280
Ma3         TGCTAGTGGATAGTCATGTATGTTTGAGATGGGTTGTAGGCCCATCCCGCCC 281
ISR         TGCTAGTGGATAGTCATGTATGTCTGAGATGGGTTATAGGC-CATCCCGCCC 279
Pa58        TGCTAGTGGATAGTCATGTATGTTTGAGATGGGTTATAGGCCCATCCCGCCC 280
Ma68        TGCTAGTGGATAGTCATGTATGTTTGAGATGGGTTATAGGCCCATCCCGCCC 280
Chiba       TGCTAGTGGATAGTCATGTATGTTTGAGATGGGTTATAGGCCCATCCCGCC- 281
Yamaguchi   TGCTAGTGGATAGTCATGTATGTTTGAGATGGGTTATAGGCCCATCCCGCC- 280
YS          TGCTAGTGGATAGTCATGTATGTTTGAGATGGGTTATAGGCCCATCCCGCCC 281
1Kochi      TGCTAGTGGATAGTCATGTATGTTTGAGATGGGTTATAGGCCCATCCCGCC- 282
Nagasaki    TGCTAGTGGATAGTCATGTATGTTTGAGATGGGTTATAGGCCCATCCCGCC- 282
KS          TGCTAGTGGATAGTCATGTATGTTTGAGATGGGTTGTAGGCCCATCCCGCCC 282
Kouchi      TGCTAGTGGATAGTCATGTATGTTTGAGATGGGTTGTAGGCCCATCCCGCCC 282
HM          TGCTAGTGGATAGTCATGTATGTTTGAGATGGGTTGTAGGCCCATCCCGCCC 279
            ********************** *********** ***** *********
```

(c)

```
CABYV-X     -CCGCTCTGTGGAGACGAGCGTGACTCCACCCGGCATCCAGTGGGCCCGACCAAATCACT 59
MNSV-N      TTTGCTTTGTGGAGATGAGCGTGACTCCACCCGGCATCCAGTGTGCCTGTCCAAATCACT 60
               *** ********* ***************************** *** * **********

CABYV-X     GATGACATCAAGCCAAAGATGTAAAATTGGAACGACTCCGAAAGGATAGGCAACGAACGT 119
MNSV-N      GGT---------CT---------------------------------------------- 65
            * *         *

CABYV-X     TCCCACCTTAGTGGAAACAGGGGGACTCCCCCTGGCATTTCGGTGT 165
MNSV-N      ---------------------------------------------
```

(d)

Figure 9. The 3´-UTR of MNSV-N contains a sequence of 55 nt that is highly similar to the 3´-UTR of CABYV. (**a**) Nucleotide sequence similarity plot (performed with AlignX program from the Vector NTI software package (Invitrogen)), comparing nucleotide sequence of avirulent *Melon necrotic spot virus* (MNSV) isolates versus MNSV-N and MNSV264 versus MNSV-N. The X-axis represents the nucleotides of the virus sequence, with a window size of 5. The Y-axis represents the nucleotide similarity, being 1.0 for identical, 0.5 for similar nucleotides and lower depending on the number of different nucleotides and the number of sequences compared. (**b**) Alignment (CLUSTAL X) of the 3´-UTRs of all Dutch-type MNSV isolates (avirulent) and MNSV-N showing that MNSV-N contains an insertion of 55 nt after the tenth nucleotide of its 3´-UTR. High similarity between the sequences of all these MNSV isolates can be observed after this insertion (95 %). The previously identified 3´-CITE sequence, highly conserved in avirulent isolates (4 variations in the 45 nt), but also in MNSV-N (only 1 nucleotide different from other isolates), is highlighted in a grey box. The last 10 nt at the 3´end, invariant in all MNSV isolates, are framed. On MNSV-N sequence 3´-end of constructs N37, N65 and N81 are marked with an arrow. GenBank accession numbers of MNSV sequences included in the alignment are Mα5-AY122286, HM-GU480022.1, Chiba-AB250684, Yamaguchi-AB250687, Yamaguchi CP gene (YS) -AB189944**,** Nagasaki-AB250686, Al-DQ339157, Dutch-NC001504, ISR (Israel)-DQ922807, Kochi-AB250685, Kouchi CP gene (KS)-AB189943, Mα24-EU589616, Mα71-EU589619, Mα3-EU589618, Mα68-EU589622, Pα58-EU589620, Pα57-EU589621, Pα54-EU589617. (**c**) Alignment of the first 65 nt of the 3´-UTR of MNSV-N (including the first 10 nt conserved in avirulent isolates (indicated by vertical line) plus the 55 nt insertion) with the complete 3´-UTR sequence of *Cucurbit aphid-borne yellows virus* isolate CABYV-Xinjiang (Genbank accession: EU636992). Identical nucleotides are marked below with an asterisk. (**d**) Recombination hypothesis generated by the RDP3 software, a computer program for characterizing recombination events in sequence alignments using several different recombination analysis methods and tests for recombination hot-spots. The sequences included in this analysis are the 3´-UTRs of MNSV (see above) and CABYV isolates (Genbank accession numbers are CABYV-Xinjiang: EU636992; CABYV-Beijing: EU000535; CABYV-FJ: GQ221223; CABYV-JAN: GQ221224; CABYV-R_TW82: JQ700306; CABYV-C_TW20: JQ700305.). RDP3 colors similar sequences with similar colors. The predicted recombination in MNSV-N starts at nucleotide position 4 and ends at nucleotide 63. The statistical significance is very high, with a P value < 0.01.

3.3. The recombined sequence allows MNSV-N to break *nsv*-mediated resistance

We identified the virulence determinant of MNSV-N by construction of chimeric mutants. For these experiments we decided to use the background of the MNSV-264 genome, since the sequence similarity of the genome without the 3´-UTR of MNSV-N is higher with this isolate (95 %, the same % for MNSV-Al and other dutch-type isolates) than with MNSV-Mα5 (91 %). Thus, we exchanged the 3´-UTRs of MNSV-N and the infectious chimeric virus 264/3´-Mα5 (genome of MNSV-264 with its 3´-UTR exchanged with the one of MNSV-Mα5, thus able to infect susceptible but not resistant melon (Truniger *et al.*, 2008)). This new chimeric virus (264/3´N) was able to infect not only susceptible, but also resistant melon, similar to MNSV-264, as shown by mechanical inoculation of susceptible and resistant melons with *in vitro* transcribed RNA from this clone (264/3´-N) (Fig. 10a). This result was confirmed by inoculating melon protoplasts with this RNA (Fig. 10b).

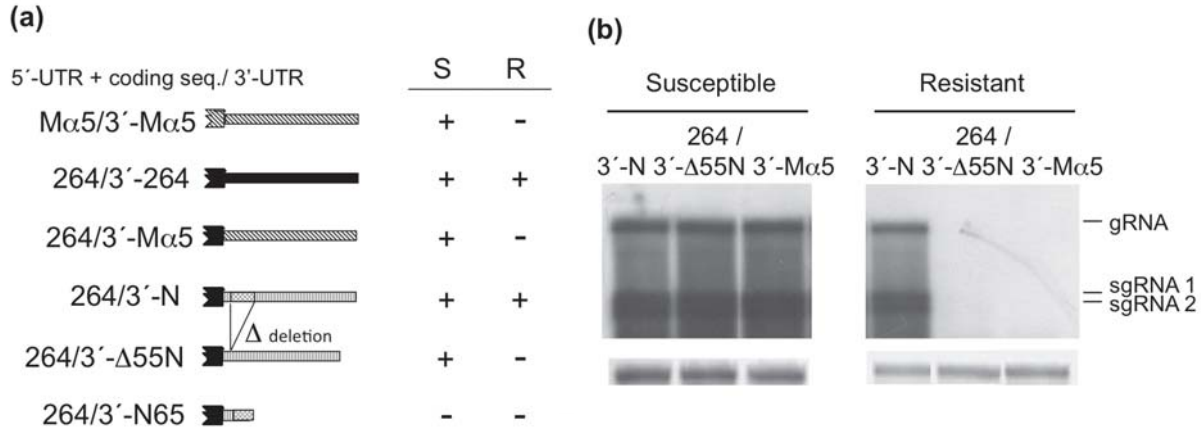

Figure 10. The 55 nt insertion acquired by recombination contains the virulence determinant of MNSV-N (a) On the left, schematic representation of the wild-type and chimeric constructs studied, obtained by exchanging the 3´-UTRs. The chimeric viruses consisted of the genome of MNSV-264 with its 3´-UTR exchanged for the one of MNSV-Mα5 (264/3´-Ma5), of MNSV-N (264/3´-N), of MNSV-N without the 55 nt insertion present in its 3´-UTR (264/3´- D55-N) or with only the first 65 nt of the 3´-UTR of MNSV-N (264/3´-N65). In vitro transcribed RNA from these constructs was mechanically inoculated on expanded cotyledons of susceptible (Nsv/-) (S) and resistant (nsv/nsv) (R) melon. Appearance of necrotic lesions was monitored and presence (+) or absence (-) of infection was confirmed by dot-blot. (b) Accumulation of these chimeric MNSV RNAs in susceptible and resistant melon protoplasts at 24 hpi as detected by Northern blot analysis. The non-viable chimeric mutant 264/3´-N65 is not shown. Positions of genomic (gRNA) and subgenomic RNAs (sgRNA1/2) are indicated. The cRNA probe was complementary to the 3´-UTR of MNSV-Mα5 and detected efficiently MNSV-N. The amount of total RNA loaded was visualized by methylene blue staining of the 28S rRNA (bottom panel).

Thus, although the 3´-UTR sequences of the two resistance breaking isolates, MNSV-N and -264, showed low similarity (see above), the virulence determinants of both were located in their 3´-UTRs (Truniger *et al.*, 2008). To determine if the recombined sequence itself is required for breaking resistance, the multiplication capacity of mutants that have this sequence deleted was analysed in susceptible and resistant melon plants and protoplasts (Fig. 10a and b). While the chimeric virus containing the 3´-UTR of MNSV-N (264/3´-N) was able to multiply in both melon varieties, the deletion mutant (264/3´-Δ55-N), although viable in susceptible melon, lost this capacity in resistant melon. From this result it can be concluded that the recombined sequence is necessary for resistance breaking. As expected, since the 3´-UTR sequence is expected to contain a diversity of functional elements (for example involved in replication (Zhang & Simon, 2003; Wu *et al.*, 2009)), a chimeric virus with only the recombined sequence at the 3´-UTR (264/3´-N65) was not viable neither in melon plants (Fig. 10a) nor in protoplasts of any of the two varieties (not shown).

3.4. The recombined sequence is a 3´-cap-independent translational enhancer (3´-CITE)

In a previous study, a 44-nt fragment of the 3´-UTR sequence of avirulent isolates had been shown to be essential for viral multiplication, functioning as a 3´-CITE in susceptible melon (Truniger *et al.*, 2008). This 3´-CITE sequence (nucleotides 142-186) was found to be highly conserved in this new isolate, with only one nucleotide difference (Fig. 9b, grey box). Thus, MNSV-N contained the avirulent 3´-CITE, that was not functional in resistant melon, and not, as might be expected from localisation of the virulence determinant in the 3´-UTR, the different 3´-CITE of MNSV-264 (functional in both susceptible and resistant melon) (Truniger *et al.*, 2008). These and the above data suggested that the 3´-UTR of MNSV-N could possibly contain a second new 3´-CITE, functional in resistant melons, possibly located in the recombined region.

Therefore, we studied the role of the 3´-UTR of MNSV-N in cap-independent translation initiation. For this, we flanked the firefly luciferase gene (*luc*) with the 5´- and/or 3´-UTRs of this new isolate and studied the *in vivo* translation efficiency in

susceptible and resistant melon protoplasts. In susceptible as well as in resistant melon, the 5´-UTR of MNSV-N alone, like the 3´-UTR, was not able to enhance cap-independent translation (Fig. 11, first and eight bar above (susceptible) and below (resistant), respectively), while the presence of both UTRs of MNSV-N resulted in a > 40-fold increase of the translation efficiency (third bar). Thus, the 3´-UTR of MNSV-N was able to enhance cap-independent translation to levels similar to those of the 3´-UTRs of MNSV-Mα5 in susceptible melon and MNSV-264 in resistant melon.

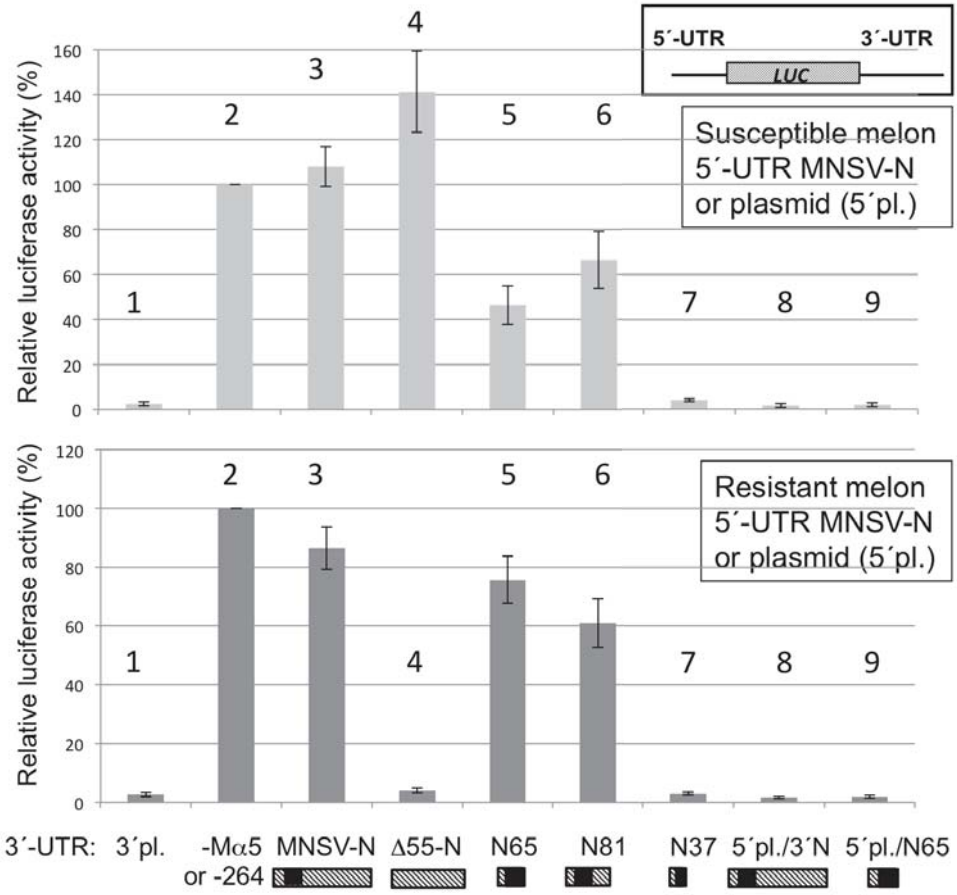

Figure 11. The recombined sequence is a 3´-CITE that is functional in resistant melon. *In vivo* cap-independent translation assayed in melon protoplasts. Each bar represents the relative luciferase activity (corresponding to the translation efficiency) obtained with a construct (as indicated below) either in susceptible (upper part) or resistant (lower part) melon protoplasts. The reference values are the activity obtained with the construct of the *luc* gene flanked by both 5´- and 3´-UTRs either of MNSV-Mα5 in susceptible (=100 %; second bar - upper graph), or of MNSV-264 in resistant melon protoplasts (=100 %; second bar - lower graph). All constructs, with exception of these two positive controls and the two constructs in the last two bars (that contain plasmid sequence at the 5´-end (5´pl.)), contained the 5´-UTR of MNSV-N and the different 3´ends indicated below. 3´-UTRs: 3´pl. = plasmid sequence; Mα5 or 264 = 3´-UTR of MNSV-Mα5 or -264; MNSV-N or 3´N = 3´-UTR of MNSV-N; Δ55N = 3´-UTR of MNSV-N with the 55 nt of insertion deleted; N65/81/37 = first 65/81/37 nt of the 3´-UTR of MNSV-N, respectively. Error bars are +/-.

In order to determine if the 55-nt insertion was involved in translational control, this sequence was deleted from the 3´-UTR of MNSV-N. The shortened 3´-UTR (Δ55-N) still enhanced cap-independent translation in susceptible melon, even increasing its activity, but was unable to facilitate translation in resistant melon (fourth bar). These results suggested that the shortened 3´-UTR of MNSV-N still contained a 3´-CITE that is functional in susceptible, but not in resistant melon. Thus, the recombined sequence was necessary for cap-independent translation.

In order to determine if the extra sequence in the MNSV-N 3'-UTR is sufficient for cap-independent translation in resistant melon, three different constructs were tested containing the first 81, 65 or 37 nt of the 3´-UTR of MNSV-N together with its 5´-UTR flanking the *luc*. The two longer fragments, N65 and N81, enhanced translation in both susceptible and resistant melon (bars 5 and 6, respectively), while the shorter one, N37, lost this capacity (bar 7). These results suggested that the first 65 nt of the 3´-UTR of MNSV-N, that are highly similar to the first 65 nt of the 3´-UTR of CABYV-Xinjiang, were sufficient to function as a 3´-CITE that is active in susceptible and in resistant melon. The activity of this 3´-CITE was dependent on the presence of the 5´-UTR *in cis*; no translation activity controlled by the 3´-UTR of MNSV-N (3´N) or only its first 65 nt (N65) was found in the absence of the 5´-UTR (bars 8/9).

3.5. The newly identified 3´-CITE belongs to a new structural class of 3´-CITEs and functions in the absence of eIF4E

The prediction of the secondary structure of the first 65 nt of the 3´-UTR of MNSV-N obtained by Mfold was different to the previously described 3´-CITEs, suggesting that this was a new class of translation enhancer element formed by two stem-loops (Fig. 7b). Thus, the secondary structure of this new 3´-CITE in solution was studied by Selective 2´-Hydroxyl Acylation analyzed by Primer Extension (SHAPE)(Wilkinson *et al.* 2006a) using benzoyl cyanide (BzCN) (Mortimer & Weeks 2008). This chemical quickly modifies flexible and therefore possibly single-stranded nucleotides in a sequence-independent manner, forming 2´-O-adducts that block reverse transcriptase. The RNA segment used in this structure probing assay was

inserted into the SHAPE cassette described in (Wang *et al.* 2010) and the functionality of the 3'-CITE in this context was confirmed by *trans*-inhibition assay (Fig. 12) using as reporter mRNA the luciferase construct with the 5´- and 3´-UTR of MNSV-Mα5 flanking the *luc* gene (Truniger *et al.* 2008b). Both the MNSV-N 3´-CITE alone and in the context of the cassette used for SHAPE analysis inhibited translation of reporter mRNA when added in 200-fold excess indicating structural and functional integrity of the 3'CITE in the SHAPE cassette.

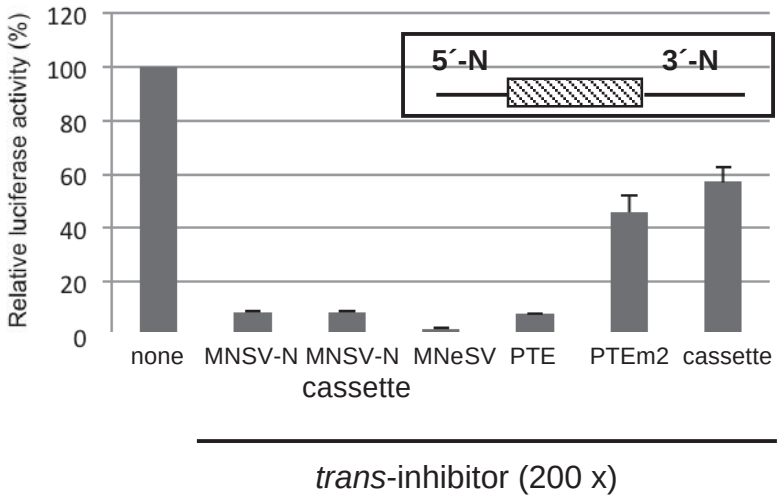

Figure 12. *Trans*-inhibition assays testing functionality of MNSV-N 3´-CITE in SHAPE cassette. Relative luciferase activity of 8 nM 5´-N-luc-3´-N construct (*luc* gene flanked by 5´- and 3´-UTR of *Melon necrotic spot virus* isolate MNSV-N) in wheat germ extract competed *in trans* with a 200-fold excess of 3´-CITE RNAs (Wang *et al.*, 2011).

Primer extension after modification with BzCN revealed two highly modifiable regions forming the loops of two stem-loop structures (Fig. 13), consistent with the structure predicted by Mfold. The first stem-loop (SL1) consists of 34 nucleotides (3990-4023), including two highly reacting bases U4003 and G4004 and one with weak activity, G4006, in the loop. The second stem-loop (SL2) is formed by 25 nucleotides with four strongly modified nucleotides located in the loop (C4033, G4036, U4037 and C4038) and three nucleotides with weak activity (A4040, A4041, U4043). Magnesium titration experiments showed that the folding of this structure was independent of this divalent cation. Thus, the 3´-CITE folded into two helices protruding from a central hub in magnesium independent manner. This structure was supported by the nucleotide variations found in the 3´-UTR sequences of the known Asiatic-type CABYV isolates

(light blue arrows Fig. 13b), since most of them were located in the unpaired loop regions L1 or L2. Additionally, two of the five variations that appeared in base-paired regions did not disrupt base-pairing (orange arrows). The other three possibly had little effect on the structure since they were located in the base of the stems (grey arrows)(see alignment Fig. 9).

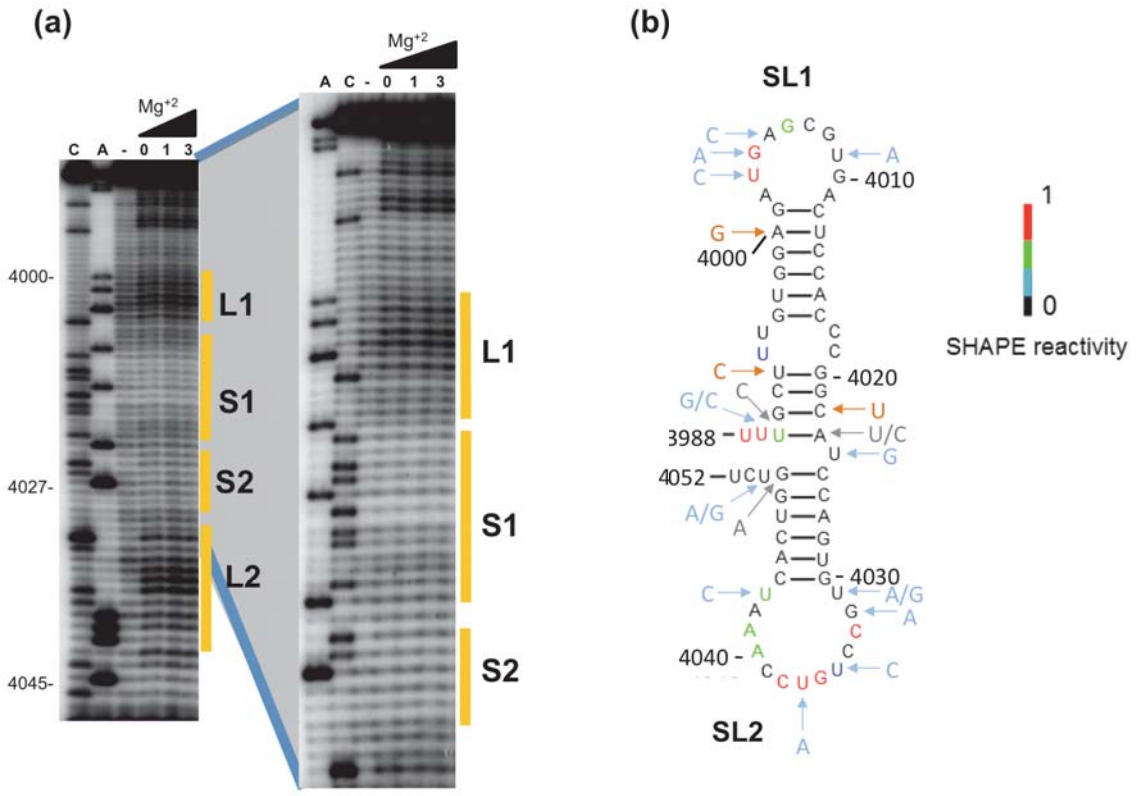

Figure 13. Secondary structure probing of the new 3´-CITE. (**a**) Structure probing by SHAPE of the first 65 nt of the 3´-UTR of *Melon necrotic spot virus* isolate MNSV-N, including the new 3´-CITE. Primer extension products separated on denaturing PAGE of RNA treated (forth to sixth lane (concentrations of Mg^{2+} (mM) added are indicated above, (0/1/3)) or untreated (third lane, (-)) with BzCN. The sequencing ladder was generated by reverse transcription of unmodified RNA in the presence of dideoxyCTP (ddCTP) (lane C) or ddATP (lane A). Positions of A4000, A4027 and A4045 are indicated on the left. The positions in the PAGE corresponding to the stems (S1/S2) and loops (L1/L2) of stem-loop structures, SL1 and SL2, are marked at the right. (**b**) Secondary structure of new 3´-CITE probed in panel A. SHAPE reactivity of nucleotides superimposed on secondary structure predicted by Mfold. Color-coded bases indicate the levels of BzCN modification, with warmer color indicating greater modification (inset). The nucleotide variations found with respect to the 3´-UTRs of the Asiatic-type *Cucurbit aphid-borne yellows virus* (CABYV) isolates are indicated by arrows: in orange for nucleotide variations that maintain the secondary structure in double-stranded regions since they do not disrupt base-pairing, in light blue nucleotide variations located in single-stranded regions, arrows in grey indicate three sequence variations in double-stranded regions predicted to disrupt base-pairing.

Data on resistance breaking suggested that the new 3´-CITE could function either with the different eIF4E variants expressed by susceptible or resistant melon, or independently of eIF4E. To learn if this new 3´-CITE was eIF4E-dependent, its activity in melon protoplasts of a previously described eIF4E knock-down line was studied (Rodríguez-Hernández *et al.*, 2012). Through expression of a hairpin construct targeting and thus silencing melon *eIF4E* its expression had been shown to be reduced more than 6-fold. As can be seen in Fig. 14(a), low cap-independent translation activity was obtained for the construct with 5´- and 3´-UTRs of MNSV-Mα5 flanking the *luc* gene, in agreement with the eIF4E-dependence of its 3´-CITE (Truniger *et al.*, 2008; Rodríguez-Hernández *et al.*, 2012). On the other hand, the construct with both wild-type MNSV-N UTRs and even with only the first 65 nt of the 3´-UTR (N65) resulted in 8-10 fold higher translation activity. This result shows that translation controlled by the new 3´-CITE in melon can occur in the absence of *Cm*-eIF4E. Consequently, MNSV-N was able to infect eIF4E-silenced melon plants (Fig. 14b).

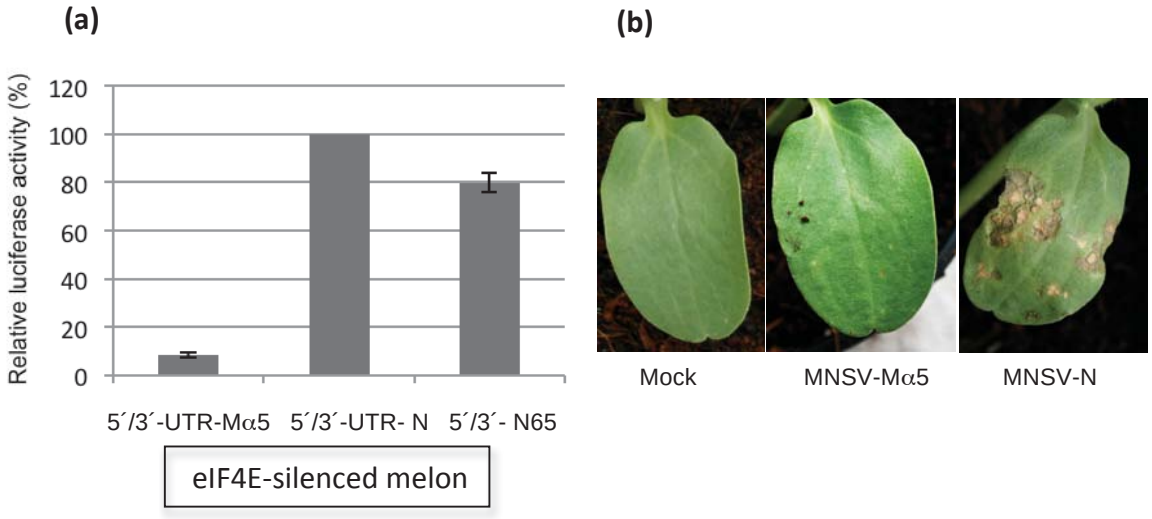

Figure 14. Dependence on eIF4E of the new 3´-CITE. (**a**) Translation efficiency of *luc* gene flanked by 5´- plus 3´-UTR of *Melon necrotic spot virus* (MNSV) isolates MNSV-Mα5 (5´/3´-Mα5) or of MNSV-N (5´/3´-N; defined as 100 %) or 5´-UTR plus only the first 65 nt of 3´-UTR of MNSV-N (5´/3´-N65) in melon protoplasts from eIF4E-silenced transgenic melon. Error bars are +/-. (**b**) Cotyledons of eIF4E-silenced melon plants at 9 days after inoculation with MNSV-Mα5 or -N. Typical strong necrosis indicates multiplication of MNSV-N in these plants. Very small single necrotic lesions appear with MNSV-Mα5, suggesting that the residual eIF4E expression (about 20 %) still allows some, but strongly reduced, multiplication of this isolate (Rodríguez-Hernández *et al.*, 2012)

4. DISCUSSION

In this study we provide the first direct proof for the hypothesis that 3´-CITEs are in nature modular transferrable RNA elements and show that this phenomenon can be associated with an advantage for the recombinant virus created. We have characterized a new 3´-CITE in MNSV, the third characterized in this virus. This new 3´-CITE gives the natural recombinant virus the capacity to infect resistant melon cultivars (*nsv/nsv* genotype). It was most probably acquired through an exquisitely specific recombination event, leading to the acquisition of only the translational enhancer element; the parental viruses can be clearly identified among still existing viruses, an Asiatic isolate of CABYV (CABYV-Xinjiang) and MNSV. Thus, we call this new class of 3' CITE, the CABYV-Xinjiang-like translation element, short CXTE. The first two 3´-CITEs characterized in MNSV were the one present in all avirulent MNSV isolates (and highly conserved), unable to infect the resistant melon, and that of MNSV-264, able to overcome this resistance (Truniger *et al.*, 2008). The 3´-CITE of MNSV-264 was also proposed to have been acquired through recombination, but in this isolate the complete 3´-UTR was accepted from an unknown heterologous source (Nieto *et al.*, 2011).

Modularity and transferability of 3´-CITEs have been proposed before, because different types of 3´-CITEs can be found in a single genus and the same type of 3´-CITE appears in different virus genera (Nicholson & White, 2011). A first direct, but artificial, evidence came from the viability of engineered chimeric viruses: the Y-shaped 3´-CITE from CIRV was exchanged with the I-shaped one from MNeSV or the PTE-like 3´-CITE of *Cucumber leaf spot virus* (CLSV). The results also supported the modularity of 3´-CITEs (Nicholson *et al.*, 2013). In these experiments, the 3´-CITEs exchanged belonged to viruses from the same family as CIRV, the *Tombusviridae*. Additionally, all three 3´-CITEs are known to depend on eIF4E/eIF4G for proper functioning (Nicholson *et al.*, 2010; Wang *et al.*, 2011; Nicholson *et al.*, 2013). However, in the case of the natural resistance-breaking MNSV isolates, MNSV-264 and MNSV-N, the possible recombination events occurred between viruses of different families, these being identified as *Tombusviridae* and *Luteoviridae* for MNSV-N. Additionally, the 3´-CITEs of these two isolates have been shown to function in the absence of eIF4E, in contrast to

the 3´-CITEs of avirulent MNSVs (Fig. 14 and (Rodríguez-Hernández *et al.*, 2012)). These results suggest that 3´-CITEs, when interchanged, can be active in very similar (belonging to the same family) and very heterologous (belonging to different families) viral genomes, even if they recruit different translation initiation factors for their activity.

Our results also confirm that eIF4E-mediated resistance breaking by MNSV is controlled by the host-specificity of its 3´-CITE. While the 3´-CITEs of the avirulent isolates are not functional in resistant melon, the 3´-CITEs of MNSV-N and -264 are active in this melon genotype. Remarkably, the previously identified MNSV 3´-CITEs (from avirulent isolates and MNSV-264) have both been predicted to be I-shaped (Truniger *et al.*, 2008; Nicholson *et al.*, 2010). In contrast, the new 3´-CITE described here has a double stem-loop structure that is different from all 3´-CITEs described to date (Miller *et al.*, 2007; Nicholson & White, 2011). The *in vivo* translation experiments and 3´-UTR sequence alignment analyses lead to the conclusion that the 3´-UTR of MNSV-N contains two 3´-CITEs: one is functional only in susceptible melons and the other functional in both susceptible and resistant types. To our knowledge the existence of more than one 3´-CITE with varying mechanisms and different host-specificity in the same viral genome has not been observed before. The 3'-UTR of PEMV RNA2 has also been reported to contain two 3' CITEs, a PTE-like CITE and a T-shaped CITE like that of *Turnip crinkle virus*, but the effect, if any, of these two CITEs on host-specificity is unknown (Gao *et al.*, 2012).

How would cap-independent translation occur in the presence of both the CXTE and the I-shaped 3´-CITE? In susceptible melon both 3´-CITEs would be active, while in resistant melon and in absence of eIF4E only the CXTE would be functional. We have shown that both 3´-CITEs depend on the presence of the 5´-UTR of MNSV-N *in cis* for their activity (Fig. 11) (Truniger *et al.*, 2008). Long-distance RNA-RNA interactions have been shown to be essential for translation, transcription and replication of viral RNAs (Wu *et al.*, 2009). Thus, RNA circularization in the case of MNSV-N would occur through the I-shaped 3´-CITE/5´-UTR sequence complementarity (V. Truniger, unpublished results). In the chimeric virus 264/3´-N the same interaction of this 3´-CITE with the 5´-UTR of MNSV-264 would occur, since the 5´-UTR sequences of these two

isolates are highly conserved (the first 24 nt, containing the complementary sequence stretch, are even identical) (Fig. 15). But interestingly, the CXTE of MNSV-N alone also showed 5´-UTR dependent *in vivo* cap-independent translation enhancing capacity in melon protoplasts (N65; Fig. 11). This suggests an additional mechanism for viral genome circularization occurring during translation controlled by the CXTE. We are currently studying this aspect. Also alternative mechanisms for the circularization of viral genomes have been described (Stupina *et al.*, 2008; Stupina *et al.*, 2011; Iwakawa *et al.*, 2012).

```
5-264     GGATTACTCTAGCCGGATCCCCGACTCTCTTGTTTCTGTAAGTTAGTTCGTGTATTGGTC 60
5-MNSV-N  GGATTACTCTAGCCGGATCCCCGATTCTCTTGTTTCTGTAAGTGAGTTCGTGTATTGATC 60
          ************************ ****************** ************* **
5-264     ATCTGTCTTGATCAGTATAGGTTAGCA 87
5-MNSV-N  GTCTGTCTTAATCAATATAGGTTAGCA 87
           ******** **** ************
```

Figure 15. Sequence alignment of the 5´-UTRs of isolates MNSV-264 and MNSV-N. Alignment performed with ClustalX. Genbank accession of *Melon necrotic spot virus* isolate MNSV-264 is AY330700. Identical nucleotides are marked below with an asterisk.

Imprints of RNA recombination can be found within the genomes of natural populations of plant viruses. RNA recombination seems to be particularly frequent among members of the family *Potyviridae*, the largest family of plant RNA viruses, but also members of the family *Luteoviridae* seem to be very recombination prone, and they have been proposed to have emerged from intergeneric recombination events. Thus, several recombinants between poleroviruses and luteoviruses have been described (e.g. Moonan *et al.*, 2000; Domier *et al.*, 2002). These two genera have been proposed to have emerged from a common ancestor and diverged into different genera by recombination with a sobemovirus and a tombusvirus, respectively (Miller *et al.*, 2002; Pagán & Holmes, 2010). Also stable intergeneric recombinants between polero- and sobemovirus yielded to the new virus species *Poinsettia latent virus* (PnLV, polemovirus (aus dem Siepen *et al.*, 2005)). Some luteoviruses have even been suggested to have acquired host-chloroplast sequences (Mayo & Jolly, 1991).

Our results strongly suggest the occurrence of a recombination event between a polerovirus and a carmovirus, viruses belonging to different families. This is supported by the very high nucleotide sequence identity of the fragment inserted at the 5´-end of the 3´-UTR of MNSV-N with the first 60 nt of the 3´-UTR of CABYV and supported by recombination-detecting algorithms. The presence of MNSV and CABYV co-infecting field-grown cucurbit plants makes this recombination event plausible (Kassem *et al.*, 2007). In this case, recombination has resulted in a broadened host range, supporting the studies that indicate that recombination may assist host switching (García-Arenal & McDonald, 2003; Chare & Holmes, 2006; Codoñer & Elena, 2008; Sztuba-Solińska *et al.*, 2011) The analysis by García-Arenal and McDonald (García-Arenal & McDonald, 2003) on the durability of different resistance genes against different viruses showed that pathosystems for which no resistance-breaking strains had been reported were those in which recombinants or reassortants were relatively rare. This result suggested that viruses that undergo genetic exchange were more prone to generating resistance-breaking strains than those that do not. The new MNSV isolate studied here is one example. In this case, the recombination event is the direct reason for resistance-breaking. This is one of the first rare recombination events in a plant RNA virus that have been proven to result in resistance-breaking or host switching. The adaptation of the multipartite virus CMV to the host alstroemeria through recombination between its RNAs has been described earlier (Chen *et al.*, 2002), but in this case the recombinant virus does not infect an otherwise non-susceptible host.

The acquisition of the host-switching ability by a virus may impose a reduction in its fitness in the original host, since the new host may impose different selective requirements (Elena *et al.*, 2011). While this was the case for MNSV-264, the first *nsv* resistance-breaking isolate described, no reduced virulence with the original host has been observed for MNSV-N. Under field conditions, MNSV-264 was not able to become prevalent in MNSV populations, as concluded from the inability to identify it again (M.A. Aranda, unpublished results) (Diaz *et al.*, 2004). Our analyses indicate that MNSV-N is slightly less virulent than MNSV-Al in susceptible melons, but its virulence is definitely higher than that of MNSV-264 in resistant melons. These results suggest that MNSV-N may be a more important threat for melon cultivation than MNSV-264 was,

especially since the use of resistant melon cultivars is increasing (M.A. Aranda, unpublished observations).

Interestingly, the MNSV-264 3'-UTR has <50% nucleotide sequence identity to its counterpart in the other avirulent MNSV strains sequenced to date, whereas the coding regions of all strains show >85% identity (Diaz *et al.*, 2004). In this case, the different 3´-UTR of MNSV-264, gave this isolate the capacity to overcome the melon resistance (Diaz *et al.*, 2004), but this reduced virulence in melon. On the other hand, the precise insertion into the MNSV-N genome of only the 3´-CITE sequence that is functional in resistant melon, did not affect the virulence of this isolate.

In conclusion, we have provided the first direct proof that 3´-CITEs consist of modular elements that can be transferred among viral species most probably through RNA recombination, interacting differentially with host elements to confer host specificity and giving the virus the possibility to infect new hosts.

5. REFERENCES

aus dem Siepen M., Pohl J.O., Koo B.-J., Wege C. and Jeske H. 2005. Poinsettia latent virus is not a cryptic virus, but a natural polerovirus–sobemovirus hybrid. *Virology* **336**(2): 240-250.

Bujarski J.J. 2013. Genetic recombination in plant-infecting messenger-sense RNA viruses: overview and research perspectives. *Frontiers in Plant Science* **4**.

Codoñer F.M and Elena S.F. 2008. The promiscuous evolutionary history of the family Bromoviridae. *Journal of General Virology* **89**(7): 1739-1747.

Chao L. and Matthews C. 1992. Mueller´s ratchet and the advantage of sex in the RNA virus f6. *Evolution* **46**: 289-299.

Chao L. and Trang T. 1997. The advantege of sex in the RNA phage f6. *Genetics* **14**: 953-959.

Chare E.R. and Holmes E.C. 2006. A phylogenetic survey of recombination frequency in plant RNA viruses. *Archives of Virology* **151**(5): 933-946.

Chen Y.-K., Goldbach R. and Prins M. 2002. Inter- and Intramolecular Recombinations in the Cucumber Mosaic Virus Genome Related to Adaptation to Alstroemeria. *Journal of Virology* **76**(8): 4119-4124.

Das R., Laederach A., Pearlman S.M., Herschlag D. and Altman R.B. 2005. SAFA: Semi-automated footprinting analysis software for high-throughput quantification of nucleic acid footprinting experiments. . *RNA* **11**: 344-354.

Diaz-Pendon J., Fernandez-Munoz R., Gomez-Guillamon M. and Moriones E. 2005. Inheritance of resistance to Watermelon mosaic virus in Cucumis melo that

impairs virus accumulation, symptom expression, and aphid transmission. *Phytopathology* **95**: 840 - 846.

Díaz J.A., Bernal J.J., Moriones E. and Aranda MA. 2003. Nucleotide sequence and infectious transcripts from a full-length cDNA clone of the carmovirus Melon necrotic spot virus. *Archives of Virology* **148**(3): 599-607.

Diaz JA, Nieto C, Moriones E, Aranda MA. 2002. Spanish Melon necrotic spot virus isolate overcomes the resistance conferred by the recessive *nsv* gene of melon. *Plant Disease* **86**(6): 694-694.

Diaz JA, Nieto C, Moriones E, Truniger V, Aranda MA. 2004. Molecular characterization of a Melon necrotic spot virus strain that overcomes the resistance in melon and nonhost plants. *Molecular Plant-Microbe Interactions* **17**(6): 668-675.

Díez J, Marcos J, Pallás V 1998. Carmovirus isolation and RNA extraction. In: Foster G, Taylor S eds. *Plant Virology Protocols*: Humana Press, 211-217.

Dolja VV, Kreuze JF, Valkonen JPT. 2006. Comparative and functional genomics of closteroviruses. *Virus Research* **117**(1): 38-51.

Domier LL, McCoppin NK, Larsen RC, D'Arcy CJ. 2002. Nucleotide sequence shows that Bean leafroll virus has a Luteovirus-like genome organization. *Journal of General Virology* **83**(7): 1791-1798.

Domingo E. 2010. Mechanisms of viral emergence. *Veterinary Research* **41**(6): 38.

Dreher TW, Miller WA. 2006. Translational control in positive strand RNA plant viruses. *Virology* **344**(1): 185-197.

Elena SF, Bedhomme S, Carrasco P, Cuevas JM, de la Iglesia F, Lafforgue G, Lalić J, Pròsper À, Tromas N, Zwart MP. 2011. The evolutionary genetics of emerging plant RNA viruses. *Molecular Plant-Microbe Interactions* 24(3): 287-293.

Escriu F, Fraile A, García-Arenal F. 2007. Constraints to genetic exchange support gene coadaptation in a tripartite RNA virus. *PLoS Pathogens* **3**(1): e8.

Fernández-Cuartero B, Burgyan J, Aranda MA, Salanki K, Moriones E, García-Arenal F. 1994. Increase in the relative fitness of a plant virus RNA associated with its recombinant nature. *Virology* **203**: 373-377.

Gao F, Kasprzak W, Stupina VA, Shapiro BA, Simon AE. 2012. A ribosome-binding, 3' translational enhancer has a T-shaped structure and engages in a long-distance RNA-RNA interaction. *Journal of Virology* **86**(18): 9828-9842.

García-Arenal F, McDonald BA. 2003. An analysis of the durability of resistance to plant viruses. *Phytopathology* **93**(8): 941-952.

Genoves A., Navarro J.A. and Pallas V. 2006. Functional analysis of the five melon necrotic spot virus genome-encoded proteins. *Journal of General Virology* **87**(8): 2371-2380.

Gomez P., Sempere R.N., Elena S.F. and Aranda M.A. 2009. Mixed Infections of Pepino Mosaic Virus Strains Modulate the Evolutionary Dynamics of this Emergent Virus. *Journal of Virology* **83**(23): 12378-12387.

Gosalvez-Bernal B., Genoves A., Antonio Navarro J., Pallas V. and Sanchez-Pina M.A. 2008. Distribution and pathway for phloem-dependent movement of Melon necrotic spot virus in melon plants. *Molecular Plant Pathology* **9**(4): 447-461.

Holmes E.C. 2008. Evolutionary history and phylogeography of human viruses. *Annual Review of Microbiology* **62**(1): 307-328.

Holmes EC. 2009. The evolutionary genetics of emerging viruses. *Annu. Rev. Ecol. Evol. Syst.* **40**: 353-372.

Iwakawa H.-O., Tajima Y., Taniguchi T., Kaido M., Mise K., Tomari Y., Taniguchi H. and Okuno T. 2012. Poly(A)-binding protein facilitates translation of an uncapped/nonpolyadenylated viral RNA by binding to the 3′ untranslated region. *Journal of Virology* **86**(15): 7836-7849.

Jaag H.M. and Nagy P.D. 2010. The combined effect of environmental and host factors on the emergence of viral RNA recombinants. *PLoS Pathogens* **6**(10): e1001156.

Jegouic S., Joffret M.-L., Blanchard C., Riquet F.B., Perret C., Pelletier I., Colbere-Garapin F., Rakoto-Andrianarivelo M. and Delpeyroux F. 2009. Recombination between polioviruses and co-circulating Coxsackie A viruses: role in the emergence of pathogenic vaccine-derived polioviruses. *PLoS Pathogens* 5(5): e1000412.

Juarez M., Legua P., Mengual C.M., Kassem M.A., Sempere R.N., Gómez P., Truniger V. and Aranda M.A. 2013. Relative incidence, spatial distribution and genetic diversity of cucurbit viruses in eastern Spain. *Annals of Applied Biology* **162**: 362-370.

Kassem M., Sempere R., Juarez M., Aranda M. and Truniger V. 2007. Cucurbit aphid-borne yellows virus Is Prevalent in Field-Grown Cucurbit Crops of Southeastern Spain. *Plant Disease* **91**: 232 - 238.

Kneller E.L.P., Rakotondrafara A.M. and Miller W.A. 2006. Cap-independent translation of plant viral RNAs. *Virus Research* **119**(1): 63-75.

Kraft J.J., Treder K., Peterson M.S. and Miller W.A. 2013. Cation-dependent folding of 3′ cap-independent translation elements facilitates interaction of a 17-nucleotide conserved sequence with eIF4G. *Nucleic Acids Research* **41**(5): 3398-3413.

Mallor C., Luis-Arteaga M., Alvarez J.M., Montaner C. and Floris E. 2006. Resistance to Melon necrotic spot virus in Cucumis melo L.. 'Doublon' artificially inoculated by the fungus vector Olpidium bornovanus. *Crop Protection* **25**(5): 426-431.

Martin D.P., Lemey P., Lott M., Moulton V., Posada D. and Lefeuvre P. 2010. RDP3: a flexible and fast computer program for analyzing recombination. *Bioinformatics* **26**: 2462-2463.

Mayo M.A. and Jolly C.A. 1991. The 5′-terminal sequence of potato leafroll virus RNA: evidence of recombination between virus and host RNA. *Journal of General Virology* **72**(10): 2591-2595.

Miller W.A., Liu S. and Beckett R. 2002. Barley yellow dwarf virus: Luteoviridae or Tombusviridae? *Molecular Plant Pathology* **3**(4): 177-183.

Miller W.A., Wang Z. and Treder K. 2007. The amazing diversity of cap-independent translation elements in the 3′-untranslated regions of plant viral RNAs. *Biochemical Society Transactions* **035**(6): 1629-1633.

Miller W.A. and White K.A. 2006. Long-distance RNA-RNA interactions in plant virus gene expression and replication. *Annual Review of Phytopathology* **44**(1): 447-467.

Moonan F., Molina J. and Mirkov T.E. 2000. Sugarcane yellow leaf virus: An emerging virus that has evolved by recombination between luteoviral and poleroviral ancestors. *Virology* **269**(1): 156-171.

Mortimer S.A. and Weeks K.M. 2008. Time-Resolved RNA SHAPE Chemistry. *Journal of the American Chemical Society* **130**(48): 16178-16180.

Moury B., Desbiez C., Jacquemond M. and Lecoq H. 2006. Genetic diversity of plant virus populations: towards hypothesis testing in molecular epidemiology. In: Karl Maramorosch AJS, Thresh JM eds. *Advances in Virus Research*: Academic Press, 49-87.

Nicholson B.L. and White K.A. 2011. 3′ Cap-independent translation enhancers of positive-strand RNA plant viruses. *Current Opinion in Virology* **1**(5): 373-380.

Nicholson B.L., Wu B., Chevtchenko I. and White K.A. 2010. Tombusvirus recruitment of host translational machinery via the 3′ UTR. *RNA* **16**(7): 1402-1419.

Nicholson B.L., Zaslaver O., Mayberry L.K., Browning K.S. and White K.A. 2013. Tombusvirus Y-shaped translational enhancer forms a complex with eIF4F and can be functionally replaced by heterologous translational enhancers. *Journal of Virology* **87**(3): 1872-1883.

Nieto C., Morales M., Orjeda G., Clepet C., Monfort A., Sturbois B., Puigdomenech P., Pitrat M., Caboche M., Dogimont C., Garcia-Mas J., Aranda M.A. and Bendahmane A. 2006. An eIF4E allele confers resistance to an uncapped and non-polyadenylated RNA virus in melon. *The Plant Journal* **48**(3): 452-462.

Nieto C., Rodríguez-Moreno L., Rodríguez-Hernández A.M., Aranda M.A. and Truniger V. 2011. Nicotiana benthamiana resistance to non-adapted Melon necrotic spot virus results from an incompatible interaction between virus RNA and translation initiation factor 4E. *The Plant Journal* **66**(3): 492-501.

Ohshima K., Tomitaka Y., Wood J.T., Minematsu Y., Kajiyama H., Tomimura K. and Gibbs A.J. 2007. Patterns of recombination in turnip mosaic virus genomic sequences indicate hotspots of recombination. *Journal of General Virology* **88**(1): 298-315.

Pagán I. and Holmes E.C. 2010. Long-term evolution of the Luteoviridae: time scale and mode of virus speciation. *Journal of Virology* **84**(12): 6177-6187.

Parisien M. and Major F. 2008. The MC-Fold and MC-Sym pipeline infers RNA structure from sequence data. *Nature* **452**: 51-55.

Rodríguez-Hernández A.M., Gosalvez B., Sempere R.N., Burgos L., Aranda M.A. and Truniger V. 2012. Melon RNA interference (RNAi) lines silenced for Cm-eIF4E show broad virus resistance. *Molecular Plant Pathology* **13**(7): 755-763.

Sambrook J. and Russell D.W. 2001. Molecular Cloning: A Laboratory Manual. 3rd ed. Cold Spring Harbor Laboratory Press, Cold Spring Harbor, N.Y. U.S.A.

Shen R. and Miller W.A. 2004. The 3' untranslated region of Tobacco necrosis virus RNA contains a Barley yellow dwarf virus-like cap-independent translation element. *Journal of Virology* **78**(9): 4655-4664.

Simon A.E. and Miller W.A. 2013. 3′ cap-independent translation enhancers of plant viruses. *Annual Review of Microbiology* **67**(1): 21-42.

Stupina V., Meskauskas A., McCormack J., Yingling Y., Shapiro B., Dinman J. and Simon A. 2008. The 3' proximal translational enhancer of Turnip crinkle virus binds to 60S ribosomal subunits. *RNA* **14**(11): 2379-2393.

Stupina V.A., Yuan X., Meskauskas A., Dinman J.D. and Simon A.E. 2011. Ribosome bnding to a 5' translational enhancer is altered in the presence of the 3' untranslated region in cap-independent translation of Turnip crinkle virus. *Journal of Virology* **85**(10): 4638-4653.

Sztuba-Solińska J., Urbanowicz A., Figlerowicz M. nad Bujarski J.J. 2011. RNA-RNA recombination in plant virus replication and evolution. *Annual Review of Phytopathology* **49**(1): 415-443.

Treder K., Pettit Kneller E.L., Allen E.M., Wang Z., Browning K.S. and Miller W.A. 2008. The 3' cap-independent translation element of Barley yellow dwarf virus binds eIF4F via the eIF4G subunit to initiate translation. *RNA* **14**(1): 134-147.

Truniger V, Nieto C, González-Ibeas D, Aranda M. 2008. Mechanism of plant eIF4E-mediated resistance against a Carmovirus (*Tombusviridae*): cap-independent translation of a viral RNA controlled *in cis* by an (a)virulence determinant. *The Plant Journal* **56**(5): 716-727.

van Regenmortel M.H.V., Fauquet C.M., Bishop D.H.L., Carstens E.B., Estes M.K., Lemon S.M., Maniliff J., Mayo M.A., McGeoch D.J., Pringle C.R. and Wickner R.B. 2000. *Virus Taxonomy:Seventh report of the International Committee on Taxonomy of Viruses. Academic Press, San Diego.*

Wang Z., Kraft J.J., Hui A.Y. and Miller W.A. 2010. Structural plasticity of Barley yellow dwarf virus-like cap-independent translation elements in four genera of plant viral RNAs. *Virology* **402**(1): 177-186.

Wang Z., Parisien M., Scheets K. and Miller W.A. 2011. The cap-binding translation initiation factor, eIF4E, binds a pseudoknot in a viral cap-independent translation element. *Structure* **19**(6): 868-880.

Wang Z., Treder K. and Miller W.A. 2009. Structure of a viral cap-independent translation element that functions via high affinity binding to the eIF4E subunit of eIF4F. *Journal of Biological Chemistry* **284**(21): 14189-14202.

Wilkinson K.A., Merino E.J. and Weeks K.M. 2006. Selective 2[prime]-hydroxyl acylation analyzed by primer extension (SHAPE): quantitative RNA structure analysis at single nucleotide resolution. *Nat. Protocols* **1**(3): 1610-1616.

Wu B., Pogany J., Na H., Nicholson B.L., Nagy P.D. and White K.A. 2009. A discontinuous RNA platform mediates RNA virus replication: building an integrated model for RNA–based regulation of viral processes. *PLoS Pathogens* **5**(3): e1000323.

Zhang G. and Simon A.E. 2003. A multifunctional Turnip crinkle virus replication enhancer revealed by in vivo functional SELEX. *Journal of Molecular Biology* **326**(1): 35-48.

Chapter 2

Analysis of the interacting partners eIF4F and 3´-CITE required for MNSV cap-independent translation

1. INTRODUCTION

Translation initiation is a rate-limiting step that is tightly regulated by the availability of initiation factors. In canonical eukaryotic translation initiation, recognition of the mRNA by the translation machinery is facilitated through the binding of the 5' m^7G cap structure to the eukaryotic translation initiation factor (eIF) 4E, which is part of the eIF4F complex (Marcotrigiano *et al.* 1997; Gross *et al.* 2003). In mammals, eIF4F is a heterodimer composed of the cap-binding protein, eIF4E, the multifunctional scaffolding protein, eIF4G, and the helicase, eIF4A. In plants, eIF4F is a heterodimer consisting of eIF4E and eIF4G but eIF4A is not part of the complex (Hinnebusch & Lorsch 2012). EIF4G binds simultaneously to eIF4E and the poly(A)binding protein (PABP), which interacts with the poly(A) tail (Aitken & Lorsch 2012), thus, mRNA is circularized by a protein bridge (Gallie 2002). EIF4G also associates with eIF3, recruiting the 40S subunit of the ribosome and initiating the scanning of the mRNA in the 5´ to 3´direction (Jackson *et al.* 2010; Park *et al.* 2011).

Many positive-strand RNA viruses do not possess a 5´cap structure and/or a 3´poly(A) tail but instead have evolved a variety of non-canonical mechanisms to directly recruit eIFs to the viral RNA for translation initiation (Kneller *et al.* 2006; Miller & White 2006a). Plant viruses within the family *Tombusviridae* and *Luteoviridae* (single stranded, positive sense and uncapped RNA genomes) harbor cap-independent translation enhancers (CITEs) in their 3´-UTRs (Simon & Miller 2013a). It has been reported that these 3´-CITEs require and directly bind eIFs, recruiting the ribosomes through different interactions with eIFs. Thus, *Barley yellow dwarf virus*-like translation element (BTE) interacts with the eIF4G subunit and the *Panicum mosaic virus*-like translation enhancer (PTE) requires the eIF4E subunit (Wang *et al.* 2011; Kraft *et al.* 2013a). On the other hand, the translation enhancer domain (TED) from the *Satellite tobacco necrosis virus*, the Y-shaped translational enhancer of CIRV and the I-shaped translational enhancer of *Maize necrotic streak virus* (MNeSV), the last two 3´-CITEs present in several viruses of the *Tombusviridae* family, bind and require the intact eIF4F complex (Gazo *et al.* 2004; Nicholson *et al.* 2010; Nicholson *et al.* 2013).

We previously showed that cap-independent translation of *Melon necrotic spot virus* (MNSV, family *Tombusviridae*, genus C*armovirus*) RNA is controlled by a 3´-CITE and is dependent on the presence of the 5´-UTR *in cis.* This translation enhancer was not functional *in vitro* in wheat germ extract (Truniger *et al.* 2008a). Genetic resistance to MNSV in melon was shown to result from a single amino acid change in $eIF4E_{H228}$ ($eIF4E_{H228L}$, *nsv* allele) (Nieto *et al.* 2006b) annulling virus genome translation (Díaz *et al.* 2004). Thus, translation of most MNSV genomes, including MNSV-Mα5, is eIF4E-dependent. On the other hand, analysis of eIF4E knock down lines strongly suggests that the resistance breaking isolates MNSV-264 and MNSV-N may rely on other factors than eIF4E (Rodríguez-Hernández *et al.* 2012; Miras *et al.* 2014). Chimeric 3´-UTR mutants from isolates MNSV-Mα5 and MNSV-264 showed that a stem-loop structure (SLC) acts as a resistance-breaking determinant through its capacity to control cap-independent translation in a host-dependent manner (Truniger *et al.* 2008a; Nieto *et al.* 2011a). Based on RNA secondary structure predictions, the 3´-CITEs from MNSV-Mα5 and MNSV-264 have been classified as I-shaped structures (ISS) but with several differences to the other ISS identified to date (Nicholson *et al.* 2010).

Here we describe structural and functional analyses of the MNSV-Mα5 3´-CITE, which is nearly invariable in all MNSV isolates that are unable to multiply in resistant melons (Truniger *et al.* 2008a). We also analyzed its translation initiation factor partner, identifying critical residues of eIF4E from melon (*Cm*eIF4E) implicated in *in vivo* cap-independent translation. Our results provide biochemical evidence regarding a specific interaction between eIF4F and the 3´-CITE and show that this binding correlates with the ability of the 3´-CITE to facilitate cap-independent translation.

2. EXPERIMENTAL PROCEDURES

2.1. Plant material

The *Cucumis melo* cultivars used were the cantaloupe-type accessions C-35 and C-46 ("La Mayora" germplasm collection, Málaga, Spain). C-35 carries the $eIF4E_{H228}$ allele and is susceptible to all MNSV isolates. Cultivar C-46 is homozygous for $eIF4E_{H228L}$

(*nsv* allele) and is resistant to all MNSV isolates, except for resistant breaking isolates MNSV-264 and MNSV-N.

2.2. Plasmids and RNA preparation by *in vitro* transcription

Luc constructs with the 5´- and 3´-UTRs from MNSV-Mα5 flanking the firefly luciferase gene have been previously described (Truniger *et al.* 2008a). Constructs containing only 30, 45 or 53 nucleotides from the SLC of the 3´-UTR of MNSV in absence or presence of the GC-clamp, as well as the constructs including mutations in the Ma5TE, were obtained by PCR amplification using construct 5´-UTRα5-luc with reverse primers including the corresponding SLC sequence, *DpnI* digestion to eliminate input DNA, followed by *in vitro* transcription (RiboMAX Large Scale RNA production, Promega). The Ma5TE SHAPE plasmid was prepared by cloning the Ma5TE sequence into the *EcoRI*/*SmaI* sites of the SHAPE cassette (Wang *et al.* 2009). The *SmaI*-linearized Ma5TE SHAPE plasmid was transcribed using the MEGAshortscript^{TM} kit (Ambion). RNAs used in UV-crosslinking assays were directly transcribed from PCR-amplified and gel-purified DNA including the T7 promoter. RNAs were transcribed in the presence of [α-^{32}P] UTP and purified with MicroSpin G-25 columns (GE Healthcare). Truncated *CmeIF4G* versions eIF4G$_{p10}$ and eIF4G$_{p20}$ (1003-1092 and 980-1159, respectively) were amplified by PCR from full-length *eIF4G* plasmid pTOPO-Cm-4G and cloned by LIC technology into the p2CT expression vector (Macrolab, UC Berkeley, CA, USA) yielding p2CT-4Gp10 and p2CT-4Gp20. Plasmid p2AT-4E was constructed by PCR-amplification of the *CmeIF4E* gene from the previously constructed expression vector pET15b-4EVed (Nieto *et al.* 2006b) and LIC-cloned in vector p2AT (Macrolab). For expression of eIF4F$_{p10}$ and eIF4F$_{p20}$ complexes, dicistronic expression vectors were generated by cloning into plasmid p2D (Macrolab), yielding p2D-4Fp10 and p2D-4Fp20: *eIF4E* was cloned into cassette 1 and into *BamHI*/*XbaI* restriction sites and truncated *eIF4G* versions were cloned into cassette 3 and into *SbfI*/*AscI* restriction sites. All *Cm*eIF4E and *Cm*eIF4G$_{p20}$ mutants were generated by site-directed mutagenesis in plasmids pET15b-4EVed (H228) and p2CT-eIF4Gp20, respectively (Supplementary Table 2). For transient *Cm*eIF4E expression in complementation experiments, eIF4E constructs were cloned into binary vector pBIN61 using *XbaI*/*XmaI* restriction sites. All mutants were confirmed by DNA sequencing.

2.3. *In vivo* translation in melon protoplasts

In vivo translation in melon protoplasts was performed as previously described (Truniger *et al.* 2008a). Briefly, 10 μg of *in vitro*-transcribed RNA was electroporated into 1x 10^6 protoplasts (Díaz *et al.* 2004). After 5-6 h incubation in the dark at 25 °C, protoplasts were lysed in 1xPLB (Passive lysis buffer, Promega). *Firefly* and *Renilla* luciferase activities were measured with the Luciferase assay system (Promega). These experiments were carried out at least six times for each construct.

2.4. Protein expression and purification

All proteins were expressed in *E. coli* Rosetta™ (DE3) pLysS cells (Novagen) that were grown in LB medium at 37 °C to an OD_{600} of 0.6. At this point IPTG was added to a final concentration of 0.4 mM to induce protein expression at 37 °C for 2 hours. Cells were re-suspended in Nickel Buffer A (25 mM HEPES pH 7.5, 400 mM NaCl, 20 mM imidazole, 10% glycerol, 1 mM dithiothreitol (DTT)) and supplemented with DNaseI (Roche) and protease inhibitor cocktail (Roche) and lysed by sonication. Expressed eIF4Fp20 and eIF4Fp10 were loaded on a HisTrap HP column (GE Healthcare) and eluted with Nickel Buffer B (as for Nickel Buffer A but with 400mM imidazole). After buffer exchange, eluted proteins were quantified by spectrometry at OD_{280}. To get rid of the His_6-tag and the MBP-tag, TEV protease was added to a 1:20 mass ratio and incubated overnight at 4 °C. Finally, these proteins were again loaded into the same HisTrap HP column and eluted with Nickel Buffer B and loaded onto a size exclusion Superdex 200 16/60 column (GE Healthcare). Protein 4Gp20 was expressed and purified as eIF4F proteins except for the second nickel-affinity step. Purification of eIF4E was carried out as previously described in (Nieto *et al.* 2006b). Buffers from all preparations were exchanged to the final buffer 25 mM HEPES pH 7.5, 200 mM NaCl and 10% glycerol.

2.5. Protein pull-down assays

For the pull-down experiments, proteins from empty p2CT expressing MBP and constructs p2CT-4Gp20 and pET15b-4E (H228 and mutants), were expressed in *E. coli* Rosetta™ (DE3) pLysS cells as described above. Pull-down was performed with cleared lysates, using the same volume of $eIF4G_{p20}$ lysate for each interaction experiment and similar amounts of the eIF4E lysates (H228 and mutants), as controlled by Western

blot using a rabbit polyclonal antibody against melon eIF4E (input). Incubation was with 20 µL of amylose resin (New England Biolabs) for 1 hour at 4 °C. The beads were washed three times with lysis buffer and eluted with 60 µL of 25 mM maltose. Maltose binding protein (MBP) was expressed and incubated with lysate or purified His-eIF4E as negative control. Proteins were analyzed by 12% of SDS-PAGE followed by Coomassie blue staining (eIF4G$_{p20}$ and MBP visualization) or Western blot (eIF4E visualization).

2.6. Analysis of RNA structure and footprinting

Determination of secondary RNA structure in solution was performed using Selective 2´-Hydroxyl Acylation analyzed by Primer Extension (SHAPE) as previously reported (Miras 2015). Briefly, ^{32}P-labeled Ma5TE RNA was refolded in SHAPE buffer alone or with specified proteins and treated with benzoyl cyanide (BzCN; Sigma-Aldrich) and reverse transcribed by primer extension of a radiolabeled primer. Reactions were resolved in a 10% denaturing polyacrylamide gel, dried and exposed to a phosphorimager screen. Normalized BzCN reactivity values for each nucleotide were calculate by SAFA Footprinting software (Laederach *et al.* 2008) and plotted by GraphPad software (GraphPad Software, Inc) with standard deviation. A normalized reactivity of 1.0 is defined as the average intensity of the top 10% most reactive peaks, excluding a few highly reactive nucleotides taken to be outliers (Low & Weeks 2010). RNA secondary structure was determined by MC-Fold computer program (Parisien & Major 2008a), using SHAPE reactivity data.

2.7. UV-crosslinking assays

UV-crosslinking assays were employed as described previously (Chodosh 2001; Huang *et al.* 2012) with slight modifications. Labeled RNA (0.02 pmol per reaction) was incubated in binding buffer (25 mM HEPES pH 7.5, 200 mM NaCl, 2 mM $MgAc_2$, 1 mM DTT, 10% glycerol, 20 units/mL RNase inhibitor, 0.1 mg/mL BSA, 30 µg/µL yeast tRNA) with recombinant proteins for 15 minutes at 30 °C. Reaction mixtures were place on a Petri dish on ice directly underneath the bulb (15 cm distance) of a 254-nm UV light source (UVP, model CL1000) for 15 min. Samples were mixed with SDS-PAGE loading buffer, boiled and loaded in a 12% SDS-PAGE. After drying, the gel was exposed to a phosphorimager screen.

2.8. Translation complementation by transiently-expressed eIF4E

*Cm*eIF4E$_{H228}$ and mutant proteins were transiently expressed from binary plasmids in cotyledons of resistant melon C46 by agroinoculation in the presence of the tombusvirus silencing suppressor P19 as previously described (Nieto *et al.* 2011a). At 3-4 days post-agroinfiltration, protoplasts were prepared from infiltrated tissues. *In vivo* translation assays were performed as described above by electroporating separately with two 5´-UTR-luc-3´-UTR RNA constructs, differing in the UTRs flanking the luciferase gene that were either from MNSV-264 or from MNSV-Mα5. Translation controlled by the 3´-CITE of MNSV-264 can take place in protoplasts from eIF4E knocked-down lines, strongly suggesting that it can function in the absence of eIF4E (Rodríguez-Hernández *et al.* 2012) and therefore serves for normalization of the different protoplast preparations. In agreement with Truniger *et al.* (2008) eIF4E-dependent translation controlled by the 3´-CITE of MSNV-Mα5 in resistant melon was very low, but transiently expressed eIF4E$_{H228}$ was able to complement translation (Nieto *et al.,* 2006). For each protoplast preparation the translation efficiency obtained with the construct controlled by the 3´-CITE of MNSV-264 was set to 100 % and translation controlled by the 3´-CITE of MSNV-Mα5 was related to it. The expression levels of eIF4E were analyzed in protein extracts (extraction buffer: 0.1 M Tris HCl pH 9.0, 0.1 M NaCl, 5 M Urea, 10 mM EDTA, 0.1 M β-mercaptoethanol) of infiltrated cotyledons and visualized by Western blot using a rabbit polyclonal antibody against melon eIF4E peptide “QNPRGRGGDEDEEL” (aa22-35; GenScript).

2.9. Yeast complementation

Saccharomyces cerevisiae strain JO55 contains a deletion in its endogenous *eIF4E* gene and requires complementation with an external eIF4E for growing, for example the human eIF4E expressed from the pGAL-eIF4E-URA3 plasmid in a galactose-dependent manner (Altmann *et al.* 1989). For the analysis of the complementation capacity of the melon eIF4E mutants, the coding sequence of the eIF4E variants were introduced into the *SpeI*/*BamHI* restriction sites of the Trp-selectable yeast-*Escherichia coli* shuttle vector p424-GDP/TRP1 (Mumberg *et al.* 1995). The constructs obtained in *E. coli* were transformed into JO55 selected on galactose-containing minimal medium in the absence Ura and Trp. Yeast cells were grown at 30

°C in liquid Gal/Raf-Ura-Trp medium until OD_{600} of 1, washed with sterile water and serially diluted in 10-fold steps until reaching 1000-fold. Drops (5 μL) of dilutions were placed on both control Gal/Raf-Ura-Trp solid medium and nitrogen base medium containing 2% glucose in the absence of Ura/Trp. JO55 transformed with an empty p424-GPD/TRP1 vector was used as negative control. The positive control was JO55 transformed with *Arabidopsis thaliana eIF4E* gene present in vector p424-GPD/TRP1:At-eIF4E (Charron *et al.* 2008).

2.10. Molecular modeling

The melon eIF4E model was built with the Swiss Model Workspace ("http://swissmodel.expasy.org") using as template the *P. sativum* crystal structure of eIF4E (PDB 2WMC)(Ashby *et al.* 2011). Models were evaluated by means of the Model Assessment package provided by SWISS-MODEL. Structure alignment of melon eIF4E model and *D. melanogaster* eIF4E:$eIF4G_{602-638}$ (PDB 4UEC) (Peter *et al.* 2015a) was made with PyMol (Schrodinger, LLC).

3. Results

3.1. The 3´-CITE of MNSV maps to a 45 nucleotide sequence

To determine if the SLC from MNSV-Mα5 was sufficient to enhance translation and to also further map the minimal sequence required for this activity, we flanked the firefly luciferase gene (LUC) with the 5´-UTR of MNSV-Mα5 at its 5´-end, and with either the complete MNSV-Mα5 3´-UTR, the SLC (SLC-53), or two progressive deletions of SLC (SLC-45 and SLC-30) at its 3´-end (Fig. 16a), and studied the *in vivo* cap-independent translation efficiency of the corresponding RNAs in melon protoplasts. We also produced a set of RNAs with a 5 base-pair G-C clamp added to the end of the 3´-stem-loop structure to stabilize it (SLC-30c, SLC-45c and SLC-53c; Fig. 16b). While the MNSV 3´-UTR enhanced translation to more than 15 fold with respect to its negative control, the RNA with SLC-30 (with or without clamp), and the RNAs with SLC-45 and SLC-53 showed only low translational activity. However, addition of the clamp to SLC-45 and SLC-53 resulted in a ≈4-7-fold increase in the translation efficiency levels

(Fig. 16c), suggesting that stabilization of these structures through addition of the clamp was necessary for their cap-independent translational activity outside the context of the complete 3´-UTR. Similar stabilization by a clamp had been previously shown to be required for activity in the case of the 3´-CITE of MNeSV (Nicholson *et al.,* 2010).

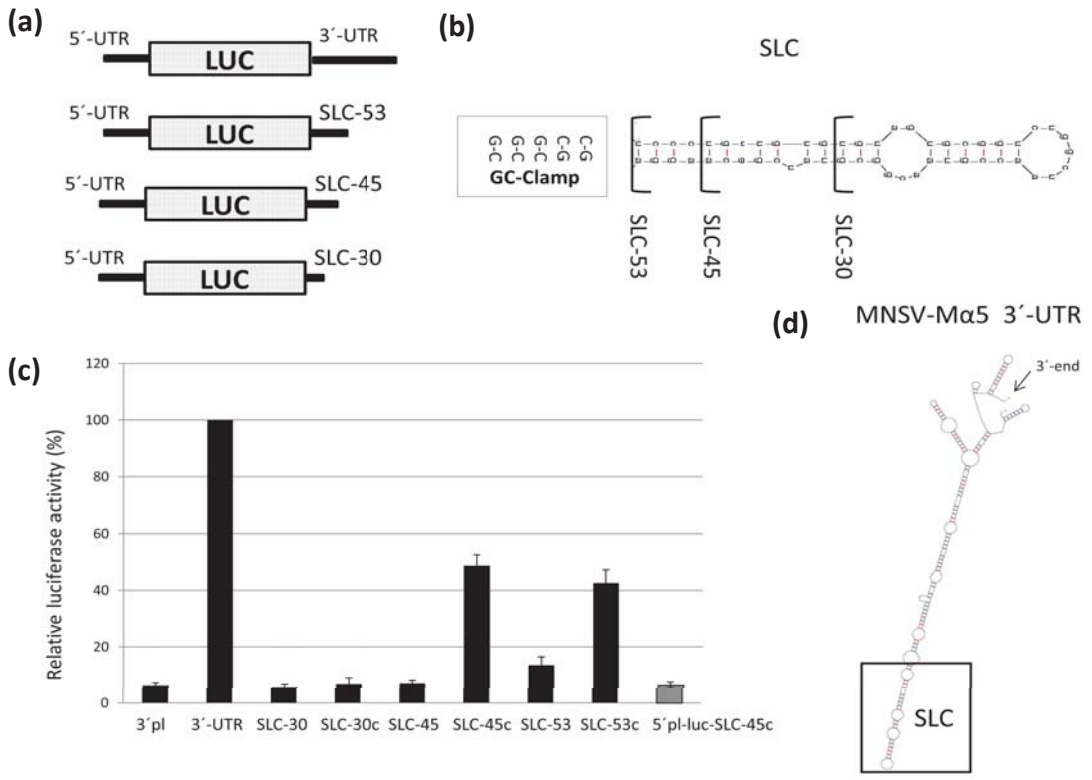

Figure 16. Mapping the minimal sequence of the MNSV-Mα5 3´-UTR required for cap-independent translation. (a) Schematic representation of reporter constructs consisting of the luciferase gene flanked by 5´-UTR and 3´-UTR or 5´-UTR and SLC variants SLC-53, SLC-45 and SLC-30, respectively, of MNSV-Mα5. **(b)** Mfold prediction of SLC showing the fragments SLC-53 (53 nucleotides (nts)), SLC-45 and SLC-30 corresponding to the different sequences added at the 3´end of the luciferase gene. The GC-clamp added at the end of these variants is shown in a box. **(c)** Relative luciferase activity (%) in melon protoplasts (Y-axis) obtained with different constructs (X-axis) differing in their 3´ends. The luciferase activity obtained with the construct 5´-UTR-luc-3´-UTR was set as 100% (second bar). 3´ends: 3´pl = plasmid sequence; 3´-UTR = 3´-UTR; SLC-30 = 30 nts from SLC (4085-4114); SLC-45 = 45 nts from SLC (4079-4122); SLC-53 = SLC (53 nts; 4074-4126). SLC-30c, SLC-45c and SLC-53c correspond to constructs with the clamp added to the SLC fragment analyzed. The last column corresponds to the activity obtained with a construct with SLC-45c at the 3´end and plasmid sequence instead of the 5´-UTR at the 5´end. Error bars are +/-. **(d)** MNSV-Mα5 3´-UTR secondary structure as predicted by Mfold; the box marks SLC.

Therefore, these results showed that when stabilized SLC was able to enhance cap-independent translation to at least 50% of the activity conferred by the complete 3´-UTR (Figure 16d), and that the minimal 3´-CITE sequence needed was 45 nucleotides

long. We named this 45 nucleotide RNA element MNSValpha5-like Translation Enhancer (Ma5TE). The activity of Ma5TE was dependent on the presence of the MNSV 5´-UTR *in cis* (last column in Figure 16c).

3.2. The Ma5TE belongs to the I-shaped structural class of 3´-CITEs

The Ma5TE secondary structure in solution was characterized by Selective 2´-Hydroxyl Acylation analyzed by Primer Extension (SHAPE) technology using benzoyl cyanide (BzCN) to monitor its folding in the presence of different magnesium concentrations. This chemical interrogates the conformation of each nucleotide by reacting with possibly single-stranded nucleotides in a sequence-independent manner, forming a 2´-O-adducts that block reverse transcriptase (Wilkinson *et al.*, 2006, Mortimer & Weeks, 2007). Chemical modification was followed by primer extension (Fig. 17a) and the data obtained revealed a stem-loop structure with two internal loops (Fig. 17b). The lower internal loop (IL1) included seven unpaired bases, from which U4115 and A4116 were strongly modified. Based on standard Watson-Crick base pairing and M-fold predictions, a different structure for IL1 was expected (Fig. 16b). The middle bulge (IL2) contained a highly reactive adenosine in position 4109. The apical loop (L) was highly accessible to BzCN suggesting that seven bases were unpaired. Using 1 mM of magnesium concentration, the nucleotides in the L loop showed high reactivity to BzCN. However, increasing Mg^{2+} concentration to 3 mM decreased reactivity, suggesting that conformation of this loop is highly dependent on the Mg^{2+} concentration. Likewise, the conformation of IL1 seemed to be dependent on magnesium, but modifications were found to be weaker than for L. Interestingly, the structure shown in Fig. 17b was supported by the highly conserved SLC-sequences found in all the other MNSV isolates (Fig. 17c), since the only six nucleotide variations were found in positions either in or adjacent to loops L or IL1 (Fig. 17b, black arrows) thus supposedly not affecting the basic Ma5TE conformation.

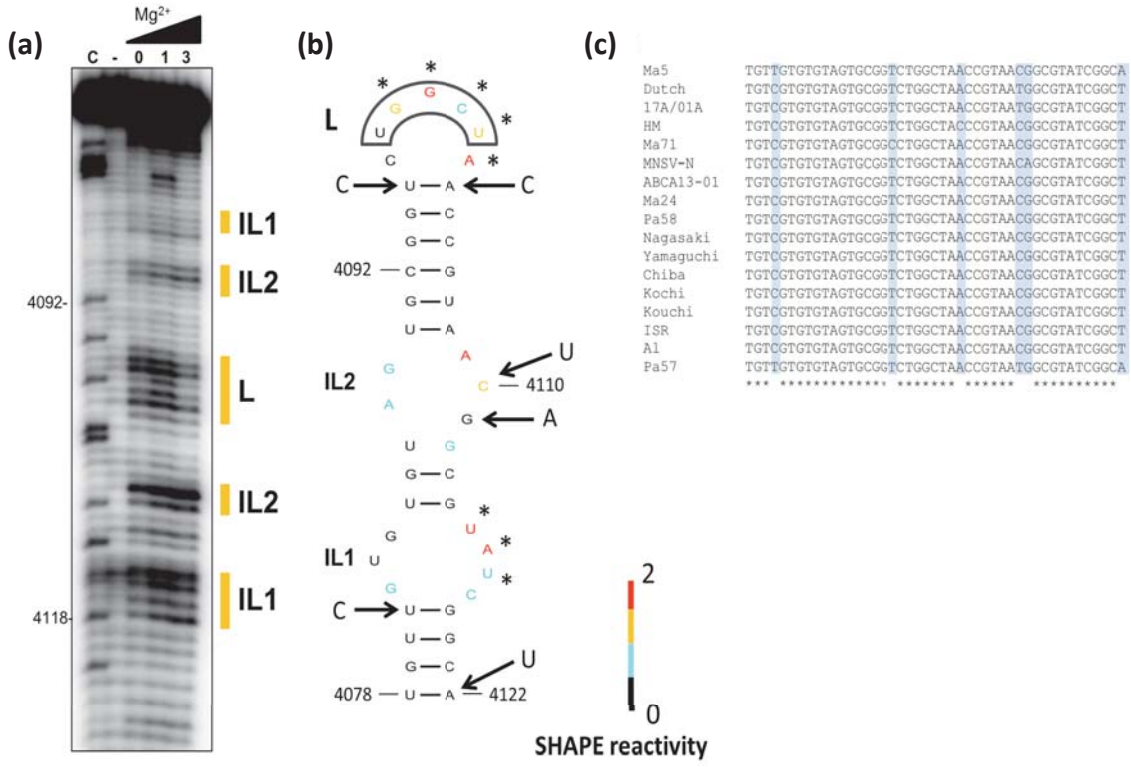

Figure 17. Chemical solution structure probing of Ma5TE. (a) Structure probing by SHAPE of SLC-45 (nucleotides 4079-4112 in the MNSV-Mα5 sequence). Primer extension products from RNAs modified with BzCN using increasing Mg^{2+} concentrations (0-3 mM) (lanes 3, 4 and 5). "-": untreated RNA; "C" sequencing ladder generated with dideoxy-CTP on unmodified RNA. Positions marking nucleotides C4092 and C4118 are indicated on the left. The regions of modified nucleotides corresponding to the internal loops (IL1/2) and final loop (L) are marked on the right side of the PAGE. **(b)** Secondary structure of Ma5TE according to the SHAPE reactivity data on the best-fitting predicted MC-Fold secondary structure. Levels of BzCN modification are indicated in a color-coded scale where red color points to the strongest modification. The pentanucleotide proposed to be involved in long-distance interaction with the 5´-UTR (to be published) is marked in L and arrows point to nucleotide variations found with respect to the SLC sequence of other MNSV isolates. Asterisks indicate the nucleotides whose accessibility change with changing Mg^{2+} concentrations, as they are increasingly modified at 1 mM Mg^{2+} but appear less modified at 3 mM Mg^{2+}. **(c)** Alignment of the Ma5TE sequences conserved in the 3´-UTR of all MNSV isolates. Nucleotide variations are shaded in light blue. GenBank accession numbers of MNSV sequences included in the alignment are Mα5-AY122286, Dutch-NC001504, 17A/01A-D12536.2, HM-GU480022.1, Mα71-EU589619, N-KF060715, ABCA13-01 (KR094068) Mα24-EU589616, Pα58-EU589620, Nagasaki-AB250686, Yamaguchi-AB250687, Chiba-AB250684, Kochi-AB250685, Kouchi CP gene (KS)-AB189943, ISR (Israel)-DQ922807, Al-DQ339157, Pα57-EU589621.

3.3. The Ma5TE interacts with eIF4F

Genetic evidence indicates that eIF4E is required for the cap-independent translation of MNSV-Mα5 RNAs controlled by SLC (Nieto *et al.* 2006b; Truniger *et al.* 2008a; Rodríguez-Hernández *et al.* 2012). Thus, we hypothesized that eIF4E or eIF4F may interact directly with the 3´-CITE. To study this we analyzed the *in vitro* interaction of SLC-45c with purified recombinant *Cm*eIF4F complexes by UV-crosslinking followed by

gel retardation assays. We were not able to purify *Cm*eIF4G full length due to its instability associated to its rapid proteolytic processing (data not shown), as previously described for eIF4G from wheat (Mayberry *et al.* 2007). Thus, our eIF4F complexes were formed by eIF4E and two different eIF4G fragments, $eIF4G_{p20}$ ($eIF4G_{980\text{-}1159}$) and $eIF4G_{p10}$ ($eIF4G_{1003\text{-}1092}$). Factors eIF4E, $eIF4G_{980\text{-}1159}$ ($4G_{p20}$) and $eIF4F_{p20}$ ($4F_{p20}$) and $eIF4F_{p10}$ ($4F_{p10}$, Figure 18A) were expressed and purified from *E. coli*. Ma5TE was only able to form a RNA:protein complex with $eIF4F_{p20}$ but not with $eIF4F_{p10}$ (Figure 18B), while no interaction with the individual polypeptides eIF4E or $eIF4G_{p20}$ could be detected. The formation of the $eIF4F_{p20}$/Ma5TE complex was detectable starting with a 150 nM concentration of $eIF4F_{p20}$ (Figure 18c).

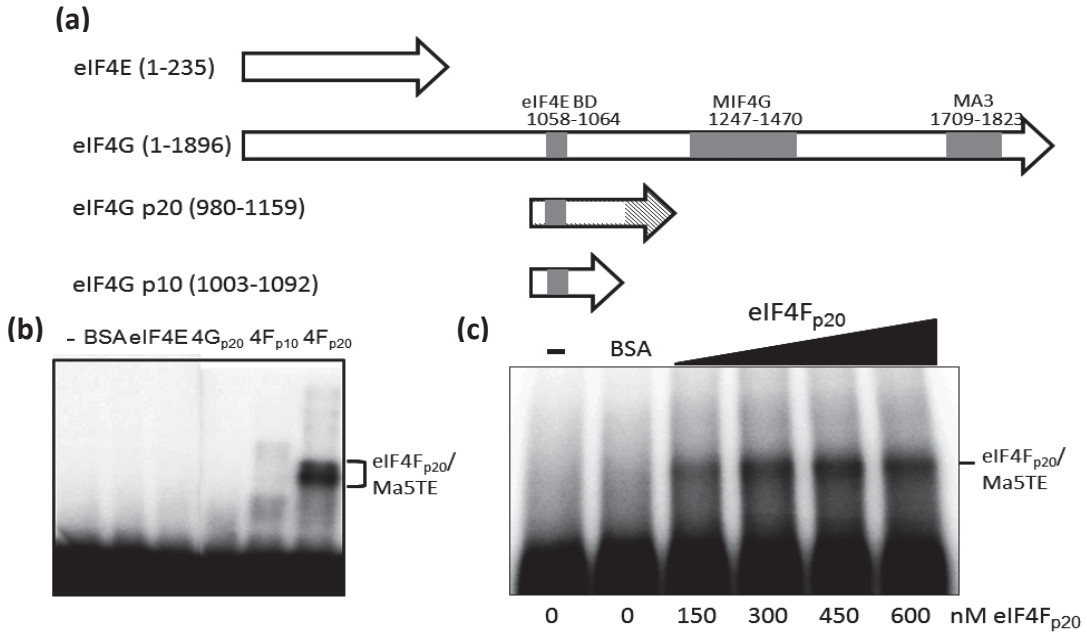

Figure 18. Identification of the interaction between eIF4F and Ma5TE. (a) Schematic representation of melon eIF4E and subunits of eIF4G. Factor-binding domains in eIF4G predicted by Pfam are shaded in grey: eIF4E-binding, MIF4G and MA3 domains. The eIF4E-binding domain was kept in the two truncated eIF4G proteins ($eIF4G_{p20}$ and $eIF4G_{p10}$). The region of $eIF4G_{p20}$ crucial for binding of eIF4F to Ma5TE appears striped. **(b)** UV-crosslinking followed by 12% SDS-PAGE separation of labelled Ma5TE (SLC-45c) in absence (-) or presence of 400 nM of each protein: ovalbumin (BSA), eIF4E, $eIF4G_{980\text{-}1159}$ ($4G_{p20}$), $eIF4F_{p10}$ ($4F_{p10}$) and $eIF4F_{p20}$ ($4F_{20}$). The retarded Ma5TE due to complex formed with $eIF4F_{p20}$ is marked on the right. **(c)** $eIF4F_{p20}$/Ma5TE complex formation using increasing $eIF4F_{p20}$ concentrations (nM, as indicated below).

These results suggest that the MNSV 3´-CITE binds eIF4F either through interaction with eIF4E following its conformational change as induced by its binding to $eIF4G_{p20}$, or through a double interaction with eIF4E and the p20 fragment of eIF4G.

Having established that Ma5TE is able to bind eIF4F$_{p20}$, we studied this interaction using footprinting analysis to determine the specific binding site by looking for protected nucleotides in the 3´-CITE structure. The SHAPE analysis of the Ma5TE/eIF4F$_{p20}$ complex revealed that in the presence of eIF4F$_{p20}$, the highly accessible adenosine in position 4109 was protected, while nucleotides G4093, G4094 and C4105, which were not accessible in the absence of eIF4F$_{p20}$, became accessible (Fig. 19a).

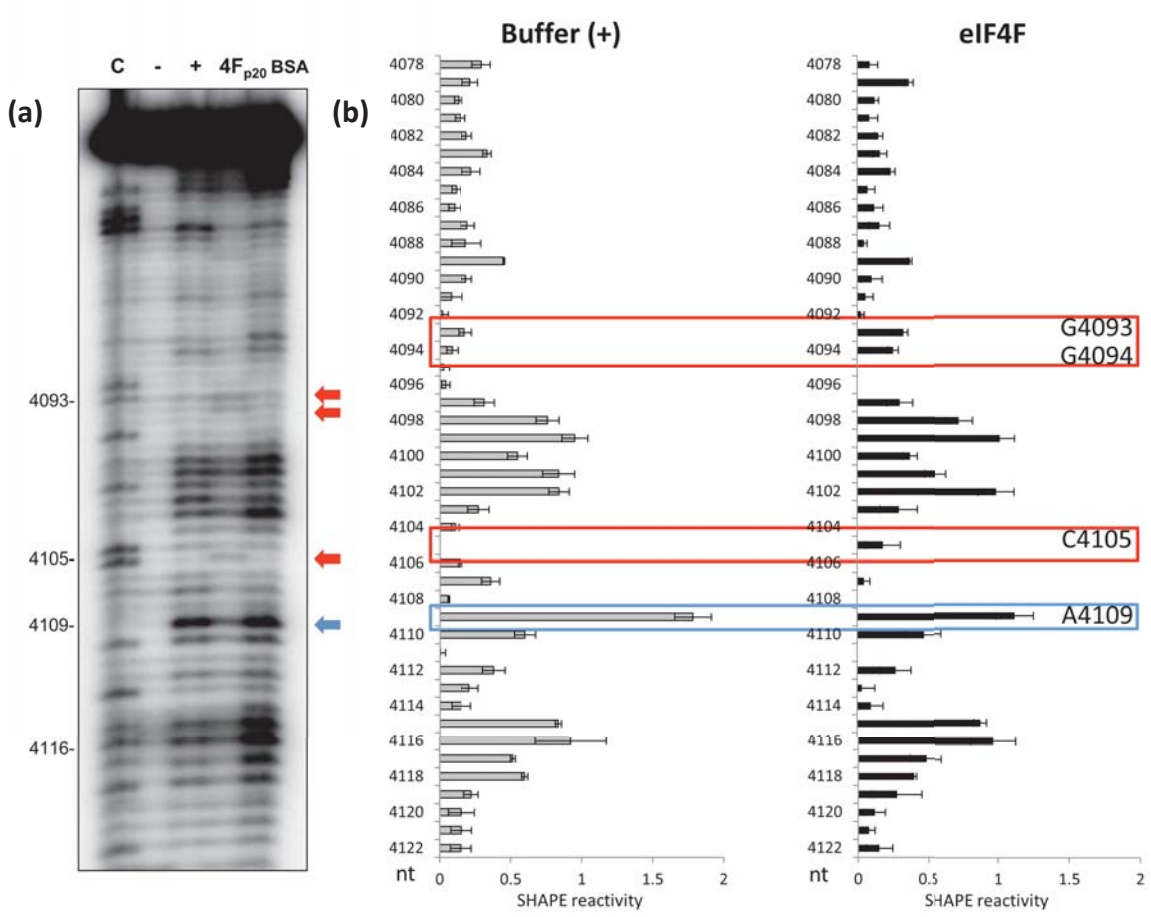

Figure 19. Mapping of the eIF4F-binding sites on the Ma5TE sequence. (a) BzCN modification analysis of Ma5TE in buffer (+ lane) and incubated with eIF4F$_{p20}$ (4F$_{p20}$) or non-binding protein BSA. Proteins were added to a final concentration of 1 µM. "C" corresponds to the sequencing ladder obtained using ddCTP. The second lane shows unmodified RNA (-). Nucleotides protected in the presence of eIF4F$_{p20}$ are marked with a blue arrow, while red arrows mark residues with increased accessibility. **(b)** SHAPE reactivity profiles (diagonal bars) in absence (Buffer) or in presence of eIF4F$_{p20}$. Values correspond to the mean SHAPE reactivity (±SD) of four independent experiments. SHAPE reactivity is measured in a scale where 0 represents unreactive nucleotides and 2 the maximum reactivity. Nucleotide positions are shown on the *y*-axis. Nucleotides that were protected or strongly modified are boxed in blue or red, respectively.

Statistical analysis showed significant differences in the reactivity levels of these nucleotides in the absence *vs*. presence of eIF4F$_{p20}$ (boxed positions in Fig. 19b).

Note that the quantification program normalizes bands intensity for each lane, correcting potential problems arising from unequal loading, as could be the case between lanes 3/5 and 4 in Fig. 4a. No conformational changes in the 3´-CITE structure were observed by the addition of eIF4E, $eIF4G_{p20}$ or BSA to the Ma5TE (data not shown). To investigate the importance of these residues in cap-independent translation and eIF4F binding, we performed a mutational analysis. The mutations introduced into the 5´-UTR-luc-SLC45c construct were A4109C, A4109G, G4093C or C4105G (Fig. 20a). Mutated RNAs were tested as before, in cap-independent translation assays in melon protoplasts; none of the mutated RNAs were able to enhance translation (Fig. 20b), showing that these nucleotides were essential. Thus, their ability to interact with eIF4F was analyzed. UV-crosslinking experiments followed by SDS-PAGE with the Ma5TE mutant A4109C revealed the loss of its binding capacity to $eIF4F_{p20}$, confirming the importance of this residue in this interaction (Fig. 20c).

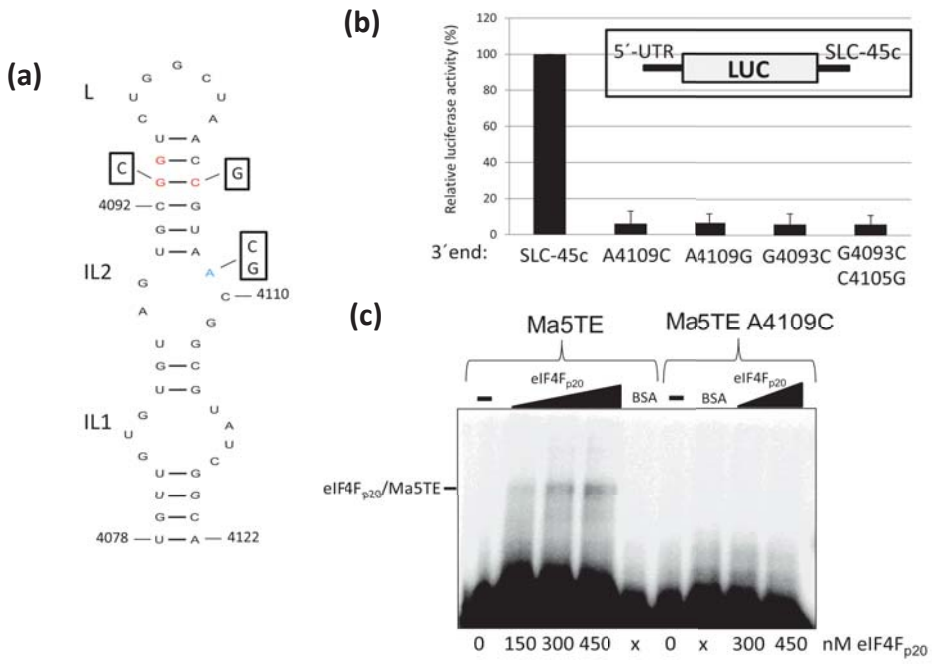

Figure 20. Identification of nucleotides of Ma5TE involved in eIF4F binding. (a) SHAPE Ma5TE secondary structure analysis showing the nucleotides protected in the presence of eIF4Fp20 in blue and the ones with increased accessibility in red. The Ma5TE point mutations studied are boxed. (b) Relative luciferase activity (%) in susceptible melon protoplasts of the constructs with the luciferase gene flanked by 5´-UTR and Ma5TE (WT and mutated). The activity obtained with WT Ma5TE was set as 100% (column 1). Ma5TE mutations analyzed: A4109C, A4109G and G4093C without and with the complementary mutation C4105G. Error bars are +/-. (c) UV-crosslinking of labelled Ma5TE and mutant Ma5TE A4109C with eIF4Fp20 followed by SDS-PAGE separation. The eIF4Fp20/Ma5TE complex was visible only with WT Ma5TE. Factor concentration (nM) is indicated below.

3.4. Identification of eIF4E residues involved in Ma5TE-driven translation

EIF4E from susceptible melon ($eIF4E_{H228}$) transiently expressed in resistant melon (homozygous for $eIF4E_{H228L}$) is able to complement the multiplication of MNSV (Nieto *et al.,* 2006) depending on the nature of its 3´-CITE (Truniger *et al.,* 2008). Translation of most MNSV isolates is eIF4E-dependent. In contrast, translation of the resistance–breaking isolate MNSV-264 RNA can take place normally in protoplasts from eIF4E knocked-down lines, suggesting that it can function in the absence of eIF4E (Rodríguez-Hernández *et al.,* 2012; Truniger *et al.*, unpublished). These results provided the basis for the design of an experimental system to test eIF4E mutants in relation to their ability to support Ma5TE-driven translation. Thus, we transiently expressed eIF4E in cotyledons of resistant melons by agroinfiltration, prepared protoplasts from these cotyledons and studied the ability of the transiently-expressed eIF4E to complement cap-independent Ma5TE-controlled translation of 5´-UTR-luc-3´-UTR RNAs (Fig. 21a). Our results showed that cap-independent eIF4E-dependent translation in the presence of $eIF4E_{H228}$ increased 6-fold with respect to transient expression of only the silencing suppressor p19 (Fig. 21a, columns 1, 2), reaching nearly 50% of the translation activity obtained with the construct 5´-UTR-luc-3´-UTR of the resistance breaking isolate used to normalize the different protoplasts preparations. In contrast, transient over-expression of $eIF4E_{H228L}$ did not result in increased luciferase activity (Fig. 21a, column 3), validating this experimental system for our purpose.

We then modeled the melon eIF4E 3D structure based on the *Pisum sativum* eIF4E crystal structure (Ashby *et al.*, 2011) (Fig. 22a). As shown before, amino acid position 228 resides in the carboxy-terminal arm of the protein, in close proximity to the cap-binding pocket (Fig. 22a) (Nieto *et al.*, 2006, Nieto *et al.*, 2011). It has been proposed that net amino acid charge at this position is relevant for determining melon susceptibility to MNSV (Nieto *et al.,* 2006). We therefore designed substitution H228R to try to elucidate if cap-independent translation of MSNV could be dependent on the positive charge of this amino acid. Our results showed that the *in vivo* cap-independent eIF4E-dependent translation efficiency also increased 6-fold in the

presence of eIF4E$_{H228R}$, similar to eIF4E$_{H228}$ (Fig. 21a, columns 2-4) supporting the above hypothesis.

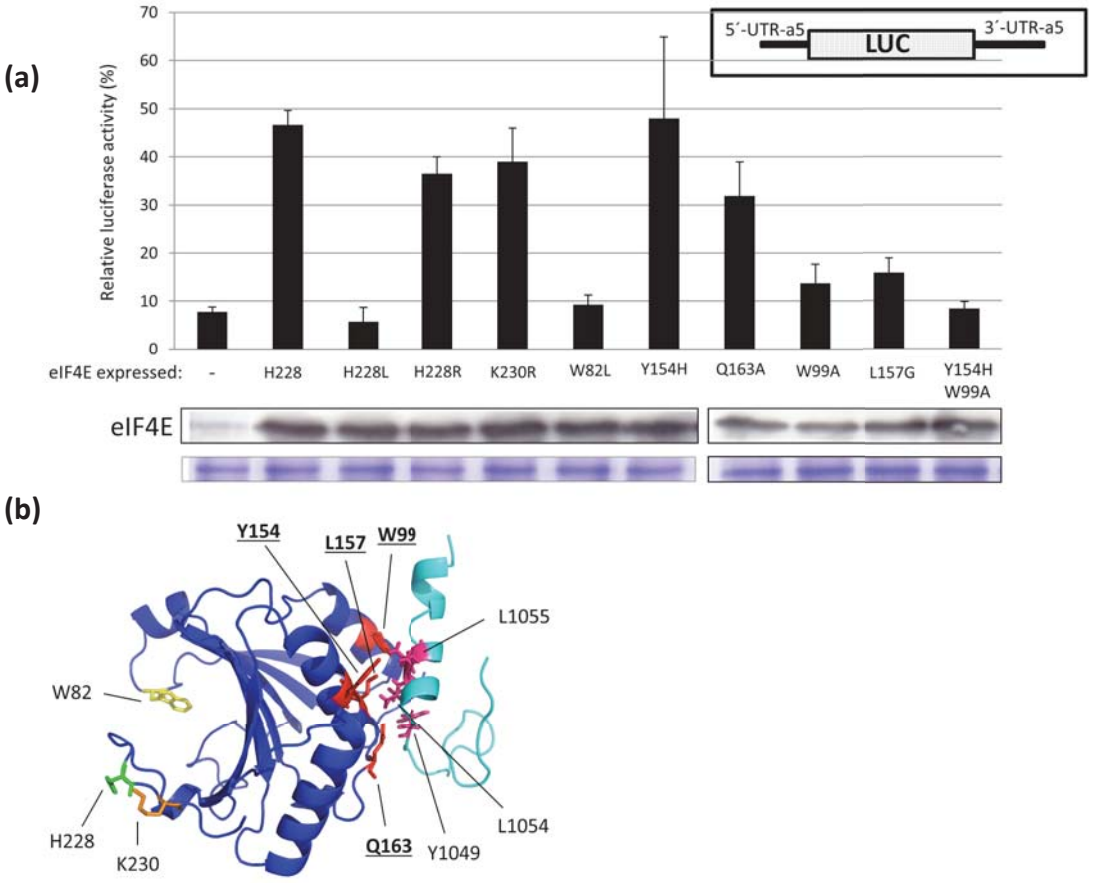

Figure 21. Effect of substitutions in eIF4E on cap-independent Ma5TE-mediated translation. (a) Relative luciferase activity (%) obtained with luciferase constructs (5´-UTR-luc-3´-UTR) in resistant melon protoplasts expressing transiently eIF4E from susceptible melon (H228 and mutants). For normalization of the different protoplast preparations, luciferase activity obtained with construct 5´-UTR-luc-3´-UTR from resistant breaking MNSV (MNSV-264) was set to 100% for each protoplast preparation. Translation of MNSV-264 has been shown to be eIF4E-independent (Rodríguez-Hernández *et al.,* 2012). The transiently expressed eIF4E mutants are indicated below each bar: "-": silencing suppressor P19 alone; H228: susceptible eIF4E; H228L: resistance allele; engineered eIF4E mutations: H228R; K230R (in residues proposed to be involved in RNA binding); W82L (in cap-binding pocket); Y154H, Q163A, W99A, L157G and Y154H-W99A (in residues proposed to be involved in eIF4G interaction). Error bars are +/-. Panels below show expression of each eIF4E mutant in resistant melon cotyledon visualized by western blot using antibodies against melon eIF4E. Low expression of endogenous eIF4E ("-") can be detected. The panel below shows the loading control visualized by Coomassie blue staining. **(b)** Predicted structure of melon eIF4E (dark blue) based on *P. sativum* eIF4E crystal structure in complex with eIF4G$_{602-638}$ from *D. melanogaster* (light blue). Residues of eIF4E suggested to be involved in the interaction with eIF4G (W99, Y154, L157 and Q163, underlined in bold) are drawn with red sticks. Residue W82 located in the cap-binding pocket, H228 and K230 are colored in yellow, green and orange, respectively. Residues in eIF4G of conserved canonical eIF4E-binding motif YxxxxLϕ (YSRDFLL in melon, Y1049, L1054 and L1055) are shown in pink.

Moreover, we studied the effect of the substitution K230R, as RNABindR, a server for predicting and analyzing RNA-binding sites in proteins (Walia *et al.*, 2014), predicted that this amino acid position forms part of an RNA-binding motif including H228. Transient expression of this mutant in resistant melon resulted in a similar translation efficiency to that obtained with $eIF4E_{H228}$ (Fig. 21a, column 5), suggesting either that the maintenance of the positive charge of this residue is important to support Ma5TE-driven translation or that K230 residue is not essential for it.

Since Ma5TE was able to interact with $eIF4F_{p20}$ but not with eIF4E, we hypothesized that disrupting the binding of eIF4E to eIF4G would result in loss of Ma5TE-driven translation. To test this hypothesis, we compared our 3D model with the recently published crystal structure of *Drosophila melanogaster* eIF4E:$eIF4G_{602-638}$ complex (Peter *et al.*, 2015) (Fig. 22b), identifying several residues in the melon eIF4E that could be implicated in eIF4G-binding through interactions with the conserved motif YxxxxLϕ (C domain) of eIF4G (Fig. 21b). Thus, we studied if point mutations in these residues of eIF4E, proposed to be involved in eIF4G binding, would affect cap-independent translation controlled by Ma5TE.

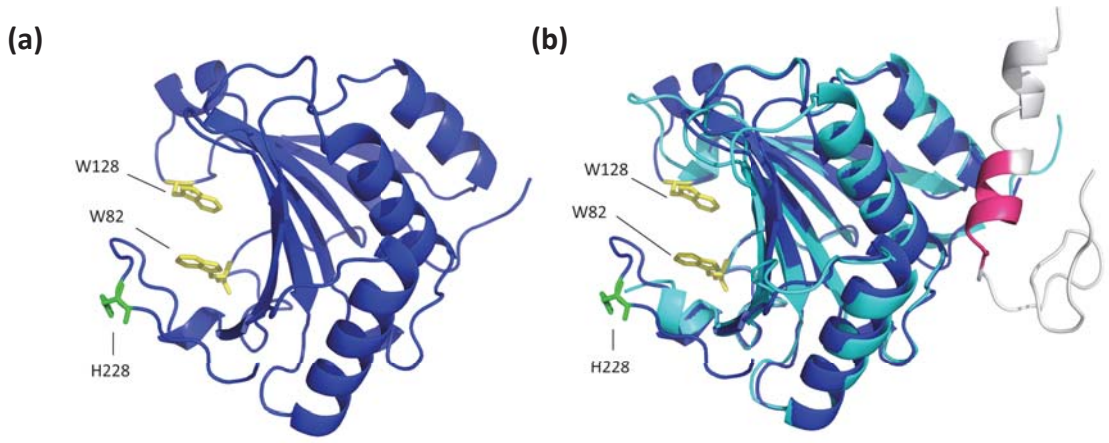

Figure 22. Position of the mutations on the predicted structure of melon eIF4E. (a) 3D model of melon eIF4E based on the *P. sativum* eIF4E crystal structure (Ashby *et al.,* 2011). The two residues, W82 and W128, involved in π-π stacking with the cap aromatic ring are colored in yellow and amino acid H228, responsible for eIF4E-dependent resistance to MNSV in melon, is indicated in green. **(b)** Melon eIF4E model (dark blue) superimposed with *D. melanogaster* eIF4E:$eIF4G_{602-638}$ crystal complex (eIF4E in light blue and $eIF4G_{602-638}$ in grey) (Peter *et al.,* 2015). The root mean square deviation (RMSD) value of 0.612 suggests a very similar folding. Conserved canonical eIF4E-binding domain YxxxxLϕ is shown in pink.

Substitutions Q163A and Y154H did not affect the complementation abilities of these mutant eIF4Es, while amino acid substitutions W99A and L157G reduced this ability. Likewise, simultaneous amino acid substitutions W99A and Y154H in eIF4E abolished its cap-independent translation activity (Fig. 21a, columns 7-11). Additionally, a mutation introduced into the cap-recognition pocket, W82L, rendered this eIF4E mutant unable to complement cap-independent translation (Fig. 21a, column 6), suggesting that residues involved in cap-binding were also essential for cap-independent translation controlled by Ma5TE, thus for multiplication of MNSV.

Next, we analyzed binding of tagged eIF4G$_{p20}$ to eIF4E by performing *in vitro* interaction experiments using pull-down assays (Fig. 23).

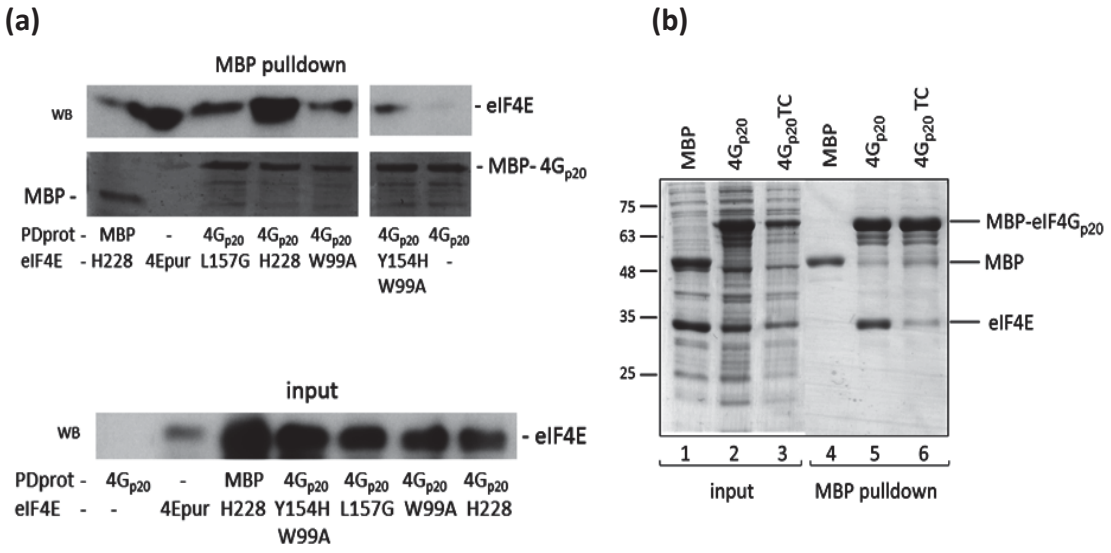

Figure 23. Mutations in eIF4E and eIF4G$_{p20}$ involved in their interaction. MBP pull-down assays showing the interaction of eIF4E (H228 and mutants) and MBP-eIF4G$_{980-1159}$ (4G$_{p20}$ and mutant). **(a)** Pulldown of eIF4E$_{H228}$ and mutant proteins through their interactions with eIF4G$_{p20}$. Upper gel shows pulled down eIF4E (MBP pulldown) visualized by Western blot (WB) with melon eIF4E specific antibody. The same gel was stained with Coomassie to compare the similar amount of eluted eIF4G$_{p20}$ in each experiment. The third gel visualizes the amount of eIF4E present in the input by Western blot. The factors interacting in each experiment are described below the gels, as pulldown protein (PDprot) either MBP or eIF4G$_{p20}$, and as partner the eIF4E proteins (H228 or mutant L157G, W99A or double mutant W99A/Y154H). **(b)** Interaction of eIF4G$_{p20}$ and triple mutant in canonical 4E-binding domain, (4G$_{p20}$TC) with purified eIF4E$_{H228}$ protein. The input (lanes 2 and 3) and bound fractions (lanes 5 and 6) were analyzed by 12% SDS-PAGE followed by Coomassie blue staining. As negative control for the specificity of the interaction, we incubated eIF4G$_{p20}$ alone or MBP with lysate (A) or purified (B) eIF4E.

We studied the three eIF4E mutants that affected cap-independent translation, W99A, L157G and the double mutant Y154H-W99A and found that their eIF4G$_{p20}$ binding capacity was reduced in comparison to eIF4E$_{H228}$ (Fig. 23a). This result confirms

the role of these eIF4E residues in eIF4G binding and, as a consequence, in cap-independent translation. Additionally, the effect of $eIF4G_{p20}$ protein containing three substitutions in its YxxxxLϕ motif was studied. The finding that much less eIF4E could be pulled-down as complex with the mutant $eIF4G_{p20}$ protein, supported the importance of the canonical eIF4E-binding domain of eIF4G in the interaction with eIF4E (Fig. 23b).

To confirm that the amino acid changes introduced into eIF4E did not affect protein folding, we studied the ability of these mutant proteins to accomplish all the functions related to growth, including mRNA translation initiation, taking advantage of the eIF4E-deficient yeast strain JO55 (Altmann *et al.* 1989) that needs to be complemented with a functional eIF4E to be able to grow with glucose. Nearly all mutations in melon eIF4E analyzed allowed for the functional complementation in yeast, confirming their functionality. One exception was the amino acid change W82L (Figure 24).

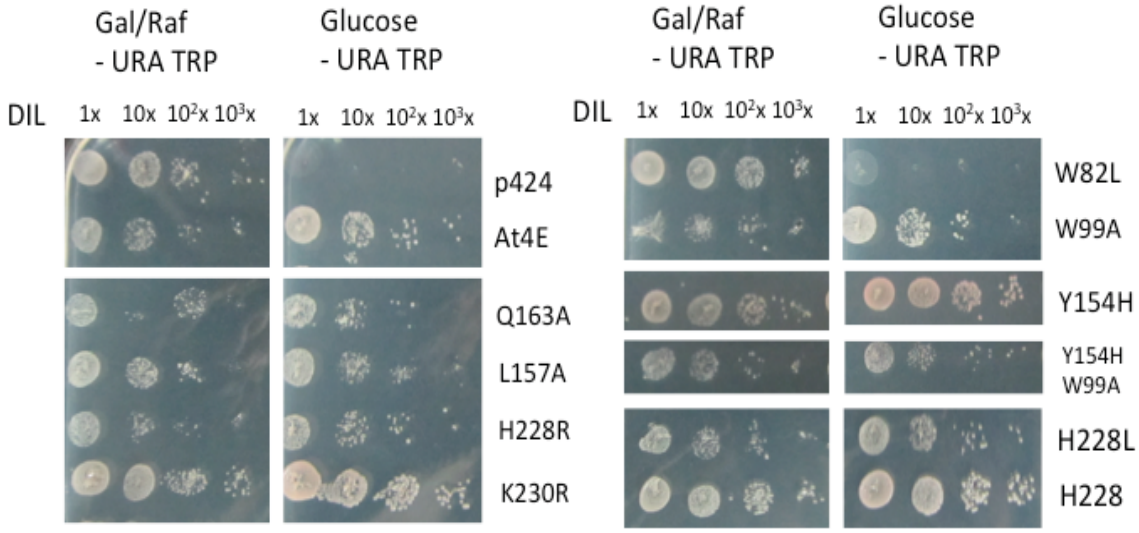

Figure 24. Complementation of translation by eIF4E mutants in eIF4E-deficient yeast. Yeast strain JO55 was transformed with plasmid p424 expressing *A. thaliana* eIF4E (At4E), or melon eIF4E (H228 or mutant). Yeast cultures were spotted either undiluted (1x) or diluted (10x, 10^2x and 10^3x) on Gal/Raf and Glucose selective media (both media -Ura/-Trp). The negative control with the empty p424 and the cap-binding pocket mutant W82L were unable to complement translation, thus to grow on glucose.

Since this residue is involved in cap-binding and also conserved in yeast eIF4E, it was not surprising to find that it was not functional. Interestingly, some of the mutations in the melon eIF4E residues that were supposed to be involved in the interaction with eIF4G, affected translation in yeast and in melon differently: substitutions W99A and L157G did not support cap-independent translation but were able to restore growth to an eIF4E-deficient yeast strain (Table 3).

Table 3. Summary of the complementation experiments

Class of mutation	**Mutation**	**Cap-independent translation assay**[a]	**Yeast complementation**[b]
nsv allele	H228L	-	+
Charge dependence	H228R	+	+
RNA-binding motif	K230R	+	+
Cap-binding	W82L	-	-
eIF4G binding	W99A	-	+
	Y154H	+	+
	L157G	-	+
	Q163A	+	+
	W99A-Y154H	-	+

[a] +, mutation complements cap-independent translation; -, unable to complement cap-independent translation.

[b] +, yeast growth on glucose was supported; -, no growth on glucose.

4. DISCUSSION

A wide range of positive-strand RNA viruses use 3´-CITEs to efficiently translate their proteins in a cap-independent manner in their hosts (Simon & Miller 2013a). In this study we characterized Ma5TE, the 3´-CITE of MNSV-Mα5, which is highly conserved among MNSV isolates, providing evidence that it drives cap-independent eIF4E-dependent translation by recruiting the eukaryotic initiation factor 4F. Key amino acids in melon eIF4E involved in this mechanism were identified.

We mapped Ma5TE to a 45-nucleotide long sequence, the smallest 3´-CITE found in RNA viruses (Simon & Miller 2013a). These stabilized 45 nucleotides, when

located in the 3´-end of a reporter construct, were able to mediate cap-independent translation *in vivo* in susceptible melon protoplasts. From all the 3´-CITEs identified until now, only the 3´-CITE of MNSV-N has also been shown to be able to promote *in cis* translation *in vivo* in the absence of the remaining 3´-UTR sequence (Miras *et al.* 2014). For Ma5TE activity, a G-C clamp had to be attached to the CITE sequence, possibly increasing its stability. Such a G-C clamp was previously shown to be necessary for stabilizing the MNeSV 3´-CITE before it showed activity *in trans* and in *in vitro* translation experiments (Nicholson *et al.* 2010). As observed with the complete 3´-UTR, translation enhancement controlled by Ma5TE was also dependent on the presence of the 5´-UTR from MNSV-Mα5 *in cis*. Our unpublished results suggest that a long-distance 5´-3´-UTR interaction based on sequence complementarity is required for efficient translation (Truniger, manuscript in preparation).

Experimental determination of the secondary structure of Ma5TE confirmed that it belonged to the I-Shaped Structure (ISS) class of 3´-CITEs, and was similar to the one from MNeSV (Nicholson & White, 2011) (Fig. 25a). Both MNeSV ISS and Ma5TE seemed to be Mg^{2+}-dependent for folding; while the MNeSV ISS formed non-canonical interactions in the lower internal loop 1 (IL1) in presence of Mg^{2+}, the Ma5TE IL1 and apical loop (L) appeared to "breathe", making these regions more accessible when Mg^{2+} was present. Analysis of the ISS-CITEs revealed that Ma5TE had two internal loops that were smaller than those found in the characterized MNeSV 3´-CITE and in the other predicted I-shaped structures from the MNSV-264 isolate, the aureusviruses *Maize white line mosaic virus* (MWLMV) and *Johnsongrass chlorotic stripe mosaic virus* (JCSMV) and the tombusvirus *Cucumber Bulgarian virus* (CBV) (Carstens, 2010, Scheets & Redinbaugh, 2006) (Fig. 25b). In the case of the MNeSV 3´-CITE, the lower internal loop (IL1) was proposed to be important for its interaction with eIF4F, and more specifically, the guanosine residue at position 6 (marked in light blue in Fig. 25a and b) was shown to be involved in eIF4F binding (Nicholson *et al.,* 2010). This guanosine residue was conserved in Ma5TE as well as in the other I-shaped structures. On the other hand, our footprinting analysis of Ma5TE showed reduced modification of A4109 in the presence of $eIF4F_{p20}$. *In vivo* translation and *in vitro* binding analysis proved the importance in translation of this residue, likely through its interaction with eIF4F. This

adenosine is conserved and remains unpaired in all known I-Shaped Structures (marked in red in Fig. 25a and b). In line with these results, mutation of this conserved adenosine in MNeSV ISS showed that it was also important for this CITE's activity (Nicholson *et al.,* 2010).

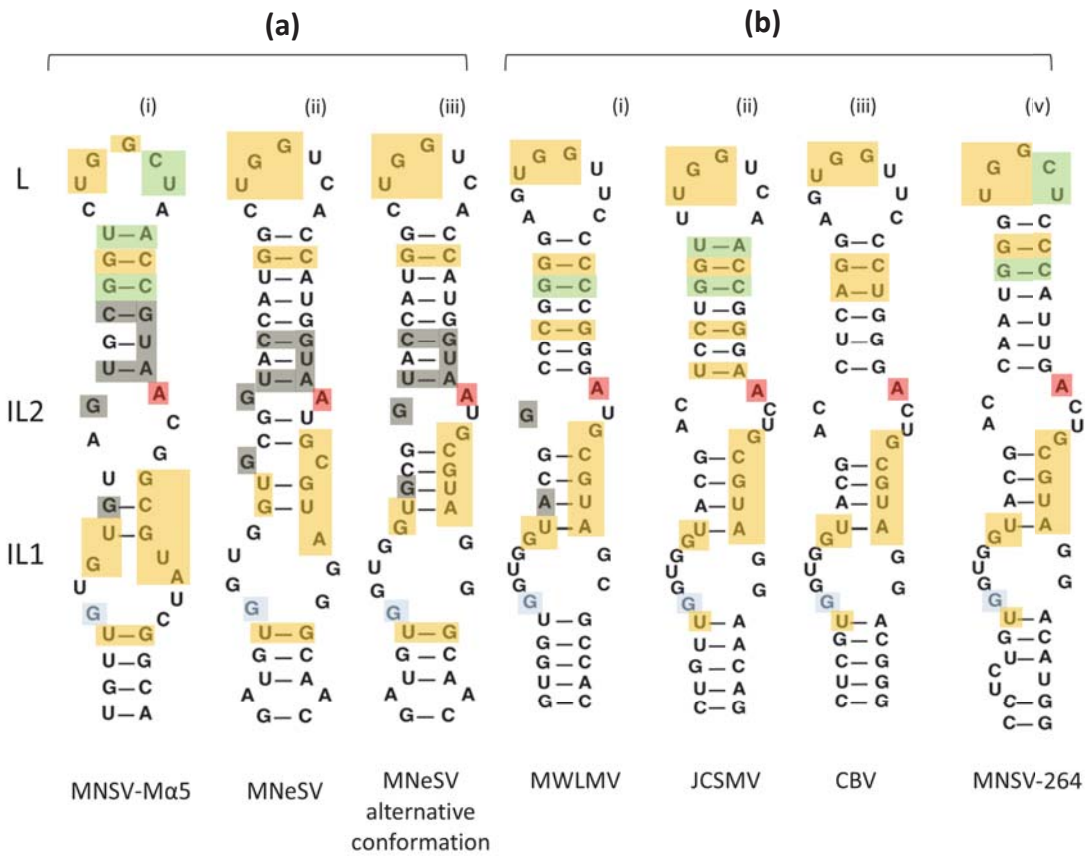

Figure 25. Comparison of sequence and structure of I-shaped structured 3´-CITEs. (a) Ma5TE and MNeSV ISS secondary structures. The Ma5TE (i) and MNeSV ISS (ii) secondary structures were probed by SHAPE analysis, while MNeSV ISS alternative conformation (iii) was predicted by Mfold based on *in vivo* evolution studies (Nicholson *et al.,* 2013). **(b)** MWLMV (i), JCSMV (ii), CBV (iii) and MNSV-264 (iv) Mfold-predicted secondary structures of non-characterized ISS. The adenosine residue involved in the interaction of Ma5TE with eIF4F is shaded in red and the guanosine residue important for MNeSV 3´-CITE interaction with eIF4F is marked in light blue. Nucleotides shaded in orange are conserved in all ISS and the ones in grey correspond to those conserved between Ma5TE and MNeSV ISS. The nucleotides shaded in green are conserved between Ma5TE and non-characterized ISS.

By looking at the conserved sequences of these ISS-CITEs, it can be observed that Ma5TE has a higher nucleotide similarity with the MNeSV 3´-CITE, which is eIF4F-dependent (marked in grey in Fig. 25), than with the other predicted I-shaped CITEs. One of these predicted ISS-CITEs belongs to the resistance-breaking MNSV isolate, MNSV-264 (Truniger *et al.* 2008a). This 3´-CITE is known to be active in the absence of

eIF4E (Rodríguez-Hernández *et al.* 2012). Interestingly, the MNSV-264 3´-CITE conserves the adenosine and guanosine residues, both important for eIF4F interaction of Ma5TE and MNeSV 3´-CITE. The identity of the translation initiation factor required for MNSV-264 ISS activity and the nature of the nucleotides involved in its binding are still unknown. Although active in the absence of eIF4E, this 3´-CITE may also maintain its ability to bind and promote translation by interacting with this initiation factor. Two different groups of ISS-CITEs could exist depending on the translation initiation factors they recruit: the ones that are more similar to Ma5TE and MNeSV would bind to eIF4F, while the less similar ones would be eIF4F-independent.

The resistance to MNSV in melon was shown to result from a single amino acid change in eIF4E (Nieto *et al.* 2006b). This finding led to the proposal that a direct interaction between Ma5TE and $eIF4E_{H228}$ existed. On the other hand, the results presented here suggest that Ma5TE does not bind to eIF4E alone, but only when complexed with eIF4G. This could be explained by a possible allosteric effect: binding of eIF4G would result in the conformational change of eIF4E, rearranging the residues involved and thus allowing for its interaction with Ma5TE. Conformational changes in eIF4E upon binding to eIF4G or 4EBP have been suggested before (Gross *et al.* 2003; Papadopoulos *et al.* 2014). Interestingly, Ma5TE has been shown to interact with a truncated version of eIF4F, $eIF4F_{p20}$, but not with the smaller $eIF4F_{p10}$. This suggests that the extra sequence of $eIF4G_{p20}$, missing in $eIF4G_{p10}$, is crucial for inducing the conformational change in eIF4E, which is important for Ma5TE binding. Another explanation could be that this extra sequence contains an RNA-binding motif required for its interaction with Ma5TE.

As just mentioned above, the only amino acid that differs between the eIF4E from susceptible and resistant melon is the histidine at position 228 that is changed into leucine (Nieto *et al.* 2006b). $EIF4E_{H228L}$ is unable to promote cap-independent translation controlled by Ma5TE (Truniger *et al.* 2008a). Regarding this residue, we previously proposed that net positive amino acid charge could be important for cap-independent translation controlled by Ma5TE (Nieto *et al.* 2011a). Our mutational analysis showed that substitution of this residue for another positively-charged amino

acid (arginine) did not affect its activity in cap-independent translation, confirming the importance of this positive charge.

Previous studies have suggested that the interaction of the *Panicum mosaic virus*-like translation enhancer (PTE) with eIF4F involves the cap-binding pocket of eIF4E (Wang *et al.* 2009). In agreement with this, our results showed that substitution of one of the tryptophan residues of melon eIF4E involved in cap-binding reduced its capacity to promote *in vivo* cap-independent translation driven by Ma5TE and to restore growth of an eIF4E-deficient yeast strain. (Altmann *et al.* 1989; German-Retana *et al.* 2008; Ashby *et al.* 2011). This result allows us to propose that an intact cap-binding pocket is required for efficient cap-independent translation controlled by Ma5TE, suggesting that this 3´-CITE could be interacting with eIF4F via the cap-binding pocket of eIF4E. On the other hand, other cases have been described where substitutions in the cap-binding pocket have affected the structural conformation of eIF4E, even affecting its stability (Niedzwiecka *et al.* 2002b; Rutkowska-Wlodarczyk *et al.* 2008). Since the mutation introduced in melon eIF4E also annulled its capacity to complement translation in yeast, we cannot exclude this possibility.

Among the substitutions in melon eIF4E shown to impair its interaction with eIF4G, the substitution W99A disrupted cap-independent translation controlled by the Ma5TE. The finding that mutations in the corresponding residue of *S. cerevisiae* eIF4E abolished its binding to eIF4G, while in *D. melanogaster* eIF4E the mutation disrupted its binding to both eIF4G and eIF4E-binding protein CUP (Ptushkina *et al.* 1998; Nelson *et al.* 2004; Kinkelin *et al.* 2012), supports additionally the finding that the loss of activity in cap-independent translation in melon of the mutant eIF4E results from its reduced binding to eIF4G. In contrast, the corresponding residue in lettuce eIF4E was not involved in *in vitro* binding to eIF4G and its substitution did not reduce viral accumulation of *Lettuce mosaic virus* (German-Retana *et al.* 2008). In addition, substitution L157G in melon eIF4E was also not able to complement cap-independent translation, and its binding to $eIF4G_{p20}$ was shown to be affected. No studies about a possible role in eIF4G-binding of the corresponding residue in eIF4E from other species exist yet. Interestingly, the two mutations in eIF4E from melon did not affect its ability

to complement growth of an eIF4E-deficient yeast strain, suggesting that these residues in melon eIF4E may not be important for its complexing with yeast eIF4G.

In conclusion, we have provided direct proof that Ma5TE binds eIF4F from melon, by identifying the essential nucleotides required. For this binding, it is not essential that eIF4F be intact, since a fragment of eIF4G complexed with eIF4E is sufficient, possibly due to induction of conformational changes in eIF4E or due to the presence of an RNA-binding motif in the eIF4G fragment. Finally, mutational analyses of eIF4E revealed amino acids involved in cap-independent translation providing information for the possible engineering of eIF4E mutants that disrupt cap-independent translation of viral RNAs.

5. REFERENCES

Aitken, C.E. and Lorsch, J.R. 2012. A mechanistic overview of translation initiation in eukaryotes. *Nature Structural & Molecular Bioogy* **19,** 568-576.

Altmann, M., Muller, P.P., Pelletier, J., Sonenberg, N. and Trachsel, H. 1989. A mammalian translation initiation factor can substitute for its yeast homologue in vivo. *Journal of Biological Chemestry* **264,** 12145-12147.

Ashby, J.A., Stevenson, C.E.M., Jarvis, G.E., Lawson, D.M. and Maule, A.J. 2011. Structure-based mutational analysis of eIF4E in relation to sbm1 resistance to Pea seed-borne mosaic virus in Pea. *PLoS ONE* **6,** e15873.

Carstens, E.B. 2010. Ratification vote on taxonomic proposals to the International Committee on Taxonomy of Viruses (2009). *Archives of Virology* **155,** 133-146.

Charron, C., Nicolaï, M., Gallois, J.L., Robaglia, C., Moury, B., Palloix, A. and Caranta, C. 2008. Natural variation and functional analyses provide evidence for co-evolution between plant eIF4E and potyviral VPg. *Plant Journal* **54,** 56-68.

Chodosh, L.A. 2001. UV Crosslinking of Proteins to Nucleic Acids. *Current Protocols in Molecular Biology* **Chapter 12**, Unit 12.5.

Díaz, J.A., Nieto, C., Moriones, E., Truniger, V. and Aranda, M.A. 2004. Molecular characterization of a Melon necrotic spot virus strain that overcomes the resistance in melon and nonhost plants. *Molecular Plant-Microbe Interactions* **17,** 668-675.

Gallie, D.R. 2002. Protein-protein interactions required during translation. *Plant Molecular Biology* **50,** 949-970.

Gazo, B.M., Murphy, P., Gatchel, J.R. and Browning, K.S. 2004. A Novel Interaction of Cap-binding Protein Complexes Eukaryotic Initiation Factor (eIF) 4F and eIF(iso)4F with A Region in the 3′-Untranslated Region of Satellite Tobacco Necrosis Virus. *Journal of Biological Chemestry* **279,** 13584-13592.

German-Retana, S., Walter, J., Doublet, B., Roudet-Tavert, G., Nicaise, V., Lecampion, C., Houvenaghel, M.C., Robaglia, C., Michon, T. and Le Gall, O. 2008. Mutational analysis of plant cap-binding protein eIF4E reveals key amino acids involved in biochemical functions and potyvirus infection. *Journal of Virology* **82,** 7601-7612.

Gross, J.D., Moerke, N.J., Von Der Haar, T., Lugovskoy, A.A., Sachs, A.B., McCarthy, J.E.G. and Wagner, G. 2003. Ribosome loading onto the mRNA cap is driven by conformational coupling between eIF4G and eIF4E. *Cell* **115,** 739-750.

Hinnebusch, A.G. and Lorsch, J.R. 2012. The Mechanism of Eukaryotic Translation Initiation: New Insights and Challenges. *Cold Spring Harbor Perspectives Biology* **4**, a011544.

Huang, Y.W., Hu, C.C., Liou, M.R., Chang, B.Y., Tsai, C.H., Meng, M., Lin, N.S. and Hsu, Y.H. 2012. Hsp90 interacts specifically with viral RNA and differentially regulates replication initiation of Bamboo mosaic virus and associated satellite RNA. *PLoS Pathogens* **8,** e1002726.

Jackson, R.J., Hellen, C.U.T. and Pestova, T.V. 2010. The mechanism of eukaryotic translation initiation and principles of its regulation. *Nature Reviews Molecular Cell Biology* **11,** 113-127.

Kinkelin, K., Veith, K., Grünwald, M. and Bono, F. 2012. Crystal structure of a minimal eIF4E–Cup complex reveals a general mechanism of eIF4E regulation in translational repression. *RNA* **18,** 1624-1634.

Kneller, E.L.P., Rakotondrafara, A.M. and Miller, W.A. 2006. Cap-independent translation of plant viral RNAs. *Virus Research* **119,** 63-75.

Kraft, J.J., Treder, K., Peterson, M.S. and Miller, W.A. 2013. Cation-dependent folding of 3' cap-independent translation elements facilitates interaction of a 17-nucleotide conserved sequence with eIF4G. *Nucleic Acids Research* **41,** 3398-3413.

Laederach, A., Das, R., Vicens, Q., Pearlman, S.M., Brenowitz, M., Herschlag, D. and Altman, R.B. 2008. Semiautomated and rapid quantification of nucleic acid footprinting and structure mapping experiments. *Nature Protocols* **3,** 1395-1401.

Low, J. T. and Weeks, K. M. 2010. SHAPE-directed RNA secondary structure prediction. *Methods* **52**, 150-158.

Marcotrigiano, J., Gingras, A.C., Sonenberg, N. and Burley, S.K. 1997. Cocrystal structure of the messenger RNA 5' cap-binding protein (eIF4E) bound to 7-methyl-GDP. *Cell* **89,** 951-961.

Mayberry, L.K., Dennis, M.D., Leah Allen, M., Ruud Nitka, K., Murphy, P.A., Campbell, L. and Browning K.S. 2007. Expression and Purification of Recombinant Wheat Translation Initiation Factors eIF1, eIF1A, eIF4A, eIF4B, eIF4F, eIF(iso)4F, and eIF5. *Methods Enzymology* **430**, 397-408.

Miller, W.A. and White, K.A. 2006. Long-distance RNA-RNA interactions in plant virus gene expression and replication. *Annual Review of Phytopathology* **44**, 447-467.

Miras, M., Sempere, R.N., Kraft, J.J., Miller, W.A., Aranda, M.A. and Truniger, V. 2014. Interfamilial recombination between viruses led to acquisition of a novel translation-enhancing RNA element that allows resistance breaking. *New Phytologist* **202,** 233-246.

Miras, M., Sempere, R.N., Kraft, J.J., Miller, W.A., Aranda, M.A. and Truniger, V. 2015. Determination of the Secondary Structure of an RNA fragment in Solution: Selective 2`-Hydroxyl Acylation Analyzed by Primer Extension Assay (SHAPE). *Bio-protocol* **5,** e1386.

Mortimer, S.A. and Weeks, K.M. 2007. A fast-acting reagent for accurate analysis of RNA secondary and tertiary structure by SHAPE chemistry. *Jorunal of the American Chemical Society* **129,** 4144-4145.

Mumberg, D., Müller, R. and Funk, M. 1995. Yeast vectors for the controlled expression of heterologous proteins in different genetic backgrounds. *Gene* **156,** 119-122.

Nelson, M.R., Leidal, A.M. and Smibert, C.A. 2004. Drosophila Cup is an eIF4E-binding protein that functions in Smaug-mediated translational repression. *EMBO Journal* **23,** 150-159.

Nicholson, B.L. and White, K.A. 2011. 3′ Cap-independent translation enhancers of positive-strand RNA plant viruses. *Current Opinion in Virology* **1,** 373-380.

Nicholson, B.L., Wu, B., Chevtchenko, I. and White, K.A. 2010. Tombusvirus recruitment of host translational machinery via the 3′ UTR. *RNA* **16,** 1402-1419.

Nicholson, B.L., Zaslaver, O., Mayberry, L.K., Browning, K.S. and White, K.A. 2013. Tombusvirus Y-shaped translational enhancer forms a complex with eIF4F and can be functionally replaced by heterologous translational enhancers. *Journal of Virology* **87,** 1872-1883.

Niedzwiecka, A., Marcotrigiano, J., Stepinski, J., Jankowska-Anyszka, M., Wyslouch-Cieszynska, A., Dadlez, M., Gringas, A.C., Mak, P., Darzynkiewicz, E., Sonenberg, N., Burley, S.K. and Stolarski, R. 2002. Biophysical Studies of eIF4E Cap-binding Protein: Recognition of mRNA 5′ Cap Structure and Synthetic Fragments of eIF4G and 4E-BP1 Proteins. *Journal of Molecular Biology* **319,** 615-635.

Nieto, C., Morales, M., Orjeda, G., Clepet, C., Monfort, A., Sturbois, B., Puig-Domènech, P., Pitrat, M., Caboche, M., Dogimont, C., Garcia-Mas, J., Aranda, M.A. and Bendahmane, A. 2006. An eIF4E allele confers resistance to an uncapped and non-polyadenylated RNA virus in melon. *Plant Journal* **48,** 452-462.

Nieto, C., Rodríguez-Moreno, L., Rodríguez-Hernández, A.M., Aranda, M.A. and Truniger, V. 2011. Nicotiana benthamiana resistance to non-adapted Melon necrotic spot virus results from an incompatible interaction between virus RNA and translation initiation factor 4E. *Plant Journal* **66,** 492-501.

Papadopoulos, E., Jenni, S., Kabha, E., Takrouri, K. J., Yi, T., Salvi, N., Luna R.E., Gavathiotis, E., Mahalingam, P., Arthanari, H., Rodriguez-Mias, R., Yefidoff-Freedman, R., Aktas, B.H., Chorev, M., Halperin, J.A. and Wagner, G. 2014. Structure of the eukaryotic translation initiation factor eIF4E in complex with 4EGI-1 reveals an allosteric mechanism for dissociating eIF4G. *Proceedings of the National Academy of Sciences USA* **111,** 3187-3195.

Parisien, M. and Major, F. 2008. The MC-Fold and MC-Sym pipeline infers RNA structure from sequence data. *Nature* **452,** 51-55.

Park, E.H., Walker, S.E., Lee, J.M., Rothenburg, S., Lorsch, J.R. and Hinnebusch, A.G. 2011. Multiple elements in the eIF4G1 N-terminus promote assembly of eIF4G1•PABP mRNPs in vivo. *EMBO Journal* **30,** 302-316.

Peter, D., Igreja, C., Weber, R., Wohlbold, L., Weiler, C., Ebertsch, L., Weichenrieder, O. and Izaurralde, E. 2015. Molecular Architecture of 4E-BP Translational Inhibitors Bound to eIF4E. *Molecular Cell* **57,** 1074-1087.

Ptushkina, M., Von der Haar, T., Vasilescu, S., Frank, R., Birkenhäger, R. and McCarthy, J.E.G. 1998. Cooperative modulation by eIF4G of eIF4E-binding to the

mRNA 5' cap in yeast involves a site partially shared by p20. *EMBO Journal* **17,** 4798-4808.

Rodríguez-Hernández, A.M., Gosalvez, B., Sempere, R.N., Burgos, L., Aranda, M.A. and Truniger, V. 2012. Melon RNA interference (RNAi) lines silenced for Cm-eIF4E show broad virus resistance. *Molecular Plant Pathology* **13,** 755-763.

Rutkowska-Wlodarczyk, I., Stepinski, J., Dadlez, M., Darzynkiewicz, E., Stolarski, R. and Niedzwiecka, A. 2008. Structural Changes of eIF4E upon Binding to the mRNA 5′ Monomethylguanosine and Trimethylguanosine Cap. *Biochemistry* **47,** 2710-2720.

Scheets, K. and Redinbaugh, M.G. 2006. Infectious cDNA transcripts of Maize necrotic streak virus: Infectivity and translational characteristics. *Virology* **350,** 171-183.

Simon, A.E. and Miller, W.A. 2013. 3′ cap-independent translation enhancers of plant viruses. In: *Annual Review of Microbiology* pp. 21-42.

Truniger, V., Nieto, C., González-Ibeas, D. and Aranda, M.A. 2008. Mechanism of plant eIF4E-mediated resistance against a Carmovirus (Tombusviridae): Cap-independent translation of a viral RNA controlled in cis by an (a)virulence determinant. *Plant Journal* **56,** 716-727.

Walia, R.R., Xue, L.C., Wilkins, K., El-Manzalawy, Y., Dobbs, D. and Honavar, V. 2014. RNABindRPlus: A Predictor that Combines Machine Learning and Sequence Homology-Based Methods to Improve the Reliability of Predicted RNA-Binding Residues in Proteins. *PLoS ONE* **9,** e97725.

Wang, Z., Parisien, M., Scheets, K. and Miller, W.A. 2011. The cap-binding translation initiation factor, eIF4E, binds a pseudoknot in a viral cap-independent translation element. *Structure* **19,** 868-880.

Wang, Z., Treder, K. and Miller, W.A. 2009. Structure of a viral cap-independent translation element that functions via high affinity binding to the eIF4E subunit of eIF4F. *Journal of Biological Chemestry* **284,** 14189-14202.

Wilkinson, K.A., Merino, E.J. and Weeks, K.M. 2006. Selective 2′-hydroxyl acylation analyzed by primer extension (SHAPE): Quantitative RNA structure analysis at single nucleotide resolution. *Nature Protocols* **1,** 1610-1616.

6. SUPPORTING INFORMATION

Supplementary Table 1. Primers used in this study

Primer	Sequence (5´-3´)	Application
SLC30_ R	CGCCGTTACGGTTAGCCAGACCGCACTACATTACACGGCGATCTTTCCGCCC	Luciferase construct SLC 30 nts
SLC30c_R	GGGCCCGCCGTTACGGTTAGCCAGACCGCACTACAGGCCCTTACACGGCGATCTTTCCGCCC	Luciferase construct SLC30 clamped version
SLC45_R	TGCCGATACGCCGTTACGGTTAGCCAGACCGCACTACACACAACATTACACGGCGATCTTTCCGCCC	Luciferase construct SLC 45 nts
SLC45c_R	GGGCCTGCCGATACGCCGTTACGGTTAGCCAGACCGCACTACACACAACAGGCCCTTACACGGCGATCTTTCCGCCC	Luciferase construct SLC45 clamped version
SLC53_R	TCCTTGCCGATACGCCGTTACGGTTAGCCAGACCGCACTACACACAACAGGGATTACACGGCGATCTTTCCGCCC	Luciferase construct SLC 53 nts
SLC53c_R	GGGCCTCCTTGCCGATACGCCGTTACGGTTAGCCAGACCGCACTACACACAACAGGGAGGCCCTTACACGGCGATCTTTCCGGCCC	Luciferase construct SLC53 clamped version
45cMut a-c_R	GGGCCTGCCGATACGCCGGTACGGTTAGCCAGACCGCACTACACACAACAGGCCCTTACACGGCGATCTTTCCGCCC	Mutant A4109C
45cMut a-g_R	GGGCCTGCCGATACGCCGCTACGGTTAGCCAGACCGCACTACACACAACAGGCCCTTACACGGCGATCTTTCCGCCC	Mutant A4109G
45cMut g-c_R	GGGCCTGCGCACTACACACAACAGTTAGCCAGACCGCACTACACACAACAGGCCCTTACACGGCGATCTTTCCGCCC	Mutant G4093C
45cMut gc-cg_R	GGGCCTGCCGATACGCCGTTACCGTTAGCCAGACGGCACTACACACAACAGGCCCTTACACGGCGATCTTTCCGCCC	Mutant G4093C-C4105G
eIF4Gp10_F	TACTTCCAATCCAATGCAAATGAGGCTATTAAAGAAGATG	eIF4G$_{p10}$ cloning in p2CT
eIF4Gp10_R	TTATCCACTTCCAATGTTATTAATTGGTATGAGTACTCATTAAAG	
eIF4Gp20_F	TACTTCCAATCCAATGCAGTAGCACATTCAGAGAGTATTG	eIF4G$_{p20}$ cloning in p2CT
eIF4Gp20_R	TTATCCACTTCCAATGTTATTAACCAGGTCGGAAACCCGCAGTA	
4E_F	TTTAAGAAGGAGATATAGATCATGGTAGTTGAAGATTCGATGAAAG	eIF4E cloning in p2AT
4E_R	TTATGGAGTTGGGATCTTATTACACCATATATTTATTCTTCGC	
MaTE_SHAPE_F	CTGATGAATTCTGTTGTGTGTAGTGC	Ma5TE structure probing
MaTE_SHAPE_R	TGCCGATACGCCGTTAC	
SL45cT7_F	AATTTAATACGACTCACTATAGGGGCCTGTTGTGTGTAGTGCGGTCTG	Ma5TE PCR amplification for UV-crosslinking assay
SL45c_R	GGGCCTGCCGATACGCCGTTAC	

SL45cmutT7_F	AATTTAATACGACTCACTATAGGGGCCTGTTGTGTGTAGTGCGC	Ma5TE mutant
4E_W82L_F	CAAGCCACCCTTGGTGCGTCT	eIF4E Mutation, W82L
4E_W82L_R	AGACGCACCAAGGGTGGCTTG	
4E_W99A_F	TCTACCGTCGAGGAGTTCGCGAGTGTTTACAACAACATT	eIF4E Mutation, W99A
4E_W99A_R	AATGTTGTTGTAAACACTCGCGAACTCCTCGACGGTAGA	
4E_Y154H_F	TCTGATAATGGCTGGTTGCACACGCTGCTTGCTATGATC	eIF4E Mutation, Y154H
4E_Y154H_R	GATCATAGCAAGCAGCGTGTGCAACCAGCCATTATCAGA	
4E_L157G_F	GGCTGGTTGTACACGCTGGGTGCTATGATCGGAGAACAG	eIF4E Mutation, L157G
4E_L157G_R	CTGTTCTCCGATCATAGCACCCAGCGTGTACAACCAGCC	
4E_Q163A_F	CTTGCTATGATCGGAGAAGCATTTGACTGTGGTGATGAA	eIF4E Mutation, Q163A
4E_Q163A_R	TTCATCACCACAGTCAAATGCTTCTCCGATCATAGCAAG	
4E_H228R_F	GCAAAGAAATTCGATAGACGTGCGAAGAATAAATATATG	eIF4E Mutation, H228R
4E_H228R_R	CATATATTTATTCTTCGCACGTCTATCGAATTTCTTTGC	
Triple mut C_F	GGAGATATGGCCAAGAAGGCATCTAGGGATTTTGCAGCAAAGTTTG CCGAGCAGTTT	eIF4G$_{p20}$ Y1049A-L1054A-L1055A
Triple mut C_R	AAACTGCTCGGCAAACTTTGCTGCAAAATCCCTAGATGCCTTCTTGG CCATATCTCC	

Supplementary Table 2. Mutants and constructs used in this study

Protein	Mutation	Type of mutation
$eIF4E_{1\text{-}235\ full\ length}$	WT	
	W82L	Cap-binding pocket
	H228L	*nsv* resistance allele
	H228R	Maintenance of positive charge in $eIF4E_{H228}$ allele (RNA-binding motif)
	K230R	RNA-binding motif
	W99A	Dorsal surface
	Y154H	Dorsal surface
	Q163A	Dorsal surface
	L157G	Dorsal surface
	Y154H-W99A	Dorsal surface
$eIF4G_{980\text{-}1159}$	WT	
	Y1049A-L1054A-L1055A	Canonical eIF4E-binding domain

Chapter 3

Crystal structure of a plant eIF4E in complex with eIF4G reveals a universal bipartite binding mode for eIF4E interacting proteins in higher eukaryotes

1. INTRODUCTION

The initiation of eukaryotic protein synthesis is a key control and highly regulated step in gene expression (Sonenberg & Hinnebusch 2009). Its end is to assemble the large (60S) and small (40S) ribosomal subunits into an active 80S ribosome able to locate the correct start codon of the mRNA. This is facilitaded by the coordinated action of at least 12 protein initiation factors (Jackson *et al.* 2010; Hinnebusch 2011; Hinnebusch & Lorsch 2012). In cap-dependent translation, binding of the eukaryotic translation initiation factor 4F (eIF4F) to the 7-methyl guanosine cap (m^7G cap) at the 5' end of mRNA drives the attachment of the latter to the ribosomal 43S preinitiation complex. In mammals, eIF4F is build up of three proteins: the mRNA 5' cap binding protein eIF4E, the RNA helicase eIF4A, and the scaffolding protein eIF4G, which contains binding domains for eIF4E, eIF4A, eIF3 and poly(A)binding protein (PABP) (Marcotrigiano *et al.* 1997; Pestova *et al.* 2001; Gross *et al.* 2003). In contrast, plant eIF4Fs are heterodimers consisting of eIF4E and eIF4G but lacking eIF4A (Hinnebusch & Lorsch 2012). EIF4G binds simultaneously to eIF4E and PABP, which is able to interact with the mRNA poly(A) tail (Aitken & Lorsch 2012) resulting in a transient circularization of the mRNA. EIF4G also associates with eIF3, recruiting the 40S subunit of the ribosome and initiating the scanning of the mRNA in the 5´ to 3´direction (Jackson *et al.* 2010) (Park *et al.* 2011). EIF4G interacts with eIF4E through a highly conserved $Y(X)_4L\phi$ amino acid sequence, where X is variable and ϕ is hydrophobic. EIF4E-binding proteins (4E-BPs) also contain this motif (Mader *et al.* 1995; Marcotrigiano *et al.* 1999) and inhibit translation initiation by competing for the same binding site on the eIF4E surface thus blocking the assembly of translation active complexes (Mader *et al.* 1995; Matsuo *et al.* 1997; Marcotrigiano *et al.* 1999; Gross *et al.* 2003). In addition to the aforementioned canonical or C domain, 4E-BPs and eIF4G also contain a downstream non-canonical (NC) motif that binds to a highly conserved hydrophobic lateral surface of eIF4E (Mizuno *et al.* 2008; Gosselin *et al.* 2011; Kinkelin *et al.* 2012; Paku *et al.* 2012; Lukhele *et al.* 2013; Igreja *et al.* 2014). This NC domain enhances eIF4G-eIF4E affinity and is required for 4E-BPs to be able to compete with eIF4G and repress translation (Paku *et al.* 2012; Lukhele *et al.* 2013; Igreja *et al.* 2014). How NC motifs, which are poorly conserved in terms of amino acid sequence similarity

from ortholog genes, bind to the same conserved eIF4E surface remains elusive. Recently, structural analyses have revealed that, besides the canonical N-terminal alpha-helical motif binding to the dorsal surface of eIF4E, two additional structural elements are present in 4E-BPs: (1) an elbow loop downstream the canonical domain, which induces the bending of the peptide backbone thus allowing the (2) non-canonical loop to bind the hydrophobic pocket on the lateral surface of eIF4E (Kinkelin *et al.* 2012; Igreja *et al.* 2014; Peter *et al.* 2015a; Peter *et al.* 2015b). Despite this NC extra anchoring point showing the largest structural differences between the different complexes, they all contact the same hydrophobic lateral surface of eIF4E through hydrophobic interactions and main chain hydrogen bonds (Kinkelin *et al.* 2012; Peter *et al.* 2015a; Peter *et al.* 2015b).

Structural information of eIF4E bound to eIF4G is still scant for higher eukaryotes and so far focusing only on the canonical binding domain. A competition model, based on the solution structure of yeast eIF4E-eIF4G complex has been proposed in which the C-terminal region downstream of the canonical domain folds back towards the flexible N-terminal tail of eIF4E (Kinkelin *et al.* 2012; Peter *et al.* 2015a; Peter *et al.* 2015b). However, analysis of eukaryotic eIF4G amino acid sequences downstream of the canonical domain from different species suggests that eIF4G could also exploit the above commented eIF4E second binding surface. Our high resolution structure of a plant eIF4E in complex with a eIF4G peptide containing both motifs together with our functional analysis shows that eIF4G binds to eIF4E through both, the canonical and non-canonical domains. On the light of our results a universal bipartite mode of binding to eIF4E is proposed.

2. EXPERIMENTAL PROCEDURES

2.1. Plasmids

The plasmids expressing melon eIF4G-WT and eIF4E were previously described in Miras et al., 2016. Briefly, eIF4G (residues 1003-1092) and eIF4E (residues 51-235) were amplified by PCR from plasmids pTOPO-Cm-4G and pET15b-4EVed (Nieto et al.,

2006) and cloned by LIC technology into the p2CT (which provides an N-terminal MPB tag followed by a TEV protease cleavage site) and p2AT expression vectors, respectively (Macrolab, UC Berkeley, CA, USA) yielding p2CT-eIF4G-p10 and p2AT-eIF4E-WT (Miras et al., 2016). For expression of the eIF4F complex, a dicistronic expression vector was generated by cloning into plasmid p2D (Macrolab), yielding p2D-4Fp10: eIF4E was cloned into cassette 1 using *BamHI*/*XbaI* restriction sites and eIF4G-WT was cloned into cassette 3 using *SbfI*/*AscI* restriction sites. All *Cm* eIF4E and *Cm* eIF4G mutants were generated by site-directed mutagenesis using plasmids pET15b-4EVed (H228) and p2CT-eIF4G-p10, respectively, and the oligonucleotide sequences provided in Supplementary Table 1. For transient *Cm* eIF4E expression in the complementation experiments, the eIF4E constructs were cloned into the binary vector pBIN61 using *XbaI*/*XmaI* restriction sites. All mutants were confirmed by DNA sequencing and are listed in Supplementary Table 4.

Luc construct with the 5´- and 3´-UTR from MNSV-Mα5 and MNSV-264 flanking the firefly luciferase gene has been previously described (Truniger *et al.* 2008a). Reporter RNA was obtained by *in vitro* transcription (RiboMAX Large Scale RNA production, Promega).

2.2. Protein expression and purification

All proteins were expressed, as previously described in Miras et al., 2016, in *E. coli* Rosetta^{TM} (DE3) pLysS cells (Novagen) that were grown in LB medium at 37 °C to an OD_{600} of 0.6. At this point IPTG was added to a final concentration of 0.4 mM to induce protein expression at 37 °C for 2 hours. Cells were re-suspended in Nickel Buffer A (25 mM HEPES pH 7.5, 400 mM NaCl, 20 mM imidazole, 10% glycerol, 1 mM dithiothreitol (DTT)) and supplemented with DNaseI (Roche) and protease inhibitor cocktail (Roche) and lysed by sonication. Expressed eIF4Fp10 was loaded on a HisTrap HP column (GE Healthcare) and eluted with Nickel Buffer B (as for Nickel Buffer A but with 400mM imidazole). After buffer exchange, eluted protein was quantified by spectrometry at OD_{280}. The His_6-tag and the MBP-tag were removed after cleavage with TEV protease at a 1:20 mass ratio and incubated overnight at 4 °C. Finally, this protein was again

loaded into the same HisTrap HP column and eluted with Nickel Buffer B and loaded onto a size exclusion Superdex 200 16/60 column (GE Healthcare). eIF4E (51-235) was expressed from p2A-eIF4E-WT as described above and purified taking advantage of its affinity for HisTrap HP column (GE Healthcare). Finally, protein was passed through a final size exclusion chromatography column (Superdex 200 16/60 , GE Healthcare). Purification of full-length eIF4E was carried out as previously described in (Nieto *et al.* 2006). All proteins were concentrated to a final concentration of 10 mg/ml and buffers were exchanged to the final buffer 25 mM HEPES pH 7.5, 200 mM NaCl and 10% glycerol.

2.3. Crystallization, Data Collection and Processing

Crystals were obtained using the hanging drop vapour diffusion method. Briefly, 1µl of protein solution (10 mg/ml) was mixed with an equal volume of reservoir solution and incubated at 20°C until crystals suitable for X-ray difraction were obtained. eIF4E crystals were grown using XXX as precipitant and eIF4E-CAP complex was obtain by incubating native crystals O/N in the presence of 1:1.1 excess of ligand. eIF4E-eIF4G complex was crystallized using 1.4-1.6 M Ammonium sulphate, 100mM Na Acetate pH 4.5 as reservoir solution. Small needles were obtained when plates were incubated at 20ºC. Suitable crystals for X-ray data collection were obtained using micro-seeding techniques. Data was collected using synchrotron radiation at ALBA-CELLS after flash freezing under liquid nitrogen using 20% glycerol as cryo-protectant. Diffraction images from one single crystal for each complex were processed using XDS (Emsley & Cowtan 2004) and SCALA (Collaborative computational project 1994).

2.4. eIF4E-eIF4G Structure Solution and Refinement

Initial phases were determined by molecular replacement with the program MOLREP (Collaborative computational project 1994) using the crystal structure of wheat eIF4E as a searching model ((Monzingo *et al.* 2007); PDB ID: 2IDR). Rigid body refinement was using REFMAC5 (Murshudov *et al.* 1997). Manual rebuilding was performed using COOT (Emsley & Cowtan 2004) and refinement using Refmac5 and

PHENIX (Brünger *et al.* 1998). Statistics for both data collection and refinement are summarized Supplementary Table 5.

2.5. Protein pull-down assays

For the pull-down experiments shown in Fig. 34 and 35, eIF4G (WT and mutants) were expressed with a N-terminal MBP tag in *E. coli* Rosetta™ (DE3) pLysS cells as described above. The bacterial cells were resuspended in 2 mL of lysis buffer and lysed by sonication. Purified eIF4E (1 µM) was added to the cleared lysates, adjusted to 300 µl with lysis buffer and incubated with 30 µl of amylose resin (New England Biolabs) for 1h at 4°C. The beads were washed three times with lysis buffer and eluted with 60 µl of lysis buffer containing 25 mM maltose. Maltose binding protein (MBP) was expressed and incubated with purified eIF4E as negative control. Proteins were analyzed by 12% of SDS-PAGE followed by Coomassie blue staining.

In Fig. 36, MBP-tagged eIF4G-WT and eIF4E (WT and mutants) were expressed in *E. coli* Rosetta™ (DE3) pLysS cells as described above. Pull-down was performed with cleared lysates, using the same volume of eIF4G-WT lysate for each interaction experiment and similar amounts of the eIF4E lysates (WT and mutants), as controlled by Western blot using a rabbit polyclonal antibody against melon eIF4E (input). Proteins were analyzed by 12% of SDS-PAGE followed by Western blot using a rabbit polyclonal antibody against melon eIF4E (Miras *et al.,* 2016).

2.6. Binding efficiency

For binding affinity experiments shown in Fig. 35, eIF4G lysates from WT and mutants (C, NC and C-NC) were adjusted at the same concentration with lysis buffer. Serial concentrations of 0.5, 1, 2 and 3 µM of purified eIF4E were added to each eIF4G lysate and incubated with amylose resin for 1h at 4°C. Elution and staining were followed as before.

Band intensities of pulled-down eIF4Es were quantified with Quantity One software and plotted versus total eIF4E input. Apparent dissociation constants were calculated using a one-site binding model (GraphPad Prism).

2.7. Translation complementation by transiently-expressed eIF4E

*Cm*eIF4E WT and mutant proteins were transiently expressed from binary plasmids in cotyledons of $eIF4E_{H228L}$ allele-melon by agroinoculation in the presence of the tombusvirus silencing suppressor P19 as previously described (Nieto *et al.* 2011). At 3-4 days post-agroinfiltration, protoplasts were prepared from infiltrated tissues. *In vivo* translation assays were performed as previously described (Truniger *et al.* 2008a) by electroporating separately with two 5´-UTR-luc-3´-UTR RNA constructs, differing in the UTRs flanking the luciferase gene that were either from isolate MNSV-Mα5 (eIF4E-dependent) or from the eIF4E-independent isolate MNSV-264. Translation of MNSV-264 can take place in protoplasts from eIF4E knocked-down lines, strongly suggesting that it can function in the absence of eIF4E (Rodríguez-Hernández *et al.* 2012) and therefore serves for normalization of the different protoplast preparations. In agreement with Truniger *et al.* (2008), eIF4E-dependent translation controlled by the Ma5TE of MSNV-Mα5 in resistant melon was very low, but transiently expressed eIF4E WT (H228 allele) was able to complement translation (Nieto *et al.,* 2006). After 5-6 h incubation in the dark at 25 °C, protoplasts were lysed in 1xPLB (Passive lysis buffer, Promega). *Firefly* and *Renilla* luciferase activities were measured with the Luciferase assay system (Promega).

For each protoplast preparation the translation efficiency obtained with the construct of MNSV-264 was set to 100 % and translation of MSNV-Mα5 was related to it. The expression levels of eIF4E were analyzed in protein extracts (extraction buffer: 0.1 M Tris HCl pH 9.0, 0.1 M NaCl, 5 M Urea, 10 mM EDTA, 0.1 M β-mercaptoethanol) of infiltrated cotyledons and visualized by Western blot using a rabbit polyclonal antibody against melon eIF4E (Miras *et al.,* 2016).

2.8. Yeast complementation

Saccharomyces cerevisiae strain JO55 lacks its endogenous *eIF4E* gene and requires complementation with an external eIF4E to survive, for example the human eIF4E expressed from the pGAL-eIF4E-URA3 plasmid in a galactose-dependent manner (Altmann *et al.* 1989). For the analysis of the complementation capacity of the melon eIF4E mutants, the cDNAs encoding each of the eIF4E variants were introduced into the *SpeI*/*BamHI* restriction sites of the Trp-selectable yeast-*Escherichia coli* shuttle vector p424-GDP/TRP1 (Mumberg *et al.* 1995) and used to transform into JO55 selected on galactose-containing minimal medium in the absence Ura and Trp. After transformation yeast cells were grown at 30 °C in liquid Gal/Raf-Ura-Trp medium until OD_{600} of 1, washed with sterile water and serially diluted in 10-fold steps until reaching 1000-fold. Drops (5 μL) of dilutions were placed on both control Gal/Raf-Ura-Trp solid medium and nitrogen base medium containing 2% glucose in the absence of Ura/Trp. JO55 transformed with an empty p424-GPD/TRP1 vector was used as negative control. The positive control was JO55 transformed with *Arabidopsis thaliana eIF4E* gene present in vector p424-GPD/TRP1:At-eIF4E (Charron *et al.* 2008).

3. RESULTS AND DISCUSSION

3.1. Crystal structure of the eIF4F complex

To understand the binding mode of eIF4G to eIF4E, we crystallized and determined the structures of free *Cm* eIF4E and in complex with a *Cm* eIF4G peptide at 2.56 Å and 1.9 Å resolution, respectively (Fig. 26). Previous structural studies with other eIF4Es from diverse organisms have shown that the full-length protein can be recalcitrant for crystallization, however N-terminally truncated versions of eIF4E have been successfully crystalized while they keep their cap-binding abilities (Marcotrigiano *et al.* 1997; Matsuo *et al.* 1997; Marcotrigiano *et al.* 1999; Monzingo *et al.* 2007).

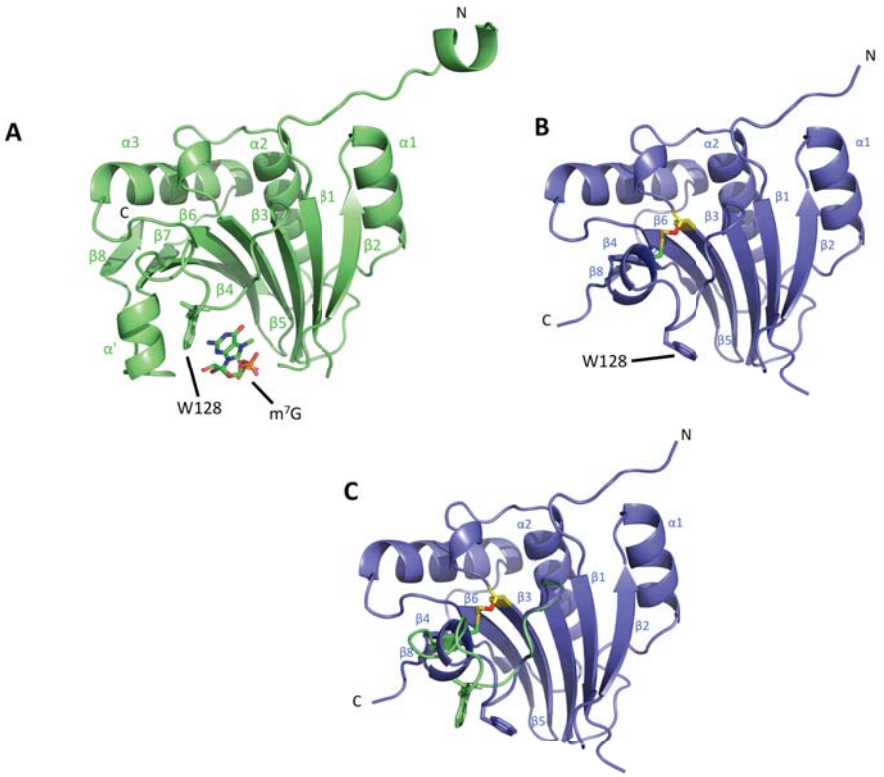

Figure 26. Structures of melon eIF4E. A) Ribbon diagram of the free *Cm* eIF4E$_{51-235}$ in complex with m^{7}G. The m^{7}G is located in the cap-binding pocket. Residue W128, in direct interaction with cap, is shown as sticks. B) Ribbon representation of *Cm* eIF4E$_{51-235}$ in complex with the eIF4G peptide. Residue W128 involved in cap-binding interaction is represented as stick and the disulfilde bond is shown in yellow sticks. C) Structural alignment of the structures of free (green) and complexed (blue) *Cm* eIF4E reveals differences in the conformation of the loops involved in cap-pocket. Residues 51-121 and 139-235 from free *Cm* eIF4E were omitted for clarity. Selected secondary structure elements are labeled in the same color as the corresponding protein.

Preliminary studies using the I-TASSER server (Yang *et al.* 2015) predicted that the first 50 residues of *Cm* eIF4E are likely to be disordered. Thus, we designed a N-terminal truncated *Cm* eIF4E, eIF4E$_{51-235}$, for crystallization. The *Cm* eIF4G peptide used in the complex was chosen based on a combination of sequence conservation and secondary structure prediction. Thus, we used the peptide *Cm* eIF4G$_{1003-1092}$, which contains the canonical eIF4E binding motif and a downstream extra sequence that includes a hydrophobic patch conserved in other eIF4Gs that was predicted by I-TASSER to be structured.

The obtained *Cm* eIF4E structure, free or in complex with *Cm* eIF4G$_{1003-1092}$, is similar to those of other eIF4Es from diverse organisms (Marcotrigiano *et al.* 1999; Marcotrigiano *et al.* 2001; Gross *et al.* 2003; Paku *et al.* 2012; Papadopoulos *et al.* 2014; Peter *et al.* 2015a). The X-ray data from free *Cm* eIF4E cocrystallized with m^{7}G revealed four independent copies of eIF4E in the crystallographic asymmetric unit. *Cm* eIF4E adopts a crescent-shaped conformation formed by a strongly bent β sheet of eight antiparallel β-strands (Fig. 26A). The convex surface is decorated by three α-helices that form the dorsal surface. The cap-binding pocket is located on the concave, ventral surface, and contains the cap-analog m^{7}G sandwiched between two conserved tryptophan rings (W82 and W128) in an aromatic stack, although in none of the crystals the W82 is visible in the electron density map. The free *Cm* eIF4E structure most closely resembles that of pea (PDB ID: 21DV; (Ashby *et al.* 2011)). A superposition of the pea eIF4E protein with its melon homolog gives a root mean square deviation (RMSD) of 0.37 Å over 171 structurally equivalent residues.

The most significant difference between the two *Cm* eIF4E protein structures, free or in complex, appears to be the formation of a disulfide bond between cysteine C133 and C171 when eIF4E is bound to the eIF4G peptide (Fig. 26B). The formation of this disulfide linkage may avoid the presence of the cap in the cap-binding pocket as was proposed in the wheat eIF4E (Monzingo *et al.* 2007). In the free melon eIF4E, the two S_γ atoms are in close proximity (4.1 A), but are not bridged. The two Cys residues involved are strictly conserved among plant orthologs (Fig. 27) but the biological significance of this observation remains uncertain (Monzingo *et al.* 2007).

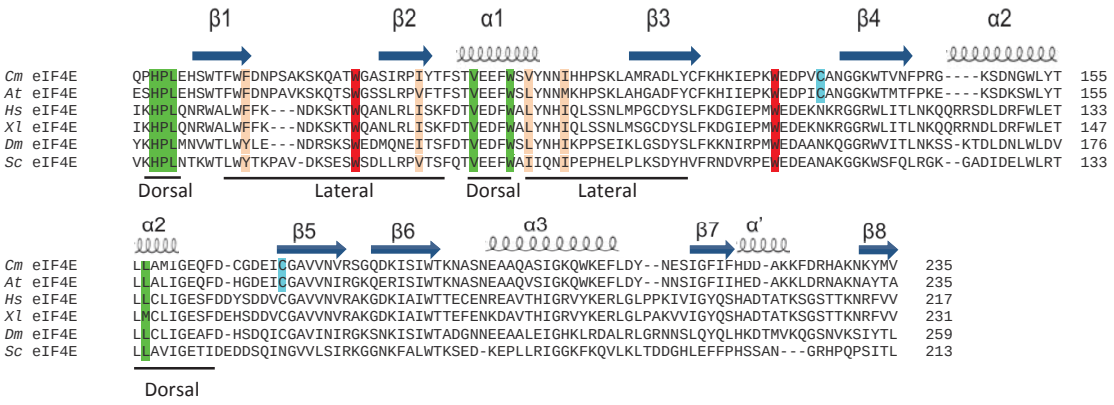

Figure 27. Structure-based sequence alignment of eIF4E orthologous proteins. Amino acids involved in canonical and non-canonical interactions that are invariant in the different 4E sequences are labeled in green and orange, respectively. Plant-specific cysteines forming disulfide bridge are marked in blue and the tryptophans residues coordinating the m^7G cap are labelled in red. Schematic representation of secondary structure is pointed above the alignment and the lateral and dorsal binding surfaces are indicated by a line below the sequences. Input sequences belong to *Cucumis melo* (*Cm*), *Arabidopsis thaliana* (*At*), *Homo sapiens* (*Hs*), *Xenopus laevis* (*Xl*), *Drosophila melanogaster* (*Dm*) and *Saccharomyces cerevisiae* (*Sc*).

Another difference consist of a structural rearrangement in the loop that harbors W128. This loop is extended away from the surface and displaces W128 out of the cap-binding cavity in the complex (Fig. 26C). However, this difference can be explained, at least partially, by the absence of the ligand in the cap-binding pocket, as equivalent structures have been foud for other eIF4E proteins crystallized without the substrate, indicating similar aberrant movements of the loops that are supposed to bind the cap analog (Volpon *et al.* 2006; Monzingo *et al.* 2007; Rosettani *et al.* 2007; Siddiqui *et al.* 2012).

The structural details of the interacting eIF4G peptide revealed a short N-terminal α-helix and a loop connected by a linker region (Fig. 28). Each of these three structural elements bind to a defined eIF4E surface: 1) The N-terminal α-helix is formed by the canonical binding motif and interacts with the dorsal surface of eIF4E. 2) An elbow loop after the canonical α-helix that bends the peptide backbone by approximately 90°, orienting the linker region downward to engage the lateral surface of eIF4E. 3) The loop contacts a hydrophobic pocket on the lateral surface of eIF4E, suggesting the existence of a second non-canonical binding motif. Importantly, this second motif was identified before in *Drosophila melanogaster* and in vertebrates

eIF4E-binding proteins (4E-BP) (Kinkelin *et al.* 2012; Igreja *et al.* 2014; Peter *et al.* 2015a; Peter *et al.* 2015b), but it was not previously identified in eIF4G.

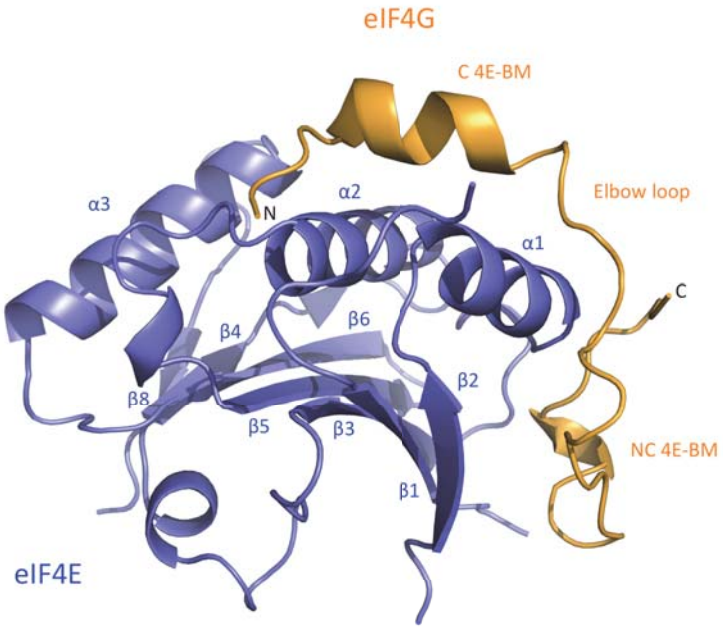

Figure 28. Structure of melon eIF4E-eIF4G complex. Ribbon diagram of the complex with *Cm* eIF4E$_{51-235}$ and *Cm* eIF4G$_{1003-1092}$ colored in blue and orange, respectively. *Cm* eIF4G contains a canonical eIF4E binding-domain (C 4E-BM) and a non-canonical eIF4E binding-domain (NC 4E-BM). Selected secondary structure elements are named in the same color as the corresponding protein.

3.2. Structure of the canonical eIF4E binding site of *Cm* eIF4G

As expected, the canonical binding motif of *Cm* eIF4G folds into an α-helix that docks at the convex dorsal surface of *Cm* eIF4E by interactions similar to those previously described for other eIF4Gs and 4E-BPs (Marcotrigiano *et al.* 1999; Gross *et al.* 2003; Brown *et al.* 2007; Rosettani *et al.* 2007). The first residue of the consensus sequence Y(X_4)Lϕ, Y_{1059} is located at the extended chain portion of the peptide N-terminus of the α-helix and contacts the backbone of the residues H60, P61 and L62 in *Cm* eIF4E (Fig. 29). The next residues defined by the consensus sequence, L1064 and L1065 (ϕ in the consensus motif), form the first turn of the helix. These residues form hydrophobic contacts with the *Cm* eIF4E residues V95, W99 and L157 (Fig. 29). In addition, arginine and phenylalanine amino acids flank these hydrophobic residues of the canonical motif. The side chain of residue R1061 from the eIF4G peptide contacts

with Y154 from *Cm* eIF4E while F1067 from eIF4G contacts with W99 of *Cm* eIF4E (Fig. 29). All these residues are well conserved in all eukarya eIF4Es and participate in other eIF4Gs and 4E-BPs in the interaction through the canonical motif (Fig. 27) (Marcotrigiano *et al.* 1999; Kinkelin *et al.* 2012; Peter *et al.* 2015a).

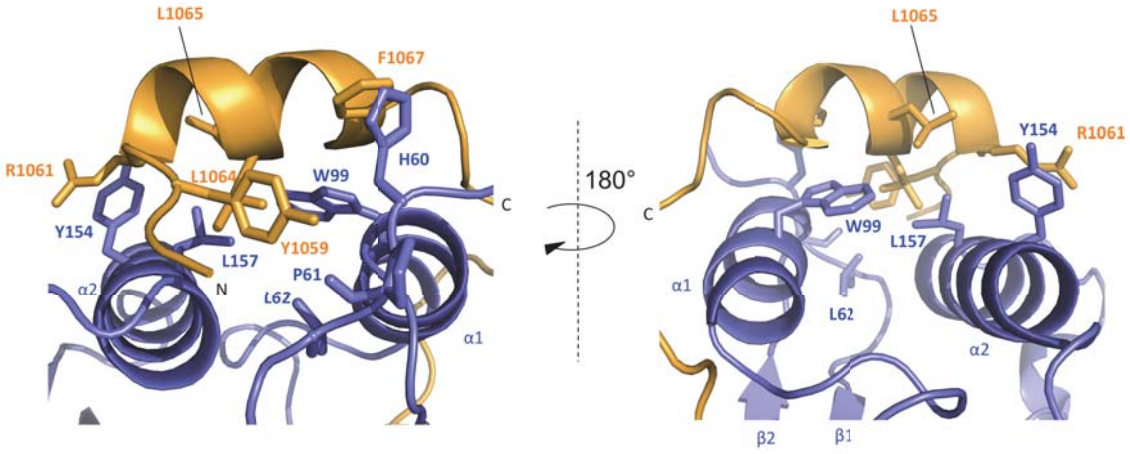

Figure 29. Interaction of the canonical motif of *Cm* eIF4G with the dorsal surface of *Cm* eIF4E. Close-up views of the interaction between the dorsal surface of eIF4E (blue) and the canonical helix of eIF4G (orange). Selected interface residues are shown as blue sticks for eIF4E and as orange sticks for eIF4G.

3.3. The elbow loop

The proposed non-canonical motif is connected to the canonical α-helix by a linker region, which forms a characteristic elbow loop that enables eIF4G to engage two orthogonal surfaces on eIF4E. The elbow loop is anchored to the lateral surface of eIF4E by $N104^{4E}$. This linker is also present in 4E-BPs but differs in sequence, containing conserved serine and threonine residues that can be phosphorylated (Peter *et al.*, 2015). These residues do not contribute to the binding interface, strongly suggesting that phosphorylation does not directly interfere with complex formation. Phosphorylation has been shown to reduce the efficiency of 4E-BPs to interact with eIF4E and decrease potency of 4E-BPs as translational repressors (Peter *et al*., 2015).

3.4. Structure of the non-canonical binding site of *Cm* eIF4G

A second anchoring point on the lateral surface of eIF4E is provided by a conserved hydrophobic pocket. This pocket is formed by residues F70, I89, Y90, V101

and I105 and is engaged by the eIF4G residues that form the non-canonical binding motif providing an additional binding site. I89^{4E}, a conserved residue (Fig. 27), is central in the interaction with eIF4G and provides a hydrophobic core around which hydrophobic residues F1078 and I1084 from eIF4G are arranged (Fig. 30).

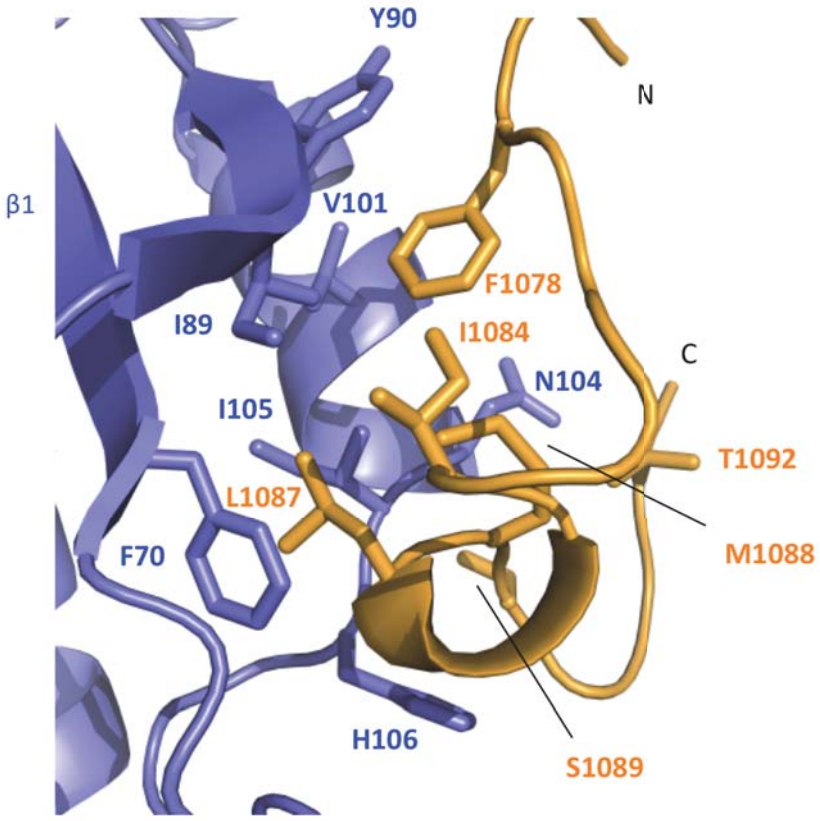

Figure 30. The non-canonical eIF4E interaction loop. Close-up view of the *Cm* eIF4G (orange) showing all interactions with the lateral surface of *Cm* eIF4E (blue). Selected residues mediating the interactions are shown in blue sticks for eIF4E and orange sticks for eIF4G.

Interestingly, I89^{4E} has also been shown to be involved in binding to eIF4G in yeast (Gross *et al.* 2003). Comparison of *Cm* eIF4E-eIF4G with the solution structure of the yeast eIF4E-eIF4G complex shows a partial overlapping that suggests that yeast eIF4G may also bind a lateral surface of eIF4E (Fig. 31).

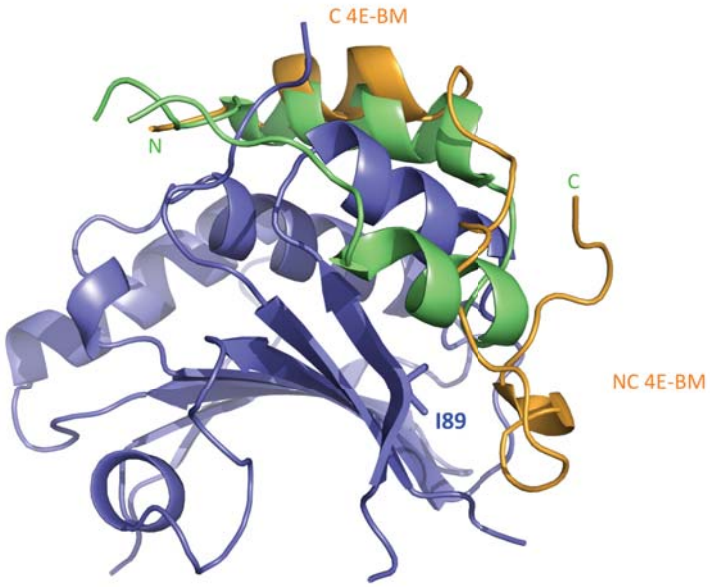

Figure 31. Superposition of the yeast eIF4G on the *Cm* eIF4E-eIF4G complex. *Sc* eIF4G (green) and *Cm* eIF4G (orange) are in contact with residue I89 in the lateral surface of *Cm* eIF4E (blue). *Sc* eIF4E and *Sc* $eIF4G_{215-273}$ (PDB ID: 1RF8; Gross et al., 2003) have been omitted for clarity.

On the beta-turn of *Cm* eIF4G, $L1087^{4G}$ contacts with main-chain conserved residues $F70^{4E}$ and $I105^{4E}$ and engages the hydrophobic pocket. $M1088^{4G}$ makes side-chain contacts with $I105^{4E}$ and with the carbonyl oxygen of $H106^{4E}$. In the N-terminus of the non-canonical motif, $F1078^{4G}$ contacts with $V101^{4E}$ on α-helix α1 and $Y90^{4E}$ on β-strand β1. In addition to the hydrophobic interactions, $S1089^{4G}$ and $T1092^{4G}$ show hydrogen bonds with $N104^{4E}$ located on α-helix α1.

Despite the lack of sequence conservation in putative non-canonical motifs in eIF4G, an alignment of sequences from plants, vertebrates and insects, indicates that hydrophobic residues in the region of the non-canonical binding motif are conserved (Fig. 32).

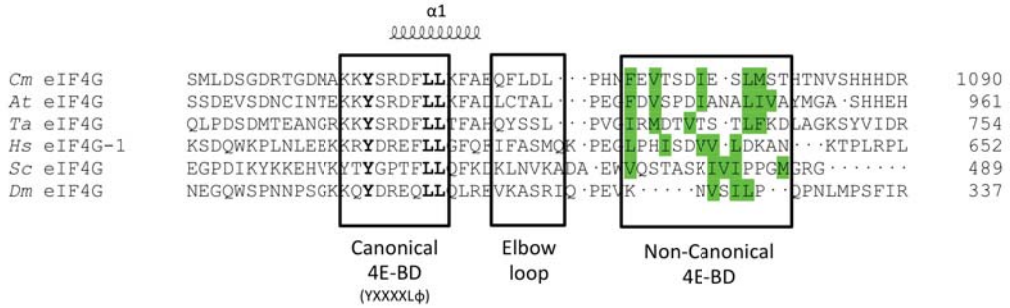

Figure 32. Structure-based sequence alignment of eIF4G orthologous. Hydrophobic residues that form the non-canonical eIF4E motif are conserved across all kingdoms. The canonical and non-canonical eIF4E binding domains (4E-BD) and the elbow loop are framed. The invariant amino acid residues of the canonical domain are typed in bold and hydrophobic residues conserved in the non-canonical domain are green colored. eIF4G sequences are from *Cucumis melo* (*Cm*), *Arabidopsis thaliana* (*At*), *Triticum aestivum* (*Ta*), *Homo sapiens* (*Hs*), *Saccharomyces cerevisiae* (*Sc*) and *Drosophila melanogaster* (*Dm*).

Moreover, the hydrophobic pocket of *Cm* eIF4E is also conserved in *Drosophila melanogaster* and *Homo sapiens*. Previous results showed that this hydrophobic patch makes contacts with 4E-BPs through their non-canonical motifs (Fig. 33) (Kinkelin *et al.* 2012; Peter *et al.* 2015a; Peter *et al.* 2015b). This may explain why a peptide from the 4E-BP Cup that encompasses a non-canonical binding domain but lacking a canonical motif is sufficient to bind eIF4E and to compete with a fragment of eIF4G in the work of Nelson *et al.* (2004). Igreja *et al.* (2013) and Peter *et al.* (2015) suggested that eIF4G lacks the non-canonical binding motif and competition with 4E-BP for binding eIF4E was due to contacting the lateral surface. However, our structural data shows that eIF4G also contains this motif with 4E-BPs and is able to bind eIF4E in both dorsal and lateral surfaces.

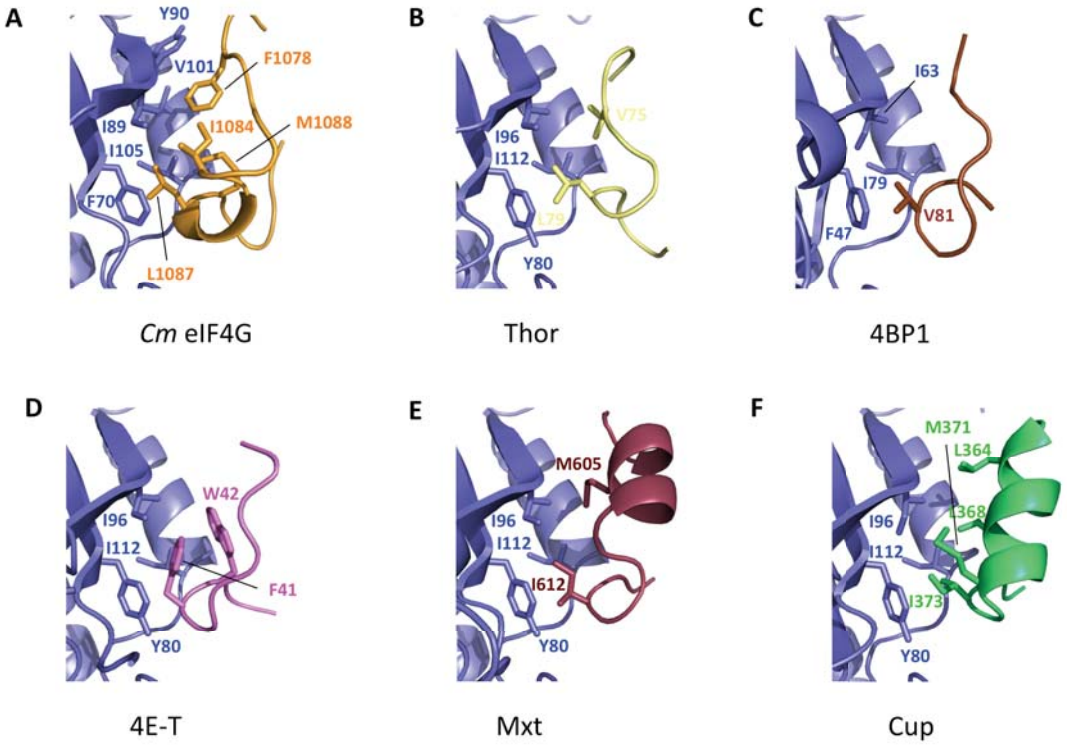

Figure 33. Structures of the eIF4E lateral hydrophobic pocket interacting with eIF4G and 4E-BPs. Conservation of Hydrophobic residues in all interacting domains of different eIF4Es. A-F) Close-up views of eIF4E hydrophobic patch and residues involved in the binding of: A) *Cm* eIF4E and eIF4G; B) *Dm* eIF4E and 4E-BP Thor; C) *Hs* eIF4E and 4E-BP 4EBP1; D) *Dm* eIF4E and 4E-BP 4E-T; E) *Dm* eIF4E and 4E-BP Mxt and F) *Dm* eIF4E and 4E-BP Cup.

3.5. Structure validation

To validate the proposed role of residues of eIF4E and eIF4G in their interaction, we mutated these in both proteins and performed *in vitro* pull-down assays (Fig. 34). All eIF4G fragments were expressed as N-terminal fusions of the maltose binding protein (MBP), which was used as a tag in this affinity chromatography. We tested recombinant fragments of wild type $eIF4G_{1003\text{-}1092}$ (eIF4G-WT) and mutated versions of it for its binding to full length eIF4E. EIF4G mutants included those located in the canonical (eIF4G-C), non-canonical (eIF4G-NC) and both (eIF4G-C-NC) eIF4E-binding sites. EIF4G-C carried three alanine substitutions in the well-conserved canonical domain YxxxLL. In eIF4G-NC the hydrophobic residues F1078, I1084 and L1087 of the proposed non-canonical motif were substituted by aspartic acid. Results showed that substitutions in either the canonical or the non-canonical binding-domain did not

disrupt the association of eIF4G with eIF4E (Fig. 34, lanes 3-8). Substitutions in the canonical binding-domain seemed to reduce but not to abolish formation of the complex (Fig. 34, lanes 5-6), contrasting with previous work where this mutations disrupted eIF4E binding in *Dm* eIF4G (Igreja *et al.* 2014). Moreover, mutants in the non-canonical binding site pulled-down comparable amounts of eIF4E as eIF4G-WT (Fig. 34, lanes 3-4 and 7-8). By contrast, no binding to eIF4E was observed when amino acid substitutions in the canonical and non-canonical binding-domains (eIF4G-C-NC) were combined (Fig. 34, lanes 9-10).

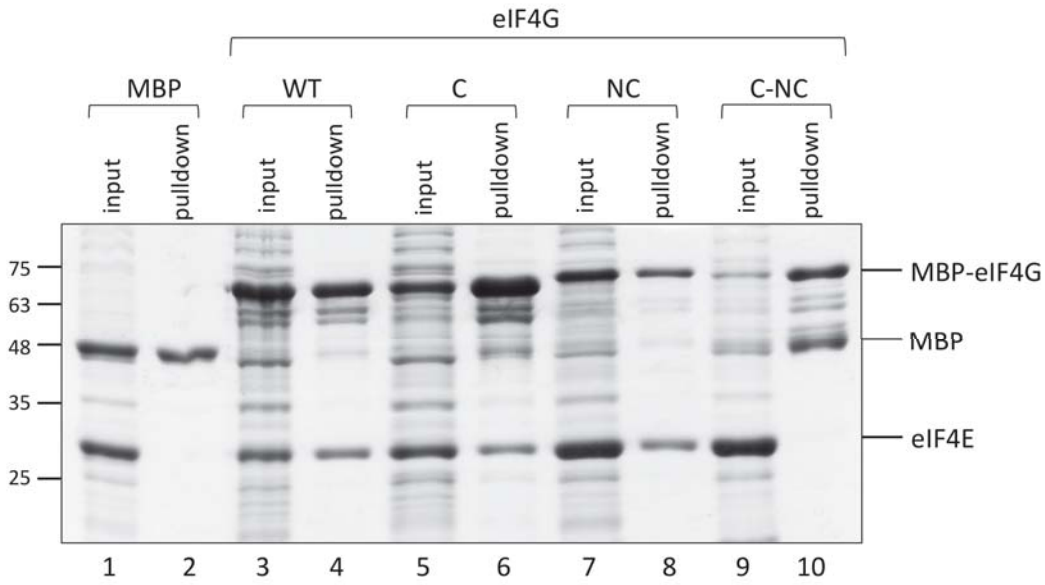

Figure 34. Interaction of *Cm* eIF4E and eIF4G *in vitro*. MBP pull-down assay showing the interaction of eIF4E (wild type, full length) and MBP-eIF4G (residues 1003-1092; either WT or mutated in canonical motif (C), non-canonical motif (NC) or both motifs (C-NC)). The input and bound fractions were analyzed by SDS-PAGE followed Coomassie blue staining.

To confirm these results, we compared the binding efficiencies of each mutant in pull-down assays using increasing concentrations between 0.5 µM and 3 µM of eIF4E with a fixed concentration of eIF4G (Fig. 35). EIF4G-WT and eIF4G-NC seemed to display similar affinities for eIF4E, slightly higher than eIF4G-C, as they bound eIF4E at the lowest concentration (Fig. 35 B, C and D, lane 5). On the other hand, as shown in the previous figure no binding was observed for the eIF4G-C-NC mutant. We quantified band intensities of the pulled-down eIF4E and plotted them versus the eIF4E concentrations used (Figure 10, F). When a hyperbolic binding curve was fitted to the

resulting concentration data, apparent dissociation constants (K_d) of 2.15 µM, 2.67 µM and 1.90 µM were obtained for eIF4G-WT, eIF4G-C and eIF4G-NC, respectively. Therefore, each of the binding domains seems to be sufficient for a similarly efficient interaction, and only simultaneous disruption of the two binding sites results in binding disruption, at least in this *in vitro* analysis.

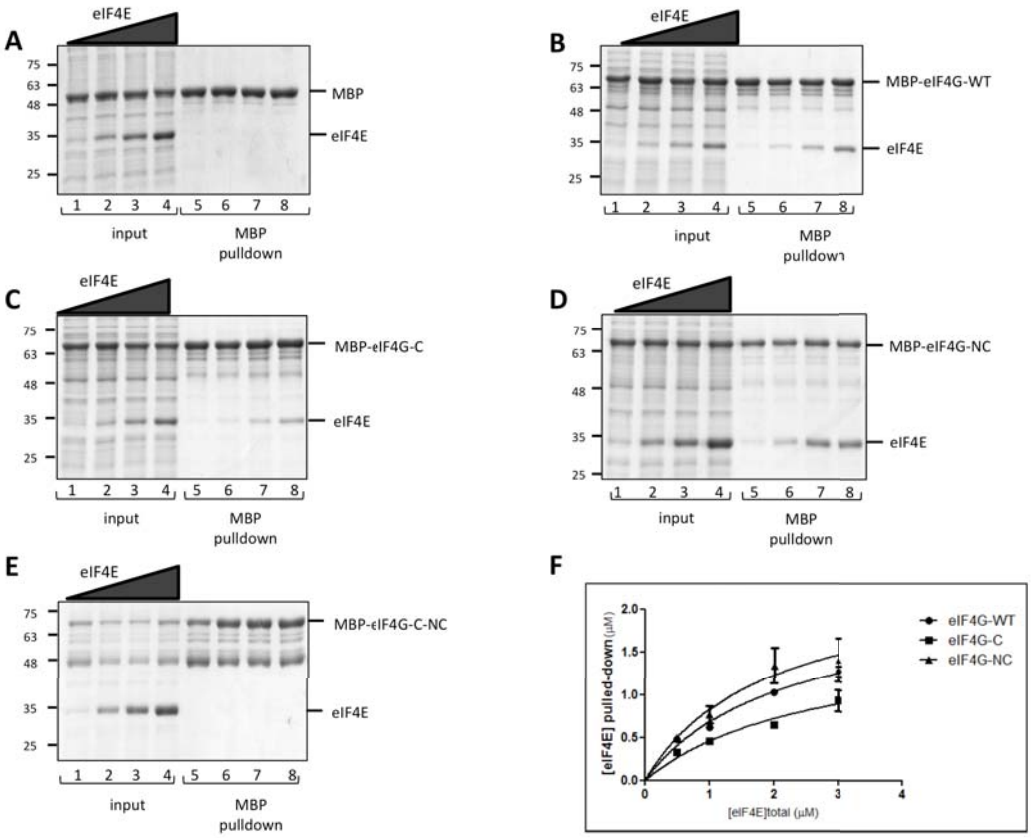

Figure 35. Binding affinity of the *Cm* eIF4E and eIF4G interaction. MBP pull-down showing the interaction of eIF4E and MBP-eIF4G-WT (B) and MBP-eIF4G mutants C, NC and C-NC (C-E). MBP served as a negative control (A). F) graph representing the specific binding obtained in several experiments as in (B, C, D). Data were fitted using a one-site binding model.

To determine whether the non-canonical binding domain of eIF4G interacts with the lateral surface of eIF4E (Fig. 30), we examined the effect of substitutions of eIF4E residues proposed to be involved in eIF4G binding, including F70A, I89A, W99A and Y154H, even as double and triple mutants Y154H-W99A, F70A-I89A, Y154H-W99A-F70A and Y154H-I89A-F70A. Lysates of mutant eIF4Es and MBP-tagged eIF4G-WT were incubated and pulled-down eIF4E was visiualized by Western blot analysis.

Substitutions W99A and Y154H-W99A on the dorsal surface of eIF4E reduced its eIF4G-binding capacity to 70% and 33%, respectively, compared to eIF4E-WT (Fig. 36, lanes 3 and 5). Substitution in residue W99 of yeast and fly eIF4E was previously shown to affect eIF4G and 4E-BPs binding to eIF4E (Ptushkina *et al.* 1998; Nelson *et al.* 2004; Igreja *et al.* 2014). On the other hand, substitution of the hydrophobic residues of the lateral pocket of eIF4E, F70A and double mutant F70A-I89A reduced its eIF4G-binding efficiency to 77% and 43% compared to eIF4E-WT, respectively (Fig. 36, lanes 6 and 8). Interestingly, binding was affected to similar extents for single and double mutants in dorsal and lateral surfaces. When substitutions in both surfaces were combined, binding was strongly impaired, resulting in 30% and 21% of the eIF4E-WT efficiency (Fig. 36, lanes 7 and 9). These results suggest that eIF4G needs to interact with both the dorsal and lateral surfaces of eIF4E for efficient binding.

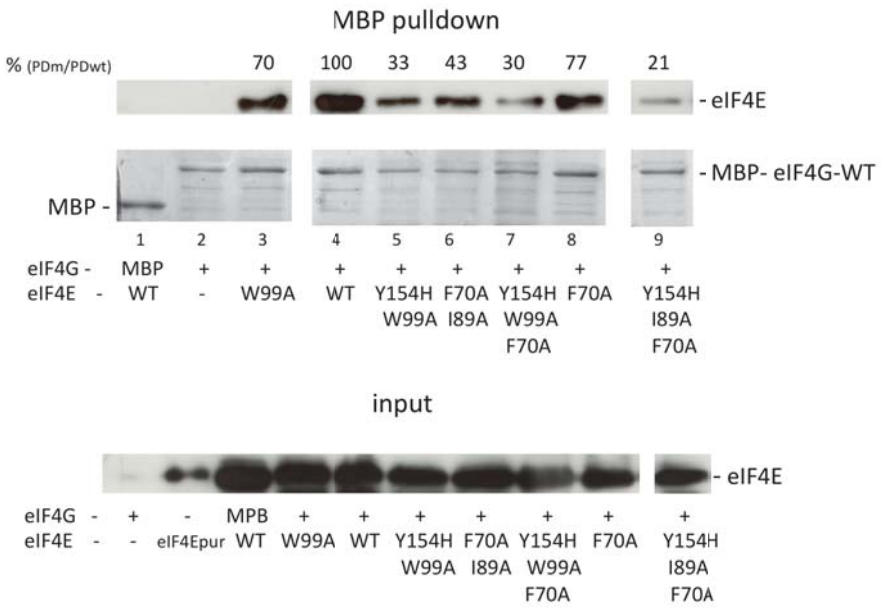

Figure 36. Mutations in *Cm* eIF4E involved in eIF4G interaction. MBP pull-down of eIF4E (WT and mutant) proteins through their interactions with MBP-eIF4G. Upper gel shows pulled down eIF4E (MBP pulldown) visualized by Western blot (WB) with a melon eIF4E specific antibody. The same gel was stained with Coomassie to compare the similar amount of eluted eIF4G in each experiment. The third gel visualizes the amount of eIF4E present in the input analyzed by Western blot. Bands from WB and from eIF4E input were quantified and a binding ratio was calculated based on eIF4E-WT:eIF4G band intensity. The interacting factors in each experiment are shown below the gels, that are the pull-down proteins, either MBP or MBP-eIF4G, and the interacting eIF4E proteins (WT or mutants).

3.6. Testing substitutions in eIF4G-binding residues of eIF4E in a translation efficiency assay

Recently, we developed a translation efficiency assay to test eIF4E mutants *in vivo* (Miras et al., 2016). This assay is based on the cap-independent translation enhancer (CITE) located in the 3'-UTR of *Melon necrotic spot virus* (MNSV, family *Tombusviridae*) named Ma5TE, which requires and has a strong specificity for eIF4E alleles to efficiently drive translation of messenger RNAs bearing it (Nieto *et al.*, 2006; Truniger *et al*., 2008; Rodriguez-Hernandez *et al*., 2012). Briefly, this assay is based on the capacity of eIF4E-WT to complement the Ma5TE-controlled translation of RNAs when it is transiently expressed in melons that carry the $eIF4E_{H228L}$ allele in homozygosis, which normally do not support Ma5TE-driven translation (Nieto *et al.*, 2006; Miras *et al*., 2016). Thus, we transiently expressed eIF4E mutants in $eIF4E_{H228L}$ melons and studied their ability to complement Ma5TE-controlled translation of reporter RNAs consisting of the luciferase gene flanked by the 5'- and 3'-UTRs of MNSV. Recapitulating previous results (Miras *et al*., 2016), our data showed that transient expression of eIF4E-WT increased Ma5TE-driven translation 6-fold with respect to translation in absence of eIF4E-WT (Fig. 37, columns 1 and 2), reaching nearly 50% of the translation activity of an eIF4E-independent reporter RNA used to normalize the data (see Materials and Methods for details); in contrast, transient over-expression of $eIF4E_{H228L}$ did not support translation (Fig. 37, column 3). We then studied the effect on translation of the eIF4E substitutions that reduced eIF4G-binding *in vitro*. In agreement with the pull-down assays, single and double substitutions in residues of the dorsal surface of eIF4E, in contact with the canonical binding domain of eIF4G, resulted in a drastic reduction of the Ma5TE-driven translation efficiency (Fig. 37, columns 4 and 5). Substitutions in the lateral surface of eIF4E, involved in interactions with the non-canonical binding domain in eIF4G, also reduced the translation efficiency (Fig. 37, columns 6 and 7). Congruently, eIF4E-mutants with substitutions in residues of both surfaces are unable to complement translation in this assay (Fig. 37, columns 8 and 9). These results strongly support the importance of the eIF4E residues implicated in binding to eIF4G through/at the non-canonical domain for eIF4F-dependent translation. The interaction of both eIF4E surfaces with eIF4G is required for efficient translation.

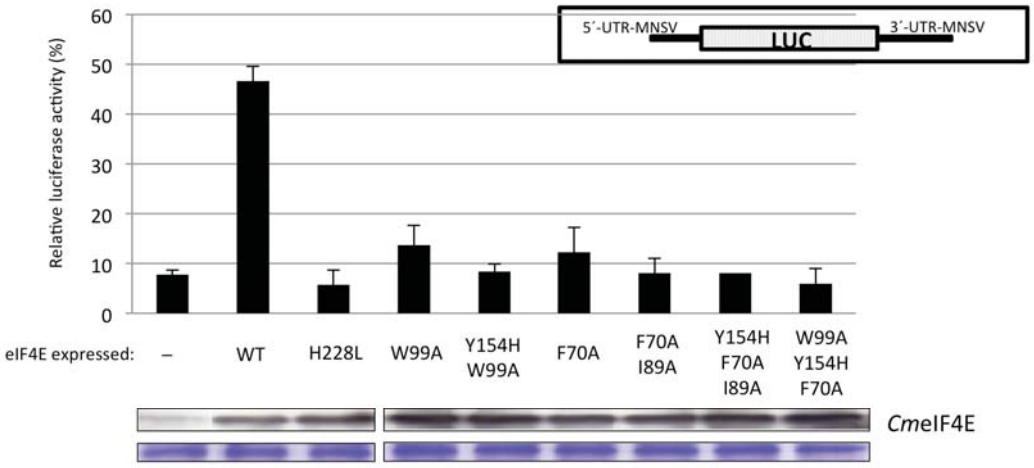

Figure 37. Effects of substitutions in eIF4E on translation efficiency assay. Relative luciferase activity (%) obtained with luciferase construct (5´-UTR-luc-3´-UTR) in eIF4E$_{H228L}$ melon protoplasts, expressing transiently different eIF4E variants (WT and mutants). For normalization of the different protoplast preparations, luciferase activity obtained with an eIF4E-independently translated reporter RNA construct 5´-UTR-luc-3´-UTR (UTRs from MNSV-264)was set to 100% for each protoplast preparation. The transiently expressed eIF4E mutants are indicated below each bar: "-": silencing suppressor P19 alone; WT; engineered eIF4E mutations: H228L; W99A and Y154H-W99A (in residues in the dorsal surface proposed to be involved in canonical eIF4G interaction); F70A and F70A-I89A (in residues in the lateral surface proposed to be involved in non-canonical eIF4G interaction); and mutations in both surfaces Y154H-F70A-I89A and W99A-Y154H-F70A. Error bars are SD +/-. Panels below show expression of each eIF4E mutant in melon cotyledon visualized by western blot using antibodies against melon eIF4E. The panel below shows the loading control visualized by Coomassie blue staining.

To confirm the correct folding of the mutant proteins tested, we studied their ability to complement growth of the eIF4E-deficient yeast strain JO55 (Altmann *et al*., 1989). This assay is a good indicator in yeast of all the functions related to growth, including mRNA translation (Altmann *et al*., 1989; German-Retana *et al*., 2008; Charron *et al*., 2008; Ashby *et al*., 2011). Almost all eIF4E mutants analyzed complemented yeast growth, confirming their functionality in this organism (Fig. 38), with exception of the triple mutant Y154H-F70A-I89A (Fig. 38) harboring substitutions in two residues involved in non-canonical binding to eIF4G, suggesting that this interaction is essential for yeast growth.

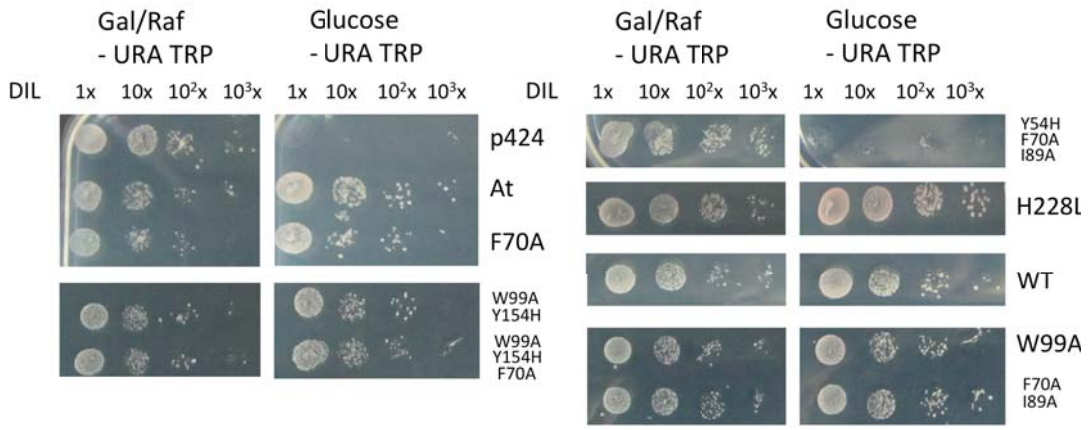

Figure 38. Complementation of translation by eIF4E mutants in eIF4E-deficient yeast. Yeast strain JO55 was transformed with plasmid p424 expressing *A. thaliana* eIF4E (At4E), or melon eIF4E (WT or mutant). Yeast cultures were spotted either undiluted (1x) or diluted (10x, 10^2x and 10^3x) on Gal/Raf and Glucose selective media (both media -Ura/-Trp). The negative control with the empty p424 and the cap-binding pocket triple mutant Y154H-F70A-I89A were unable to complement translation, thus to grow on glucose.

4. Conclusions

Our results provide the structural basis for the mode of binding eIF4G to eIF4E. While the canonical binding domain interact as expected at a conserved patch in the dorsal surface of eIF4E, a novel non-canonical binding domain was discovered. This second binding site of eIF4G docks also at a conserved surface and overlaps with the binding site of 4E-BPs (Peter *et al.*, 2015). Our data strongly suggests a universal bipartite binding mode for eIF4E binding, where eIF4G and 4E-BP repressors compete for both dorsal and lateral surfaces (Fig. 39). Phosphorylation of linker residues in 4E-BPs may interfere with the competition mechanism regulating the binding to eIF4E. These observations may contribute to a better knowledge in the design of inhibitors that compete with binding motifs on eIF4E and in this way regulate translation.

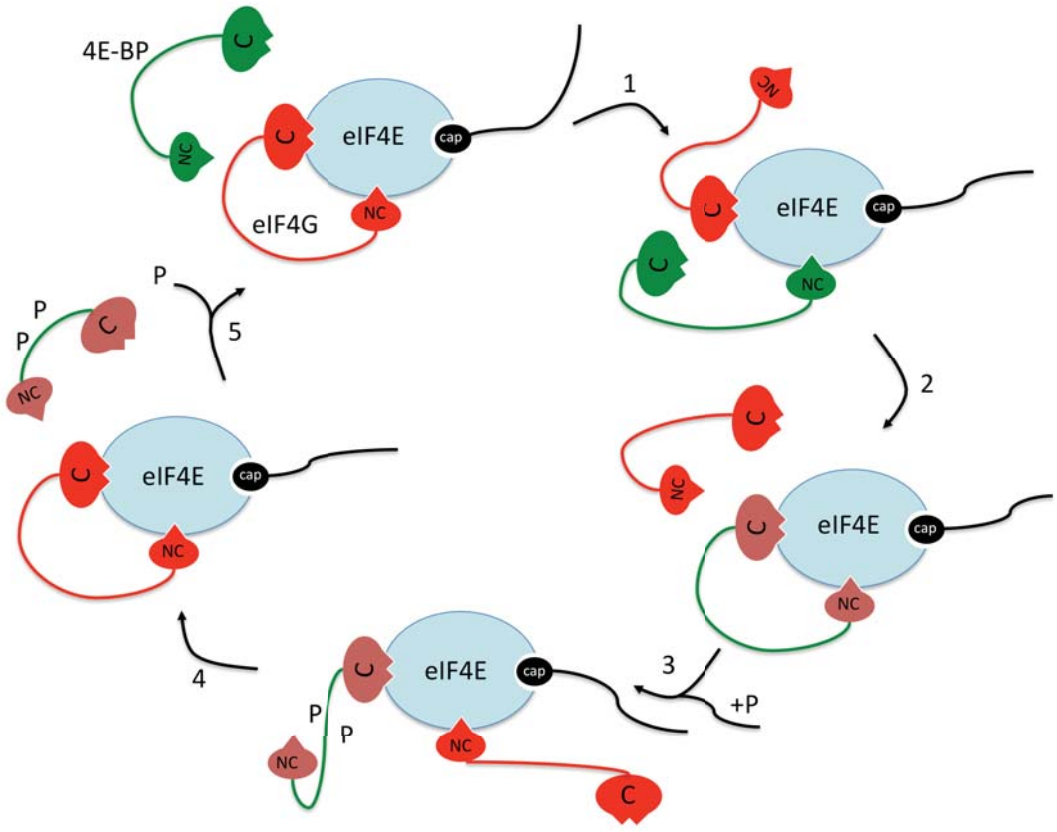

Figure 39. Competition model for eIF4E binding. EIF4E (blue) contains dorsal and lateral surfaces that bind to the C and NC motifs of eIF4G (red) and 4E-BPs (green). When eIF4G is bound to both surfaces, 4E-BPs compete for binding the lateral surface via its non-canonical motifs (1). After docking, 4E-BPs displace eIF4G from the dorsal surface of eIF4E and repress translation (2). Phosphorylation of 4E-BPs destabilizes their binding with eIF4E (3). Therefore, eIF4G can bind to both surfaces and resume translation (4). Dephosphorilation of 4E-BPs is required for binding to eIF4E (5).

5. REFERENCES

Aitken C.E. and Lorsch J.R. 2012. A mechanistic overview of translation initiation in eukaryotes. *Nature Structural and Molecular Biology* **19**: 568-576.

Altmann M., Muller P.P., Pelletier J., Sonenberg N. and Trachsel H. 1989. A mammalian translation initiation factor can substitute for its yeast homologue in vivo. *Journal of Biological Chemistry* **264**: 12145-12147.

Ashby J.A., Stevenson C.E.M., Jarvis G.E., Lawson D.M. and Maule A.J. 2011. Structure-based mutational analysis of eIF4E in relation to sbm1 resistance to Pea seed-borne mosaic virus in Pea. *PloS one* **6**.

Brown C.J., McNae I., Fischer P.M. and Walkinshaw M.D. 2007. Crystallographic and mass spectrometric characterisation of eIF4E with N 7-alkylated cap derivatives. *J Mol Biol* **372**: 7-15.

Brünger A.T., Adams P.D., Clore G.M., DeLano W.L., Gros P., Grosse-Kunstleve R.W., Jiang J.S., Kuszewski J., Nilges M. and Pannu N.S. 1998. Crystallography & NMR system: a new software suite for macromolecular structure determination. *Acta Crystallographica Section D: Biological Crystallography* **54**: 905-921.

Charron C., Nicolaï M., Gallois J.L., Robaglia C., Moury B., Palloix A. and Caranta C. 2008. Natural variation and functional analyses provide evidence for co-evolution between plant eIF4E and potyviral VPg. *Plant Journal* **54**: 56-68.

Collaborative computational project N. 1994. The CCP4 suite: programs for protein crystallography. *Acta Crystallogr D Biol Crystallogr* **50**: 760-763.

Emsley P. and Cowtan K. 2004. Coot: model-building tools for molecular graphics. *Acta Crystallographica Section D: Biological Crystallography* **60**: 2126-2132.

German-Retana S., Walter J., Doublet B., Roudet-Tavert G., Nicaise V., Lecampion C., Houvenaghel M.C., Robaglia C., Michon T. and Le Gall O. 2008. Mutational analysis of plant cap-binding protein eIF4E reveals key amino acids involved in biochemical functions and potyvirus infection. *Journal of Virology* **82**: 7601-7612.

Gosselin P., Oulhen N., Jam M., Ronzca J., Cormier P., Czjzek M. and Cosson B. 2011. The translational repressor 4E-BP called to order by eIF4E: new structural insights by SAXS. *Nucleic acids research* **39**: 3496-3503.

Gross J.D., Moerke N.J., Von Der Haar T., Lugovskoy A.A., Sachs A.B., McCarthy J.E.G. and Wagner G. 2003. Ribosome loading onto the mRNA cap is driven by conformational coupling between eIF4G and eIF4E. *Cell* **115**: 739-750.

Hinnebusch A.G. 2011. Molecular mechanism of scanning and start codon selection in eukaryotes. *Microbiology and Molecular Biology Reviews* **75**: 434-467.

Hinnebusch A.G. and Lorsch J.R. 2012. The Mechanism of Eukaryotic Translation Initiation: New Insights and Challenges. *Cold Spring Harbor Perspectives in Biology* **4**.

Igreja C., Peter D., Weiler C. and Izaurralde E. 2014. 4E-BPs require non-canonical 4E-binding motifs and a lateral surface of eIF4E to repress translation. *Nature Communications* **5**.

Jackson R.J., Hellen C.U.T. and Pestova T.V. 2010. The mechanism of eukaryotic translation initiation and principles of its regulation. *Nature Reviews Molecular Cell Biology* **11**: 113-127.

Kinkelin K., Veith K., Grünwald M. and Bono F. 2012. Crystal structure of a minimal eIF4E–Cup complex reveals a general mechanism of eIF4E regulation in translational repression. *Rna* **18**: 1624-1634.

Lukhele S., Bah A., Lin H., Sonenberg N. and Forman-Kay J.D. 2013. Interaction of the eukaryotic initiation factor 4E with 4E-BP2 at a dynamic bipartite interface. *Structure* **21**: 2186-2196.

Mader S., Lee H., Pause A. and Sonenberg N. 1995. The translation initiation factor eIF-4E binds to a common motif shared by the translation factor eIF-4 gamma and the translational repressors 4E-binding proteins. *Molecular and cellular biology* **15**: 4990-4997.

Marcotrigiano J., Gingras A.C., Sonenberg N. and Burley S.K. 1997. Cocrystal structure of the messenger RNA 5' cap-binding protein (eIF4E) bound to 7-methyl-GDP. *Cell* **89**: 951-961.

Marcotrigiano J., Gingras A.C., Sonenberg N. and Burley S.K. 1999. Cap-dependent translation initiation in eukaryotes is regulated by a molecular mimic of eIF4G. *Molecular Cell* **3**: 707-716.

Marcotrigiano J., Lomakin I.B., Sonenberg N., Pestova T.V., Hellen C.U.T. and Burley S.K. 2001. A conserved HEAT domain within eIF4G Directs Assembly of the Translation Initiation Machinery. *Molecular Cell* **7**: 193-203.

Matsuo H., Li H., McGuire A.M., Fletcher C.M., Gingras A.-C., Sonenberg N. and Wagner G. 1997. Structure of translation factor eIF4E bound to m7GDP and interaction with 4E-binding protein. *Nature Structural & Molecular Biology* **4**: 717-724.

Mizuno A., In Y., Fujita Y., Abiko F., Miyagawa H., Kitamura K., Tomoo K. and Ishida T. 2008. Importance of C-terminal flexible region of 4E-binding protein in binding with eukaryotic initiation factor 4E. *FEBS letters* **582**: 3439-3444.

Monzingo A.F., Dhaliwal S., Dutt-Chaudhuri A., Lyon A., Sadow J.H., Hoffman D.W., Robertas J.D. and Browning K.S. 2007. The structure of eukaryotic translation initiation factor-4E from wheat reveals a novel disulfide bond. *Plant Physiology* **143**: 1504-1518.

Mumberg D., Müller R. and Funk M. 1995. Yeast vectors for the controlled expression of heterologous proteins in different genetic backgrounds. *Gene* **156**: 119-122.

Murshudov G.N., Vagin A.A. and Dodson E.J. 1997. Refinement of macromolecular structures by the maximum-likelihood method. *Acta Crystallographica Section D: Biological Crystallography* **53**: 240-255.

Nelson M.R., Leidal A.M. and Smibert C.A. 2004. Drosophila Cup is an eIF4E-binding protein that functions in Smaug-mediated translational repression. *The EMBO Journal* **23**: 150-159.

Nieto C., Morales M., Orjeda G., Clepet C., Monfort A., Sturbois B., Puigdomènech P., Pitrat M., Caboche M., Dogimont C. et al. 2006. An eIF4E allele confers resistance to an uncapped and non-polyadenylated RNA virus in melon. *Plant Journal* **48**: 452-462.

Nieto C., Rodríguez-Moreno L., Rodríguez-Hernández A.M., Aranda M.A. and Truniger V. 2011. Nicotiana benthamiana resistance to non-adapted Melon necrotic spot virus results from an incompatible interaction between virus RNA and translation initiation factor 4E. *Plant Journal* **66**: 492-501.

Paku K.S., Umenaga Y., Usui T., Fukuyo A., Mizuno A., In Y., Ishida T. and Tomoo K. 2012. A conserved motif within the flexible C-terminus of the translational regulator 4E-BP is required for tight binding to the mRNA cap-binding protein eIF4E. *Biochemical Journal* **441**: 237-245.

Papadopoulos E., Jenni S., Kabha E., Takrouri K.J., Yi T., Salvi N., Luna R.E., Gavathiotis E., Mahalingam P., Arthanari H. et al. 2014. Structure of the eukaryotic translation initiation factor eIF4E in complex with 4EGI-1 reveals an allosteric mechanism for dissociating eIF4G. *Proceedings of the National Academy of Sciences of the United States of America* **111**: E3187-E3195.

Park E.H., Walker S.E., Lee J.M., Rothenburg S., Lorsch J.R. and Hinnebusch A.G. 2011. Multiple elements in the eIF4G1 N-terminus promote assembly of eIF4G1•PABP mRNPs in vivo. *EMBO Journal* **30**: 302-316.

Pestova T.V., Kolupaeva V.G., Lomakin I.B., Pilipenko E.V., Shatsky I.N., Agol V.I. and Hellen C.U.T. 2001. Molecular mechanisms of translation initiation in eukaryotes. *Proceedings of the National Academy of Sciences* **98**: 7029-7036.

Peter D., Igreja C., Weber R., Wohlbold L., Weiler C., Ebertsch L., Weichenrieder O. and Izaurralde E. 2015a. Molecular architecture of 4E-BP translational inhibitors bound to eIF4E. *Molecular cell* **57**: 1074-1087.

Peter D., Weber R., Köne C., Chung M.-Y., Ebertsch L., Truffault V., Weichenrieder O., Igreja C. and Izaurralde E. 2015b. Mextli proteins use both canonical bipartite and novel tripartite binding modes to form eIF4E complexes that display differential sensitivity to 4E-BP regulation. *Genes & development* **29**: 1835-1849.

Ptushkina M., Von der Haar T., Vasilescu S., Frank R., Birkenhäger R. and McCarthy J.E.G. 1998. Cooperative modulation by eIF4G of eIF4E-binding to the mRNA 5' cap in yeast involves a site partially shared by p20. *EMBO Journal* **17**: 4798-4808.

Rodríguez-Hernández A.M., Gosalvez B., Sempere R.N., Burgos L., Aranda M.A. and Truniger V. 2012. Melon RNA interference (RNAi) lines silenced for Cm-eIF4E show broad virus resistance. *Molecular Plant Pathology* **13**: 755-763.

Rosettani P., Knapp S., Vismara M.-G., Rusconi L. and Cameron A.D. 2007. Structures of the human eIF4E homologous protein, h4EHP, in its m 7 GTP-bound and unliganded forms. *J Mol Biol* **368**: 691-705.

Siddiqui N., Tempel W., Nedyalkova L., Volpon L., Wernimont A.K., Osborne M.J., Park H.-W. and Borden K.L.B. 2012. Structural insights into the allosteric effects of 4EBP1 on the eukaryotic translation initiation factor eIF4E. *J Mol Biol* **415**: 781-792.

Sonenberg N. and Hinnebusch A.G. 2009. Regulation of translation initiation in eukaryotes: mechanisms and biological targets. *Cell* **136**: 731-745.

Truniger V., Nieto C., González-Ibeas D. and Aranda M. 2008a. Mechanism of plant eIF4E-mediated resistance against a Carmovirus (Tombusviridae): Cap-independent translation of a viral RNA controlled in cis by an (a)virulence determinant. *Plant Journal* **56**: 716-727.

Truniger V., Nieto C., González-Ibeas D. and Aranda M. 2008b. Mechanism of plant eIF4E-mediated resistance against a Carmovirus (Tombusviridae): cap-independent translation of a viral RNA controlled in cis by an (a) virulence determinant. *The Plant Journal* **56**: 716-727.

Volpon L., Osborne M.J., Topisirovic I., Siddiqui N. and Borden K.L.B. 2006. Cap-free structure of eIF4E suggests a basis for conformational regulation by its ligands. *EMBO Journal* **25**: 5138-5149.

Yang J., Yan R., Roy A., Xu D., Poisson J. and Zhang Y. 2015. The I-TASSER Suite: protein structure and function prediction. *Nature methods* **12**: 7-8.

6. SUPPORTING INFORMATION

Supplementary Table 3. Primers used in this study

Primer	Sequence (5´-3´)	Application
4E_F	TTTAAGAAGGAGATATAGATCATGGCGTCCCTAGTGCATCAGCC	$eIF4E_{51-235}$ cloning in p2AT
4E_R	TTATGGAGTTGGGATCTTATTACACCATATATTTATTCTTCGC	
4E_I89A_F	GGTGCGTCTATTCGACCGGCGTATACCTTCTCTACCGTC	eIF4E Mutation, I89A
4E_I89A_R	GACGGTAGAGAAGGTATACGCCGGTCGAATAGACGCACC	
4E_F70A_F	CACTCTTGGACCTTTTGGGCGGATAACCCATCTGCCAAA	eIF4E Mutation, F70A
4E_F70A_R	TTTGGCAGATGGGTTATCCGCCCAAAAGGTCCAAGAGTG	
4E_W99A_F	TCTACCGTCGAGGAGTTCGCGAGTGTTTACAACAACATT	eIF4E Mutation, W99A
4E_W99A_R	AATGTTGTTGTAAACACTCGCGAACTCCTCGACGGTAGA	
4E_Y154H_F	TCTGATAATGGCTGGTTGCACACGCTGCTTGCTATGATC	eIF4E Mutation, Y154H
4E_Y154H_R	GATCATAGCAAGCAGCGTGTGCAACCAGCCATTATCAGA	
Triple mut C_F	GGAGATATGGCCAAGAAGGCATCTAGGGATTTTGCAGCAAAGTTTG CCGAGCAGTTT	eIF4G C, Y1049A-L1054A-L1055A
Triple mut C_R	AAACTGCTCGGCAAACTTTGCTGCAAAATCCCTAGATGCCTTCTTGG CCATATCTCC	
Triple mut NC_F	CTGGACCTTCCTCATAACGACGAAGTTACATCTGATGACGAGTCTGA CATGAGTACTCATACCAAT	eIF4G NC, F1078D-I1084D-L1087D
Triple mut NC_R	ATTGGTATGAGTACTCATGTCAGACTCGTCATCAGATGTAACTTCGT CGTTATGAGGAAGGTCCAG	

Supplementary Table 4. Mutants and constructs used in this study

Protein	Mutation	Type of mutation
$eIF4E_{1\text{-}235\ full\ length}$	WT	
	H228L	resistance allele
	W99A	Dorsal surface
	Y154H-W99A	Dorsal surface
	F70A	Lateral surface
	F70A-I89A	Lateral surface
	Y54H-F70A-I89A	Dorsal and lateral surface
	W99A-Y154H-F70A	Dorsal and lateral surface
$eIF4E_{51\text{-}235}$	WT	
$eIF4G_{1003\text{-}1092}$	WT	
	Y1049A-L1054A-L1055A	Canonical eIF4E-binding domain
	F1078D-I1084D-L1087D	Non-canonical eIF4E binding motif
	Y1049A-L1054A-L1055A-F1078D-I1084D-L1087D	Canonical and non-canonical binding motifs

Supplementary Table 5. X-ray data collection statistics and refinement

Data Collection	4EG	4E	4E+CAP
Resolution range (outermost shell) (Å)	29.3-1.9 (1.99-1.9)	47.1-2.2 (2.32-2.2)	47.1-2.56 (2.7-2.56)
Space group	$P2_1$	$P2_12_12_1$	$P2_12_12_1$
Cell dimensions	a=38.1; b=70.3; c=42.8; β=93.6	a=57.7; b=109.0; c=122.1	a=57.7; b=108.9; c=122.8
Number of total/unique reflections	66637/17809	145891/39619	125316/24722
Rmerge (%)	7.9 (60.8)	10.3 (38.4)	24.4 (88.1)
I/sigmaI	11.2 (2.1)	7.9 (2.8)	4.2 (1.5)
Completeness (%)	99.8 (99.7)	99.3 (97.8)	96.7 (78.2)
Redundancy	3.7 (Collaborative computational project)	3.7 (3.6)	5.1 (4.8)
Refinement statistics			
R_{work} %	18.9 (23.5)	18.5 (26.2)	21.8 (25.3)
R_{free} %	22.9 (29.3)	21.1 (27.1)	25.6 (26.1)
Number of residues			
Protein	151 (eIF4E) 37 (eIF4G)	703	703
Solvent	61	142	
Ion (SO_4)	2		
Glycerol		5	
Ligand (CAP)			2
Rmsd			
Bond lengths (Å)	0.007	0.015	0.006
Bond angles (°)	1.031	1.660	1.194
Average temperature factors (Å)			
Protein	29.6	25.7	18.4
Solvent	32.3	40.9	

Ion	44.8		
Glycerol		77.6	
Ligand			27.5
Model quality/Ramachandran plot (%)			
Residues in favored regions	98.4	97.3	95.6
Residues in allowed regions	1.6	2.4	4.1

Resumen

La mayor parte de los RNAs mensajeros (mRNAs) eucarióticos tienen una estructura cap en el extremo 5´ (5´-cap) y una cola de poly(A) [3´-poly(A) tail] en el extremo 3´, y ambos elementos actúan sinérgicamente para estimular la traducción del mRNA. Esta estimulación traduccional depende de la formación de un lazo que se cierra gracias a interacciones múltiples: el factor 4E de iniciación de la traducción en eucariotas (eIF4E) se une al 5´-cap, la proteína de unión a poly(A) se une al 3´-poly(A), y eIF4G se une simultáneamente a ambas proteínas. La formación de este lazo cerrado es un requisito para la traducción eficiente de la mayoría de los mRNAs, ya que parece que estimula el reclutamiento del complejo de iniciación de la traducción 43S hacia la región 5´-no traducida (5´-UTR) de los transcritos celulares (revisado en Sonenberg y Dever, 2003). Los mRNAs virales han evolucionado desarrollando diversos mecanismos para reclutar la maquinaria de traducción del huésped, proporcionando a los virus la capacidad de competir con los mRNAs del huésped y evitar mecanismos de defensa que actúan al nivel de la iniciación de la traducción (revisado en Dreher y Miller, 2006). Sólo aproximadamente un 20% de los virus de RNA de cadena positiva tienen RNAs genómicos y subgenómicos con 5´-cap y 3´-poly(A) típicos de los mRNAs eucarióticos (van Regenmortel *et al*., 2000) y, así, lo más frecuente es que sólo tengan una, o no tengan ninguna, de estas estructuras, sino que usen estructuras terminales alternativas para la expresión de sus genes (Dreher y Miller, 2006; Kneller *et al*., 2006). Los virus de la familia *Tombusviridae* y los del género *Luteovirus* no tienen ni 5´-cap ni 3´-poly(A), sino que inician la traducción independiente de cap en el extremo 5´ de sus RNAs con la ayuda de una estructura que reside en los 3´-UTRs y que actúa como estimulador de la eficiencia traduccional independiente de cap (cap-independent translational enhancer, 3´-CITE) (Miller y White, 2006). El 3´-CITE mejor estudiado es el del Virus del enanismo y amarilleo de la cebada (*Barley yellow dwarf virus,* BYDV; familia *Luteoviridae*, género *Luteovirus*), el cual se ha mostrado recientemente que se une a eIF4F a través de su subunidad eIF4G (Treder *et al*., 2008). Todos los demás miembros del género *Luteovirus*, y todos los de los géneros *Necrovirus* y *Dianthovirus* (familia *Tombusviridae*) contienen un 3´-CITE parecido al de BYDV. Otros 3´-CITEs no relacionados estructuralmente han sido identificados en los 3´-UTRs de tombusvirus como el Virus del enanismo arbustivo del tomate (*Tomato bushy stunt virus*), el Virus del listado necrótico del maíz (*Maize necrotic streak virus*), el Virus del mosaico del

mijo (*Panicum mosaic virus*), el Virus de las manchas cloróticas en anillos del hibisco (*Hibiscus chlorotic ringspot virus*) y el Virus del arrugado del nabo (*Turnip crinkle virus*) (Miller *et al*., 2007). Las secuencias y estructuras de estos 3´-CITEs no tienen una similitud obvia y se han asignado a ocho clases estructurales distintas (Miller *et al.*, 2007). A pesar de esta falta de similitud, casi todos los 3´-CITEs que han sido descritos hasta ahora contienen tramos cortos de secuencia que se sabe (en unos pocos casos) o se ha propuesto (en la mayoría de los casos) que interaccionen con secuencias complementarias en los correspondientes 5´-UTRs, una interacción a larga distancia que es necesaria para la traducción independiente de cap (Miller y White, 2006). Así, Fabian y White (2004) han propuesto que ocurran interacciones 5´-3´ para diversos virus que pertenecen a la familia *Tombusviridae*, incluyendo el Virus de la necrosis del tallo del guisante (*Pea stem necrosis virus*, PSNV), que pertenece al mismo género que MNSV. Significativamente, la secuencia que potencialmente interacciona y que se ha identificado (6 nt) en el 3´-CITE de PSNV es parcialmente idéntica (4 nt) a la secuencia de un bucle de una estructura tallo-bucle conservada en todos los aislados de MNSV (Truniger *et al*., 2008). En dos casos se han identificado interacciones directas entre 3´-CITEs y factores de iniciación de la traducción: el 3´-CITE del Satélite del virus de la necrosis del tabaco interacciona específicamente con eIF4F y eIF(iso)4F así como con las subunidades de unión a cap eIF4E y eIF(iso)4E (Gazo *et al.*, 2004), y el 3´-CITE de BYDV se une a eIF4F, interaccionando preferentemente con eIF4G, y esta interacción correlaciona con la capacidad del 3´-CITE de BYDV para estimular la traducción independiente de cap (Treder *et al.*, 2008). Por tanto, los resultados obtenidos mediante el análisis de unos pocos casos sugieren que los 3´-CITEs sean responsables de reclutar factores del huésped implicados en la iniciación de la traducción y que, mediante una interacción RNA:RNA a larga distancia entre los extremos 3´- y 5´- de los RNAs virales, éstos sean puestos en contacto con el 5´-UTR. Sin embargo, existe muy poca información sobre las conformaciones estructurales que adoptan los elementos (RNAs y proteínas) que intervienen en estas interacciones.

El Virus de las manchas necróticas del melón (Melon necrotic spot virus, MNSV), objeto de estudio de la presente Tesis Doctoral, presenta un genoma de ARN monocatenario con sentido positivo de aproximadamente 4,3Kb con al menos cinco

marcos de lectura abiertos (Open reading frames, ORFs). La estrategia de traducción de los ORFs del genoma de MNSV es la misma que la de otros Carmovirus donde la expresión de la p29 y p89 se llevaría a cabo a partir del ARN genómico, mientras que el resto de proteínas se expresarían a partir de dos mensajeros subgenómicos. (Figura 5). Ni su ARN genómico ni los subgenómicos presentan estructuras 5´-cap (m^7G^5pppNp) ni cola 3´-poli(A), típicas de los ARN mensajeros eucarióticos (Diaz et al., 2003; Riviere and Rochon, 1990). Sin embargo, en sus regiones 3´ no traducibles (3´UTR) contienen secuencias que actúan como activadores de su traducción, que es independiente de cap (3´-CITE) (Truniger et al., 2008).

El ORF más próximo al extremo 5´ codifica una proteína de 29 kDa (p29) y finaliza en un codón ámbar. Si la traducción no se detiene en dicho codón se obtiene una proteína de 89 kDa (p89) que contiene el dominio polimerasa de ARN dependiente de ARN (RNA dependent RNA polymerase, RdRp) y que junto con la p29, está implicada en la replicación del virus. Los dos ORFs situados en la parte central del genoma constituyen el bloque de dos genes típico de los carmovirus (Double gene block, DGB), que en el caso de MNSV codifican las proteínas p7A y p7B, de 7 kDa cada una, separadas por un codón de parada ámbar en la mayoría de aislados. Estas proteínas participan en el movimiento célula a célula del virus (Genovés et al., 2006). El ORF situado en el extremo 3´ codifica la proteína de la cápsida (CP) de un tamaño de 42 kDa.

Existen herramientas moleculares eficientes para el estudio de MNSV, incluyendo clones infectivos (Diaz et al., 2004; Genovés et al., 2006). En nuestro laboratorio, hemos estudiado con detalle determinados aspectos relacionados con la traducción de los RNAs de MNSV, debido primariamente a nuestro interés por caracterizar un mecanismo de resistencia a MNSV en melón. En melón, existen al menos dos fuentes de resistencia a MNSV, el cultivar 'Gulfstream' y la entrada Coreana PI 161375, estando la resistencia de ambas líneas controlada por el mismo gen recesivo, nsv (Coudriet et al., 1981). El gen nsv es efectivo frente a todas las cepas de MNSV conocidas hasta ahora, excepto frente a MNSV-264 (Diaz et al., 2004). Los análisis de protoplastos de melones susceptibles y resistentes inoculados con MNSV

que hemos llevado a cabo mostraron que la resistencia conferida por este gen actúa a nivel unicelular (Diaz et al., 2004). Significativamente, los estudios realizados utilizando mutantes quiméricos entre MNSV-264 y una cepa no virulenta mostraron que el determinante genético en el virus responsable de la rotura de la resistencia reside en el 3´-UTR de su RNA genómico (Diaz et al., 2004). Utilizando una combinación de clonaje posicional y microsintenia con Arabidopsis thaliana, delimitamos genética y físicamente el locus nsv a un único clon BAC e identificamos eIF4E de melón (Cm-eIF4E) como gen candidato. Ensayos de complementación in vivo utilizando un ensayo biolístico de expresión transitoria confirmaron Cm-eIF4E como producto de nsv. Un único cambio de amino ácido en la posición 228 de la proteína es responsable de la resistencia a MNSV (Nieto et al., 2006). La expresión de la proteína y ensayos de afinidad por cap mostraron que el Cm-eIF4E codificado por plantas resistentes no parece estar afectado en su unión a cap con respecto al Cm-eIF4E codificado por plantas susceptibles (Nieto et al., 2006). La construcción y análisis de más virus quiméricos nos permitió delimitar los determinantes de virulencia y avirulencia a 49 y 26 nucleótidos, respectivamente. Analizamos también la eficiencia traduccional de un gen chivato (luc) flanqueado por 5´- y 3´-UTRs de virus virulentos, avirulentos y quiméricos, in vitro (en extractos de germen de trigo) e in vivo (en protoplastos de melón), obteniendo los siguientes resultados: (i) el determinante de avirulencia intermedia la eficiencia de la traducción independiente de cap tanto in vitro como in vivo, (ii) el determinante de avirulencia promueve la traducción independiente de cap eficientemente in vitro pero sólo cuando el eIF4E de melón susceptible se añade al extracto de germen de trigo y, coherentemente, solo en protoplastos de melón susceptible, pero no en protoplastos de melón resistente; Por tanto, los determinantes de virulencia y avirulencia funcionan como 3´-CITEs (Truniger et al., 2008). (iii) estas actividades requieren la presencia en cis del 5´-UTR de MNSV. En análisis preliminares hemos identificado pequeños tramos de secuencias complementarias en los extremos 5´- y 3´-UTR virales, que están muy conservados entre los aislados de MNSV secuenciados, lo que sugiere que ocurra una interacción directa RNA:RNA entre estos extremos. Los resultados descritos nos han permitido proponer un modelo para explicar el mecanismo de la resistencia mediada por eIF4E (nsv) a MNSV en melón, en el cual la circularización del RNA viral se consigue mediante el apareamiento de bases a

través de una interacción a larga distancia entre 5´- y 3´-UTR. En melón susceptible, una interacción entre el 3´-CITE de MNSV-avirulento y Cm-eIF4ES (de melón susceptible) permite una eficiente traducción independiente de cap, mientras que en melón resistente esta interacción, y por tanto, la traducción, es ineficiente, previniendo la multiplicación viral. Por otra parte, el 3´-CITE de MNSV-264 quizá pueda interaccionar con ambas versiones de Cm-eIF4E, aunque menos eficientemente con Cm-eIF4ES que con Cm-eIF4ER (de melón resistente), ya que su traducción es menos eficiente en protoplastos de melón susceptible. Alternativamente, el factor del huésped que interaccione con el 3´-CITE de MNSV-264 quizá sea la isoforma de Cm-eIF4E o, quizá sea otro factor de iniciación de la traducción (Truniger et al., 2008).

Recientemente, ha sido identificado un segundo aislado capaz de superar esta resistencia. El determinante de virulencia del primer aislado había sido localizado en una parte de su extremo 3´ no traducido (3´-UTR), la cual le confería la capacidad de traducción independiente de cap no sólo en melón susceptible, sino también en resistente (Truniger et al., (2008) The Plant Journal 56:716-727). La secuencia nucleotídica del nuevo aislado, denominado MNSV-N, muestra una alta similitud con el resto de aislados de MNSV que no superan la resistencia, incluso en su 3´-UTR. Sin embargo, el inicio de su 3´-UTR contiene una inserción de 55 nucleótidos (nt) que es casi idéntica al comienzo del 3´-UTR del virus del amarilleo de las cucurbitáceas transmitido por pulgones (Cucurbit aphid-borne yellows virus) (CABYV), indicando que MNSV-N es un recombinante entre MNSV y CABYV. Mediante la construcción de virus quiméricos hemos localizado el determinante de virulencia de MNSV-N en su 3´-UTR. Estudios de traducción in vivo en protoplastos de melón han demostrado que el 3´-UTR de MNSV-N controla la traducción independiente de cap en melón susceptible y resistente del transcrito de un gen delator, siendo la inserción de 55 nt dentro del 3´-UTR esencial para la traducción en melón resistente, pero no en susceptible; estos resultados sugieren que esta capacidad sea responsable de la superación de la resistencia. La estructura secundaria del 3´-UTR de este aislado está siendo estudiada actualmente.

Así mismo, hemos comprobado que la traducción de MNSV-N probablemente sea independiente de eIF4E, al ser este aislado capaz de infectar plantas cuya expresión de eIF4E ha sido reducida a través de silenciamiento génico posttranscripcional.

En el segundo capítulo, se realizó un análisis estructural y funcional del 3'-CITE y del factor asociado a él, eIF4F, que ambos controlan la traducción de los ARNs de MNSV. Para ello, primero se delimitó a 45 nucleótidos la secuencia mímina capaz de estimular la traducción *in vivo*. A continuación, estudiamos su estructura secundaria y su capacidad para unir al complejo eIF4F mediante ensayos de filterbinding y UV-crosslinking. La experimentos de estructura secundaria no dieron una estructura en forma tallo-lazo con dos regiones internas desapareadas. Los ensayos de footprinting revelaron la unión a eIF4F a través de una de las zonas desapareada del 3'-CITE. A continuación, se realizaron ensayos mutando dicha que conllevaron la pérdida de traducción y de unión a eIF4F. Por último, los ensayos de mutantes en eIF4E llevados a cabo, nos sugieren que el complejo eIF4F es necesario para la traducción de estos ARNs, ya que la rotura de la interacción eIF4E:eIF4G está asociada con una pérdida de la actividad traduccional.

Por último, en el tercer capítulo estudiamos el modo de interacción entre eIF4E y eIF4G ya que hemos determinado que es necesaria para la traducción de los ARNs virales de MNSV. Para ello se cristalizó la subunidad eIF4E, libre y unida a una versión truncada de $eIF4G_{1003-1092}$. La estructura de eIF4E de melón es muy parecida a las ya cristalizadas anteriormente. La diferencia entre la estructura de eIF4E sola y en complejo con el péptido de eIF4G, radica en la formación de un puente disulfuro. Este puente disulfuro fue previamente descrito en la eIF4E de trigo. Sin embargo, se desconoce su implicación. La difracción por rayos X de los cristales del complejo eIF4F reveló un segundo dominio de unión en eIF4G. Este segundo dominio, o dominio no-canónica, está en contacto con la superficie lateral de eIF4E, la cuál está compartida por otras proteínas que contienen también este segundo dominio de unión. Estos

datos sugieren que la interacción eIF4E:eIF4G es bipartita y que hay una competición entre eIF4G y otras proteínas por estas superficies de eIF4E para regular la traducción.